UNBOUND GRANULAR BASES FOR ROADS

GOVERT T.H. SWEERE

UNBOUND GRANULAR BASES FOR ROADS

GOVERT T.H. SWEERE

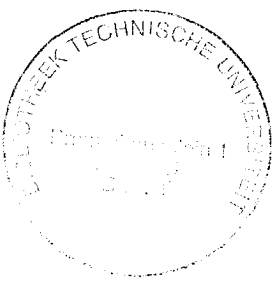

PROEFSCHRIFT

ter verkrijging van de graad van doctor
aan de Technische Universiteit Delft,
op gezag van de Rector Magnificus, prof. drs. P.A.Schenck,
in het openbaar te verdedigen ten overstaan van een commissie
aangewezen door het College van Dekanen
op donderdag 20 september 1990
te 16.00 uur.

door

GODEFRIDUS THEODORUS HENRICUS SWEERE

geboren te Zevenbergen,
civiel ingenieur

Dit proefschrift is goedgekeurd door de promotoren

prof.ir. H.J.Th. Span en

prof. S.F. Brown, D.Sc., C.Eng.

ACKNOWLEDGEMENT

The research described in this dissertation was carried out at the Road and Railroad Research Laboratory of the Faculty of Civil Engineering of Delft University of Technology. The author wishes to express his appreciation to his colleagues at the Laboratory for their cooperation and support.

This research was supported by the Netherlands Technology Foundation (STW), the Road and Hydraulic Engineering Division of Rijkswaterstaat (DWW) and the Centre for Research and Contract Standardization in Civil and Traffic Engineering (CROW).

EXECUTIVE SUMMARY

This study deals with the mechanical properties of unbound granular road base materials. An extensive laboratory and in-situ experimental investigation is described, in which the various methods for determination of the mechanical properties of granular materials are examined for their applicability. Further, the mechanical behaviour of unbound materials under influence of changes in the moisture content is investigated and a study into the modelling of the stress-dependent mechanical behaviour of granular materials is presented. Finally, an experimental case study into the structural contribution of granular bases to flexible pavements is described.

The laboratory investigation involved a large range of granular materials, which was investigated in cyclic load triaxial tests. These tests yield fundamental parameters that describe the resilient stiffness and the resistance to permanent deformation of the materials tested. In addition to the granular base coarse materials, a total of six sands used widely in pavement construction in the Netherlands was incorporated in the laboratory testing program. Further, laterites were investigated since they form the main road building material in the tropics.

Chapter 2 gives an extensive review of the literature on the various topics of this dissertation. Each of the paragraphs of this chapter summarizes the literature on the topics which are later dealt with in the subsequent chapters of this dissertation.

Chapter 3 deals with the specifications for unbound road base material. In addition to the Dutch specifications for such materials, those used in the USA and the UK are also dealt with. Further, specifications for tropical road base materials are described. Finally, the South-African specifications for "Waterbound Macadam" are summarized, because of the particular composition of this gap-graded, high stiffness material.

Chapter 4 describes the materials used in the test program of the research described in this dissertation. Four main groups of materials are distinguished, being conventional granular road base materials, recycled granular road base materials, sands and laterites. This chapter also describes the coding system which is used throughout this dissertation to denote the various materials.

Chapter 5 discusses the laboratory testing of the wide range of materials. First, a description is given of the range of standard tests which were carried out to obtain a reference with common pavement engineering practice. Next, the cyclic load triaxial equipment built for this investigation is described, together with the actual testing procedures and the results of that testing. Finally, an investigation into development of simplified testing procedures for determination of fundamental mechanical properties is described.

In Chapter 6, the mechanical behaviour of granular materials as influenced by changes in the moisture content is discussed. The background of the development of suction in unsaturated granular materials is described. Subsequently, the influence of suction on the

mechanical behaviour of granular materials is investigated in cyclic load triaxial tests on granular materials at different moisture contents.

Chapter 7 deals with the modelling of the stress-dependent mechanical properties of granular materials. Four models describing the resilient behaviour of such materials are discussed, two of which are in terms of principal stresses and strains and the other two use volumetric and shear components of stress and strain to describe the resilient stiffness of the materials. For the modelling of the permanent deformation of granular materials too, both ways of describing stresses and strains are used.

Chapter 8 deals with the in-situ determination of the stiffness of granular materials. Four types of tests were performed on the granular bases of a specially built test pavement incorporating sub-sections with different granular materials in the base course. The main purpose of this investigation was the development of a quick means of determining in-situ the stiffness of the granular base and expressing it in a fundamentally sound parameter. The "Dynamic Plate Bearing Test" presented here appears most applicable for this purpose.

A case study into the structural contribution of granular bases to flexible pavements is presented in Chapter 9. On a specially built instrumented test pavement asphalt tensile strains caused by simulated traffic loading were measured for five different pavement structures. The results of this investigation indicate the structural importance of the granular bases applied.

Chapter 10, finally, summarizes the research described in this dissertation and draws the overall conclusion of the study performed. Also, recommendations for further research and for implementation of the results presented here are given. A list of references and three appendices then conclude this dissertation. The appendices give a listing of the materials investigated, a separate Material Information Sheet describing each material tested in terms of grading and the results of standard tests and an overview of triaxial specimen data, respectively.

ONGEBONDEN STEENFUNDERINGEN VOOR WEGEN

SAMENVATTING

Deze studie handelt over het mechanisch gedrag van ongebonden granulaire materialen voor toepassing in wegconstructies. Een uitgebreid laboratorium en in-situ onderzoek wordt beschreven, waarin de diverse methoden ter bepaling van de mechanische eigenschappen van granulaire materialen zijn geevalueerd. Verder wordt het mechanisch gedrag van granulaire materialen onder invloed van veranderingen in het vochtgehalte behandeld en wordt een studie gepresenteerd naar de modellering van het spanningsafhankelijke mechanisch gedrag van granulaire materialen. Tenslotte wordt een case study naar de constructieve bijdrage van ongebonden steenfunderingen aan flexibele verhardingsconstructies beschreven.

Het uitgevoerde laboratorium-onderzoek omvatte een grote reeks materialen, welke zijn onderzocht in triaxiaalproeven met cyclische belasting. Deze proeven leveren als uitkomst fundamentele parameters, welke het elastisch vervormingsgedrag en de ontwikkeling van permanente vervorming onder een groot aantal lastherhalingen beschrijven. Naast de gecompliceerde triaxiaalproeven is ter referentie ook een groot aantal relatief eenvoudige standaardproeven uitgevoerd. Naast ongebonden funderingsmaterialen is ook een zestal in Nederland veel gebruikte zanden onderzocht, terwijl ook een aantal laterieten is opgenomen in het experimentele programma. Deze laatste materialen vormen het belangrijkste wegenbouw materiaal in de tropen.

Hoodstuk 2 geeft een uitgebreid overzicht van de literatuur over de onderwerpen van deze dissertatie. Elk van de paragrafen van dit hoofdstuk geeft een samenvatting van de literatuur over de onderwerpen welke vervolgens in de opeenvolgende hoofdstukken van deze dissertatie worden behandeld.

In hoofdstuk 3 worden vervolgens de specificaties voor ongebonden steenfunderingsmaterialen behandeld. Naast de in Nederland gehanteerde specificaties wordt een korte beschrijving gegeven van Amerikaanse en Engelse specificaties. Ook worden specificaties behandeld welke in tropische gebieden worden gehanteerd. Tenslotte wordt ingegaan op de Zuid-Afrikaanse specificaties voor "Waterbound Macadam", zijnde een steenfunderingsmateriaal met een heel typische gradering en daardoor een zeer hoge stijfheid.

In hoofdstuk 4 wordt een beschrijving gegeven van de materialen welke in het in deze dissertatie gerapporteerde onderzoek zijn beproefd. Vier hoofdgroepen van materialen worden onderscheiden, te weten klassieke steenfunderingsmaterialen, alternatieve steenfunderingsmaterialen, zanden en laterieten. Dit hoofdstuk beschrijft ook de codering welke in deze dissertatie wordt gebruikt ter aanduiding van de verschillende materialen.

Hoodstuk 5 beschrijft de laboratorium-beproeving van de grote reeks materialen. Begonnen wordt met de beschrijving van de uitgevoerde standaardproeven als Proctor en CBR. Vervolgens wordt de voor dit onderzoek gebouwde triaxiaalapparatuur beschreven, tezamen met de procedures van de eigenlijke beproeving van de materialen. Het hoofdstuk wordt afgesloten met de beschrijving van een onderzoek naar de

mogelijkheid om fundamentele vervormingsparameters van ongebonden materialen af te leiden uit de resultaten van relatief eenvoudige proeven.

Hoodstuk 6 beschrijft het mechanisch gedrag van ongebonden materialen onder invloed van veranderingen in het vochtgehalte. Na een theoretische beschrijving van de achtergronden van het ontstaan van negatieve waterspanningen in onverzadigde korrelige materialen wordt aan de hand van resultaten van triaxiaalproeven bij verschillende vochtgehalten onderzocht wat de invloed van die negatieve waterspanning op het mechanisch gedrag is.

In hoofdstuk 7 wordt de modellering van het mechanisch gedrag van ongebonden materialen behandeld. Voor de beschrijving van het elastisch gedrag van ongebonden materialen wordt een viertal modellen gepresenteerd, te weten twee modellen welke het gedrag van het materiaal beschrijven in termen van hoofdspanningen en hoofdrekken en twee modellen in termen van volume- en schuifrekken. Ook bij de modellering van de permanente vervorming van korrelige materialen onder invloed van een groot aantal lastherhalingen wordt van beide benaderingswijzen gebruik gemaakt.

Hoofdstuk 8 behandeld de beproeving van granulaire materialen in-situ. Op een speciaal aangelegd proefvak met een aantal verschillende steenfunderingen is een viertal proeven uitgevoerd met als doel het ontwikkelen van een snelle en fundamenteel juiste proef voor het bepalen van de in-situ stijfheid van granuaire materialen. De hier gepresenteerde "dynamische plaatbelastingsproef" komt hierbij als meest veelbelovend naar voren.

In hoofdstuk 9 wordt een case study naar de structurele bijdrage van ongebonden steenfunderingen aan flexibele verhardingen beschreven. Op een speciaal aangelegd geïnstrumenteerd proefvak zijn de onder gesimuleerde verkeersbelasting optredende asfaltrekken gemeten voor een vijftal verschillende constructies. De resultaten van dit onderzoek duiden op een grote structurele bijdrage van de toegepaste steenfunderingen.

In hoofdstuk 10 wordt tenslotte een samenvatting van deze dissertatie gepresenteerd, gevolgd door de algemene conclusies van het uitgevoerde onderzoek en de daaruit voortvloeiende aanbevelingen. Deze dissertatie wordt afgesloten met een overzicht van de geraadpleegde literatuur en een drietal bijlagen, welke achtereenvolgens een overzicht van de onderzochte materialen geven, per materiaal een aparte beschrijving in termen van gradering en de resultaten van standaardproeven en tenslotte een overzicht van dichtheid en vochtgehalte van de onderzochte triaxiaalproefstukken.

TABLE OF CONTENTS

1 INTRODUCTION AND SCOPE OF THIS STUDY

1.1 INTRODUCTION

One of a nation's most important economic assets is its road infrastructure. It provides an opportunity of transportation for both people and goods and, most importantly, it provides door-to-door transportation. This causes the major part of all transportation to take place entirely by road and other ways of transportation to be preceded and followed by road transport. As an example, within the Netherlands over 90% of all people-transportation, expressed in man×kilometer, takes place by road. For goods, 70% of all goods×kilometers are produced by road based transportation [1].

The replacement-value of the whole road network in the Netherlands is estimated to be around one hundred milliard guilders. On a yearly basis, some 2.2 milliard guilders is invested into the road network system. Of this total, some 1.3 milliard guilders is yearly spent on construction of new state roads and reconstruction of existing ones. The economic role of the road infrastructure and the amount of money invested in its construction and maintenance indicate the importance of good pavement design and management procedures. Poorly designed road pavements will cause premature failure, which will lead to high reconstruction costs and to great economical loss due to traffic stagnation. Overdesigned pavements on the other hand will involve a waste of limited funds.

A good pavement design procedure should use the beneficial strength and stiffness characteristics of all materials employed to their fullest extent. For the granular materials applied in pavement constructions, the knowledge concerning these material characteristics is still relatively limited. The test methods used to determine the engineering characteristics of granular materials are still mostly based on empiricism. The parameters obtained from these tests cannot be used as input to today's mechanistic pavement design procedures. Therefore, these procedures do not use the granular materials to their full structural capacity and attribute only a limited structural role to the granular layers.

This dissertation aims at providing more insight into testing and analysis of granular materials for use in pavement structures. As an introduction, the technical background of the study performed will be described in the next paragraph of this chapter. Paragraph 1.3 will then deal with the scope and limitation of this study, followed by a description of the organization of this dissertation in Paragraph 1.4.

1.2 TECHNICAL BACKGROUND

Many of the pavement design procedures presently employed are still empirically based. They were developed from years of experience with existing roads, supplemented with the analysis of test sections or even major research projects like the AASHO Road test (2), which was carried out by the American Association of State Highway Officials in the late nineteen-fifties. Material specifications too are mainly based on experience and practical considerations. Test methods for characterization of the mechanical properties of the pavement materials and the subgrade are often still empirically based and only yield a rough estimate of the fundamental material parameter required for pavement design.

This empirical approach to material characterization and pavement design has been used for many years and initial shortcomings of the methods used have been eliminated by updating them with newly gathered experience. Within the limits of this experience with respect to, for instance, axle loads and materials applied, these empirical testing and design methods form a sound basis for pavement design. Thanks to their empirical nature, they are often very well implemented and, most importantly, simple in nature. The testing techniques require only standard laboratory equipment and the pavement design techniques simply use charts from which the proper design for a given set of circumstances can be read.

The major drawback of empirical methods is that they indeed only operate within the limits of the experience on which they are based. Extrapolation from that experience to, for instance, higher axle loads or new materials can lead to major problems. Because of this drawback,

increasing effort is presently being spent throughout the world in the development of so-called analytical or mechanistic design procedures. These methods are based on the analytical capability to calculate stress, strain or deflection in a pavement subjected to an external load, or the effects of temperature and moisture. These analytical calculations of the so-called pavement response are subsequently extrapolated to long-term pavement performance, which is a function of physical distress such as cracking and rutting.

The rapid increase in power of digital computers has greatly enhanced the development of the analytical procedures required for calculation of stresses and strains in pavements. Although the calculation procedures themselves are almost standard nowadays, the determination of the required input parameters to describe the mechanical behaviour of the granular materials in the pavement structure still poses problems. Most of the available analytical procedures rely on standard testing procedures like the Califirnia Bearing Ratio test to obtain, through empirical correlations, values for fundamental material parameters like Young's modulus. The translation of the calculated pavement response to actual pavement performance is presently being studied worldwide. Accelerated loading of test pavements plays a major role in this research, next to long-term monitoring of the structural condition of roads under normal traffic.

Since the development and implementation of mechanistic design procedures will still require a considerable number of years to come, major road authorities still rely on empirical design procedures. Both the design procedure published in 1984 by the British Department of Transport [3] and the procedure published in 1986 by the American Association of State Highway and Transportation Officials [4] are, in essence, empirical design methods. In the Netherlands, the use of the analytically based Shell Pavement Design Manual [5] is now quite standard. It contains a design procedure based on calculation of stresses and strains in a linear elastic multi-layered pavement structure using the computer program BISAR [6]. Some of the input parameters to the BISAR calculations are derived from standard tests, using correlation formulae to convert standard test results into the fundamental input parameters required for BISAR. As an example, the elastic stiffness of the subgrade is estimated from its CBR-value. No fundamentally sound

test methods for determination of strength and stiffness characteristics of subgrade and unbound granular base materials are given in the manual. The specifications and test methods [7] presently employed in the Netherlands for these materials are for the greater part empirically based.

In the Netherlands, the lack of fundamentally sound specifications and testing techniques became a problem when initiatives were taken to use recycled materials like crushed concrete in unbound granular road bases. These materials did not fit into any empirical knowledge with regard to either specifications and testing methods or to design. This has been one of the major incentives for the study described in this dissertation. It deals with the structural contribution of unbound granular bases to road pavements from a fundamental point of view. A comprehensive laboratory and in-situ testing program forms the basis of the knowledge presented. This knowledge was gathered and developed in a close co-operation with universities, research agencies and practising engineers in the Netherlands and abroad.

1.3 SCOPE AND LIMITATION OF THIS STUDY

This study focuses on laboratory and in-situ testing techniques for unbound granular road base materials and provides an experimental assessment of their structural contribution to pavement structures. Since most of the major roads in the Netherlands have flexible pavements, the actual testing and analysis of the structural contribution of unbound granular layers were performed on asphalt pavements. Thanks to their fundamental nature, however, the testing techniques and the material parameters presented can also be used for design and analysis of other types of pavements.

To analyse material behaviour, a wide range of materials was investigated. The main focus lies with temperate zone unbound granular materials, including conventional materials like lava and limestone and recycled materials like crushed concrete and crushed masonry. To expand the scope of the materials tested, laterites were also included in the test program. These natural occurring materials form the main

road building material in the tropics. The same principles apply to the testing and analysis of these materials, but the variation in their mechanical properties and the susceptibility to changes in moisture content is far larger than for the temperate zone materials with man-made gradings.

For two reasons, the behaviour of sands was also studied. Firstly, major roads in the Netherlands all contain sand layers of substantial thickness, which causes sands to be structurally important. Secondly, thanks to the relatively small particle size of sands the mechanical parameters of these materials can be determined using relatively small test specimens. Because of this, testing of sands is far less cumbersome than testing of coarse graded base course materials, which require very large test specimens for their mechanical analysis. Therefore, most of the pilot-testing in this study was performed on sands.

This study does not contain a detailed analysis of the clayey subgrade materials, which are found in parts of the Netherlands. The reason for this is that, in case of occurrence of such subgrades, the clayey material is replaced by sand to a substantial depth in construction of main roads. This causes the clayey subgrade materials to be of less structural importance with respect to the required thickness of the various layers of the pavement. It should be noted that clayey materials in the subgrade do play an important role in the settlement of the road. Study of this phenomenon clearly lies beyond the scope of this study.

The main emphasis in this study lies with the laboratory testing of the wide range of materials mentioned. Fundamentally sound testing techniques are described that yield the parameters required as input to today's mechanistic pavement design procedures. Simplified testing techniques are developed that allow for determination of fundamental material parameters with relatively simple equipment. An analysis of the susceptibility of the stiffness of granular materials to changes in moisture content is presented. The modelling of the stress dependent behaviour of granular materials with respect to both elastic and permanent deformation is discussed in detail.

In addition to the main laboratory analysis, also in-situ investigations on a specially constructed test pavement were performed. These investigations focused on development of a fundamentally sound proof testing technique for granular road bases and on an experimental assessment of the structural significance of granular bases in flexible pavements.

The link between the fundamental stress-strain characteristics determined through laboratory testing and the actual in-situ behaviour of the materials in pavements is formed by an analytical tool capable of accurately dealing with the stress-dependent behaviour of granular road base materials. Development of such an analytical tool lies beyond the scope of this dissertation. Hence, no analytical coupling will be presented between the laboratory and in-situ behaviour of the materials investigated. No attempts will be made to use linear elastic pavement models presently available for such a coupling, since these models by definition cannot accurately deal with the stress dependency of granular materials. In a parallel research project, a finite element approach to pavement modelling is being developed at the time of writing of this dissertation, using the experimental data gathered here as input to design calculations and for validation purposes.

1.4 ORGANIZATION OF THIS DISSERTATION

This dissertation was written with two main purposes in mind. The first purpose is of a scientific nature, namely documenting the results of the study performed. As stated earlier, this study involves a vast experimental program, the results of which have already been published by the author and his co-workers in a number of conference papers and laboratory reports. The scientific purpose of this dissertation involves grouping together the data obtained, putting them in a broader context derived from international literature and drawing the overall conclusions of the study. The second purpose of this dissertation is of a practical nature, namely serving as a reference work for practising engineers and students. The very nature of pavement engineering calls for a direct translation of scientific work into practically applicable knowledge.

The scientific purpose of this work causes it to contain a detailed theoretical background of the technical field dealt with and sufficient experimental data to allow other researchers to check the theory presented and to work with the data gathered in their own research. Complex models for the description of the stress-dependent material behaviour will be presented, realizing that these models are not yet implemented and practically usable at this time. The practical purpose of this work causes it to contain a detailed review of existing practice with respect to specifications, testing techniques and design procedures. Simple models for the description of stress-dependent material behaviour will be presented, next to the fundamentally sound more complex models. Attention will be given to the development of simplified testing techniques that still allow for determination of fundamentally sound mechanical parameters. In addition to the fundamental material characteristics presented, the materials investigated will be characterized using the results of standard tests in order to provide reference values with every-day engineering practice.

The division into chapters of this dissertation is as follows. After this introduction, Chapter 2 presents a review of the literature on the topics of this study. The main purpose of this literature review is to provide a detailed background of the technical field dealt with in this study and to acquaint the reader with the terminology used in this dissertation. Chapter 3 then deals with the material specifications which are presently being used, both for the temperate zone areas like Europe and North America and for tropical areas. The materials investigated in this study are described in Chapter 4, giving a compositional analysis of the materials and the results of standard tests like for instance Proctor and CBR. Chapter 5 then deals with the range of laboratory testing techniques that are used to characterize the mechanical behaviour of unbound base course materials. Standard and non-standard testing techniques are discussed, and correlations between the results of these tests are investigated.

The mechanical behaviour of unbound granular materials can be greatly affected by water, if a substantial amount of fine material is present. The theoretical background of this influence is described in Chapter 6, and the effect of water content on mechanical behaviour is illustrated using laboratory testing results. In Chapter 7, the

modelling of material stiffness for pavement design is dealt with. Simple and complex models for describing both elastic and permanent deformation as a function of stress are presented. Chapters 8 and 9 subsequently deal with the testing performed on a specially constructed pavement. Chapter 8 focuses on development of a quick means of fundamentally sound proof testing of granular road bases, while Chapter 9 describes an experimental assessment of the structural contribution of granular materials to flexible pavements. Chapter 10, finally, summarizes the overall conclusions of this study and presents recommendations that focus on implementation of the knowledge presented in this dissertation.

2 LITERATURE REVIEW

2.1 INTRODUCTION

To set a detailed technical background for this dissertation, this chapter contains a review of the literature on the subjects dealt with. The main purpose is presenting the reader with the "state of the art" on unbound granular materials research. Furthermore, the terminology used in this research field to describe, for instance, materials and testing techniques will be presented here. The shortcomings of the present empirical approach to material testing and pavement design will be discussed and an indication of the direction in which improvements are to be sought will be given.

In Paragraph 2.2, the terminology used in the Netherlands to denote the various layers of a flexible pavement construction will be given and compared to the terminology used in the United Kingdom and the USA. Furthermore, the terminology pertaining to the stress-strain characteristics of granular materials will be discussed. Subsequently, each paragraph of this literature review serves as an introduction to a chapter of this dissertation. Too much detail will be avoided here; the full details of the various topics will be dealt with in the relevant chapters.

2.2 TERMINOLOGY

2.2.1 Terminology for pavement structures

The terminology used in the Netherlands to denote the various layers of a pavement structure is somewhat different from the terminology used in the UK and the USA. Since the main focus of this study lies with Dutch circumstances, the Dutch terminology will be adhered to in this dissertation. To clarify this terminology, Figure 2.1 shows a

cross section of a typical pavement construction for a primary road in the Netherlands.

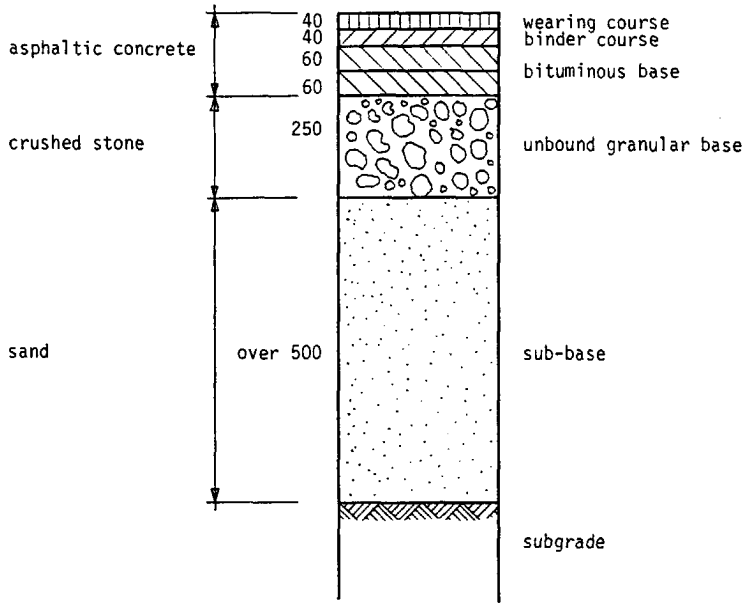

Figure 2.1: Typical pavement construction for a primary road in the Netherlands (layer thickness in mm).

Going from top to bottom in Figure 2.1, the following layers can be distinguished:

- The wearing course consisting of dense asphaltic concrete. This layer provides the skid resistance required by traffic and it serves as an impermeable layer protecting the lower pavement layers from the ingress of water. A recent development is the application of a pervious macadam wearing course providing horizontal drainage through the wearing course and reducing traffic noise.
- The binder course, consisting of coarse graded asphaltic concrete. The main function of this layer is levelling of the lower layers. In case of a pervious macadam wearing course a dense bituminous binder course is applied.
- The bituminous base, consisting of one or more layers of gravel asphaltic concrete. These are the main structural layers of the pavement construction.
- The unbound granular base, consisting of crushed stone, slag or recycled materials. This layer has a structural role and serves as a working platform for the construction of the upper layers.

- The sub-base, consisting of sand. In case of weak subgrades, this layer replaces the upper part of the subgrade, thereby providing a smooth transition in stiffness from the stiff upper layers to the weak subgrade.
- The subgrade.

The construction shown in Figure 2.1 contains both a bituminous and an unbound granular base. Other options are full-depth asphalt concrete constructions, where the unbound granular base is replaced by say 6 cm of gravel asphaltic concrete or layers of sand asphalt. Also, a sand-cement base layer may be applied. For secundary and tertiary roads, either the unbound granular base layer or one or more of the bituminous bound layers are omitted.

Typical about Dutch pavement constructions for major roads is the application of layers of sand of substantial thickness in the sub-base. In other countries, the sub-base often consists of low quality granular materials such as gravel-clay mixtures.

The main difference in terminology lies with the base layers. In the Netherlands, either a fully bound (bituminous or cement) base is applied, or a combination of a bound (bituminous) ànd an unbound granular base. The recently published UK-design method [3] and USA-design method [4] both prescribe either a bound òr an unbound granular base. The combination of a bituminous base ànd a granular base is not denoted as such in the UK and USA design guides; granular layers below a bituminous base are refered to as "sub-bases".

2.2.2 Terminology for stress-strain characteristics

Figure 2.2A shows a typical stress-strain curve as obtained from a conventional monotonic loading triaxial test. On increasing the stress, the strain gradually increases until the yield stress of the specimen is reached. After that, the strain increases further even if the stress is decreased. Such stress-strain behaviour is described as "plastic behaviour" and hence the strain in monotonic loading failure tests is termed "plastic strain".

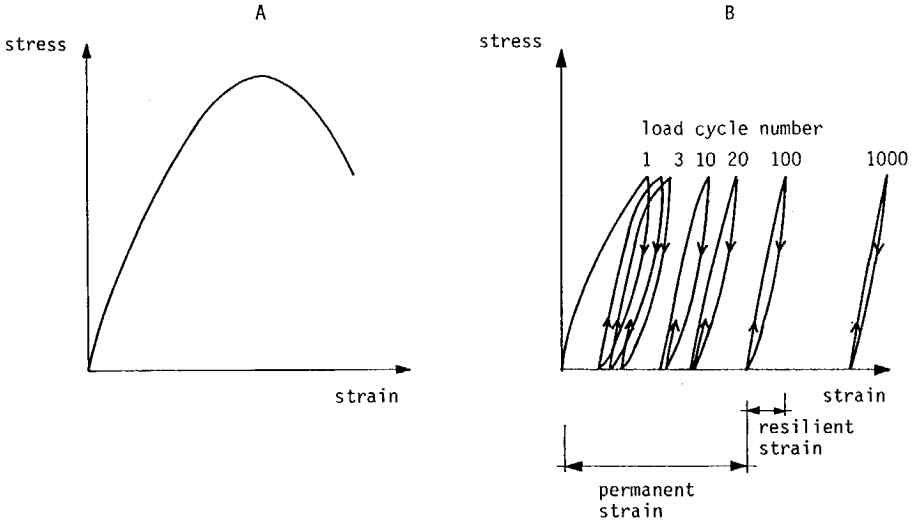

Figure 2.2: Stress-strain behaviour of a granular material.
A: Monotonic loading to failure.
B: Cyclic loading.

Figure 2.2B shows the stress-strain behaviour of a material as studied for pavement design purposes. Here, the behaviour of the material under a large number of stress applications is of interest. Triaxial tests for studying that behaviour are refered to in the literature as "repeated load" or "cyclic load" triaxial tests. Since in classical soil mechanics the term "repeated load" is used to denote triaxial tests with only a few stress repetitions, the term "cyclic load" triaxial tests will be used in this dissertation to denote tests with up to one million load applications.

The initial part of the stress-strain curve depicted in Figure 2.2B is similar to that from the monotonic load test. Before reaching the yield stress, however, the stress on the triaxial specimen is released and part of the strain is recovered. At increasing numbers of load repetitions, the strain of the material becomes almost entirely recoverable and is hence refered to in pavement engineering as "resilient" strain. The accumulated non-recoverable strain from each of the stress applications is in pavement engineering refered to as "permanent " strain. This terminology will be adhered to in this dissertation. The term "plastic" strain will be used to denote strain caused by yielding of the material (such as in the CBR-test), whereas

the term "permanent" strain will be used to denote accumulated strain under large numbers of load applications.

2.3 SPECIFICATIONS FOR UNBOUND GRANULAR MATERIALS

Generally speaking, two main groups of specifications can be distinguished, namely specifications for temperate zone areas and those for tropical areas. These two groups have in common that they are both empirically based and use standard testing techniques for characterizing the materials. The main difference between the two groups lies with the fact that the temperate zone specifications are often somewhat more stringent. This is partly due to the fact that in temperate zone areas pavement constructions often have to meet higher demands with respect to, for example, traffic loading and vehicle speed. Furthermore, freezing and thawing put quite stringent demands on the grading of unbound granular materials applied in the temperate zone areas, where these climatic circumstances occur. Finally, pavement engineers in tropical areas often have to work with locally available materials like laterites, since crushed stone materials cannot be afforded or are not available.

Many tropical countries, however, do not have specifications of their own and use specifications developed in temperate zone areas together with the pavement design procedures developed there. In South America, for instance, AASHTO specifications (8) are often used, together with the AASHTO Interim Guide for the Design of Pavement Structures (9). If temperate zone developed specifications are applied stringently in tropical areas, this may lead to discarding of materials which are in fact quite suited for application in tropical areas. Therefore, there clearly exists a need for specifications specially developed for tropical areas, such as those presented in the British Road Note 31 (10).

The material specifications developed for tropical areas and those for temperate zone areas have in common that they are based on simple to perform standard tests. Most specifications prescribe material composition and grading. In addition, plasticity (as determined in

Atterberg limits tests), California Bearing Ratio CBR, resistance to degradation (determined in Los Angeles Abrasion tests or crushing tests) and particle shape (flakyness) are sometimes prescribed. Table 2.1 gives a general view of the specifications used in the Netherlands, the UK, the USA and of the specifications for tropical areas from Road Note 31. Chapter 3 of this dissertation gives more details on the subject.

Table 2.1: General view of material specifications used in the Netherlands, the UK, the USA and some tropical areas.

country		the Netherlands	UK	USA	former UK colonies
specifications		Eisen 1978	DOT	AASHTO	RN31
reference		[7]	[19]	[8]	[10]
property	composition		X	X	X
	grading	X	X	X	X
	plasticity		X		X
	CBR		X		X
	degradation	X	X	X	
	flakyness	X	X		

2.4 MATERIALS

2.4.1 Introduction

In this study, the following main groups of unbound granular materials used in base and sub-base courses are dealt with:

- conventional base course materials
- recycled base course materials
- sands
- laterites.

The conventional base course materials used in temperate zone areas are mainly crushed stone materials like limestone and lava. In the Netherlands, blast furnace slag is also considered to be a conventional base course material, although it is in fact a recycled material since it involves the use of a waste product.

To replace the crushed stone materials, recycled materials are presently being used in a number of countries. The most important of these materials are granulats produced from demolition and construction waste, such as crushed concrete. Waste incineration slag is another recycled material.

In the Netherlands, sands are the material most widely used in sub-bases. In the UK and the USA, low quality coarse graded materials are often used in the sub-base layers, while locally occurring low cost materials like river gravels are used in layers below the sub-base as capping over very soft subgrades.

Laterites are naturally occurring clay-gravel mixtures with a high iron content, which causes their characteristic red colour. They are used in the tropics in surface layers, base courses and sub-base courses, depending on their quality.

This paragraph gives a review of the existing literature on these materials, limiting itself to the description of the materials. Literature dealing with structural characteristics like, for instance, material stiffness will be dealt with in later paragraphs of this chapter. Again, only major lines will be drawn here; full details will again be given in the relevant chapters.

2.4.2 Conventional materials

Of the total of six million tons of unbound granular road base material applied annually in the Netherlands, only a small portion

consists of crushed rock, namely crushed lava from Germany. About half of the total quantity of granular materials applied consists of blast furnace slag, both from the Dutch steelworks at IJmuiden and from the German steel works in the Ruhr-area. The remaining part of the total quantity of granular road base materials is presently recycled material produced from construction and demolition waste.

Lava is an eruption material, which is chemically similar to basalt. One of the main quarrying areas for this material in Western Europe is the German Eifel-area. The lava is quarried there in large quantities and processed by crusher plants to obtain the desired grading. It should be noted that the quality of the lava may differ considerably from one quarry to another and even within one quarry. Much experience has been gained over the years in the Netherlands with application of lava in unbound base courses. The main problem lies with the material variability noted above. Furthermore, lava does not have a self-cementing potential like, for instance, blast furnace slag and consequently maintains a relatively low stiffness throughout the life-cycle of the pavement.

Blast furnace slag is a residu obtained in the production of pig iron and other blast furnace processes. The main constituents of the material are CaO (28-50%), SiO_2 (28-40%) and Al_2O_3 (5-20%) [11]. Dependent on the CaO-content, the slag is either used for production of cement or as a granular material in road bases. Dependent on the way in which the hot residu from the blast furnace process is cooled down, different types of slag are obtained. Slow cooling produces a high density coarse slag, which is processed in a crusher plant to obtain the desired grading. Fast cooling with water produces granulated slag-sand, while a special process involving the use of high pressure steam produces an expanded and thus low-density slag (the so-called "pelletised slag"). Much experience has been gained over a number of years with the use of these materials in granular base courses. The high density slag has earned itself a good reputation, mainly because of its self-cementing potential. Within a period of one year, if placed in moist surroundings, a layer of this unbound granular material can change into a semi-rigid plate showing numerous small cracks, no shrinkage and no temperature-sensitivity [11]. The granulated slag-sand is most widely used for cement production and the expanded slag is used when low density is required. This material also

shows a self-cementing potential, but may be very susceptible to crushing because of its porous nature.

Outside the Netherlands, crushed rock is often used in unbound granular bases, thanks to local availability. In the UK, for instance, various types of crushed limestone are applied. Much research work on the engineering characteristics of these materials has been done at the University of Nottingham [12, 13]. Since this work involves development of models for description of material behaviour, it will be discussed in detail in relevant chapters of this dissertation.

2.4.3 Recycled materials

In the Netherlands, increasing attention has been paid for a number of years to recycling of waste products to obtain road construction materials of sufficient quality. Regarding unbound granular bases, recycling of construction and demolition waste into granulats is by now becoming quite standard. In demolishing buildings, care is taken to separate stony materials from wood, plastics and the like. The stony materials are then processed in crusher plants to obtain granulats with the required particle size distribution. Crushed masonry, crushed concrete and mixtures of these materials are commercially available, with and without cementing additives.

Co-ordinated by the Dutch Centre for Research and Contract Standardization in Civil and Traffic Engineering (Centre ROW), much research has been done since 1983 into the applicability of granulats produced from rubble in unbound granular bases. Preliminary specifications for these materials have been published [14] and extensive laboratory testing has been done [15]. Test sections containing these materials have been built and tested extensively [16, 17, 18]. In most of the chapters of this dissertation, attention will be given to these recycled materials and their mechanical behaviour will be compared to that of conventional materials.

Outside the Netherlands, granulats produced from construction and demolition waste are also used in unbound granular bases and subbases. The UK-Specifications for Highway Works [19] allow crushed

concrete for application as sub-base material. The spasmodic production in small quantities of such materials, however, has been reported to prevent large scale application (20).

2.4.4 Sub-base materials

In the western part of the Netherlands the subgrade consists of clayey materials. In the construction of major roads in this area, the subgrade is replaced to a depth of at least 50 cm by a sub-base of sand. The sand is either dredged from river estuaries or produced on land in sand pits.

On land production can be done either by excavation, followed by truck or ship transportation, or by dredging followed by hydraulic transportation. The choice between the two ways of production depends on the quantity of material to be produced, on the location the pit and on the transportation distance. Furthermore, the grading of the sand is of influence, since hydraulic transportation of coarse graded sands is quite expensive. The Dutch specifications (7) for sands for sub-bases prescribe material "from a mineral origin", with a maximum percentage of fines and a maximum loss-on-ignition value.

Outside the Netherlands, both sands and granular materials are used in sub-bases. In the UK, two types of sub-base materials are distinguished (19). "Type 1" sub-base material should consist of crushed rock, crushed slag, crushed concrete or well burned non-plastic shale. The lower quality "Type 2" material may also consist of natural sands. The situation in the USA is similar: crushed stone, gravel, slag and sands are used in sub-base courses.

2.4.5 Laterites

2.4.5.1 INTRODUCTION

Laterites are by far the most widely used road building material in the tropics. They are the product of the intense chemical weathering occurring in humid tropical areas. Due to intensive leaching, certain constituents such as quartz are removed from the parent material,

leaving a residue containing high concentrations of non-leachable materials. In laterites, iron is the predominant non-leachable material left behind in the weathering residue. In a complex process of redistribution and crystallization of iron, the characteristic soil structure of laterites is developed. Typically, this structure consists of red coloured kaolinitic clay on the one hand and hardened concretions and vains of iron on the other hand. Material of sand size is often almost completely absent. After excavation from the borrow pit, laterites therefore often have a gap-graded particle size distribution. They consist of a mixture of clay-sized material and gravel and larger sized material, with the intermediate fractions lacking.

The term "laterite" was first introduced by Buchanan in 1807 [21], to describe soils that could be readily cut from the soil profile, but hardened on exposure to air. This material was locally used as brick for building and was hence called "laterite", "later" being the Latin word for brick. Since then, much research effort has been put into the study of the genesis and hardening of laterites. This topic will be dealt with in Paragraph 2.4.5.2; for more details reference is made to a paper by the author [22] and to the standard work on laterites by Gidigasu [23]. The studies dealing with laterite genesis and hardening often go into considerable detail, using sophisticated physical and chemical techniques for determination of parameters such as material composition. The studies of engineering characteristics of laterites typically use far less sophisticated methods of analysis and mainly involve index tests for material characterization and Proctor and CBR testing. These studies will be reviewed in Paragraph 2.4.5.3.

2.4.5.2 GENESIS OF LATERITES

In general, soils are formed from parent rock in two stages: physical breakdown of the parent rock and subsequent chemical alteration of the rock debris thus formed. Characteristic of the physical weathering is that the chemical and mineralogical composition of the material is not altered; physical weathering only involves pulverization of the parent rock. In chemical weathering, reactions between the materials of the parent rock and weathering agents take place, resulting in the formation of new chemical compounds. Of the weathering agents, water is by far the most important. Usually, the water is partly dissociated into

H^+ and OH^- ions, both of which can play an active role in weathering. Water also acts as a solvent for CO_2, O_2 and organic acids. In the tropics, much water is available to act as a weathering agent due to the heavy rainfall and much CO_2 and organic acids are present due to the decay of the remains of the abundant flora. Adding the year round high temperature enhancing chemical reactions, it follows that all conditions for a very intense chemical weathering are met in the tropics. It is this very intense chemical weathering that causes the normal soil forming process to go one step further into the genesis of laterites.

Chemical weathering involves leaching of certain constituents of the parent material, or replacement of certain elements by others. Elements that are resistant to leaching remain in the material and their relative concentration is increased since other elements are leached out. Table 2.2 illustrates the phenomena of leaching, replacement and relative enrichment.

Table 2.2: Changes in chemical composition due to weathering (after [24])

	A			B			C		
	a	b	c	a	b	c	a	b	c
SiO_2	60,7	45,3	-15,4	71,5	55,1	-16,4	51,3	16,1	-35,2
Al_2O_3	16,9	26,6	+ 9,7	14,6	26,1	+11,5	15,2	29,1	+13,9
$FeO+Fe_2O_3$	9,1	12,2	+ 3,1	2,3	6,3	+ 4,0	14,3	31,9	+17,6
CaO	4,4	0,0	- 4,4	2,1	0,2	- 1,9	9,6	0,02	- 9,6
MgO	1,1	0,4	- 0,7	0,8	0,3	- 0,5	5,6	0,06	- 5,5
K_2O	4,3	1,1	- 3,2	3,9	0,14	- 3,8	0,6	0,06	- 0,5
Na_2O	2,8	0,2	- 2,6	3,8	0,05	- 3,7	2,1	0,05	- 2,0
H_2O	0,6	13,8	+13,2	0,3	10,4	+10,1	0,3	20,2	+19,9

a. parent material

b. product of weathering

c. difference between a and b

A. Kaolinitic weathering of an intermediate gneiss, Virginia

B. Kaolinitic weathering of an acid granite-gneiss, Minnesota

C. Lateritic weathering of dolerite, Guyana

Comparing in Table 2.2 the intense laterite weathering (columns C) to the more moderate kaolinitic weathering (columns A and B), a more intense leaching of SiO_2, CaO and MgO is characteristic of the lateritic weathering. The relative content of iron (FeO + Fe_2O_3) of the material is increased due to this intense leaching: in columns C a far larger increase in iron can be observed as compared to columns A and B.

After formation of a soil-like material with a high iron content due to intense chemical weathering, the next step in laterite genesis involves a complex process of redistribution and dehydration of the iron in the material. Much of the iron released during the weathering process will be present in the ferrous (Fe^{++}) form, which is soluble in water. This allows the Fe^{++} to migrate under the influence of concentration differences to places in the soil where much oxygen is present. There, the ferrous iron Fe^{++} will be oxidized to the ferric Fe^{+++} form and thus precipitate into hydraded forms of ferric oxide. Due to the precipitation, the local Fe^{++} concentration is decreased and more Fe^{++} is therefore attracted to these oxygen rich places. More and more hydraded forms of ferric oxide will thus be formed, which on further dehydration may ultimately form crystalline hematite.

The precipitation and dehydration of iron is concentrated at places with a high oxygen content such as cracks and pores. The soil-like lateritic material therefore gradually passes into a heterogeneously structured material, consisting of veins of hardened material enclosing clayey material. Upon removal of such material from the borrow-pit, the veins will be broken up into irregularly shaped concretions. The material obtained then is a so-called "gap-graded" mixture of iron concretions and clayey material. Due to the intense leaching of silicon, sandy material is not often found in laterites. Sand-sized material, however, may be present in the form of fine graded iron concretions. In this case, a more continuously graded material results.

2.4.5.3 ENGINEERING CHARACTERISTICS

The optimum soil structure for gap-graded laterites is that of a skeleton of coarse iron concretions, with clayey material filling the voids of the skeleton. The bearing capacity of the skeleton of coarse

particles is greatly enhanced by soil suction (negative pore water pressure) generated by the fine material in the voids of the skeleton. Speaking in standard pavement engineering terms, CBR-values over 200 can occur [25]. However, the laterites found in borrowpits alongside the road under construction often do not have the favourable ratio of coarse to fine particles that gives this optimum soil structure after compaction. The pavement engineer then has to work with laterites containing too much clay, in which case the soil structure after compaction can be that of a matrix of clay with coarse particles "floating" in it. In this case, the bearing capacity of the material is determined by the clay matrix, which virtually loses all its strength on wetting. For more continuously graded laterites the ratio of coarse to fine particles again is the controlling factor for the engineering behaviour of the material. Too much fine material again results in a matrix of fines, in which the coarse particles are floating. The strength and stiffness of such a material are then fully dependent on soil suction.

Engineering studies of laterites mainly involve standard tests. For material characterization purposes, particle size distribution and Atterberg limits are most widely used. Proctor-, CBR- and standard degradation tests like the Los Angeles Abrasion test are used to determine the engineering characteristics of the laterites. The reason for using only standard testing techniques often is the fact that tests are carried out on the spot in field laboratories or local engineering laboratories, where sophisticated testing equipment is lacking. The applicability of the standard testing techniques developed in temperate zones for use with tropical soils is very questionable indeed. Strict adherence to such testing techniques like those described by AASHTO [26] may lead to serious errors when testing tropical soils.

For a detailed review of a vast number of engineering studies of laterites using standard testing techniques reference is made to the work of Gidigasu [23]. The most comprehensive research program dealing with laterites from a road building point of view was initiated by the United States Agency for International Development. The program involved projects in Thailand [27], Ghana [28] and Brazil [29]. In addition to detailed geological studies dealing with laterite genesis and hardening, very comprehensive engineering studies dealing with the

behaviour of laterites in road constructions were carried out. Although still using mostly standard tests, the researchers also already used more sophisticated techniques like cyclic load triaxial tests to determine the engineering characteristics of laterites. Deflection measurements using a Benkelman Beam on in-service pavements form the basis of the pavement design procedure presented in the Brazil-report [29]. Further developments to this method were made by Medina and others in Brazil [30, 31, 32], using cyclic load triaxial tests and Benkelman Beam deflection measurements.

2.5 LABORATORY TESTING TECHNIQUES

2.5.1 Introduction

A large number of standard tests is presently being used to investigate properties of compaction, bearing capacity and degradation of unbound granular materials. Most of these tests are of an empirical nature, developed to provide input-data for empirical pavement design procedures or to provide a means of qualitative comparison of different materials.

The mechanistic pavement design procedures presently being used require fundamental material properties as input. To provide these fundamental data, new testing techniques have been developed. Due to their complexity, however, these new techniques are used to date mainly for research purposes. To circumvent the necessity of complex testing techniques, many attempts have been made over the years to estimate fundamental material properties from the results of standard tests.

The laboratory testing techniques presently being used will be reviewed in this paragraph. For ease of survey, distinction will be made between standard and non-standard testing techniques.

2.5.2 Standard laboratory testing techniques

2.5.2.1 COMPACTION

The Proctor test

The test most widely used to determine moisture-density relations of soils and unbound granular materials in the laboratory is the Proctor test (AASHTO T99-74 and T180-74) [26]. This test was developed by R.R. Proctor some fifty years ago. Originally, the test involved compaction of soils in a 4 inch (101.6 mm) mould, using a drop hammer to apply the compaction effort. Since then, various versions of this test have been developed and standardized, using basically two levels of compaction energy ("standard" and "modified") and two mould-sizes (4 and 6 inches, 101.6 and 152.4 mm).

The Proctor test is now being used for soils, sands and unbound base course materials. With the latter, severe degradation of the material tested can occur, especially in case of porous materials. The density achieved in the Proctor-test is then by no means suited as a reference value for field compaction.

The Vibrating Hammer test

The degradation problems of the Proctor-test are partly overcome in the Vibrating Hammer-test (BS 5835) [33]. This test uses a full-faced compaction plate in a 4 inch (101.6 mm) mould and a Kango-hammer to supply the compaction energy.

2.5.2.2 BEARING CAPACITY

The California Bearing Ratio

The California Bearing Ratio CBR is by far the most well-known parameter for characterizing the bearing capacity of soils and unbound granular materials. The CBR-test was developed in the USA by the California State Highway Department in the late nineteen-thirties. The test was developed initially for the evaluation in the laboratory and

in-situ of subgrade strength. Presently, the laboratory CBR-test is used throughout the world as a quick means of characterizing qualitatively the bearing capacity of soils, sands and unbound base course materials. The CBR-value still is an input value to pavement design procedures, such as the recently published AASHTO [4] and TRRL [3] design methods. Even analytical pavement design procedures such as the Shell-method [5] rely on the CBR-test to obtain through empirical correlations the fundamental stress/strain parameters required as input to the calculation of stresses and strains in pavements.

In the CBR-test (AASHTO T193-72) [26], a plunger with a circular cross-section of 3 square inches (1935 mm^2) is driven at a specified rate into a specimen of the material to be tested, compacted in a 6 inch (152.4 mm) steel mould. The forces required to cause a penetration of 0.1 and 0.2 inch (2.54 and 5.08 mm) are then expressed as percentages of the standard forces of 3000 and 4500 lb (13.5 and 20.3 kN), respectively. These standard forces are said to have been obtained from tests on a crushed stone which was defined as having a CBR of 100%. In fact, the values were probably chosen as standard values, since one can hardly imagine a material giving nicely 3000 and 4500 lb force at the specified penetrations. To simulate the in-situ condition of moisture content in the laboratory, the CBR-test can be carried out "unsoaked" (at the compaction moisture content) or "soaked" (the specimen after compaction having been immersed in water for four days before the actual CBR-testing). To simulate the in-situ overburden stress, steel rings are applied on top of the CBR-specimen; the number of rings can be adapted to the overburden stress required.

Thanks to its simplicity, the CBR-tests has become the most widely used standard test for characterizing the bearing capacity of unbound road building materials. As far as soils and sands are concerned, the test seems to be a reasonable means for assessing material strength, although the value obtained is only a relative measure of strength. Since for fine grained materials the deformation of the specimen is predominantly shear deformation, the tests provides an indirect measure of shear strength. It should be well noted here that in testing of cohesive soils close to saturation the laboratory version of the CBR-test will give lower values than the in-situ version of the test due to the development of positive pore pressures during the laboratory test [34].

In testing of coarse graded unbound base coarse materials problems arise regarding the ratio of mould and plunger dimensions to particle size of the material to be tested. If, for instance, the CBR-test is performed on a 0/40 mm graded material, the diameter of the CBR-plunger and the largest particles would be almost equal. The rigid CBR-mould of 152.4 mm internal diameter gives an unknown and uncontrollable confining stress to the material specimen. To circumvent these problems, test specifications often prescribe removal of coarse particles from the test material. AASHTO T 193-72 [26], for instance, prescribes removal of material retained on the 19 mm sieve. It should be noted that in case of coarse graded materials, this removal leads to testing of a material having a grading which differs substantially from the original material, which is bound to have a large influence on the parameter to be measured. Such testing is therefore of little use.

Because of its longtime worldwide use, the CBR-test is also being used to obtain material stiffness parameters for input to analytical design procedures. Since these procedures require fundamental material properties like Young's E-modulus for input, empirical correlations between E and CBR have been developed. These correlations will be dealt with in detail in Paragraph 2.7.2 of this literature review. It is noted here, however, that the deformation occurring in the CBR-specimen is a combination of elastic and plastic deformation. Since these two types of deformation cannot be distinguished in the test and since the ratio of elastic to plastic deformation may differ from one material to another, the CBR-test is unsuited for determination of a purely elastic parameter like an E-modulus.

The Stabilometer test

The Asphalt Institute [35] has suggested the use of the Hveem Stabilometer for determination of strength parameters of soils. The Stabilometer-test was originally developed by Hveem for testing of asphaltic concrete and is as such incorporated in the AASHTO specifications (AASHTO T246-74) [26]. The "Resistance R-value" obtained in the Stabilometer test can be used as input to the recently published AASHTO pavement design procedure [4].

In the Stabilometer test, a 4 inch (101.6 mm) diameter specimen with a height of 2.5 inch (63.5 mm) is placed in the Stabilometer. The specimen is supported at its bottom by the steel pedestal of the apparatus and at its sides by a rubber membrane. The specimen is loaded axially by a full-faced loading plunger. The resulting radial deformation of the specimen is transferred through the rubber membrane to an oil/air mixture in the Stabilometer apparatus. The resulting increase in pressure of the oil/air mixture is then a measure for soil strength.

Through its design, the Stabilometer is in fact a triaxial type of testing equipment. Since it allows for control of the lateral confining stress, it should allow for determination of more appropriate material properties like the Mohr-Coulomb strength parameters C and ϕ and Yougs's E-modulus. The apparatus, however, requires very careful calibration [36] and is only suited for testing of soils and sands because of the relatively small specimen.

2.5.2.3 RESISTANCE TO DEGRADATION

For determination of the resistance to degradation of unbound granular materials, a number of empirically based tests is available. The tests most widely used in pavement engineering are the Los Angeles Abrasion Test and the Aggregate Impact Value test. The standard test used in the Netherlands for determination of the resistance to degradation is the so-called "Verbrijzelingsproef", while in the UK the so-called "10% fines value"-test is used for this purpose.

The Los Angeles Abrasion Test

In the Los Angeles Abrasion Test (AASHTO T96-77) [26] the material to be tested is sieved into various fractions and then recombined to a specified grading. A sample with a total weight of 5000 g is then placed in the Los Angeles machine, which is basically a steel drum with an internal diameter of 711 mm that can be rotated by an electric motor. To the sample material in the drum, a total of 12 steel balls having a combined weight of approximately 5000 g is added. The drum is

then rotated for 500 revolutions, after which the particle size distribution of the sample material is determined. From the shift in grading between the original sample and the sample after testing the Los Angeles Abrasion value can then be calculated.

The Aggregate Impact Value test

The Aggregate Impact Value test (BS 812) [37] gives a relative measure of the resistance of an aggregate to impact loading. The test is carried out on material passing a 14 mm sieve and retained on a 10 mm sieve and is, therefore, in fact only suited for testing aggregates containing large percentages of particles larger than 14 mm if the material has the same composition throughout all fractions, such as in case of crushed rock. Then, the resistance to degradation of the fraction 10-14 mm is a measure of that resistance of the whole material. However, for heterogeneous materials like crushed rubble the test is unsuited, since the material in the fraction 10-14 mm may very well be different from the rest of the material.

The sieved material is compacted by tamping in three layers in a cylindrical steel mould having an internal diameter of 102 mm and an internal depth of 50 mm. Subsequently, a 100 mm diameter steel hammer with a mass of 13.5-14 kg is dropped 15 times on the compacted specimen from a specified height. The test material is then removed from the mould and sieved on a 2.36 mm sieve. The ratio of the mass of material passing this sieve to the original mass of the material in the mould expressed as a percentage is then measure for the resistance of the material tested to impact loading.

The 10% Fines Value Test

The 10% Fines Value Test (BS 812) [37] gives a relative measure of the resistance of an aggregate to crushing under a gradually applied compressive load. The test is quite similar to the Aggregate Impact Value Test, the main difference being application of a gradually increasing load as opposed to impact loading. The test is suited for both strong and weak materials, whereas the Aggregate Impact Value Test is suited only for strong materials (Aggregate Impact Value > 30).

As the Aggregate Impact Value Test, the 10% Fines Value Test is performed on material passing a 14 mm sieve and retained on a 10 mm sieve. The material is compacted by tamping in three layers in a cylindrical mould having an internal diameter of 154 mm and an internal depth of 125-140 mm. Subsequently, a 152 mm diameter piston is placed on the compacted material in the mould and subjected to a gradually increasing load. The test material is then removed from the mould, sieved on a 2.31 mm sieve, and the "percentage of fines" is calculated as the ratio of the mass passing the 2.36 mm sieve to the original mass of the sample. The maximum load exerted in the test should be of such magnitude, that a percentage of fines is reached between 7.5 and 12.5. The test should be repeated once at that maximum load, and from the mean percentage of fines from the two tests the "10% Fines Value" can then be calculated as the load required to cause a percentage of fines of 10. The 10% Fines Value is therefore expressed in kN.

The Verbrijzelingsproef

In the Dutch "Verbrijzelingsproef" (test no. 17, Eisen 1978) [7], the material to be tested is sieved, using 45, 31.5, 22.4, 16 and 11.2 mm sieves. From the largest fraction by weight obtained between two successive sieves, a representative sample is then taken. A specified weight of sample material is then placed in a steel mould with an internal diameter of 159.6 mm. A full faced steel plunger is placed on top of the sample material in the mould and then loaded with 200 kN for a total of 120 seconds. From the shift in grading caused by the loading the Verbrijzelingsfactor VF can then be calculated.

2.5.3 Non-standard laboratory testing techniques

2.5.3.1 THE CYCLIC LOAD TRIAXIAL TEST

As early as 1955, H.B. Seed and his co-workers recognized the need for a more fundamental approach to soils testing for pavement engineering purposes [38]. Starting from the already well known static triaxial test [39], they concluded that the monotonic slow stress increase used in this test does not necessarily give a satisfactory indication of

the performance of soil under conditions of repeated loading. Therefore, a triaxial test set-up with a standard lever-type of loading frame was equiped with an actuator to apply and remove the weights from the hanger of the frame. A clever control system allowed for application of a constant deviator stress for a period of one second, followed by a load-off period of two seconds, without having impact loading effects. The tests were carried out with a constant confining stress.

Seed et al. [40] recognized that their load-on/load-off form of stress application was a simplification and that their testing technique at best simulated a slow moving wheel. Allen and Thompson [41] and Barksdale [42] later showed that for accurate simulation of field conditions more complicated stress versus time functions are needed, such as sinusoidal and triangular pulse shapes. From their calculations they showed that the pulse durations occurring in pavements under traffic at normal speeds (70 km/h) vary from 0.02 s at the surface of the pavement to 0.1 s at a depth of 70 cm.

Application of sinusoidal or triangular pulse shapes at these short pulse times requires sophisticated closed-loop servo-hydraulic equipment, which is only available at a limited number of research laboratories. Therefore, most cyclic load triaxial testing nowadays still is being done with pulse times of around 1 s. As far as testing of granular materials under drained conditions is concerned, this longer pulse time has no significant effect on resilient strain parameters. Evidence for this will be given in this dissertation, both from literature and from own investigations. It should be noted here that the rate of loading does have a significant effect on resilient strain properties when testing low permeability materials at high degrees of saturation. Positive pore pressures may then develop in the triaxial specimen, with a resulting lower effective stress and a drop in material stiffness.

In their cyclic load triaxial apparatus, Seed et al. [38] used a conventional triaxial cell with a specimen diameter of 1.4 inch (35.6 mm). Later, cyclic load triaxial equipment was developed having larger specimen diameters to allow for testing of coarser materials than the clay tested by Seed et al. The Transportation Research Board's Special

Report 162 on "Test procedures for characterizing dynamic stress-strain properties of pavement materials" [43] suggests a minimum specimen diameter of 2.5 inch (63.5 mm), or 4 to 5 times the maximum size of particle in the material to be tested. The larger of the two diameters thus obtained should be used. AASHTO's "Standard method of test for resilient modulus of subgrade soils" (AASHTO T 274-82) [26] prescribes a minimum specimen diameter of 2.8 inch (71 mm), or six times the largest particle size. The TRB and the AASHTO publication agree on a minimum specimen height of two times the specimen diameter.

The ratio of specimen diameter to maximum particle size still is a topic of discussion in testing of unbound granular base course materials. Since most cyclic load triaxial equipment presently available has specimen diameters of 150 mm or less, this equipment only allows for testing of material with a maximum particle size of, say, 30 mm. Therefore, triaxial tests on base course materials having nominal gradings of, for instance, 0/50 mm are usually carried out on so-called scaled-down gradings, which means that particles larger than, for instance, 25 mm are replaced by finer particles. The effect of such scaling-down of the grading on resilient characteristics of unbound granular materials has recently been studied at Nottingham University. Donbovand [44] scaled down a continuously graded granite by reducing the maximum particle size while keeping the shape of the grading curve intact. Five gradings ranging from 0-40 mm to 0-12 mm were tested in a 150 mm specimen diameter cyclic load triaxial apparatus. A significant decrease in elastic stiffness was found on reduction of the maximum particle size. Similar results were obtained in testing of a limestone. Thom [13] too found found the maximum particle size of granular materials to have a significant effect on elastic stiffness; again a decrease in particle size meant a decrease in elastic stiffness. The Nottingham results thus clearly indicate that granular materials should be tested at their full grading to obtain the stiffness parameters needed for pavement design.

Since the early work of H.B. Seed, the cyclic load triaxial test has become the test most widely used for determination of resilient and permanent strain properties of unbound granular road building materials. Due to its complexity, however, the test is still almost exclusively used for research purposes. A major step towards implementation of the cyclic load triaxial test has been the standardization

of the test by the American Association of State Highway and Transportation Officials. AASHTO T 274-92 (26) gives a detailed description of equipment, specimen preparation procedures and testing procedures. The specification allows for a sine, haversine, rectangular or triangular shaped stress pulse, which in turn allows for relatively simple loading equipment.

Another step towards implementation of more fundamental testing techniques in pavement engineering is the development of static load triaxial testing techniques giving results similar to those obtained by cyclic load techniques. The work done by other researchers on this will be reviewed in Paragraph 2.5.3.3. of this chapter. The test procedures developed will be validated and extended in Paragraph 5.5.2, using the extensive data obtained in this research.

2.5.3.2 TYPES OF CYCLIC LOAD TRIAXIAL TESTS

Elastic strain/permanent strain

The cyclic load triaxial test is basically used for determination of two types of parameters, being resilient strain parameters and permanent strain parameters.

Because of the stress-dependent behaviour of unbound granular materials, resilient strain parameters like the resilient modulus M_r have to be determined at a number of stress levels for each material tested. Brown and Hyde (45) have shown that resilient characteristics of unbound granular materials are not affected by loading history. They showed that a large number of tests for determination of resilient parameters can be carried out on the same specimen, provided that the stresses applied are kept low enough to prevent substantial permanent volume-change of the triaxial specimen.

Permanent strains in unbound granular materials are, on the contrary, affected significantly by loading history (45). Therefore, several triaxial specimens have to be tested to obtain the relationship between stress ratio applied and permanent deformation. Each test usually involves a large number (10^5 or 10^6) of load applications on each specimen, which renders the determination of permanent strain

characteristics to be quite time-consuming. This is probably the reason why far less data is available on permanent deformation of unbound granular materials than there is on resilient deformation.

Constant confining pressure/Variable confining pressure

As stated earlier, the cyclic load triaxial test was first developed from the monotonic load triaxial test by incorporating loading systems that could simply apply and remove the deviator stress, while the confining stress was kept constant. Allen and Thompson [41] reported on going one step further by applying not only a cyclic deviator stress, but also a cyclic confining stress. These Variable Confining Pressure (VCP) tests are a closer simulation of actual field conditions than the Constant Confining Pressure (CCP) tests, since in the road structure the confining stress acting on the material is cyclic in nature.

With their 6 inch specimen VCP-equipment, Allen and Thompson investigated the influence of cycling the confining stress on the resilient modulus M_r and Poisson's ratio ν of various granular materials. By comparing VCP- and CCP-test results, they showed that CCP-tests yield somewhat higher values for M_r and much higher values for ν than do VCP-tests.

Brown and Hyde [45] later showed that VCP- and CCP-tests yield the same M_r-values, provided the confining stress σ_3 in the CCP-test is equal to the mean value of σ_3 in the VCP-test. Since Allen and Thompson used the peak value of σ_3 from their VCP-tests in their CCP-tests, the higher values for M_r found in the CCP-tests were concluded to be attributable to the higher stress level in the test material.

Where VCP- and CCP-tests yield the same M_r-values, Brown and Hyde [45] also showed that the values obtained for Poisson's ratio ν in the CCP-test differ considerably from those obtained in VCP-tests. The stress-dependency of ν found in the two types of tests was completely opposite. VCP-tests yielded decreasing ν-values for increasing ratios of deviator stress over confining stress, whereas in CCP-tests ν was found to increase with increasing stress ratio. Values of ν over 0.,5 were found in the CCP-tests, thereby indicating resilient specimen dilation (volume-increase).

Using a more fundamental approach to stress-strain relationships, Brown and Hyde showed that the problem of deviating values for ν found in VCP and CCP-tests can be circumvented. Separating stresses and strains into volumetric and shear components, they showed that VCP- and CCP-tests do yield the same stress-strain relationships for those stress-ratios that do not cause specimen dilation.

With respect to permanent strain, Brown and Hyde obtained a reasonable correlation between VCP and CCP-tests, again setting σ_3 in the CCP-tests at the mean value of σ_3 in the VCP-tests. The overall conclusion is that CCP-tests are adequate for determining stress-strain relationship of granular materials, both for resilient and permanent strain provided the proper models are used to relate strains to stresses.

2.5.3.3 CORRELATIONS BETWEEN STATIC LOAD AND CYCLIC LOAD TEST RESULTS

Elastic deformation

Kalcheff and Hicks [46] investigated the effects of load duration and load frequency on the resilient modulus M_r. They tested four different crushed stone materials (maximum particle size 1 inch (25.4 mm)) in triaxial equipment with a specimen size of 6 inch (152.4 mm) diameter by 10 inch (254.0 mm) height. To check the influence of load duration, repeated static load triaxial tests (30 min load on, 30 min load off) and cyclic load tests (load duration 0.1 s) were performed. Comparison of the resilient modulus calculated from the resilient deformation from the two types of test showed no quantifiable effect of load duration on the resilient modulus.

To check the influence of load frequency, cyclic load triaxial tests were carried out at various frequencies between 10 and 80 load applications per minute. Again, no quantifiable effect on the resilient modulus was found, indicating that any reasonable frequency can be used to characterize the resilient behaviour of granular materials.

Having shown that resilient moduli can accurately be determined in repeated static load triaxial tests with a 30 min loading time, Kalcheff and Hicks suggested their "triaxial creep" procedure for routine determination of the resilient properties of granular

materials. On the one hand this procedure would eliminate the requirement of complicated cyclic load triaxial equipment for determination of resilient properties, but on the other hand the suggested procedure would involve two hours testing time for each stress level to be investigated (30 min load on, 30 min load off, repeated once). Kalcheff and Hicks suggested to use six different stress levels to determine the resilient modulus-stress relationship, which can be considered quite a minimal number. Even at this minimal number, however, testing of one material would take at least two days, thereby rendering the suggested procedure unsuited for routine application. In Paragraph 5-.5.2 of this dissertation, a far more user friendly repeated static load procedure involving shorter loading periods will be suggested.

Permanent deformation

Determination of permanent strain characteristics of granular materials in cyclic load triaxial tests is quite time-consuming. For each condition of stress, moisture content and density tests have to be run to large numbers of load applications. Because permanent strain is affected by load history, each new set of conditions requires a new specimen to be tested. To circumvent this problem of extensive cyclic load testing, several attempts have been made over the years to estimate permanent strain characteristics from static load triaxial tests.

Lentz and Baladi (47, 48) investigated the permanent strain behaviour of a sand. By performing cyclic load triaxial tests and classical static load triaxial tests they obtained relationships between the outcome of the two types of testing. The cyclic load test results were normalized with respect to parameters obtained in static load tests. The normalized cyclic deviator was shown to have a unique relationship to normalized permanent strain. This relationship was shown to be independent of moisture content, density and confining pressure. Test data from a second sand investigated met the same relationship.

The results of Lentz and Baladi would indicate that, once the relationship between normalized cyclic deviator stress and normalized permanent strain has been obtained for a group of materials (for instance sands), performance of one static load triaxial test at a given

set of circumstances would yield the required permanent strain data usually obtained in time-consuming cyclic load tests. However, Lentz and Baladi obtained their data on only two types of sands, tested to limited numbers of load applications only. The extensive data obtained in the research for this dissertation will be used in Paragraph 5.6.2 to show that the theory developed does not hold for larger groups of materials and for larger numbers of load applications.

Veverka [49] and Descornet [50] of the Belgian Road Research Centre tried another approach to circumvent the necessity of time-consuming cyclic load tests for determination of permanent strain characteristics of granular materials. Rather than estimating these characteristics from static load triaxial tests, they proposed a relationship between permanent and resilient deformation. Should such a relationship exist, permanent deformation of granular materials could simply be predicted from resilient deformation, which can be determined quite rapidly in the laboratory using cyclic load (or even repeated static load) triaxial tests, or in-situ using falling weight deflectometer measurements. The proposed relationship will be discussed in detail in Paragraph 5.6.2 and its validity will be checked using the test data obtained for sands and unbound granular base course materials.

2.6 MATERIAL BEHAVIOUR RELATED TO WATER CONTENT

2.6.1 Introduction

In the Netherlands, unbound granular base courses of major roads are constructed on a sub-base layer of sand of substantial thickness. Since the capillary rise of water in sand is limited, the unbound granular base of a properly designed and constructed road with an impervious upper pavement layer will therefore remain unsaturated. However, in the case of cracked asphalt pavements or concrete block pavements, wetting of the base layer may occur by water travelling downward through the pavement. Part of the sand sub-base layer may very well be saturated, depending on the level of the layer with respect to the level of the water table.

Contradictory as it may seem, the problems with water ingress into sub-base and base layer may be larger in countries like the UK as compared to those in the western, below-sea level part of the Netherlands. This is mainly due to design and construction practice: the thick sand layers which are standard in the Netherlands are seldomly applied abroad. In the UK, for instance, unbound granular sub-bases are placed directly on clayey subgrades, if the CBR of the subgrade is higher than 5%. For subgrades having a lower CBR-value, a "capping layer" is placed between subgrade and sub-base. The capping layer is constructed of low quality local material which may contain some plastic fines. This construction practice can lead to water travelling upward through the high capillary rise subgrade into capping layer and sub-base. In tropical areas, the problems arising from wetting of granular road building materials are even more severe, since an impervious upper pavement layer is often omitted altogether in these areas. The combination of heavy rainfall and the use of locally available materials like laterites in the upper layer of the pavement may lead to very severe problems indeed.

The wetting of unbound granular base and sub-base layers can cause a substantial reduction in material strength and stiffness, depending on the composition of the material. This paragraph deals with the general principles of the interaction between unbound materials and water. Since most of the available literature deals with soil-water interaction rather than granular material-water interaction, the literature review will start with soils. Subsequently, the limited literature on granular materials under influence of water will be dealt with. Chapter 6 of this dissertation will describe the phenomena governing the interaction in more detail and will give the results of triaxial testing carried out to investigate the influence of water on material stiffness.

2.6.2 General principles of unbound material-water interaction

In studying the interaction between unbound materials and water, first the distinction has to be made between two different conditions, being the saturated case and the unsaturated case.

In the case of saturated materials, all the voids in the unbound material are filled with water. Since both the material itself and water are virtually incompressible, application of compressive stress to a saturated soil in poorly drained conditions will lead to a substantial build-up of pore water pressure, which in turn will lead to a reduction in material strength and stiffness. These phenomena have been studied in great detail in classical soil mechanics and are relatively well understood today. For the sake of completeness they will be dealt with briefly in this chapter.

Because of its complexity, the unsaturated condition of soils and unbound granular materials is far less understood. In unsaturated soils, water is held against gravitational forces draining the water out or against evaporation of water at the soil-air interface. This water retention is caused by capillary forces arising from curved air-water interfaces in the voids of the unsaturated soil, or caused by surface forces bonding water molecules. The capillary forces depend on the size of the voids and the surface forces upon the amount and nature of the surfaces of soil grains (51).

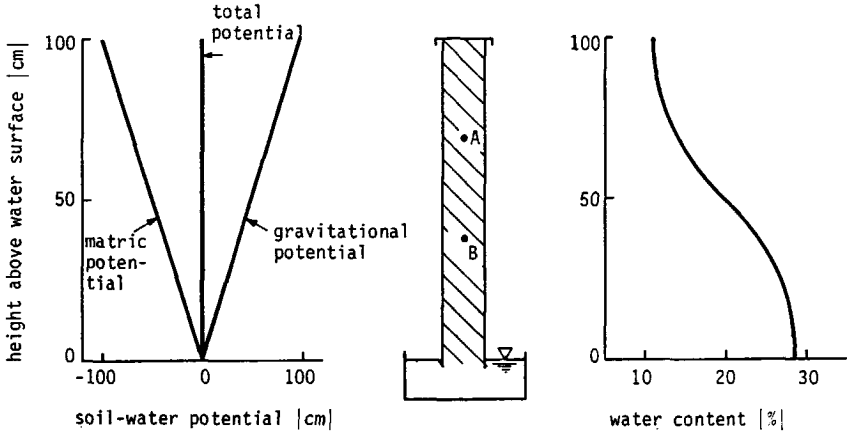

Figure 2.3: Illustration of soil-water potential concept (after (51)).

The energy with which water is held in a soil can be specified as the soil-water potential. Figure 2.3 shows an illustration of the concept of soil-water potential. A column of soil is standing in a pan of water, with the top of the column covered to prevent evaporation. After equilibrium is established, the total potential of the soil water is, by definition, constant over the height of the soil column. With the reference value of zero soil-water potential set at the level of the free water table, the gravitational potential draining the water from the soil column will increase from 0 to +100 cm over the height of the soil column, whereas the "matric" potential retaining the water in the soil will decrease from 0 to -100 cm. This matric potential is the combined effect of the capillary and surface forces retaining the water in the soil. The total potential, being the sum of gravitational and matric potential, is constant over the height of the column and thus water will not move. When a sample of soil is taken from point B in the column to point A, its water content will be reduced, resulting in a decrease (a larger negative value) of the matric potential, which will compensate for the increase in gravitational potential caused by raising the sample from point B to point A.

In Figure 2.3, the total soil-water potential is shown as the sum of gravitational and matric potential. Other component materials may also contribute to the total potential. The presence of salts in the soil, for instance, also decreases the soil-water potential (increases the water retention). Details on this "osmotic potential" will be given in Chapter 6 of this dissertation. For practical engineering purposes, the matric potential is by far the most important cause of water retention in soils. As stated, it is the combined effect of capillary forces and surface forces bounding water molecules. In sands, the surface forces are small, because of the low amount of surface and the nature of the surface. Therefore, capillary forces dominate in sands. Consequently, the matric potential is zero in saturated sand and in completely dry sand. In both cases, no curved air-water interfaces exist and, therefore, no capillary forces are present. The maximum matric potential is reached somewhere in the unsaturated region of partly filled pores.

Clay particles have a far larger surface area per unit weight than sand particles. Furthermore, the surface of clay particles has an electric charge. For these two reasons, the surface forces cannot be

neglected in clays and may dominate over the capillary forces. Therefore, the matric potential in "completely dry" clay is not zero, but will reach a maximum value. In dry clay capillary forces will be negligible, due to the absence of water. Surface forces, however, will be at their maximum and cause very large matric potentials. In fully saturated clays, the soil-water potential will only be zero when the soil has been allowed to swell freely without overburden. Clays, or soils containing a significant amount of clay, may very well be fully saturated (saturated defined as "all voids filled with water") and still show a substantial negative soil-water potential. Given enough time and supply of water, the soil will swell (increase its pore-volume) until finally the matric potential equals the gravitational potential and the total soil-water potential is zero.

Many different terms are used to describe the energy with which water is held in soils. Here, the term soil-water potential has been used so far, which is the terminology used in theoretical treatments of soil water. In more descriptive engineering usage, the terms soil-water tension and soil suction are widely used. Soil-water tension indicates that the soil water has a negative (that is: below atmospheric) pressure, whereas soil suction indicates the force with which the soil takes in water. In the remainder of this dissertation, the term soil suction will be used, following the terminology used most widely in pavement engineering. The use of the term soil suction also involves a convenient change in algebraic sign: matric potential is a negative number, whereas soil suction is a positive number.

The numerical value of soil suction varies from almost 0 kPa in nearly saturated materials up to several thousands of kPa in dessicated clays. To cope with this extended numerical range, soil suction is usually expressed in pF-units, where pF is the logarithm of the soil suction expressed in cm H_2O. Thus, pF = 3 stands for a suction of 10^3 cm H_2O (100 kPa) and pF = 7 represents 10^7 cm H_2O (10^4 kPa).

2.6.3 Material strength related to water content

As stated, the problem of positive pore water pressures occurring in fully saturated soils has long since been dealt with adequately by

classical soil mechanics. Terzaghi's famous effective stress principle states:

$$\sigma' = \sigma - u \qquad (2.1)$$

where

σ' = effective stress
σ = total stress
u = pore water pressure

It is the effective stress that dominates aspects of soil behaviour as compression and strength. Since both the total stress and the pore water pressure can be measured or calculated, depending on the situation in the laboratory of the field, the effective stress can easily be calculated using Equation 2.1. It is for this reason that most triaxial testing of clays is still being done under fully saturated conditions, thereby allowing Equation 2.1 to be used. Sands can be tested either in the fully saturated condition or completely dry. In the latter case, the whole problem of pore water pressures (positive or negative) simply does not occur.

When the effective stress is known, the shear strength of the soil can be calculated using the Mohr-Coulomb equation:

$$\tau = c' + \sigma' \tan \phi' \qquad (2.2)$$

where

τ = shear strength
c' = cohesion
σ' = effective stress
ϕ' = angle of shearing resistance

Terzaghi's effective stress law (Equation 2.1) was developed for fully saturated conditions and is therefore only valid in case of positive pore water pressures ($u > 0$). In case of partial saturation, negative pore water pressures ($u < 0$) occur and Terzaghi's law cannot be used. The following example illustrates that from a practical point of view: substituting a negative pore water pressure of $u = -10^3$ kPa (which is quite feasible in dry clay) in Terzaghi's law would yield an effective

stress and therefore a soil strength with a magnitude far beyond reality.

Bishop and Blight [52] suggested an adapted form of the effective stress law for partially saturated soils:

$$\sigma' = \sigma - u_a + \chi (u_a - u_w) \tag{2.3}$$

where

σ' = effective stress
σ = total stress
u_a = pore air pressure
u_w = pore water pressure
χ = parameter dependent on degree of saturation

χ varies between 0 and 1 with the degree of saturation, but the relationship between the two parameters is different for each soil.

Fredlund [53, 54] suggested another approach to modelling the shear strength of unsaturated soils. Rather than adapting the effective stress equation, he suggested that the suction in an unsaturated soil increases the cohesion in the soil:

$$C = c' + (u_a - u_w) \tan \phi^b \tag{2.4}$$

where

C = total (or "apparent") cohesion
c' = cohesion
$u_a - u_w$ = soil suction

ϕ^b = friction angle with respect to suction

The shear strength of the partially saturated soil can then be calculated using:

$$\begin{aligned} \tau &= C + (\sigma - u_a) \tan \phi' \\ &= c' + (\sigma - u_a) \tan \phi' + (u_a - u_w) \tan \phi^b \end{aligned} \tag{2.5}$$

This approach of increasing the cohesion for unsaturated soils was proven valid for a wide range of soils by Ho and Fredlund [55]. The

whole problem of modelling unsaturated soil strength, however, still is a large one, since accurate determination of the pore air pressure is very difficult indeed.

2.6.4 Material stiffness related to water content

In addition to its effect on soil strength, soil suction also has a significant effect on the stiffness of soils. Since this stiffness plays an important role in pavement design and analysis, the influence of soil suction should be well taken into account.

The standard approach for determination of stiffness parameters of unsaturated soil is testing of specimens prepared at the worst possible field moisture content and analyzing the test results in terms of total stresses. Thompson and Robnett [56], for instance, tested unsaturated subgrade soils for resilient characteristics. Triaxial specimens were prepared at and above the optimum moisture content and the resilient modulus M_r was calculated as the ratio of the applied deviator stress to the recoverable axial strain of the triaxial specimen. The degree of saturation of the soils was shown to have a considerable effect on the resilient modulus, but no attempt was made to relate the resilient modulus to soil suction.

In resiliency testing of soils at high degrees of saturation, care should be taken when dealing with low permeability soils. Volume change can readily turn the negative pore water pressure in the triaxial specimen into a positive pore water pressure, since the low permeability prevents sufficient drainage. This may lead to a drastic reduction of the resilient modulus or even to specimen failure. In granular materials with a high permeability these problems of positive pore water pressures do not occur, provided the triaxial specimen is allowed to drain freely. Because of the relatively low value of soil suction in these materials, test results can be interpreted in terms of total stresses in case of testing for practical purposes.

For research purposes, test results should be interpreted in terms of effective stresses. When the tested material does not contain a significant amount of clay, this can be easily done by testing the

material in the completely dry condition. In a pure sand, for instance, soil suction will be caused by capillary effects only and will thus be equal to zero in a completely dry material. Effective stresses are then equal to total stresses and test results can be interpreted correctly without the need for measurement of soil suction.

For subgrade soils containing significant amounts of clay the simple approach of testing in the completely dry condition cannot be used. The clay causes a large soil suction, which reaches its maximum in the dry condition and can therefore not be ignored. The resilient modulus M_r of saturated clayey materials is usually expressed as a function of two stress variables (the confining stress σ_3 and the deviator stress σ_d). In case of unsaturated soils, a third stress variable (the soil suction) should be added. Fredlund et al. [57] suggested the following relationship:

$$M_r = f[(\sigma_3 - u_a), (\sigma_d), (u_a - u_w)] \qquad (2.6)$$

where

M_r = resilient modulus
σ_3 = confining stress
σ_d = deviator stress
u_a = pore air pressure
$u_a - u_w$ = soil suction

From experiments, Fredlund et al. [58] later showed the influence of the confining stress σ_3 to be negligible compared to the effect of the deviator stress σ_d and the soil suction $u_a - u_w$. Based on their experimental results, they suggested the following equation:

$$\log M_r = c_{1d} - m_{1d}\sigma_d \qquad (2.7)$$

where c_{1d} and m_{1d} are functions of soil suction.

It should be borne in mind that expressing the resilient modulus M_r as function of the three stress variables σ_3, σ_d and $(u_a - u_w)$ requires measurement of the pore air pressure u_a and the negative pore water pressure u_w during the cyclic load triaxial test. Fredlund et al. [58] reported serious technical problems with this measurement.

Furthermore, preparation of triaxial specimens at a preset suction level is quite cumbersome indeed. Motan and Edil [59] used a pressure plate apparatus to adjust the suction on pre-compacted specimens to the required level, which took 4 to 12 months per specimen depending on the permeability of the material tested.

Jouve et al. [60] reported a different approach to obtaining triaxial specimens at preset suction levels. They placed the triaxial specimen between two high air-entry porous discs, which were connected to a water vessel placed at a preset level below the triaxial specimen, thereby obtaining the required negative pore water pressure u_w. A geotextile was placed between the triaxial specimen and the membrane. By connecting the geotextile to the atmosphere, the pore air pressure u_a was kept at atmospheric pressure. This procedure too is quite time-consuming: Paute [61] reported a minimum time required for specimen equilibration of one month.

The preparation of triaxial specimens at specified suction levels requires sophisticated triaxial equipment and, more importantly, much time. In testing of soils, much time is required for equilibration because of the low permeability of the material, while equilibration of triaxial specimens of granular materials requires much time since water has to travel over larger distances because of the required larger specimen size. All in all, suction controlled triaxial testing is only suited for research purposes and even then the effectivity of test procedures taking up to one year to be completed is questionable. This is probably the main reason why only limited literature is available on this subject.

A more practical approach is preparation of triaxial specimens at field moisture content and measuring the suction in the specimen using tensiometers or similar devices. Another approach is to back-analyse the value of soil suction from, for instance, unconfined compressive strength tests [62]. The simplest and still most widely used method involves testing at field moisture content and simply interpreting test results in terms of total stresses. In Chapter 6, triaxial testing of granular materials and laterites at various suction levels will be described.

2.7 MODELLING OF MATERIAL STIFFNESS FOR PAVEMENT DESIGN

2.7.1 Introduction

In 1885, Boussinesq (63) published expressions for the calculation of stresses and displacements in an elastic half-space under point loading. The more complex, multi-layered structure of a pavement was later dealt with by Burmister, who presented an analytical solution for a three-layer pavement structure in 1943 (64). Odemark in 1949 (65) presented expressions that allow for transforming mathematically a multi-layered structure into an elastic half-space. The advent of the digital computer later created the possibility of calculating stresses and strains at any given point in a linear elastic multi-layered pavement structure, using computer programs like BISAR published in 1975 (6). Finite element computer programs allow for even more accurate calculation of stresses and strains in pavements, taking into account the non-linear behaviour of the unbound materials and soils in the pavement. A milestone publication on this method of analysis was written by Duncan et al. in 1968 (66).

For all these methods of calculating stresses and strain in pavements, the stress-strain properties of the materials in the pavement have to be described by some kind of constitutive equation. In the simplest case, being the linear elastic approach, values for Young's modulus E and Poison's ratio ν are needed. The value of E for the unbound materials is often estimated using empirically based relationships between E and the CBR-value. Poisson's ratio ν is often simply chosen at a constant value, mostly $\nu = 0.35$. Also, relationships are assumed between the E-modulus of the unbound granular base and that of the subgrade (5).

The wide-spread use of the cyclic load triaxial test nowadays allows for a direct measurement of the resilient stress-strain properties of unbound granular materials. It has been shown that these materials do not exhibit linear elastic behaviour. To deal with the non-linear behaviour, the "resilient modulus" M_r was introduced as the stress-dependent ratio of the applied axial stress over the recoverable axial strain in the cyclic load triaxial test. Today, the stress-dependent resilient modulus M_r is used widely in conjunction with a constant

value of Poisson's ratio ν to describe the resilient stress-strain behaviour of granular materials. For pavement research purposes, a better modelling of the stress-strain behaviour of granular materials can be obtained by separating both stresses and strains into volumetric and shear components. The various models describing the resilient stress-strain behaviour of unbound granular materials will be discussed briefly in this paragraph. In Chapter 7, they will be dealt with in more detail using experimental data.

2.7.2 E-CBR relationships

In 1960, Heukelom and Foster [67] published relationships between Young's E-modulus and the CBR value of soils and granular materials. In a theoretical analysis, they calculated the displacement under the CBR-piston using Boussinesq's equation for the surface deflection under a circular uniform load on an elastic half space. For this fully elastic case, the CBR-displacement of 0.1 inch (2.54 mm) matches the calculated deflection if the E-modulus of the elastic half-space is taken at E = 1 CBR (E in MPa). However, since the deformation in the CBR-test is mainly plastic deformation, the actual value of the E-modulus should be considerably higher. Heukelom and Foster recognized that the ratio between plastic and elastic strain in the CBR-test varies considerably for different materials and that therefore any relationship between E and CBR is bound to show considerable scatter.

Correlating experimental data for E and CBR for a wide range of materials, Heukelom and Foster obtained the relationship

$$E = 11\ CBR \tag{2.8}$$

where

E = Young's modulus [MPa]
CBR = California Bearing Ratio [%]

In their experiments, the factor of 11 varied between 5 and 20. It should be noted that the E-values used by Heukelom and Foster were obtained from wave-velocity measurements. For testing of subgrade materials, they used a heavy mechanical vibrator and for granular base course materials a very light electro-magnetic vibrator. The stresses

applied to the base course using the light vibrator are certainly far lower than the stresses caused by actual traffic. Since unbound base course materials show a marked stress dependency, it is questionable whether the obtained E-values represent the actual stiffness of the materials investigated under traffic loading. In spite of this fundamental objection, Equation 2.8, rounded off to E = 10 CBR, has become almost in axiom in pavement engineering. Even sophisticated pavement design procedures like the Shell Pavement Design Manual use E = 10 CBR to obtain E-values of soils and unbound materials.

The British Transport and Road Research Laboratory has developed another relationship between E and CBR (3). TRRL based its relationship on a comprehensive analysis of wave propagation data, supported by information from cyclic load triaxial testing carried out at realistic stress levels and in-situ measurements of transient stress and strain in experimental pavements. The TRRL equation is:

$$E = 17.6\ (CBR)^{0.64} \qquad (2.9)$$

where

E = Young's modulus [MPa]
CBR = California Bearing Ratio [%]

It should be well noted that Equation 2.9 is a lower bound relationship, valid for 2% < CBR < 12% only.

Brown et al. (68) checked the validity of Equation 2.9 for three fine grained soils by performing both cyclic load triaxial tests and CBR-tests. Tests were carried out on saturated and partially saturated specimens, thereby yielding various stiffness- and CBR-values for each soil. As expected, the cyclic load triaxial testing of the soils yielded stress-dependent stiffness values. This stress-dependency, which is also found for coarse graded materials, in itself renders the concept of a single E-value for any unbound material unsuitable and thereby also any E-CBR relationship that does not involve a stress factor.

If one wishes to characterize the elastic stiffness of an unbound material with one single value anyhow, the elastic stiffness from cyclic load triaxial testing at a stress level representative of that

in-situ should be used. This approach was used by Brown et al.: Figure 2.4 shows the elastic stiffness of the specimens at a stress pulse of 40 kPa (expressed as E_r) plotted against CBR, together with the two well-known E-CBR relationships. From these results Brown et al. concluded that these relationships only appear to provide a rough guide to the expected soil stiffness, although the TRRL- equation is of the correct shape.

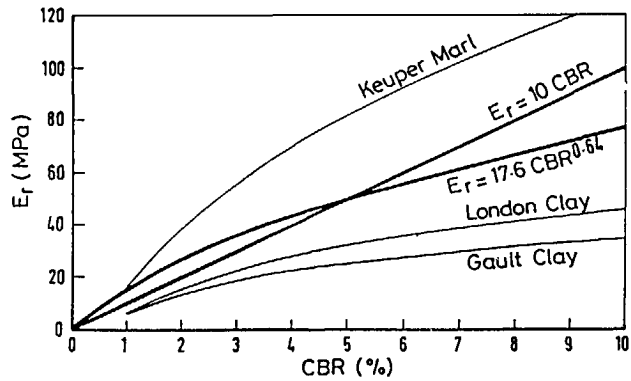

Figure 2.4: Relationship between stiffness and CBR for a stress pulse of 40 kPa (source [68]).

Where E-CBR relationships only provide a rough guide for the stiffness of soils, the use of such relationships for coarse graded granular materials of, for instance, a 0/40 mm grading involves yet another problem. These materials cannot be tested for CBR without the removal of coarse particles, because of the limited size of the CBR piston and mould. Since the coarse particles contribute significantly to material stiffness, the CBR-value determined on, for instance, material passing the 19 mm sieve can only be a very rough measure of the elastic stiffness of a 0/40 mm material. In Paragraph 5.4, CBR-values of some 30 coarse graded materials will be plotted against elastic stiffness, showing no correlation at all.

2.7.3 E_2 - E_3 relationships

The use of a single E-value for a whole layer of unbound material is theoretically not correct. Granular materials have a stress-dependent stiffness and since stress varies throughout the pavement layer, the

E-modulus will vary too. Taking account of this stress-dependency, however, requires very detailed computational work, which is certainly at the present time not yet suited for every-day use. For practical purposes, one single E-value for the whole granular base can be used, provided the main structural element of the pavement is formed by the asphalt layers. More details on this subject will be given in Paragraph 2.9, where flexible pavement design procedures will be dealt with in detail.

In their paper (67) on E-CBR relationships discussed in the previous paragraph, Heukelom and Foster also showed from their measurements that the ratio of the E-modulus of an unbound base layer E_2 to that of the underlying soil E_3 is limited to $E_2/E_3 < 2.5$. The practical explanation for this was said to be that a granular base cannot be properly compacted on a soft subgrade and that, therefore, the value of E_2 of the base course depends largely on the value of E_3 of the subgrade. In a later paper (69), this practical explanation was backed by theoretical considerations. Calculating the stresses at the bottom of the unbound base for E_2/E_3 ratio's of over 2.4, tensile stresses were found in the base under the action of the compacting roller. It was assumed that these theoretical tensile stresses would lead to decompaction of the base layer and thus to a reduction in stiffness to a point were no more tensile stresses occur.

Although the practical reasoning of not being able to properly compact an unbound base layer on a very weak subgrade is certainly valid, the numerical limitation of the E_2/E_3 ratio to maximum 2.5 is not. The values of the stiffness of the base E_2 were obtained by Heukelom and Foster from dynamic measurements at very low stress levels and are therefore not representative of the stiffness in the pavement under traffic. Their calculations of stresses in the granular base course used linear elastic theory, which was later proven to be unsuitable for that purpose (70).

The Shell Pavement Design Manual (5) also uses the concept of E_2/E_3 relationships. It states that the effective modulus of unbound base and sub-base layers depends on their thickness and the subgrade modulus, according to:

$$E_2 = k \times E_3 \quad \text{with} \quad k = 0.2\, h_2^{0.45} \quad \text{and} \quad 2 < k < 4 \qquad (2.10)$$

where

E_2 = modulus of unbound base layer [MPa]
E_3 = modulus of subgrade [MPa]
h_2 = thickness of base layer [mm]

This assumption allowed for omission of E_2 as a separate entry into the design method, thereby substantially reducing the required number of design charts.

Brown and Pappin (70) performed non-linear finite element analysis of a wide range of pavement structures, using the so-called "contour model" (see Paragraph 2.7.6) to describe the non-linear stress-strain behaviour of the granular materials in the pavements. From this non-linear analysis, they derived values for a single "equivalent stiffness E_2", that, when used as entry to parallel BISTRO-calculations, yielded the same values for critical design parameters such as asphalt tensile strain as did the non-linear calculations. The calculations were performed for a wide range of the stiffness of the subgrade E_3 . The equivalent stiffness of the granular base E_2 was shown to be constant for a given quality base course material and, hence, not to depend on the subgrade stiffness E_3. Given the constant E_2 and the varying E_3, the ratio of these two parameters ranged from $1.5 \leq E_2/E_3 \leq 7.5$, indicating that the range for E_2/E_3 given in Equation 2.10 is too narrow. Based on this information, the Addendum to the Shell Pavement Design Manual (S 02) contains correction-formulae, which allow for the use of other E_2-values than those obtained by the rigid Equation 2.10, simply by entering fictitious values for either h_2 or E_3 in Equation 2.10. In Paragraph 2.9.3.1, the Shell Pavement Design Manual and its Addendum will be discussed in detail.

2.7.4 M_r-θ relationships

The parameter most widely used nowadays to characterize the elastic stiffness of soils and unbound granular materials is the resilient modulus M_r. It was introduced by Hveem (71), who concluded that the deformation of such materials under transient loading is elastic in

the sense that it is recoverable, but that this deformation is influenced by factors which are usually not associated with elastic properties. He therefore felt that a separate terminology to describe the elastic behaviour of soils and unbound granular materials was needed and introduced the word "resiliency" to describe the behaviour of these materials under transient loads.

Hveem first determined resilient properties of unbound materials from pavement deflection testing and later [72] introduced his "Resilometer" to determine resilient properties in the laboratory. This Resilometer is in fact a cyclic load version of the Hveem Stabilometer developed earlier (see Paragraph 2.5.2.2). Seed et al. [40] adopted Hveem's terminology to describe the results of their cyclic load triaxial tests, defining the resilient modulus M_r as the ratio of the applied deviator stress to the resulting recoverable axial strain of the triaxial specimen. The results of their test on soils indicated that the resilient modulus of soils decreases with the deviator stress according to a bi-linear relationship, as shown in Figure 2.5.

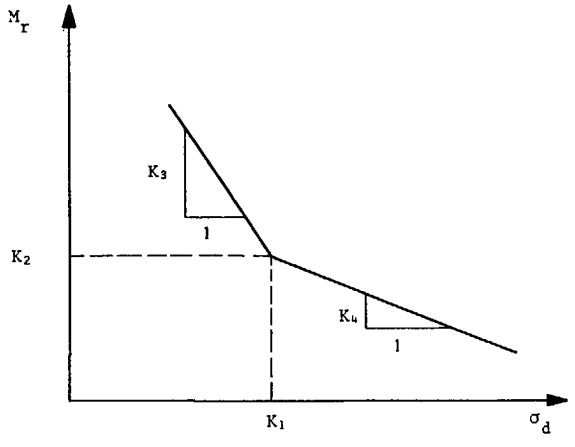

Figure 2.5: Bi-linear plot of M_r versus σ_d, for soils.

The relationships depicted in Figure 2.5 can be expressed by the following formulae [56, 31]:

$$M_r = K_2 + K_3 (K_1 - \sigma_d) \text{ for } \sigma_d < K_1 \quad (2.11)$$

$$M_r = K_2 + K_4 (\sigma_d - K_1) \text{ for } \sigma_d > K_1 \quad (2.12)$$

It should be noted that the bi-linear plot of M_r versus σ_d in Figure 2.5 refers to one level of the confining stress σ_3 only; an increase in confining stress will lead to an increase in resilient modulus.

For granular materials, Monismith et al. (73) also found the resilient modulus to increase with the confining stress σ_3. They suggested the following relationship for granular materials:

$$M_r = K \sigma_3^n \qquad (2.13)$$

where

M_r = resilient modulus
σ_3 = confining stress
K,n = material parameters

Brown and Pell (74) suggested the use of a more appropriate stress function to cope with the three dimensional problem of granular materials in pavements. They obtained stiffness values of unbound granular materials from pulse load tests on an instrumented pavement built in a test pit. By plotting the obtained M_r values on a double-logarithmic scale against the first stress invariant (being the sum of principal stresses), a straight line relationship was found. This method of representing stiffness - stress relationships for unbound granular materials has now become the standard method in pavement engineering. Figure 2.6 shows a schematic representation of this relationship, which is described by the well-known K-θ model:

$$M_r = K_1 \theta^{K_2} \qquad (2.14)$$

where

M_r = resilient modulus
θ = sum of principal stresses at maximum deviator stress
K_1, K_2 = material parameters

It should be noted that Equation 2.14 is mathematically incorrect, since the dimensions of the equation cannot be matched. A mathematically correct equation would involve rendering the stress parameter θ dimensionless by dividing it by a reference stress θ_0 of, for instance, 1 kPa. Equation 2.14 would then read:

$$M_r = K_1 \left(\frac{\theta}{\theta_0}\right)^{K_2} \qquad (2.15)$$

where

M_r	= resilient modulus	[MPa]
θ	= sum of principal stresses	[kPa]
θ_0	= reference stress = 1 kPa	[kPa]
K_1	= material parameter	[MPa]
K_2	= material parameter	[-]

The units for stiffness (MPa) and stress (kPa) used here were chosen as such for sake of conformity with engineering practice.

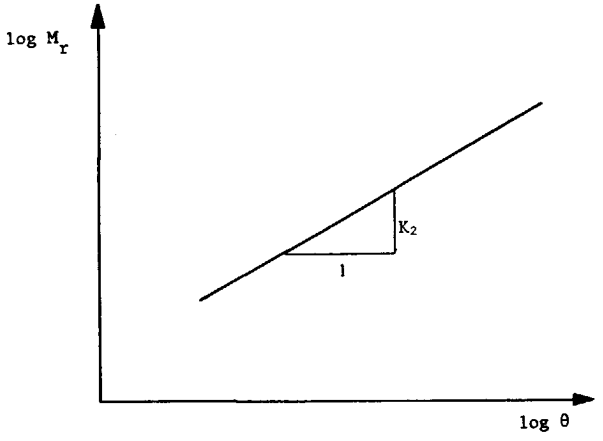

Figure 2.6: Standard log-log plot of M_r versus θ for unbound granular materials.

2.7.5 Bulk and shear moduli K and G

The main advantage of the K-θ model described in the previous paragraph is that it expresses the elastic stiffness of unbound materials in a simple to interpret parameter: the resilient modulus M_r, being an equivalent of the well-known Young's E-modulus. Stiffness expressed as M_r can therefore be readily understood by practising engineers. The model however also has a major drawback: it uses Poisson's ratio ν to model the radial strain of the material. In calculation of stresses and strains in pavements, ν is often set at a constant value. Measurement of radial strain in cyclic load triaxial

testing has however shown that Poisson's ratio ν varies with the applied stress level. At high ratio's of deviator stress over confining stress, ν can become larger than 0.5. In that case resilient specimen dilation occurs, which means that the triaxial specimen increases in volume under the application of the deviator stress. As discussed in Paragraph 2.5.3.2, Constant Confining Pressure triaxial tests and Variable Confining Pressure tests yield different values for Poisson's ratio.

Brown and Hyde [45] showed that a better description of the elastic behaviour of unbound granular materials can be obtained be separating stresses and strains into volumetric and shear components. For a three dimensional stress state, this can be done using the following equations for the stresses:

$$p = \frac{1}{3} (\sigma_1 + \sigma_2 + \sigma_3) \tag{2.16}$$

$$q = \frac{1}{\sqrt{2}} \{ (\sigma_1 - \sigma_2)^2 + (\sigma_2 - \sigma_3)^2 + (\sigma_3 - \sigma_1)^2 \}^{0.5} \tag{2.17}$$

where

p = volumetric stress component
q = shear stress component
$\sigma_1, \sigma_2, \sigma_3$ = principal stresses

The corresponding equations for strain are:

$$\varepsilon_v = \varepsilon_1 + \varepsilon_2 + \varepsilon_3 \tag{2.18}$$

$$\varepsilon_s = \frac{\sqrt{2}}{3} \{ (\varepsilon_1 - \varepsilon_2)^2 + (\varepsilon_2 - \varepsilon_3)^2 + (\varepsilon_3 - \varepsilon_1)^2 \}^{0.5} \tag{2.19}$$

where

ε_v = volumetric strain component
ε_s = shear strain component
$\varepsilon_1, \varepsilon_2, \varepsilon_3$ = principal strains

For the axisymetric case of triaxial testing, where $\sigma_2 = \sigma_3$ and $\varepsilon_2 = \varepsilon_3$, equations 2.16 through 2.19 become:

$$p = \frac{1}{3}(\sigma_1 + 2\sigma_3) \tag{2.20}$$

$$q = \sigma_1 - \sigma_3 \tag{2.21}$$

$$\varepsilon_v = \varepsilon_1 + 2\varepsilon_3 \tag{2.22}$$

$$\varepsilon_s = \frac{2}{3}(\varepsilon_1 - \varepsilon_3) \tag{2.23}$$

Volumetric and shear strains can be expressed as function of volumetric and shear stress using equations similar to Hooke's law $\varepsilon = \sigma/E$:

$$\varepsilon_v = \frac{1}{K} \cdot p \tag{2.24}$$

$$\varepsilon_s = \frac{1}{3G} \cdot q \tag{2.25}$$

where

K = bulk modulus

G = shear modulus

Because of the non-linear behaviour of granular materials, K and G should be expressed as functions of stress. In a first approach, Boyce [75] expressed K and G as a function of the mean normal stress p to a power less than 1:

$$K = K_1 \, p^{(1-n)} \tag{2.26}$$

$$G = G_1 \, p^{(1-n)} \tag{2.27}$$

where K_1, G_1 and n are material constants. The similarity with the K-θ model (Equation 2.14) is obvious, since $\theta = 3p$.

From theoretical considerations, Boyce [75] concluded that volumetric and shear strain of any elastic material have to satisfy a theorem of reciprocity according to:

$$\frac{\partial \varepsilon_v}{\partial q} = \frac{\partial \varepsilon_s}{\partial p} \tag{2.28}$$

Since K and G are functions of p only in Equations 2.26 and 2.27, the simple approach given by these equations does not satisfy Equation 2-.28. Boyce suggested to use a somewhat more complicated approach:

$$K = K_1 \, p^{(1-n)}/(1-\beta \frac{q^2}{p^2}) \tag{2.29}$$

$$G = G_1 \, p^{(1-n)} \tag{2.30}$$

where

$$\beta = (1-n) \, K_1/6G_1 \tag{2.31}$$

Substitution of Equations 2.29 and 2.30 in Equations 2.24 and 2.25 then gives the following stress-strain relationships:

$$\varepsilon_v = \frac{1}{K_1} \, p^n \, (1 - \beta \frac{q^2}{p^2}) \tag{2.32}$$

$$\varepsilon_s = \frac{1}{3G_1} \, p^n \frac{q}{p} \tag{2.33}$$

Boyce verified his model using cyclic load triaxial test data from literature. He showed that his model accurately predicts results from both Constant Confining Pressure and Variable Confining Pressure triaxial tests.

2.7.6 The contour model

A detailed examination of the resilient behaviour of a particular crushed rock was carried at the University of Nottingham [12, 76]. A 0-40 mm crushed limestone was tested in Variable Confining Pressure triaxial tests on 150 mm diameters specimens using a wide variety of stress paths, both in the triaxial compression and extension region. The test results indicated a fundamental difference between volumetric and shear strain response with respect to stress path effects. It was shown that volumetric strains are commutable in stress space, which means that the volumetric strain resulting from a stress path OA (see Figure 2.7) is equal to the volumetric strain resulting from stress paths OB plus BA.

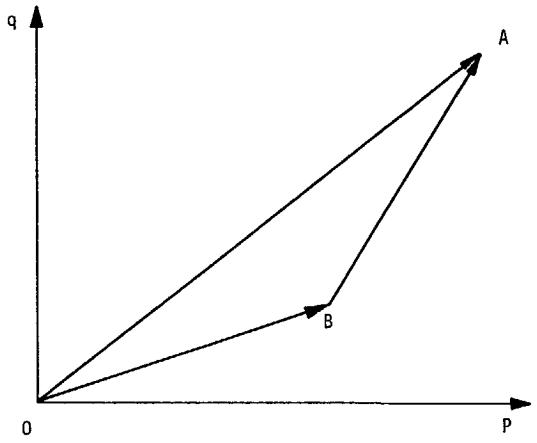

Figure 2.7: Stress paths in p-q stress space.

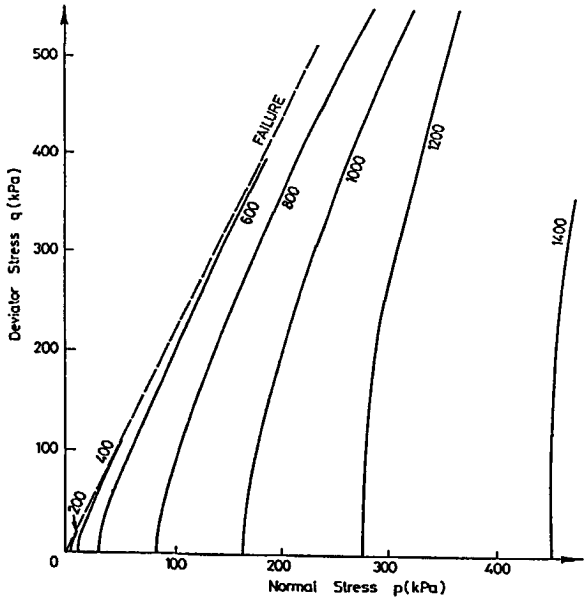

Figure 2.8: Contours of resilient volumetric strain [με] in p-q stress space (source: [12]).

This commutability allows for the use of secant moduli (moduli referring to the common origin 0) for calculation of volumetric strain caused by a given stress path. The volumetric strain caused by path BA in Figure 2.7 can be calculated by substracting the strain caused by paths OB and OA. From the Nottingham test results, it was shown that shear strains are not commutable in stress space. They are dependent

on the length of the stress path and therefore a normalizing factor with respect to stress path length was introduced. Once normalized, shear strains can be dealt with as being commutable.

To describe volumetric and shear strains as a function of stress, Pappin and Brown [76] plotted contours of volumetric and shear strain in p-q stress space. Figures 2.8 and 2.9 show examples for volumetric strains and normalized shear strains, respectively. The strain contours shown in Figures 2.8 and 2.9 were expressed mathematically, thereby obtaining the so-called contour model. Resilient volumetric strain was expressed as a function of p and q/p, using the same expression as Boyce (Equation 2.32). Resilient shear strain was expressed as a function of (q/p + constant), multiplied by a normalizing factor dependent on stress path length.

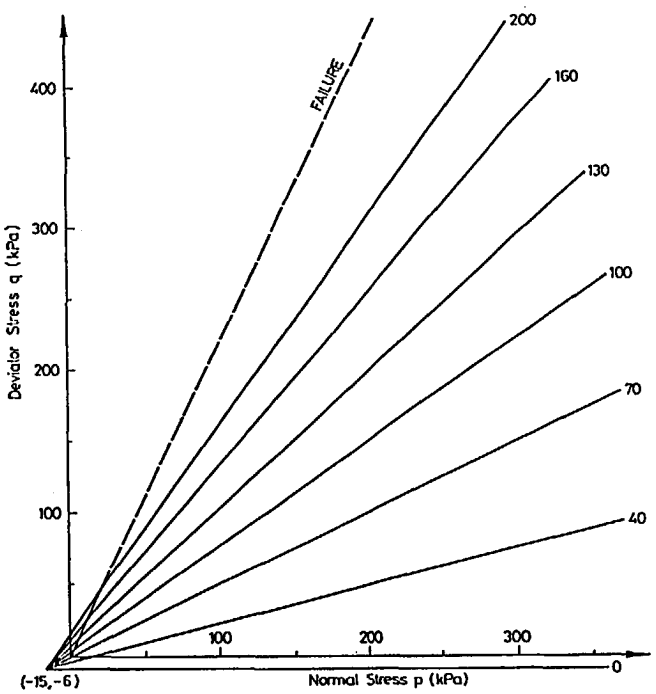

Figure 2.9: Normalized resilient shear strain contours [με] in p-q stress space (source: [12]).

Mayhew [77] applied the same approach of plotting volumetric and shear strain in p-q stress space to model his cyclic load triaxial test results on unbound road base materials. He used equations similar to

those used by Boyce (Equations 2.32 and 2.33) to express the obtained contours mathematically. Reasoning that in-service conditions of subbase and unbound granular bases only involve stress paths starting from near zero stress conditions, Mayhew concluded that the complicating factor of stress path length influence can be ignored in pavement analysis. It should, however, be noted that for deeper pavement layers the transient stress path due to traffic loading does not start at zero stress, since at greater depth the constant overburden stress becomes quite significant relative to the transient traffic-induced stresses. Moreover, recent theories [78] indicate that even in the upper unbound layers the constant stress may be quite significant. Under the action of the compaction roller, so-called "locked-in stresses" may develop, that significantly increase the stress level in the unbound layer in the unloaded condition.

From Boyce's equations for the bulk modulus K and the shear modulus G (Equations 2.29 and 2.30), it can be seen that the variation of K and G with the mean normal stress p is expressed by the same parameter n. Mayhew found that the influence of the mean normal stress p on the bulk modulus K is somewhat different from that on the shear modulus G, and therefore introduced a separate parameter m to relate G to p. This approach was later verified by Jouve et al. [60] and by the author [79]. The resulting model to describe the resilient behaviour of unbound granular materials then involves five separate parameters K_1, G_1, n, m and β:

$$\varepsilon_v = \frac{1}{K_1} \cdot p^n \cdot (1-\beta(q/p)^2) \qquad (2.34)$$

$$\varepsilon_s = \frac{1}{3G_1} \cdot p^{m-1} \cdot q \qquad (2.35)$$

In Chapter 7, the M_r-θ model, Boyce's model and the model given in Equations 2.34 and 2.35 will be used to fit triaxial data for an exemplary granular base course material and a sand.

2.7.7 Modelling of permanent deformation

As compared to the work done on modelling of resilient deformation, only limited research deals with the modelling of permanent deformation of granular materials. This is probably due to the fact that

permanent strain characteristics of unbound granular materials are often considered to be less important than resilient deformation characteristics. The latter are directly related to fatigue cracking of flexible pavements, which is virtually impossible to remedy once it has occurred to a substantial extend. Permanent deformation in unbound granular layers can simply be remedied by overlaying the pavement. Furthermore, determination of permanent deformation characteristics of unbound materials requires far more extensive testing than does determination of resilient deformation characteristics.

Barksdale (80) performed cyclic load triaxial tests with 10^5 applications on a wide variety of unbound base course materials. He plotted his results on a log-natural scale, as schematized in Figure 2.10. This way of representing permanent deformation testing results is still widely used today. The permanent axial strain $\varepsilon_{a,p}$ of the triaxial specimen is plotted against the logarithm of the number of load applications N, for different ratios of deviator stress $\sigma_1-\sigma_3$ over confining stress σ_3.

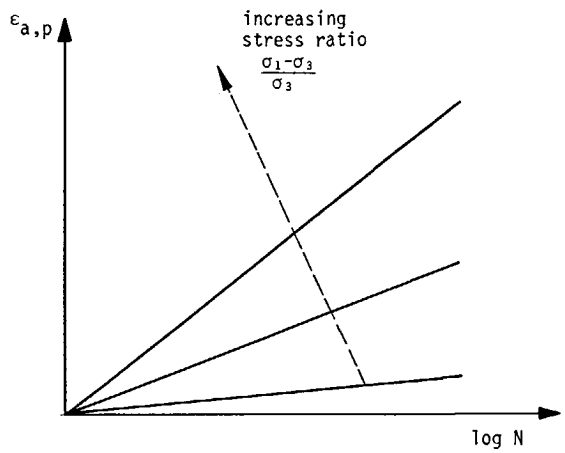

Figure 2.10: Permanent axial strain $\varepsilon_{a,p}$ versus logarithm of number of load applications N.

For given numbers of load applications N, Barksdale then replotted his data in the standard way of plotting stress-strain data from monotonic load triaxial tests, being deviator stress versus axial strain. The obtained hyperbolic stress-strain curves can be expressed by:

$$\varepsilon_{a,p} = \frac{(\sigma_1-\sigma_3)/(K\sigma_3^{\,n})}{1 - \dfrac{(\sigma_1-\sigma_3)\,R_f}{2\,(C\cos\phi + \sigma_3 \sin\phi)/(1-\sin\phi)}} \qquad (2.36)$$

where

$\varepsilon_{a,p}$ = permanent axial strain for given number of load applications N

$K\sigma_3^{\,n}$ = relationship defining the initial tangent modulus as a function of confining pressure σ_3 (K and n are constants)

C = cohesion

ϕ = angle of shearing resistance

R_f = a constant relating compressive strength to an assymptotic stress difference

Since the work of Barksdale, most researchers have used the standard way of plotting permanent strain data as depicted in Figure 2.10. The obtained straight lines on the log-natural scale can be expressed by:

$$\varepsilon_{a,p} = a + b \log N \qquad (2.37)$$

where

$\varepsilon_{a,p}$ = axial permanent strain

N = number of load applications

a,b = constants for given levels of $\sigma_1-\sigma_3$ and σ_3

Since each line depicted in Figure 2.10 requires a separate cyclic load triaxial test with a large number of load applications, much effort has been put into obtaining the constants a and b of Equation 2.37 from static load triaxial tests. This research has been dealt with in paragraph 2.5.3.3.

Recent work in France by Jouve et al [60] involves the approach of separating stresses and strains into volumetric and shear components, as discussed earlier for resilient properties (Equations 2.20 through 2.23). Permanent deformation moduli were defined as:

$$K_p(N) = p/\varepsilon_{v,p}(N) \qquad (2.38)$$

$$G_p(N) = q/3\ \varepsilon_{s,p}(N) \qquad (2.39)$$

where:

$K_p(N)$ = bulk modulus with respect to permanent deformation
$G_p(N)$ = shear modulus with respect to permanent deformation
$\varepsilon_{v,p}(N)$ = permanent volumetric strain
$\varepsilon_{s,p}(N)$ = permanent shear strain
p = mean normal stress
q = deviator stress

The permanent deformation moduli can be expressed as functions of the number of load applications N by:

$$G_p(N) = \frac{A_2 \sqrt{N}}{\sqrt{N} + D_2} \qquad (2.40)$$

$$K_p(N) = \frac{A_3 \sqrt{N}}{\sqrt{N} + D_3} \qquad (2.41)$$

where A_2, D_2, A_3 and D_3 are constants depending on the stress ratio q/p.

Equations 2.38 and 2.39 thus indicate that permanent deformation can be expressed as a function of number of load applications N and stress ratio q/p. It should, however, be well noted that a vast number of permanent strain tests is required to establish the parameters of Equations 2.40 and 2.41.

2.8 IN-SITU TESTING

2.8.1 Introduction

In Paragraph 2.5, the testing techniques used in the laboratory to characterize the mechanical properties of unbound granular materials have been dealt with. In this paragraph, the techniques for in-situ testing of unbound granular materials will be discussed. Two distinctions between laboratory and in-situ tests should be noted:

- In laboratory tests, properties are determined of the investigated material by itself, without influence of the materials in the pavement layers above and below the investigated material. Hence, laboratory tests determine actual material parameters. In-situ tests on the other hand often determine the combined properties of the layer on which the test is performed, and all layers below that layer. Then, in fact, a "structure parameter" is determined, rather than a material parameter. The latter can only be obtained through a back-analysis of the layered pavement system.

- In laboratory tests, often target values for the mechanical property at hand of the investigated material are determined. The in-situ test then is a check whether or not the target values are met in the pavement layer after construction. Because of the variability of the factors influencing the actual construction of the pavement layers, the investigated parameters are bound to show far more scatter in-situ than in the laboratory, where material specimens are made under standardized circumstances. Therefore, the required number of in-situ tests to assess material performance is usually far larger than the required number of tests in the laboratory.

The in-situ testing techniques presently being used will be reviewed in this paragraph. As was done for the laboratory testing techniques, again distinction will be made between standard and non-standard testing techniques.

2.8.2 Standard in-situ testing techniques

2.8.2.1 DEGREE OF COMPACTION

In many countries including the Netherlands, the degree of compaction of unbound layers is used as an indirect parameter for assessing the resistance to resilient and permanent deformation of unbound pavement layers. A direct measurement of this resistance is often omitted, since the tests presently available for this measurement are too cumbersome (see Paragraph 2.8.2.2). Tests often used for determination of in-situ density are the sand-cone method, the water-balloon method and the nuclear density meter method.

The sand-cone and the water-balloon methods

The sand-cone method (AASHTO T191-61) [26] and the water-balloon method (AASHTO T205-64) [26] both rely on the principle of removing material from the compacted layer and determining the volume of the resulting hole by filling it up with either a uniformly graded sand or water in a rubber balloon. The main disadvantage of these methods is that they both require overnight drying of the material removed to accurately determine its dry weight and water content. Both tests are therefore not suited to determine during the construction process whether sufficient compactive effort has been applied, for the simple reason that the answer to this question will only be obtained the next day.

The nuclear density meter

The nuclear density meter method (ASTM D 2922 and D 3017) [81] does not have this disadvantage, since it measures density and water content within a few minutes. The wet density of the material in the investigated layer is best measured by the so-called "direct transmission method", whereby the nuclear source is placed in a pre-driven hole in the layer. The value for the wet density thus obtained is then representative of the material between the source and the surface of the layer. In the determination of the moisture content, however, the upper 10 cm of material play a predominant role. Since the dry density is calculated from the wet density (measured over the whole depth of penetration of the nuclear source) and the water content (measured mainly over the upper 10 cm), errors may result in density determination on layers having a large gradient in moisture content over the height of the layer.

The dry density values measured in-situ are often not judged as absolute numbers, but as a percentage of the maximum Proctor density of the material at hand. Since the in-situ density test and the Proctor test are carried out independently, the scatter in the results of each individual test may be enhanced when the two test results are combined to give density relative to Proctor density. A recent German survey [82] has shown that a maximum combined scatter of 6.5% may occur. This

renders in-situ densities expressed as percentages of maximum Proctor density quite disputable.

2.8.2.2 BEARING CAPACITY

The California Bearing Ratio

The in-situ California Bearing Ratio test was developed from the laboratory version of the test discussed in Paragraph 2.5.2.2 as a means of measuring in-situ the bearing capacity of soils. It should be well noted that the boundary conditions of the material tested are quite different in the two versions of the test. In the laboratory version, the material is confined by the rigid boundary of the steel CBR-mould, whereas in-situ this rigid boundary is lacking. This different boundary condition may have a large influence on the outcome of the test. As noted in Paragraph 2.5.2.2, the laboratory version of the test may yield lower CBR-values when testing saturated clays because of the development of positive pore pressures. When testing granular materials, the laboratory test may yield higher values because of the larger confining stress.

The standard equipment for in-situ CBR involves a truck-mounted hand operated jack, to which the CBR-piston is connected. The weight of the truck forms the reaction for the load applied on the piston. Although the CBR-test is indeed quite simple, it is still quite cumbersome to carry out in-situ. Furthermore, because of its relatively small piston diameter (approximately 50 mm) its applicability for coarse grade unbound granular materials is questionable. Although the CBR-value still forms one of the main input parameters for many pavement design procedures, the in-situ version of the test is therefore not often used. The CBR-value of the subgrade is mostly obtained from the laboratory version of the test or through empirical correlations relating CBR to soil composition. Also, the CBR of the subgrade is sometimes assessed through empirical correlation from the results of more complex in-situ testing. Day (83), for instance, reported an investigation in the UK where the subgrade CBR was estimated from the "modulus of subgrade reaction", as determined with the plate bearing test. This is a somewhat strange approach: a very cumbersome test is carried out yielding a sound engineering parameter, which is then translated into a purely

empirical parameter which could have been obtained directly with a less cumbersome test. One of the major drawbacks of empirical pavement design procedures is shown here: the more fundamental parameter obtained from the plate bearing test cannot be used as input for the CBR-method of pavement design, for the simple reason that this method is based on experience with CBR-input only.

The Plate Bearing Test

In 1926, Westergaard [84] in his theoretical analysis of stresses in concrete pavements introduced his "modulus of subgrade reaction k" as a measure of the stiffness of the subgrade. The unit used by Westergaard for this modulus k was pressure over settlement, so $lb/inch^2/inch$ or $lb/inch^3$ (N/m^3). This modulus can be determined with a Plate Bearing Test, at stress levels which are representative of in-service conditions. Burmister [85] later reasoned that soils in natural deposits and processed and compacted in embankments and base courses of pavements are always preconditioned and prestressed materials. He therefore argued that the stiffness of these materials should be determined in-situ using Plate Bearing Tests, rather than on recompacted laboratory specimens. Nowadays, the Plate Bearing Test is used in many countries (Germany, Austria, Switzerland, USA, France, UK) for assessing the degree of compaction and/or the bearing capacity of in-situ unbound pavement layers. The implementation of the test has probably developed farthest in Germany: the Plate Bearing Test forms an essential part of the German pavement procedure [86].

The test is fundamentally sound, in the sense that it involves application of a test load similar in magnitude to traffic loading and measurement of the resulting settlement of the plate. Most countries mentioned above have their own standardized procedure for the test. The various procedures show significant differences with respect to, for instance, plate diameter, magnitude of load and number of load repetitions. Most procedures agree upon the interpretation of the test results. The stiffness of the layers is calculated from the ratio of the applied stress over the resulting settlement, multiplied by a certain constant times the plate diameter to obtain the stiffness in N/m^2 or equivalent local units. The test procedure usually involves several loading and unloading steps and calculation of the layer stiffness

from the last loading step. The increase in stiffness over the subsequent loading steps is used in some countries as a measure of the resistance to permanent deformation.

The rate of loading in the Plate Bearing Test differs considerably from traffic loading. Where actual traffic involves load-pulses in the unbound layers of around 0.1 s, the Plate Bearing Tests use load-on periods of 5 up to 30 minutes. In testing of well-drained layers of unbound granular materials the slow loading procedure probably has little effect on the outcome of the test, since the stiffness of these materials is not dependent on the rate of loading. The stiffness of poorly drained clayey material however is dependent on rate of loading. A fast rate of loading may lead to the build-up of positive pore pressures and hence to a lower stiffness, whereas under the slow rate of loading of the Plate Bearing Test pore pressures may have sufficient time to dissipate, which yields a higher stiffness. For pavement design purposes dealing with relatively high rates of loading, the Plate Bearing Test is therefore less suited for determination of the stiffness of clayey subgrades or low permeability granular materials with a high degree of saturation. It should be borne in mind that Plate Bearing Test carried out on base course layers measure the combined stiffness of that layer and all the lower layers. Therefore, the slow rate of loading might influence the combined stiffness measured on unbound granular layers built on poorly drained clayey subgrades.

In addition to this theoretical disadvantage, the static loading applied in the Plate Bearing Test has practical disadvantages as well. The applied static loading requires a heavy reaction-load, which is usually furnished by the weight of the truck on which the test equipment is mounted. Secondly, repeated application of the static loads of 5 up to 30 minutes duration requires much time. Per test point, the Plate Bearing Test requires at least one hour, which is a major disadvantage if one wishes to determine the bearing capacity of the layers of a pavement under construction in a statistically sound manner.

The solution to the theoretical and practical disadvantages of the static Plate Bearing Test is obvious: the use of some kind of impact loading device to apply the required loads could give load pulses similar to these caused by traffic, with simpler testing equipment and drastically reduced testing time. In Chapter 8 of this dissertation a

dynamic version of the Plate Bearing Test will be described which allows for a rapid assessment of in-situ stiffness under realistic conditions of magnitude and rate of loading.

2.8.3 Non-standard in-situ testing techniques

2.8.3.1 BEARING CAPACITY

The Clegg Impact Tester

The Clegg Impact Tester [87] was developed in the mid nineteen-seventies in Australia for density control of unbound base courses. The apparatus basically consists of a cylindrical drop weight contained in a guide tube. The 4.5 kg weight is dropped from a height of 450 mm onto the base layer and the maximum deceleration of the weight is measured on impact by the electronics of the tester.

Because of the similarity in dimensions between the drop-weight of the Clegg Impact Tester and the CBR piston, the Clegg Impact Test can be regarded as a dynamic version of the CBR-test. A correlation between Clegg Impact Values and CBR has been obtained [87]. The main advantage of the Clegg Impact Test is its simplicity: the apparatus is cheap and portable and one man can perform some 40 tests per hour. The Clegg Impact Tester has the same disadvantage as the CBR-test in testing of unbound base courses. The diameter of the drop-weight is small (about 50 mm) relative to the maximum diameter of the material to be tested. Furthermore, the depth of construction tested with the Clegg Impact Tester is limited. The applicability of the Clegg Impact Tester for proof testing of granular layers will be dealt with in Chapter 8, using data obtained on the test pavements built for this research.

Falling Weight Deflectometer testing on unbound base course

The Falling Weight Deflectometer (FWD) is used extensively nowadays to determine the structural condition of flexible pavements. The "deflection" (vertical displacement) of the pavement is measured simultaneously at several distances from the applied impact loading. From the "deflection bowl" obtained the elastic moduli of the various

interpretation-software. Most of the available back-analysis programs use linear elastic theory to characterize the stress-strain behaviour of the pavement materials, expressing it in one single E-value for each pavement layer.

When the FWD-measurements are carried out on pavement constructions with a thick layer of asphalt, the main structural element of the pavement is bound to be the asphalt layer with its basically linear elastic behaviour. One might argue that in that case a linear elastic back-analysis program can produce realistic stiffness values for the various pavement layers. However, the overall magnitude of the deflections is dominated by the stiffness of the subgrade, since most of the deflection is generated in that layer. Therefore, even in the relatively simple case of FWD measurements on completed constructions, the subgrade should be characterized by a non-linear elastic model, taking into account the stress dependency of the stiffness of that layer (88).

The problem of the non-linear elastic behaviour of materials becomes even larger when FWD measurements are carried out directly on the granular base layer during construction of the road. In that case, the granular base with its marked non-linear behaviour forms the main structural element of the pavement. It is therefore quite questionable whether FWD measurements on unbound pavement layers can be interpreted using linear elastic theory.

The available literature on back-analysis of layer moduli from FWD-measurements on asphalt layers being quite abundant, only very limited information is available on FWD-measurements directly on the unbound pavement layers. Work in this field has been done recently at Nottingham University, using a specially developed interpretation procedure rather than the standard linear elastic back-analysis (62, 89). Non-linear elastic models were used to characterize the stress dependent behaviour of both the subgrade and the granular base layer. Since the FWD deflection data were found to be much more variable than on bound "finished" pavements, iteration of the input to the back-analysis program was carried out manually, rather than using the automated procedure developed at Nottingham for back-analysis of FWD measurements on completed constructions (90). Although the iteration

procedure was performed manually, difficulty was generally experienced in obtaining acceptable matching of computed deflections to the measured bowls.

In Chapter 8 of this dissertation, in-situ testing performed on the granular base courses of a specially built test pavement will be described. The test program involved static Plate Bearing Tests, a dynamic variant of that test, Falling Weight Deflectometer Tests and Clegg Impact Tests.

2.9 Flexible pavement design procedures

2.9.1 Introduction

Until some twenty years ago, virtually all standardized flexible pavement design procedures were so-called empirical methods. These methods were developed from a vast experience with existing roads, sometimes supplemented with the analysis of test sections or specially built test pavements. Many countries today still rely on such empirical methods, realizing that more sophisticated mechanistic design procedures often require too many assumptions regarding material behaviour and too complicated material testing techniques to be of direct practical use. Examples of recently published empirical design methods are the procedures of the British Transport and Road Research Laboratory [3] and the American Society of State Highway and Transportation Officials [4].

The advent of the digital computer has created the possibility of the practical use of the analytical solutions to determining stresses and strains in pavement developed earlier by Boussinesq [63], Burmister [64] and Odemark [65]. Computer programs like BISTRO, BISAR, CHEVRON and CIRCLY were developed that allow for calculation of stresses and strains at any point in a multi-layered pavement structure. These programs form the analytical backbone of today's mechanistic design procedures. The programs allow for the determination of the pavement response to an external load. Comparison of the calculated values of stresses and strains to allowable values as determined in laboratory

tests allow for a first prediction of the number of loads to failure. This purely analytical exercise should, however, in all cases be supplemented by a validation process to allow the pavement response to a single loading to be translated into long-term in-situ pavement performance. Today, much effort is spent on further developing of mechanistic design procedures, both by improving the existing analytical tools for determination of the pavement response and by performing extensive long-term pavement performance studies, supplemented by accelerated loading studies of specially built test sections.

The computer programs named above all use linear elastic theory to calculate stresses and strains in pavement structures. A constant value of Young's modulus E and Poisson's ratio ν is assigned to each layer. In reality however, both E and ν vary throughout the unbound granular layers in the pavement, since these materials have a stress-dependent stiffness. The use of constant values for E and ν is therefore a simplification, allowing the use of relatively simple computer programs based on linear elastic theory. This simplification is allowable when the main structural element of the pavement is formed by the asphalt layer, with material properties being basically linear elastic for the ranges of temperature and rate of loading occurring under normal circumstances. Full-depth asphalt constructions or constructions with a thick asphalt layer on a weak granular sub-base can for design purposes be simplified to linear elastic systems. When, however, a relatively thin asphalt layer is to be designed on a thick granular layer with a high stiffness, the simplification to a linear elastic system is no longer justified. The main structural element of the pavement is then formed by the granular layer, with its marked non-linear behaviour. The stress-dependency of the stiffness of this material should then be taken into account.As a first approximation, this can be done by dividing the granular base layer into a number of sub-layers. Stress-dependency can then be taken into account by giving a lower stiffness to the deeper sub-layers. The problem however remains to obtain a correct value for the stresses in the granular base. Although subdivision of the granular base may cause the calculations to no longer yield tensile stresses in the granular base, this not necessarily means that the stresses found are the correct ones. In summary, linear elastic theory can be used to calculate critical design parameters such as asphalt tensile strain, provided an appropriate equivalent stiffness is attributed to the granular base

layer (or sub-layers). The problem, however, remains to obtain that appropriate stiffness for the granular base. Coupling to cyclic load triaxial test results is impossible, since no realistic value for the stresses in the granular base can be obtained using linear elastic theory.

The disadvantages of multi-layered linear elastic analysis can be overcome by using a finite element approach to the calculation of stresses and strains in pavements. A section of the pavements is divided both vertically and horizontally into a large number of small elements and in an iterative process each element is assigned stiffness parameters dependent on the stress level in the particular element. Sophisticated material models can be used to relate stiffness to stress. Although many researchers are presently involved in finite element calculations of pavements, no generally accepted pavement design procedure based on these calculations is today being used. Finite element calculations still are a research tool, with the main advantage of giving a far better insight into stresses and strains in pavements as compared to that obtained through linear elastic calculations.

As stated, mechanistic design procedures are based on analytical determination of the pavement response to external loads and long-term monitoring of in-service pavements to obtain data for the translation of the calculated pavement response to long-term pavement performance. The extend to which pavement design procedures have been validated by long-term performance studies differs from one method to the other. Recently developed design procedures based on finite element calculations for instance often lack sufficient in-situ validation, for the simple reason that these methods have not been around long enough to be validated with actual long-term in-situ performance data. Accelerated loading testing might solve part of this problem, but data on actual performance under normal traffic and climate are still required for a proper validation. Design procedures lacking such validation are in fact not mechanistic design procedures, but only an analytical tool to determine the pavements response. Some mechanistic design procedures presently being used do have a substantial backing from long-term pavement performance studies. The best example here is the South African pavement design procedure (91, 92, 93), which boasts validation by both long-term monitoring of in-service pavements and

extensive accelerated loading testing using a fleet of four Heavy Vehicle Simulators.

A wide variety of pavement design procedures is used in tropical areas. Some countries rely on methods developed for and in temperate zone areas, such as the AASHTO Interim Guide for the Design of Pavement Structures [9] which is widely used in Central and South America. Former British colonies in Africa use the Road Note 31 [10] procedure, which was specially developed for use in tropical and sub-tropical areas. Another example of a specially developed procedure is the Tropical Design Procedure [29] of the United States Agency for International Development USAID.

In this paragraph, a description will be given of several pavement design procedures used today. Empirical and mechanistic procedures will be dealt with separately, limiting the description to the principles of the methods. Furthermore, two pavement design procedures developed for use in tropical areas will be described. The empirical methods dealt with here are the CBR-, the TRRL-, the AASHTO- and the German method. Of these methods, the TRRL-method is in fact not entirely empirical, since it has a certain backing from structural analysis of test pavements. Over all, however, it is still considered to be an empirical method. The CBR- and the AASHTO-method are widely used purely empirical methods. The German empirical design procedure is discussed here since it relies heavily on in-situ testing of pavement layers. Under mechanistic design procedures, the Shell Pavement Design Manual will be discussed since it is today the main pavement design method used in the Netherlands. The method used in South Africa is discussed since it is at present the best validated pavement design procedure. Finally, under tropical pavement design procedures, the Road Note 31-method and the USAID Tropical Design Procedure will be described.

2.9.2 Empirical pavement design procedures

2.9.2.1 THE CBR-METHOD

By far the most well-known empirical pavement design procedure is the CBR-method. It was developed by the California Division of Highways in the late nineteen-thirties. By investigating in-service pavements of various states of deterioration, relationships were obtained between the CBR-value of the subgrade and the required pavement thickness. The method became known worldwide in the early days of World War II when it was adopted by the U.S. Corps of Engineers as the basis of a design procedure for airfield pavements.

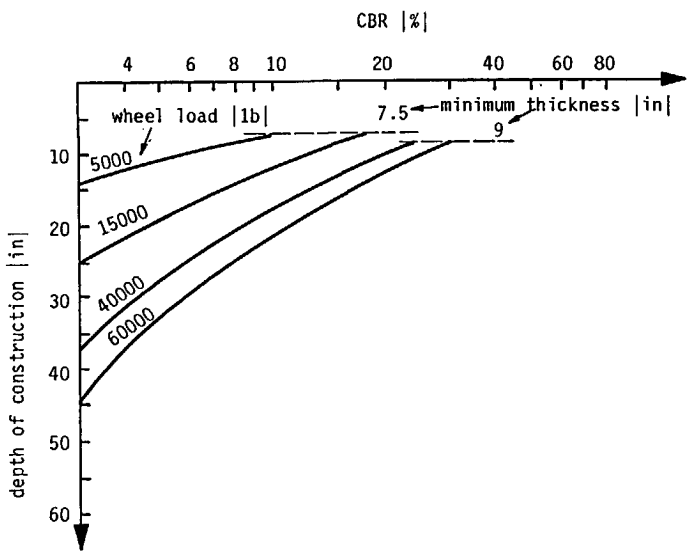

Figure 2.11: CBR design curves for airport runways (US Corps of Engineers).

Figure 2.11 shows design curves for airport runways from the Corps of Engineers procedure. The required depth of construction follows directly from the subgrade CBR and the wheel load. The design curves are based on limiting the shear stress at the top of the subgrade to a level well below failure, which in turn limits the permanent deformation of the subgrade. The curves for the large wheel loads were obtained by extrapolating from the original CBR design curve for road pavements, which is similar to the design curve for small wheel loads in the upper left hand corner of Figure 2.11. The latter curve being

based on in-situ performance of road pavements, the curves for the larger wheel loads were obtained by bringing the shear stress at the top of the subgrade under these higher loads to the same level as for the small loads by increasing the depth of construction. In this extrapolation, Boussinesq analysis was used to determine the stresses in the pavement under wheel loading.

It should be noted that in the early-day CBR design curves the number of load applications is not an entry to the design. The refinement of bringing the number of load applications into the design was later made in procedures developed from the original CBR-method. The British Road Note 29 [94], for instance, has both subgrade CBR and the cumulative number of standard axles as input to its design charts.

2.9.2.2 THE TRRL-METHOD

In 1984, the British Transport and Road Research Laboratory published its Laboratory Report LR 1132 "The structural design of bituminous roads" [3]. The report contains a design procedure for flexible pavements, which is a follow-up of the one published in Road Note 29 [94]. The method is based on the performance of experimental roads, interpreted in the light of structural theory. Through a structural back-analysis of the performance of the experimental roads, strain criteria were obtained which were subsequently used to produce the design charts. The TRRL-method involves a two-stage design: the lower layers of the pavement are designed to serve as a construction platform and to carry construction traffic, whereas the upper layers are designed to carry the normal commercial traffic. For the latter traffic, the structural contribution of the lower layers is also taken into account.

The design involves the following steps (see Figure 12):

1 The "capping layer": starting from the CBR-value of the subgrade, the decision is taken whether or not to apply a "capping layer". The main function of this layer of low cost, local material such as river gravel is to serve as a working platform, protecting the subgrade from excessive loading by construction traffic. The following thickness of the capping layer is prescribed:

- $CBR_{subgrade} < 2\%$: 600 mm capping layer
- $2\% < CBR_{subgrade} < 5\%$: 350 mm capping layer
- $CBR_{subgrade} > 5\%$: no capping layer required

2 The sub-base: this is a structurally significant layer, generally of granular material, that provides a working platform on which materials can be transported, laid and compacted. The required sub-base thickness can be read from a design chart, having subgrade CBR and construction traffic as input.

3 The base: this is the main structural element of the pavement. Three types of base are distinguished: "bituminous roadbase" (asphalt concrete), "wet mix granular roadbase" (unbound granular materials) and lean concrete. For each type, the required thickness can be read from design charts.

4 The surfacing, consisting of a binder layer and a wearing course. The main functions of the surfacing are levelling (binder layer) and providing an impervious layer with high skid resistance (wearing course). The required total thickness of the surfacing follows directly from the design charts for the various types of road base.

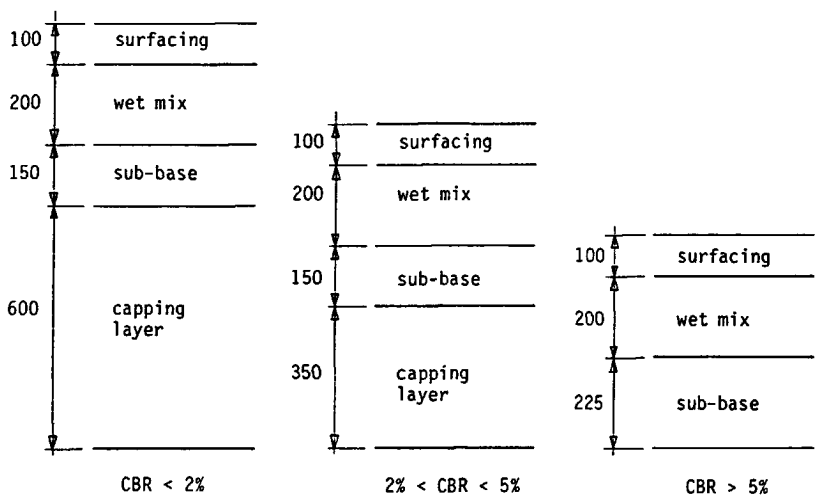

Figure 2.12: Results of TRRL-method: pavements for three soil conditions, for 10^6 standard axles of 80 kN (layer thickness in mm).

2.9.2.3 THE AASHTO-METHOD

In 1986, the American Association of State Highway and Transportation Officials published its "AASHTO guide for the design of pavement structures" (4). This guide is a final version, preceded by the AASHTO Interim Guide of 1972 and its revision of 1981. Both these documents were based on the findings of the AASHO Road Test. The final guide too is based on those findings, but new considerations were added in their interpretation, such as a concept of reliability and the use of the resilient modulus to characterize soil support.

The design involves the following steps:

1 For input to the design procedure, the soil support is characterized by the resilient modulus of the subgrade. It should be determined through cyclic load triaxial testing according to AASHTO T 274 "Resilient modulus of subgrade soils". If no equipment for this test is available, the resilient modulus can be estimated from the results of simpler laboratory tests, namely the California Bearing Ratio CBR and the Resistance R-value determined with the Hveem Stabilometer (see Paragraph 2.5.2.2).

2 From the required reliability of the design, the soil support and the expected amount of traffic, a "design structural number SN" is obtained from a nomograph in the guide.

3 The required design structural number SN is then met by selecting a combination of surfacing, base and sub-base according to

$$SN = \Sigma\, a_i\, D_i \qquad (2.42)$$

where

SN = structural number
a_i = layer coefficient
D_i = layer thickness

4 The layer coefficient a_i expresses the empirical relationship between the structural number SN of a layer and its thickness. It is a measure of the relative ability of a material to function as a structural component of the pavement. The layer coefficient a_i can

be read from a number of charts incorporated in the guide, depending on the type of material. The following types are distinguished:

- Asphalt concrete surface coarse: the structural coefficient a_1 of this layer can be read from a chart having the resilient modulus E_{AC} of the asphalt concrete at 68°F (20°C) as input. E_{AC} should be determined according to ASTM D 4123.

- Granular base layer: the structural coefficient a_2 of this layer can be read from a chart having the resilient modulus E_{BS} of the granular material as input. E_{BS} should be determined in cyclic load triaxial tests according to AASHTO T 274 "Resilient Modulus of Subgrade Soils". For those agencies that do not have the required equipment for this test, the structural coefficient can be obtained from other laboratory test data such as CBR or R-value.

- Granular sub-base layer: the structural coefficient a_3 can be read from a chart similar to that for coefficient a_2 of the base layer, having resilient modulus E_{SB}, CBR or R-value as input. This chart, however, leads to higher structural coefficients for the same input as compared to the chart for base layers. For instance, for the base layer a resilient modulus E_{BS} = 145 MPa leads to a structural coefficient a_2 = 0.10, whereas the same resilient modulus in the sub-base E_{SB} = 145 MPa leads to a structural coefficient of a_3 = 0.14. This difference clearly reflects the empirical, non-analytical approach to pavement design of the Guide. A material of a certain quality leads to a higher structural contribution when placed in the sub-base as compared to the base. Inversely, to obtain the same structural contribution, higher quality material should be applied in the base as compared to the sub-base. The background for this is that, from an empirical point of view, higher quality materials are required in the upper layers of the pavement.

- Cement treated base: the structural coefficient a_2 can be read from a chart having the resilient modulus or, alternatively, the unconfined compressive strength of the material as input.

- Bituminous treated base: the structural coefficient a_2 can be read from a chart having the resilient modulus or, alternatively, the Marshall stability of the material as input.

The AASHTO-design procedure still is a purely empirical one, although it allows for the use of fundamental material parameters from cyclic loading testing as input to the design. These fundamental parameters are not used as such in a structural analysis, but merely substitute the empirical input parameters CBR and R-value. The basis of the AASHTO method still is the performance data from the AASHO Road Test of the late nineteen-fifties.

2.9.2.4 THE GERMAN METHOD

In 1986 the German "Forschungsgesellschaft für Strassen- und Verkehrswesen" published its "Richtlinien für die Standardisierung des Oberbaues von Verkehrsflächen RSTO 86" [86]. The method distinguishes itself from the TRRL and AASHTO methods in the sense that it presents a set of standard constructions. Rather than leaving the actual choice of layer thicknesses to the pavement engineer, the method simply guides the designer to a standard construction for the particular situation of traffic loading, soil support and climate. A second distinction from the TRRL and AASHTO methods is that the German method relies heavily on in-situ testing. Plate Bearing Tests are prescribed on the subgrade and each of the successive unbound pavement layers.

The procedure for obtaining the required standard design consists of the following steps:

1 Plate Bearing Tests are performed on the subgrade, to check whether or not the stiffness of the subgrade meets the minimum requirement of the design. If not, special measures such as soil improvement are required to bring the soil support to the specified level.This approach of dealing with a weak subgrade in the design is based on the same philosophy as the TRRL-method (Paragraph 2.9.2.2). Rather than having soil support itself as an entry to the design procedure, the design starts from a standard soil support. In case the actual subgrade does not meet that standard soil support value, remedial measures are taken. In the TRRL approach a "capping layer"

is applied to bring the support to CBR = 5%, which is the basis for the design. In the German approach soil improvement is carried out to bring the soil support to the required plate bearing value.

2 From the amount of traffic to be carried, the road is classified into one of six categories ("Bauklasse I-VI").

3 The third input to the design is the climate, with respect to frost penetration. Depending on the locality and the environment a minimum thickness of non frost-susceptible material can be obtained from the guide.

4 Having obtained the traffic-category, the pavement engineer can choose a type of construction (full-depth asphalt or granular base, for instance). For each type, a construction with standard layer thickness is given.

5 If the required thickness of non frost-susceptible material (step 3) exceeds the required thickness with respect to traffic loading (step 4), an additional layer of non frost-susceptible material has to be applied.

6 Construction control is done by performing Plate Bearing Tests, first on the subgrade and later on the granular layers. For each of the traffic categories, a specified level of stiffness of the granular base as measured with the Plate Bearing Test is given.

Although the approach of performing Plate Bearing Tests on each pavement layer is a very thorough one, the practicality of a pavement design procedure incorporating this approach is questionable. The Plate Bearing Test performed according to German Standards requires over one hour per test, whereas the variability of subgrade support and compaction of granular layers requires the test to be carried out at a large number of points along the length of the road under construction. Much time is therefore required for proof testing of the various pavement layers, thereby rendering the present approach with standard Plate Bearing Tests impractical. A clear need therefore exists for a less time consuming version of the test. Research is presently underway in Germany [95] to develop a dynamic version of

the test, similar to the Dynamic Plate Bearing Test described in detail in Chapter 8 of this dissertation.

2.9.3 Mechanistic pavement design procedures

2.9.3.1 THE SHELL PAVEMENT DESIGN MANUAL

The Shell Pavement Design Manual [5] is a comprehensive guide to the design of flexible pavement structures. In addition to a basic design procedure for asphalt pavements with granular base or sub-base, it contains guides for the design of asphalt pavements with cementitious bases and for overlay design. Here, only the main principles of the basic design procedure for asphalt pavements with granular bases will be dealt with.

The Shell Pavement Design Manual is based on an analytical principle. The strains in the pavement construction caused by a standard axle-load are calculated using the computer program BISAR and the calculated values are subsequently compared to allowable strains. For the BISAR calculations, the pavement construction is divided into three horizontal layers: asphalt, unbound granular base and subgrade. All materials in the pavement are assumed to be linear elastic. The elastic properties of each of the materials are expressed by constant values of Young's modulus E and Poisson's ratio ν. For the subgrade, the E_3-modulus should be obtained from dynamic deflection measurements or from cyclic load triaxial tests. Alternatively, when results of these sophisticated testing techniques are not available, E_3 can be estimated from the CBR-value of the subgrade according to E = 10 CBR (see Paragraph 2.7.2). The stiffness of the the granular base E_2 is considered to be a function of the thickness of the base layer and of E_3 (see paragraph 2.7.3). The stiffness of the asphalt layer E_1 is estimated from mix-properties of the asphalt, such as type of bitumen and void content. Poisson's ratio ν is simply chosen at a constant value for each of the layers.

The BISAR-program allows for calculation of stresses and strains at any given point in the pavement structure. The Shell Pavement Design Manual considers two strains to be of critical importance to the design (see Figure 2.13). Limits are set to the horizontal tensile

strain at the bottom of the asphalt layer (to limit asphalt fatigue cracking) and to the vertical compressive strain at the top of the subgrade (to prevent excessive permanent deformation). In the manual, allowable values of strain are given as a function of number of load applications, for two types of asphalt and one type of subgrade. The design method also allows for the use of other relationships between the allowable strain and the number of load applications.

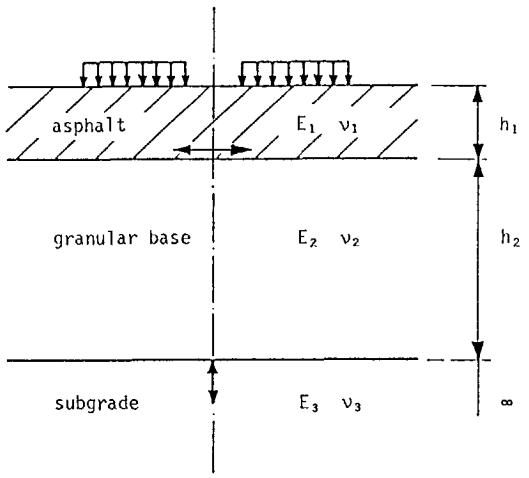

Figure 2.13: Principle of the Shell pavement design method.

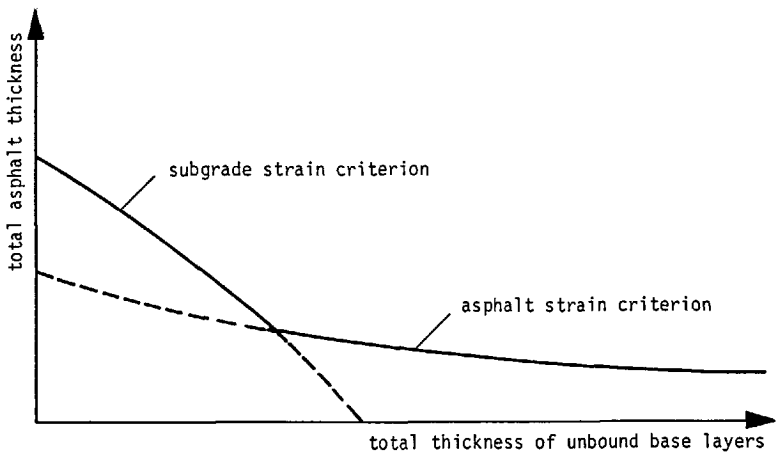

Figure 2.14: Simplified design curve from Shell Pavement Design Manual (after [S 01]).

To circumvent the necessity of the use of a computer capable of running BISAR by each user of the Shell design method, the manual contains a large number of design charts. For a large number of combinations of subgrade modulus, temperature, asphalt stiffness and asphalt fatigue characteristics ready made design charts are given in the guide that allow for obtaining directly the required layer thicknesses as a function of the number of load applications. Figure 2.14 shows a simplified design curve. For a given number of standard axle loads, subgrade support, temperature and asphalt mix the required total thickness of the asphalt layers and the unbound base layers can be read directly from the chart. A particular design curve is generally made up of two differently shaped curves, associated with the two failure criteria.

In the Addendum to the Shell Pavement Design Manual [96], some shortcomings of the original manual are recognized and correction formulae are given. Subgrade strain criteria with a higher confidence level than those of the original manual are given and a method is presented that allows for the use of stiffness values E_2 for the granular base that deviate from those used in the original manual. The latter correction should deal with one of the major drawbacks of the original manual, being the fixed ratio between the stiffness of the granular base E_2 and that of the subgrade E_3. As discussed in Paragraph 2.7.3, the original Shell Manual considers E_2 to be a straightforward function of E_3 and the thickness of the granular base h_2, according to

$$E_2 = k \times E_3 \quad \text{with} \quad k = 0.2\, h_2^{0.45} \text{ and } 2 < k < 4 \qquad (2.43)$$

This approach of fixed modular ratios stems from the work of Heukelom et al. [67, 69], which has been discussed in detail in Paragraph 2-.7.3. As discussed there, the measurements and theoretical considerations on which fixed E_2/E_3 ratios were based are incorrect by today's state of the art in pavement engineering. From a practical point of view, fixed modular ratios as indicated by Equation 2.43 are also incorrect. Equation 2.43 would mean that a base of high quality material like limestone would have the same stiffness as a base of a low quality material like river gravel when built at the same thickness on the same subgrade.

In the Addendum to the Shell Pavement Design Manual, this drawback of fixed modular ratios E_2/E_3 is recognized and a method is presented that allows for the use of other E_2 values in the design than those dictated by the rigid Equation 2.43. The Addendum suggests that if the designer wishes to use different E_2 values than those obtained from Equation 2.43, he can simply do this by entering fictitious values for E_3 or h_2 into the design. Equation 2.43, which is incorporated in the design method, than automatically adjusts E_2 to the desired level. This, however, means that E_3 and h_2 themselves do nòt have a significant influence on the design parameter (asphalt tensile strain or subgrade compressive strain) at hand, otherwise the use of fictitious values for these parameters would not be allowed. Looking at asphalt tensile strain, for instance, the Addendum states that indeed E_3 does not have a significant influence on that parameter. Where E_3 from the design charts seems to have an influence on asphalt tensile strain, it is in fact the influence of E_2 showing up. An increase in E_3 will lead - through Equation 2.43 - to an increase in E_2, and thàt increase will reduce asphalt tensile strain. However, if this is so, then of course E_2 should have been the entry into the calculation of asphalt tensile strain from the beginning, rather than E_3. The only correct approach of course is to have separate entries into the design for E_1, E_3 ànd E_2.

Brown and Barksdale [97] noted the method of fictitious E_3 and h_2 values presented in the Addendum to be a cumbersome one, dictated by the need to apply it within the existing design method. It clearly illustrates the constraints of using a chart based method rather than a computer program. The use of a separate entry for E_2, which is actually needed, would have rendered the whole set of design charts useless and with it the original Shell Pavement Design Manual itself. The widespread use of computer hardware capable of running programs like BISAR nowadays allows for a shift to computer program based design methods, that do allow for separate entries for the stiffness of all layers and for an even further refinement of design.

2.9.3.2 THE SOUTH AFRICAN METHOD

The South African method for the design of flexible pavements [91] is the most extensively validated mechanistic design procedure. Its

analytical basis is quite similar to that of the Shell Pavement Design Manual, in the sense that the African method too is based on calculations of strains in the pavement construction and limiting the calculated strains to allowable values. The method however truly is a mechanistic design procedure, since in-situ testing of pavements to determine their long term performance has been used extensively to validate and refine the design method. The analytically obtained pavement response to a standard axle load has thus been translated to in-situ pavement performance under actual traffic. The required in-situ performance data have been obtained by monitoring long term pavement performance under normal traffic and by extensive accelerated loading testing using a fleet of four Heavy Vehicle Simulators. These apparatus allow for application of large numbers of heavy axle loads within the short time of a few months.

The design procedure itself consists of the following steps:

1 The road to be designed is classified into one of three categories, dependent on its importance, required service level and traffic intensity.

2 The cumulative equivalent traffic, expressed in 80 kN standard axle loads, is classified into one of five categories.

3 The elastic properties (E-modulus) of the subgrade are estimated from its soaked CBR value, using a factor of proportionality dependent on the soil type.

4 For the granular base, recommended values of the resilient modulus to be used in the design calculation are given in the design procedure, dependent on the quality of the material. Also, allowable values of shear stresses are given, including a safety factor dependent on the road category.

5 For the asphalt, stiffness is given as a function of type of asphalt, temperature, speed of loading and depth below surface.

6 With the material parameters obtained, a structural analysis calculating strains caused by a standard wheel load is performed. At present, linear elastic theory is used for these calculations, but

finite element methods are being developed. The calculated values of strains are subsequently compared to allowable values of strains (horizontal tensile strain at the bottom of the asphalt layer and vertical compressive strain at the top of the subgrade). For these strains, allowable values are given in the guide, dependent on the number of load applications and the road category.

7 To circumvent the necessity for making computer calculations by each designer, standard designs are given in the guidelines for each combination of road and traffic category. These standard designs have been verified using extensive in-situ monitoring under normal and accelerated loading.

2.9.4 Pavement design procedures employed in the tropics

2.9.4.1 INTRODUCTION

The conditions of traffic and climate for which pavements are designed in the tropics are quite different from the conditions in the temperate zone areas of Europe and North America. Traffic is far less intense, sometimes as low as a few vehicles per day, and traffic does not put as stringent demands on riding quality as it does in temperate zones. The main function of the road is establishing a connection between two places, without questioning how long it will take or how comfortable and safe it will be to travel between them. Conditions of climate are different too: especially the heavy, concentrated rainfall in tropical areas makes cross-section design completely different from that in temperate zone areas. Economic aspects also play an important role; most third world countries simply cannot afford to build roads to western standards.

Especially for economic reasons, most countries in the tropics rely heavily on local, low cost materials for pavement construction. Laterites are by far the most widely used material in pavement construction and the layers of this material form the main structural element of the pavement. The asphalt cover is often limited to a surface seal, with the main function of preventing water ingress into the laterite layers. Alternatively, the bituminous cover is omitted altogether and the laterite layers are trafficked directly.

The design of such pavements is of course not a mechanistic one, based on structural analysis. The design methods used are based on empirical knowledge. In certain areas, empirical procedures developed for temperate zone areas are used without modification, while in others pavement design procedures developed especially for tropical regions are used. Major parts of Central and South America still use the AASHTO Interim Guide for the Design of Pavement Structures [9], which has meanwhile been succeeded by its final version [4]. Two widely used tropical pavement design procedures are the UK-developed Road Note 31-method and the USA-developed Tropical Design Procedure. Although developed by temperate zone agencies, these method pertain especially to tropical areas, both allowing for local materials like laterites to be used in the design of pavements with or without bituminous cover. The principles of these two methods will be described in brief in this paragraph.

2.9.4.2 THE ROAD NOTE 31-METHOD

Road Note 31 "A guide to the structural design of bitumen-surfaced roads in tropical and sub-tropical countries" [10] was first published by the Transport and Road Research Laboratory in 1962, and later revised in 1966 and 1977. It is appropriate for roads which are required to carry up to an average of 1500 heavy vehicles per day, thereby incorporating most non-urban roads in tropical areas. For heavier trafficked roads, reference is made in the guide to Road Note 29 [94], which was at that time the temperate zone design procedure used in the UK itself. Road Note 31 puts special emphasis on two aspects of pavement design which are of major importance in the design of roads for tropical areas. It gives a detailed procedure to estimate the moisture content at which the bearing capacity of the subgrade should be determined and it allows for a stage-construction approach, so that uncertainties in estimating the number of standard axle loads to be carried can be dealt with better.

The Road Note 31 procedure itself contains the following steps:

1 The bearing capacity of the subgrade is determined using the CBR-test, to be carried out on the soil in the wettest condition likely to occur.

2 The bituminous surfacing is fixed in Road Note 31: it is either a surface dressing (non-structural spray-and-chip treatment) or for heavier trafficked roads a 50 mm layer of premixed bituminous material.

3 The thickness of the unbound granular base is also fixed: dependent on the number of standard axles to be carried, either a 150 mm or a 200 mm base layer is prescribed.

4 The only real design-variable is the thickness of the sub-base, which can be read directly from a design chart having the CBR of the subgrade and the number of standard axles as input.

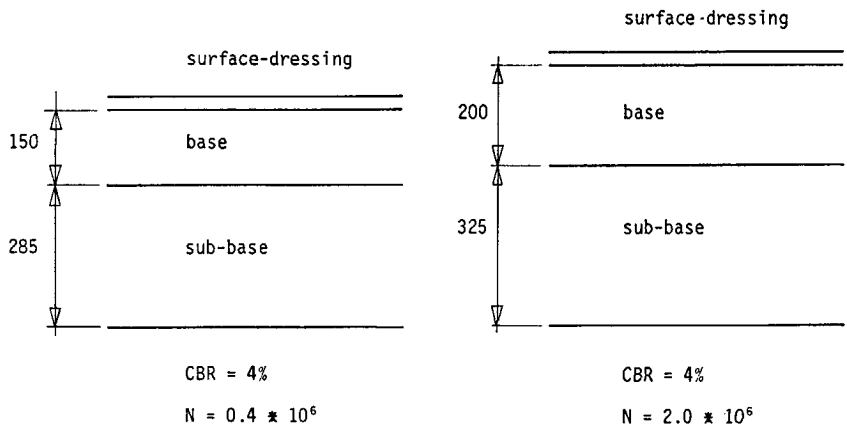

Figure 2.15: Results of Road Note 31-method: pavements for N = 0.4 × 10^6 and N = 2.0 × 10^6 18 kip (82 kN) SAL, for a subgrade of CBR = 4% (layer thickness in mm).

The difference between this tropical design procedure and temperate zone procedures described before is clear: rather than having the design-variable in the thickness of the bituminous layers, this tropical procedure has its design-variable in the thickness of the sub-base layer built from locally occurring natural materials, and clearly reduces the structural dependency on the expensive bituminous materials. As an illustration of this, Figure 2.15 shows the outcome of the Road Note 31 procedure for pavements designed for 0.4 × 10^6 and 2.0 × 10^6 18 kip (82 kN) standard axle loads, on a subgrade of CBR = 4%. The structural elements of the pavement are the base (built of for instance high quality laterite) and the sub-base (built of for

instance lower quality laterite). The surface dressing (spray-and-chip) has no structural function; it merely protects the lower pavement layers from the ingress of water and provides for skid resistance. An increase in the number of standard axle loads to be carried is met by increasing base and sub-base thickness, rather than increasing the thickness of the bituminous cover.

2.9.4.3 THE USAID TROPICAL DESIGN PROCEDURE

The USAID Tropical Design Procedure [29] was developed by the United States Agency for International Development on the basis of studies in Thailand [27], Ghana [28] and Brazil [29]. It is based on the AASHTO Interim Guide for the Design of Pavement Structures [9], using the approach of a structural number SN following from the number of standard axle loads to be carried and the subgrade support, expressed as CBR. The required structural number SN is then met by applying a number of pavement layers; the contribution of each layer to the total structural number is obtained as the product of layer thickness and "layer coefficient", which is a measure of the ability of a material to function as a structural component of the pavement.

As noted, the USAID-procedure is in principle quite similar to the AASHTO Interim Guide-procedure and thus to the final AASHTO Guide procedure described in Paragraph 2.9.2.3. It will therefore not be further detailed here. A major improvement to the AASHTO Interim Guide is that in the USAID-procedure the layer coefficients are an absolute function of material quality. In the AASHTO-Interim Guide, a material was ranked between the best and the poorest material locally available and hence the layer coefficients were only a relative function of material quality. An improvement with respect to application in tropical areas is that the USAID method also allows for the design of pavements without a structurally important bituminous cover. As was the case with the Road Note 31-method, the USAID procedure also allows for an extensive use of locally occurring unbound materials, thereby reducing the need for bituminous materials.

2.9.5 Role of granular materials in flexible pavement design

In many of the mechanistic pavement design procedures used today granular materials do not feature strongly. These design procedures focus on designing the asphalt layer, given the subgrade conditions. The main structural element of the pavement is the asphalt layer and the significance of the unbound granular base is virtually reduced to that of a working platform. The Shell Pavement Design Manual is a clear illustration of this: through the fixed E_2/E_3 relationship, the structural contribution of the unbound granular base is limited and granular materials hardly play a role in the design. Illustrative of this that in their analysis of seven years experience with the structural aspects of the Shell Pavement Design Manual, Gerritsen and Koole (98) used only full-depth asphalt constructions for the detailed case studies carried out.

In the empirical pavement design procedures employed in the tropics, the main structural element of the pavement is formed by granular layers. Here it is the asphalt cover that has a strongly reduced function. In most cases the asphalt cover only provides a seal against water ingress and often the asphalt cover is omitted altogether. Such roads are designed for very low traffic intensities and the demands on riding quality and skidding resistance are far lower than those for major roads in temperate zone areas. However, the thoroughly validated South-African catalogue of designs (91) incorporates pavements with very thin asphalt covers and thick granular layers for major inter-urban roads. For instance, for the highest road category with respect to service level, and for 12 - 50 $\times$ 10^6 80 kN standard axle loads, a pavement is prescribed of 50 mm asphalt on 150 mm "Waterbound macadam" (see Paragraph 3.4) on 300 mm cement-treated gravel. Clearly, the asphalt layer here has a very limited structural function and the cement-treated and the unbound granular layer form the main structural elements.

The reason why granular materials do not feature strongly in most temperate zone mechanistic design procedures is two-fold:

- Granular materials show a marked moisture-dependent mechanical behaviour. The phenomena governing this dependency are not yet fully understood and the mechanical parameters needed for pavement design

are, therefore, determined in the worst possible condition. Clearly, this may lead to a conservative design underestimating the structural role of the granular layer.

- Granular materials show a complex stress-dependent behaviour. Determination of fundamental stress-strain parameters requires complicated testing techniques. Complex material and pavement models are required to incorporate stress-dependency in the design. Since these requirements are often not met, pavement engineering practice again leads to a conservative design by attributing only a limited structural role to the granular layers in the pavement.

In summary, unbound granular materials are at present often not used to their fullest extend. More detailed information on their stress- and moisture-dependent behaviour is needed, and sound laboratory and in-situ testing techniques are required to determine fundamental stress-strain properties of these materials. This study aims at providing such information and at development of testing techniques for unbound granular materials that on the one hand are fundamentally sound and on the other hand are simplified to an extend that allows for implementation in every-day practice of pavement engineering.

2.9.6 Validation of design procedures

Empirical pavement design procedures are based on long-term experience with the performance of pavement constructions under the influence of traffic and climate. Mechanistic pavement design procedures are not based on such experience but on structural analysis of the pavement construction. Often, they are based on the calculation of stresses and strains in the pavement construction under a single loading and on subsequent extrapolation of this response to a single loading to long-term performance under the influence of traffic and climate.

Clearly, these mechanistic pavement design procedures need validation with in-service long-term performance data. This can on the one hand be done by analysing pavements designed according to empirical procedures, thereby in fact using experience gathered in the past to validate the newly developed mechanistic methods. When, however, mechanistic methods are developed for new conditions like heavier axle

loads or new materials, then the use of existing experience is no longer possible. Then, new information on the long-term structural performance of pavements is required. Since pavements are designed for periods of, for instance, 20 years, validation and adjustment of mechanistic design procedures on the basis of only long-term performance studies of pavements under actual traffic would require far too much time. Therefore, accelerated loading testing with, for instance, simulation of 20 years traffic in a few months time is required in addition to the long-term performance studies.

The need for long-term performance studies and accelerated loading testing cannot be stressed enough. Any structural analysis, however poor, will result in a pavement design, but certainly pavements cannot be properly designed on a single calculation of the pavement response expressed in stresses and strains to a single loading. Too many assumptions and uncertainties lie at the basis of the analytical determination of the pavement response and the required layer thicknesses to rely simply on the structural analysis for pavement design. In reality, materials do not show linear elastic behaviour, they are not homogeneous and isotropic, moduli cannot be estimated from simple tests like the CBR-test, allowable stresses and strains cannot simply be estimated from nomographs and, finally, the contractor's work will show considerable scatter along the length and even the width of the road.

The translation of the analytically determined pavement response to long-term performance under actual traffic therefore forms an essential part of mechanistic design procedures. Much effort is therefore spent throughout the world on validation and adjustment of these methods. The Long Term Pavement Performance studies being carried out under the Strategic Highway Research Program in the USA will produce extensive data in the years to come on in-service performance under actual traffic of a wide variety of pavement designs. Accelerated loading testing of pavements is increasing rapidly. This form of pavement research, spearheaded by the South Africans with their Heavy Vehicle Simulators, is presently being carried out in Australia and the USA using so-called Accelerated Loading Facilities "ALF". In the UK, the Transport and Road Research Laboratory has recently acquired its Pavement Test Facility, which is a large scale version of the Pavement Test Facility that has been used at Nottingham University for

a number of years. The Laboratoire des Ponts et Chaussées at Nantes in France has to its availability the so-called "Manège de Fatigue", which is a circular accelerated loading facility similar to the equipment available at Zürich in Switzerland. Finally, in the Netherlands a Linear Tracking Apparatus similar to the TRRL-facility is at the time writing of this dissertation being built at Delft University of Technology in the wake of the research project described in this dissertation (99).

The fact that all the research agencies mentioned have made large investments into accelerated loading facilities and yearly spend large amounts of money running these facilities clearly underlines the increasing importance of this type of research. Coupled with long-term performance studies of in-service pavements, these accelerated loading investigations will contribute significantly to the further development of mechanistic design procedures.

3 MATERIAL SPECIFICATIONS

3.1 INTRODUCTION

In the temperate zone areas of Europe and North America, most countries have their own specifications for unbound road building materials. This is partly due to local availability of materials. In the Netherlands, for instance, no suitable outcrops of bedrock exist and material specifications therefore have to allow for the use of river gravels, sands and recycled materials like crushed concrete. The climate also plays a role here. The severe winter conditions occurring in Canada and the northern states of the USA put more stringent demands on the materials to be used as compared to those used in the more moderate climates. A third factor causing differences in materials specifications is the available testing equipment. Even relatively simple equipment like sieves may differ from one country to another, causing a difference in grading specifications.

Most of the specifications presently available are recipe specifications, which prescribe, for instance, the grading and the composition of the material (see Table 2.1, Paragraph 2.3). Few specifications incorporate "end-product" properties based on testing of the laid-and-compacted granular materials, such as shear strength, stiffness and permeability. The only mechanical property often specified is resistance to degradation; a whole range of different tests, however, is used to establish some measure of this resistance.

The fact that most specifications are recipe based rather than end-product based finds its origin in the background of the specifications. Most specifications are empirically based. They were developed from experience with a certain range of materials and this range was laid down in the recipe specifications simply to prevent materials outside the range being used. Specifications are, therefore, often based on "what is available" and "what can be made" rather than on "what is needed" and "what should be made". This, first of all, leads to a technical disadvantage; materials may very well not be used to their fullest extend under the present specifications. Secondly,

introduction of new materials is strongly inhibited by recipe specifications, since these materials often do not fall into the range of materials on which the recipe specifications are based. Thirdly, international exchangeability of recipe specifications is difficult, since the available materials and construction practice differ considerably from one country to another.

What is really needed are end-product specifications, that prescribe relevant mechanical parameters like stiffness, preferably measured in-situ on the laid-and-compacted material. Such specifications may be supplemented by recipe specifications prescribing, for instance, material composition and grading in order not to loose completely the bonds with experience regarding long-term behaviour. The German pavement design practice incorporates such an approach; the materials themselves are recipe specified and the laid-and-compacted material is tested in-situ using Plate Bearing Tests to determine whether the required stiffness has been met. As discussed in Paragraph 2.9.2.4, however, the practicality of this approach is limited because of the cumbersome method used to determine in-situ stiffness.

Fast and easy to perform in-situ testing techniques as described in detail in Chapter 8 of this dissertation may open the way to specifications based on mechanical properties. It should be stressed that some form of recipe specification prescribing the materials themselves will still be needed, since the in-situ tests only determine the momentary condition of the material in-situ and at best only estimate long term behaviour. As in the actual design of pavements, knowledge about long-term performance is essential to good engineering practice. For new materials for which little or no experience is available, fundamentally sound laboratory tests simulating in-situ conditions can be used to estimate long-term in-situ performance, without having to actually build and monitor test pavements. Such testing techniques will be described in detail in Chapter 5.

In tropical areas, some countries have their own specifications. Most countries, however, rely on specifications developed for tropical areas by agencies from the temperate zone areas, or simply use temperate zone specifications without modifications. The latter case may lead to major errors, since construction practice and conditions of climate and traffic are quite different in tropical areas.

This chapter will deal with the materials specifications for temperate zone areas and for tropical areas separately. In addition, the South African specifications for "Waterbound Macadam" will be dealt with, because of the interesting special nature of this material.

3.2 MATERIAL SPECIFICATIONS FOR TEMPERATE ZONE AREAS

As stated, specifications for unbound road building materials may differ considerably from one country to another. The main reason for this is that the specifications are often production-oriented. As stated earlier, specifications are often based on local availability of materials and production equipment. The differences in applied testing techniques and equipment make any attempt at a detailed comparison of the various specifications fruitless beforehand. Therefore, a detailed listing of material specifications from temperate zone countries will be omitted here and comparison of specifications will only be done for parameters that can be reasonably compared, such as composition and grading.

Table 3.1 shows the material specifications with respect to composition, used in the Netherlands, the UK and the USA. The Dutch specifications prescribe "crushed stone" for unbound granular bases, but in addition to lava also blast furnace slag and recycled materials like crushed concrete, crushed masonry and mixtures of these two are widely used in unbound granular bases. For these crushed rubble materials, additional specifications have been developed [14]. The British specifications distinguish three material qualities: "Wet-mix Macadam" for unbound granular base layers and "Type 1" and "Type 2" materials for sub-base layers. The USA-specifications shown in Table 3.1 are the general AASHTO-specifications. It should be borne in mind the most states in the USA have specifications of their own.

Table 3.1: Composition specifications used in the Netherlands, the UK and the USA

country	the Netherlands	UK	USA
specifications	Eisen 1978	DOT	AASHTO
reference	[7]	[19]	[8]
unbound granular base	crushed stone	"Wet-mix Macadam" crushed rock crushed slag	stone gravel slag
sub-base		"Type 1": crushed rock crushed slag crushed concrete shale "Type 2": natural sands gravel crushed rock crushed slag crushed concrete shale	

Table 3.2 shows the materials specifications with respect to grading as used in the Netherlands. Three nominal gradings are distinguished: 0/40 mm, 0/80 mm and 20/80 mm. In practice, only the 0/40 mm grading is used for unbound base course materials.Table 3.3 shows the materials specifications with respect to grading as used in the UK, for the Wet-mix Macadam unbound base course material and for the Type 1 and Type 2 sub-base materials.

Table 3.2: Grading specifications used in the Netherlands [7]

sieve [mm]	mass percent passing [%]		
	nominal grading		
	0/40	0/80	20/80
90		90 - 100	90 - 100
45	90 - 100		50 - 80
31.5		60 - 90	
16	60 - 90		
8		30 - 60	
4	30 - 60		
2	20 - 50	15 - 45	
0.063	0 - 8	0 - 8	0 - 8

Table 3.3: Grading specifications used in the UK [19]

sieve [mm]	Mass percent passing [%]		
	material		
	Wet-mix Macadam	Sub-base Type 1	Sub-base Type 2
75		100	100
50	100		
37.5	95 - 100	85 - 100	85 - 100
20	60 - 80		
10	40 - 60	40 - 70	45 - 100
5	25 - 40	25 - 45	25 - 85
2.36	15 - 30		
0.600	8 - 22	8 - 22	8 - 45
0.075	0 - 8	0 - 10	0 - 10

Table 3.4 shows the materials specifications with respect to grading as used in the USA. Six gradings are distinguished, ranging from a coarse graded unbound base course material to a sand-sized grading. The AASHTO-specifications allow for the use of all these gradings in unbound base and sub-base courses.

Table 3.4: Grading specifications used in the USA (8)

sieve [mm]	mass percent passing [%]					
	grading					
	A	B	C	D	E	F
50	100	100				
25.0		75-95	100	100	100	100
9.5	30-65	40-75	50-85	60-100		
4.75	25-55	30-60	35-65	50-85	50-100	70-100
2.00	15-40	20-45	25-50	40-70	40-100	55-100
0.425	8-20	15-30	15-30	25-45	20-50	30-70
0.075	2-8	5-20	5-15	5-20	6-20	8-25

Comparison of the Dutch, British and USA grading specifications (Tables 3.2 - 3.4) shows that, even for a relatively simple material property like the particle size distribution, it is not possible to make an exact comparison. Firstly, the denomination of the materials is different in the three countries. The UK specifications clearly distinguish between unbound base and sub-base materials, whereas the Dutch and USA specifications do not. Secondly, the three countries each use different standard sieves. The Netherlands uses ISO-sieves, the UK British Standard sieves and the USA ASTM sieves. As an example, the amount of fines is therefore specified in the Netherlands as the fraction passing the 63 µm sieve, whereas the UK and the USA specify the fraction passing the 75 µm sieve. For the coarser fractions too, different sieve sizes are used in the three countries.

An exact comparison of grading specifications being impossible, only an illustrative comparison will be made here. Figure 3.1 shows the Dutch 0/40-grading, the British Wet-mix Macadam-grading and the USA A-grading. As can be seen from Figure 3.1, the UK specification is by far the most stringent. The Dutch specifications allow for quite a wide range of gradings for unbound base coarse materials: in a 0/40 mm material, 50% sand sized (0-2 mm) material is allowed. The USA A-grading specifies coarser graded material than does the Dutch 0/40-grading; however since all A-F gradings (see Table 3.4) are allowed in unbound base courses, in fact even a 100% sand-sized material (E- and F-grading) could be used as an unbound base course material.

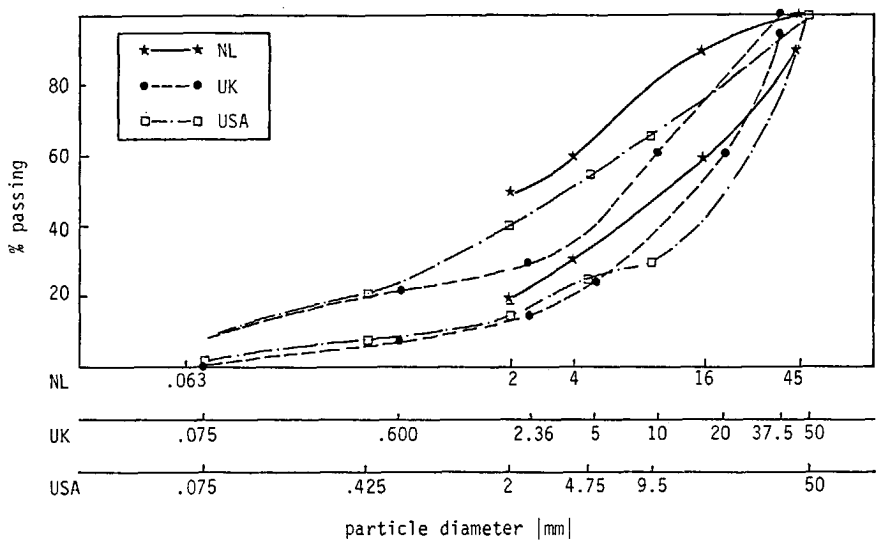

Figure 3.1: Comparison of Dutch 0/40, British Wet-mix Macadam and USA A-grading specifications.

3.3 MATERIAL SPECIFICATIONS FOR TROPICAL AREAS

As noted when discussing tropical pavement design procedures (Paragraph 2.9.4), pavement design and construction practice in the tropics differs considerably from that in temperature zone areas. The standards to which the road is built are mostly far lower then in temperate zone areas and the funds available are often limited. Hence,

locally occuring materials like laterite are used extensively as road construction material in tropical areas.

Because of the major differences in pavement design and construction, special material specifications should be available for tropical areas. However, since many tropical countries use pavement design procedures from temperate zone areas, the specifications from these areas are also applied. For instance, many countries in South America use the AASHTO Interim Guide for the Design of Pavement Structures (9) and, therefore, also apply the AASHTO specifications discussed in the previous paragraph. If these temperate zone specifications are applied stringently, the use of locally occurring quartzitic or lateritic gravels in the construction of unbound base courses is excluded, since these natural materials do not meet the specifications. Crushed stone materials then have to be used, resulting in a significant increase in costs. Therefore, in many tropical countries that use temperate zone specifications, a certain relaxation of these specifications is allowed, based on engineering judgement and local experience (100).

Relaxation of temperate zone specifications for use in tropical areas may do very well, if such a relaxation is properly documented in local specifications. On-the-job relaxation of specifications, however, is an undesirable practice. This may soon lead to the use of almost any locally available material. The laterites used in the testing program for this dissertation, for instance, were sampled from the materials used in the construction of a road in Suriname, South America. Here, too, proper specifications were lacking and local availability and engineering judgement were the main criteria for selecting the materials. As will be discussed when describing these laterites in Chapter 4, major failures resulted from this on-the-job relaxation of specifications. In summary, temperate zone specifications can and should be relaxed before application in tropical areas, but this relaxation should be well documented and be based on local research and experience. In their study of laterites in road constructions, for instance, Morin and Todor (29) suggested such an adaptation of the AASHTO-specifications to tropical conditions. They proposed broader limits for grading and Atterberg limits than those given in the temperate zone AASHTO specifications. This relaxation, however, necessitated the introduction of a minimum CBR-requirement to prevent application of unsuitable materials.

Many former UK-colonies use Road Note 31 "A Guide for the Structural Design of Bitumen Surfaced Roads in Tropical and Subtropical Countries" [10] for pavement design. As indicated in the title, the Guide was developed especially for use in tropical and subtropical areas. In addition to guides for the design of pavements, it also contains material specifications. For unbound base course materials, the Guide prescribes natural gravels or crushed stone materials. The natural gravels may be lateritic or quartzitic gravels, river gravels, decomposed rock or corals. They should have a grading that is "mechanically-stable"; typical limits of particle size distributions for mechanically-stable natural gravel are given in the Guide. The Atterberg limits of the fine fraction of the materials are specified and a minimum soaked-CBR of 80% is required. The crushed stone materials specified in Road Note 31 can be "Waterbound Macadam" (single sized stone 37.5 - 50 mm with fines rolled and washed into it), "Dry Bound Macadam" (single sized crushed stone 37.5 - 50 mm with crushed rock particles with d < 5 mm vibrated into it) or graded stone with d < 37.5 - 50 mm. CBR testing of the crushed stone materials can be omitted, since they easily achieve the required soaked-CBR of 80%. For sub-base materials, Road Note 31 specifies naturally occurring gravel or gravel/sand/clay mixtures (including laterites). A minimum CBR of 25% (at field water content and density) is required. For the deeper part of the sub-base, this CBR-requirement may be relaxed in case of material scarcity, provided the materials have a CBR of at least 8% when tested at the worst moisture conditions likely to occur.

3.4 THE SOUTH-AFRICAN "WATERBOUND MACADAM"-SPECIFICATIONS

As discussed in the previous paragraph, Road Note 31 allows for the use of "Waterbound Macadam" as a base course material. The concept of this material is the combination of coarse and fine material, placed in the base in two shifts. The coarse fraction is first layed and rolled, after which the fine material is rolled and washed with a surplus of water into the coarse material. In this way, a rigid skeleton of coarse particles is obtained, the voids of which are filled with fines. As will be discussed in Chapter 6, these fines generate high levels of soil suction when the material is dry, thereby

substantially increasing the strength and the stiffness of the material.

The South-African "Guidelines for Road Construction Materials TRH 14" [101] give detailed specifications for such "waterbound" materials. Table 3.5 shows the grading specifications for the coarse and the fine fraction of "Waterbound Macadam". The coarse fraction should consist of crushed rock, whereas the fine fraction should consist of crusher fines (high quality Waterbound Macadam WM1) or soil filler (lower quality Waterbound Macadam WM2). For the fine fraction, the Liquid Limit, Plasticity Index and Linear Shrinkage are specified.

Table 3.5: Grading specifications for coarse and fine fraction of Waterbound Macadam [101]

sieve [mm]	mass percent passing [%]		
	coarse fraction		fine fraction
75.0	100	100	
53.0	85 - 100	85 - 100	
37.5	35 - 70	0 - 30	
26.5	0 - 15	0 - 5	
19.0	0 - 5		
9.5			100
4.75			85 - 100
0.075			10 - 25

The "Guidelines for road construction materials TRH 14" also give specifications for other granular base course materials such as graded crushed stone, natural gravels and gravel-soil mixtures. These specifications will not be detailed here since these materials are rather straightforward base course materials and, hence, do not merit special attention.

3.5 CONCLUSION

Material specifications from temperate zone areas and from tropical areas were discussed in this chapter. In addition, the South-African specifications for the "waterbound macadam" granular base course material were discussed. The following conclusions can be drawn:

1. Comparison of specifications from different countries is hardly feasible, since most specifications are based on local testing techniques that differ from one country to another. Even grading specifications cannot be compared numerically because of differences in the sieves which are used.

2. Tropical countries often use specifications from temperate zone areas in conjunction with the pavement design procedures from these areas. In practice, a certain relaxation mainly based on local availability of materials is then allowed to these specifications. This is an undesirable practice. A relaxation of specifications can be necessary, but it should be well documented and based on local research and sound engineering judgement.

3. Almost all specifications presently available are of the recipe type, prescribing what the material should consist of, rather than prescribing its mechanical properties. Most specifications are empirically based and are, therefore, not open to new materials. International exchangability of specifications based on local experience is limited.

4. Specifications should be based on the required mechanical properties of the laid-and-compacted materials. Such end-product specifications could prescribe engineering properties such as shear strength, stiffness and permeability. End-product specifications are more open to new materials and are internationally exchangable, provided the engineering characteristics prescribed are expressed in sound engineering parameters.

5. The introduction of end-product specifications requires fast and simple in-situ testing techniques for establishing whether or not

the specified engineering characteristics are met by the laid-and-compacted material.

6. Since in-situ testing only establishes the momentary condition of the materials, end-product specifications should still be accompanied by a reduced set of recipe specifications to ensure proper long-term functioning of the materials. Both the end-product and the recipe specifications should be limited to relevant characteristics of the materials. The contractor should not be bound too much by over-detailed specifications excluding all possibilities of applying new materials or construction techniques.

4 MATERIALS USED IN TEST PROGRAM

4.1 INTRODUCTION

Most of the pavement design procedures presently being used still rely on standard testing techniques for the determination of strength and stiffness parameters of unbound road building materials. As far as empirical pavement design procedures are concerned, the use of these standard testing techniques is allowed within the limits of the experience on which design and testing techniques were developed. When switching, however, to mechanistic design procedures, fundamentally sound material parameters are required to characterize material strength and stiffness for input to the calculation of stresses and strains in pavements. As discussed in Chapter 2 and as will be shown in Chapter 5, such fundamental material parameters like, for instance, Young's E-modulus cannot be measured in standard testing techniques like the CBR-test.

Chapter 5 of this dissertation will deal in great detail with both standard testing techniques and fundamentally sound testing techniques like the cyclic load triaxial test. The shortcomings of the use of the standard testing techniques for assessing fundamental material parameters will be discussed and suggestions will be made for testing techniques that allow for accurate determination of fundamental material parameters with more or less standard laboratory equipment. To assess the applicability of the various types of tests, a wide variation of materials was incorporated in the test program. The materials investigated can be divided into four groups:

- Group C: conventional unbound granular base course materials like lava and limestone
- Group R: recycled unbound granular base course materials like crushed concrete and waste incineration slag
- Group S: sands
- Group L: laterites.

The main emphasis of the research described here lies with the conventional and recycled unbound granular materials, because of the structural importance of these materials. The sands were investigated because of their wide-spread use in sub-bases of major roads in the Netherlands. Furthermore, the sands were used in pilot-testing for reasons of practicability like, for instance, specimen size in cyclic load triaxial testing. The laterites were investigated since they form the main base and sub-base material in the tropics. The testing of laterites focussed on their explicit water-dependent behaviour.

To study the influence of grading and composition, part of the unbound base course materials from groups C and R were tested at different laboratory-made gradings and compositions. In addition, materials as-produced by crusher plants were tested as such. The sands and the laterites were tested at their natural grading and composition.

The four material groups C, R, S and L will be dealt with separately in this chapter. For each of the groups, the origin of the materials will be described. A list of the materials will be given, together with the codes used to denominate the materials throughout this dissertation. These material codes are the abbreviation of the Dutch names of the materials. For convenience, the codes and the Dutch and English names of the materials tested are summarized in Appendix 1. Detailed information on the grading and the results of standard tests are given in Appendix 2.

4.2 CONVENTIONAL UNBOUND GRANULAR BASE COURSE MATERIALS

4.2.1 Introduction

In Group C: conventional unbound granular base course materials, the following materials were investigated:

- lava
- stol (a natural gravel/loam mixture)
- porphyry
- limestone
- crushed gravel
- silicon-manganese slag.

Of these materials, only lava has been used widely in the Netherlands in granular base courses. Stol has been applied occasionally. Porphyry, limestone and crushed gravel were included in this research to expand the number of crushed stone materials and to obtain a reference with foreign road building practice. The industrial by-product silicon-manganese slag was included to investigate its potential as an unbound road base material.

4.2.2 Origin of the materials

The origin of the materials tested in Group C is as follows:

- lava was obtained from a quarry in the German Eifel-area
- stol was obtained from natural deposits in Limburg in the Netherlands
- porphyry was obtained from a quarry in Belgium
- limestone was obtained from a quarry in Belgium
- crushed gravel was produced in the Netherlands from gravel from the river Meuse
- silicon-manganese slag is a by-product from the manganese production in Belgium.

For two reasons, the crushed stone materials in Group C were tested at two different laboratory-made gradings. Firstly, this was done to check the influence of grading on mechanical properties. Secondly, laboratory-made gradings were used since a proper comparison of the various materials can only be made if the materials are tested at the same grading. One grading was made in conformity with the upper limit of the Dutch specifications for unbound granular base course materials 0/40 mm; the other grading was made in conformity with the lower limit of these specifications. For each material investigated, several tons of material as produced by the crusher plant were sieved into a number of fractions and subsequently recombined to obtain the desired grading.

Figure 4.1 shows the upper and lower limits of the Dutch specifications for unbound granular materials 0/40 mm. Throughout this dissertation, the upper limit of the Dutch specifications will be indicated as "B"-grading (from the Dutch "Bovenkant Eisen 1978") and the lower limit as "O"-grading (from "Onderkant Eisen 1978"). As discussed

earlier in Chapter 2, these specifications only give maximum and minimum percentages at particle diameters of 2, 4, 16 and 45 mm, and a maximum percentage passing the 63 µm sieve. To increase the accuracy of making the same grading for each material, maximum and minimum percentages at 8, 22.4 and 31.5 mm were interpolated, as shown in Figure 4.1. The materials tested were thus recombined from the fractions d > 45 mm, 45 - 31.5 mm, 31.5 - 22.4 mm, 22.4 - 16 mm, 16 - 8 mm, 8 - 4 mm, 4 - 2 mm and d < 2 mm. For practical reasons, no attempt was made to also fix the percentage passing the 63 µm sieve; this percentage was determined by sieve analyses. Full details of the grading of the materials tested are given in Appendix 2. This Appendix contains a separate information sheet for each material investigated, giving details on composition, grading, density, CBR, resistance to degradation and specific gravity. The materials stol and silicon-manganese slag were tested at their as-received grading.

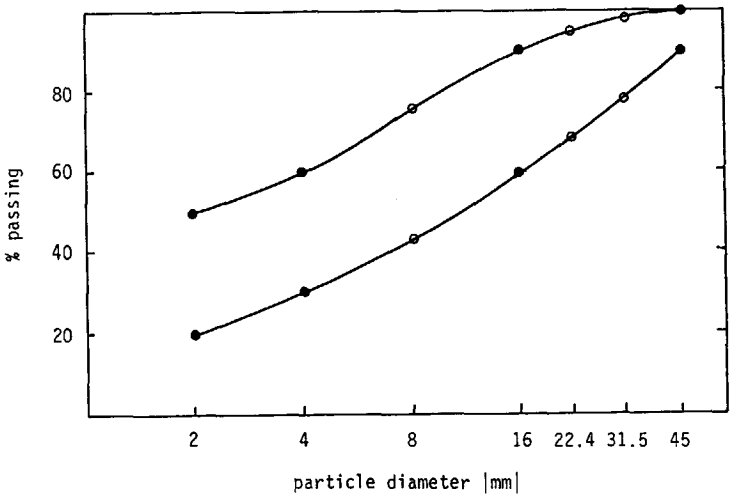

Figure 4.1: Upper and lower limit of Dutch specifications for unbound granular materials 0/40 mm.

4.2.3 The materials investigated

Table 4.1 shows the materials tested in Group C: the material number, the material name, the grading and the material code are listed in the table. For ease of survey, the materials have been numbered per group, while the material code will be used throughout this dissertation to

denote the materials. The code consists of three characters: the first two indicate the composition of the material and the third character indicates the grading. The composition code is the abbreviation of the Dutch name of the material; the grading codes are given in Table 4.2

Table 4.1: Materials tested in Group C.

material number	material name	grading	code
C01	lava	fine	LAB
C02		coarse	LAO
C03	porphyry	fine	POB
C04		coarse	POO
C05	crushed gravel	fine	GGB
C06		coarse	GGO
C07	limestone	fine	KAB
C08		coarse	KAO
C09	stol	natural	STN
C10	silicon manganese slag	commercial	SMC

Table 4.2: Grading codes.

code	grading
B	upper limit, Dutch specifications 0/40 mm
O	lower limit, Dutch specifications 0/40 mm
C	commercial, 0/40 mm
N	natural

4.3 RECYCLED UNBOUND GRANULAR BASE COURSE MATERIALS

4.3.1 Introduction

In group R: recycled unbound granular base course materials, the following materials were investigated:

- crushed masonry (two lots)
- crushed concrete (two lots)
- crushed clinker
- a mixture of 50% crushed bricks and 50% crushed concrete
- crushed rubble (three lots)
- waste incineration slag.

With the exception of the waste incineration slag, all these materials were obtained from crusher plants that recycle construction and demolition waste into granular road building materials. These types of materials have been used in increasing quantities in the Netherlands for about ten years and have since become standard materials.

Most attention in this group was given to the materials produced from construction and demolition waste, since these materials have the largest potential for replacing the classical crushed stone materials. Only one lot of waste incineration slag was investigated to check its potential as an unbound base coarse material. Although standard tests indicated this material to be of a relative good quality, the resilient stiffness of this material proved to be low. For this reason, no further testing of waste incineration slag was performed.

4.3.2 Origin of the materials

All the materials produced from construction and demolition waste were obtained from crusher plants in the Netherlands. These crusher plants generally produce three qualities: crushed concrete, crushed masonry and a 50%/50% (approximately, by volume) mixture of these two. The latter material will in this dissertation be referred to as "crushed rubble". A fourth, less current type produced by the crusher plants is crushed clinker, produced by crushing of street clinker, which is clay brick of a harder quality due to firing at elevated temperatures. None

of these materials as produced by the crusher plants have exact compositions. A commercial crushed concrete, for instance, will always contain some crushed masonry and even some wood and other non-stony material. The specifications for these materials (14) allow for small percentages of foreign materials to be present.

Part of the materials in Group R was tested at commercial compositions and gradings. For these materials, the composition and grading was determined by laboratory analysis. The results of this analysis is given on the Material Information Sheets in Appendix 2. To study the effect of material composition and grading in more detail, so-called "theoretical" materials also were tested in Group R. To obtain materials of pre-determined composition, special lots of pure concrete rubble, masonry rubble and clinker were crushed separately by crusher plants, thereby obtaining materials like 100% crushed concrete and 100% crushed masonry. For each material thus obtained, a few tons of it was subsequently sieved into the eight fractions mentioned in Paragraph 4.2.2, to allow for subsequent recombining to obtain the desired gradings of the upper and lower limits of the Dutch specifications mentioned earlier (the "B"- and "0"-grading, respectively). Laboratory-made mixtures of materials were also tested in Group R. These materials were obtained by mixing of the materials at predetermined ratios for each fraction of the materials, prior to recombining the fractions to the desired grading. Details on the grading of the theoretical materials are again given on the Material Information Sheets of Appendix 2.

The waste incineration slag tested in Group R was obtained directly from the waste incineration plant; its grading was determined by laboratory analysis. As can be seen from the Material Information Sheet for the waste incineration slag, this material does not comply with the Dutch standards for granular materials 0/40 mm. The particular slag had a maximum particle size of 22.4 mm.

4.3.3 The materials investigated

Table 4.3 shows the materials tested in Group R; the material number, the material name, the grading and the material code are given in the table. The composition of the materials is also indicated in the

table. The materials R1 through R10 are the theoretical materials, with pre-determined compositions and gradings, while the materials R11 through R15 are the commercial materials. The coding-system is equal to that used for Group C: the first two characters indicate the material, the third character the grading (see Table 4.2).

Table 4.3: Materials tested in Group R

material number	material name	grading	code	composition
R01	crushed masonry 1	fine	MGB	100% MG
R02		coarse	MGO	
R03	crushed masonry 2	fine	M2B	100% M2
R04		coarse	M2O	
R05	crushed concrete 1	fine	BGB	100% BG
R06		coarse	BGO	
R07	crushed clinkers	fine	KGB	100% KG
R08		coarse	KGO	
R09	crushed masonry/concrete	fine	FFB	50% M2
R10		coarse	FFO	50% BG
R11	crushed concrete 2	commercial	B2C	commercial
R12	crushed rubble 1	commercial	K1C	commercial
R13	crushed rubble 2	commercial	K2C	commercial
R14	crushed rubble 3	commercial	K3C	commercial
R15	waste incineration slag	commercial	AVC	commercial

4.4 SANDS

4.4.1 Introduction

In Group S, six sands from the Netherlands were investigated, ranging from very coarse to extremely fine. As stated in the literature review, sands are an important road construction material in the Netherlands. In the construction of major roads on the clayey subgrades of the western part of the country, sub-bases of sands of considerable thickness are applied to function as a haul road and a working platform during construction and as a drainage layer in the completed pavement structure. In the eastern part of the country, sands often form the natural subgrade.

4.4.2 Origin of the materials

The six sands investigated were obtained directly from the deposit; they will be denoted here by the name of the place of origin. The grading of these six sands ranged from very coarse to extremely fine, as shown in Figure 4.2. The sands are denominated in the figure by their material codes, as given in Table 4.5.

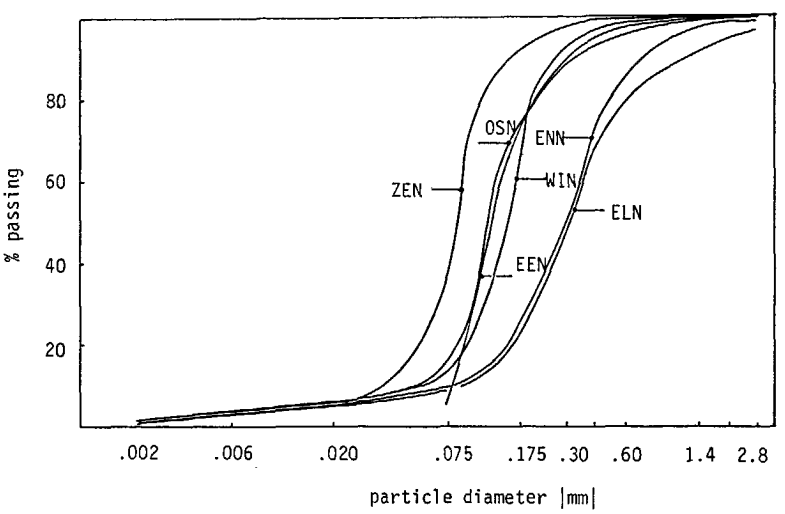

Figure 4.2: Particle size distributions of the six sands.

Table 4.4: Type of sand and manner of winning of the six sands obtained directly from the deposit

sand	type of sand	manner of winning
Echteld	river sand	wet
Echten	slope deposit	wet
Eems	estuarine sand	wet
Eastern Scheldt	estuarine sand	wet
Winterswijk	aeolien sand	dry
Zijen	basin sand	dry

Table 4.4 gives the type of sand (classification according to genesis) and the manner of winning (wet: suction dredging and dry: excavation) for these materials. Full details on these materials can be found in a publication by the former Dutch Study Centre for Road Construction [102].

4.4.3 The materials investigated

Table 4.5 shows the materials tested in Group S: the material number, the material name and the material code are given in the table.

Table 4.5: Materials tested in Group S

material number	material name	code
S01	Echteld	ELN
S02	Echten	ENN
S03	Eems	EEN
S04	Eastern Scheldt	OSN
S05	Winterswijk	WIN
S06	Zeijen	ZEN

4.5 LATERITES

4.5.1 Introduction

In Group L, six laterites from Suriname, South America were investigated. The material samples were obtained from borrowpits alongside the road Moengo-Albina in Eastern Suriname. The laterites from these borrowpits were used in a reconstruction of the road, which involved a substantial raising in level. Laterites were used as base and sub-base material and later covered with asphalt. For lack of proper specifications, the laterites used were selected mainly on the basis of engineering judgement.

Since the reconstructed road was at the same location as the existing road, the normal traffic had to be allowed to traffic the road under construction. Moreover, heavy construction traffic hauling laterite materials travelled the road fill, sub-base and base prior to asphalt paving. The heavy rain showers of the wet season occurring during the reconstruction led to substantial wetting of the unpaved road under construction, which in turn led to complete failure of certain sections of the road. Other sections of the road where different laterites had been used performed well under the adverse influence of rainfall and traffic.

Part of the laterites tested in Group L were obtained from borrowpits at the failed sections of the road, while the others were sampled from borrowpits at the intact sections of the road. Knowing the in-service performance of the laterites under the influence of wetting and traffic loading, a detailed laboratory investigation was performed to relate the performance of the various laterites to their grading [103].

4.5.2 The materials investigated

Table 4.6 shows the materials tested in Group L; the material number, the material name and the material code are given in the table. In conformity with the original publication by the author on the subject [103], the material code consist of three characters. The first character indicates the borrow pit from which the material was sampled

and the two last characters indicate the horizon in the soil profile from which the samples were taken. Details on the grading and the specific gravity of the laterites are given in the Material Information Sheets of Appendix 2.

Table 4.6: Materials tested in Group L

material number	material name	code
L01	Laterite	HA2
L02	"	AB1
L03	"	BB1
L04	"	IB1
L05	"	BB2
L06	"	AC

5 LABORATORY TESTING

5.1 INTRODUCTION

In pavement engineering, laboratory tests are used for various purposes. Firstly, they are used for material characterization, involving the determination of grading, composition, specific gravity and the like. Although the test equipment used for this purpose is relatively simple, material characterization tests may yield fundamental data. Determination of the specific gravity, for instance, yields a parameter that can be directly used in calculation of the degree of saturation of unbound materials.Some material characterization tests yield non-fundamental data. Determination of the Atterberg limits, for instance, yields parameters suited only for an empirically based assessment of material quality.

A second purpose for which laboratory tests are performed is the determination of the mechanical properties of the pavement materials. For unbound granular materials, testing focuses on compaction properties, "bearing capacity" and resistance to degradation. A large number of standard tests is available for the determination of these properties. Most of these tests, however, are far from fundamental as the materials are tested under conditions that do not represent the in-situ conditions. Furthermore, the mechanical property investigated is expressed in a parameter suited only for a relative assessment of material quality and in units devised especially for that particular test, such as % CBR. Such parameters certainly are not suited for input to present day mechanistic pavement design procedures. The standard tests presently being used only yield parameters suited for input to the empirical design methods for which the particular test was developed. Therefore, in countries with different empirical pavement design procedures, different parameters for characterizing the mechanical properties of the pavement materials are used. To allow for simple test equipment to be used, the laboratory tests are often performed on scaled-down gradings, which yields parameters that are only indicative of the properties of the original material. Next to these disadvantages, the standard tests presently being used do have their

advantages. They are indeed standardized, they express the investigated properties in widely known, easy to interpret parameters and the required testing equipment is simple.

The mechanistic pavement design procedures used today require fundamental material parameters like Young's modulus E and Poisson's ratio ν for input. Fundamentally sound testing techniques are required that determine these parameters under conditions of grading, moisture content, density and stress that are representative of the in-situ conditions. For unbound granular materials, the cyclic load triaxial test today is the main test used for that purpose. It has the advantage of being a fundamental test, meeting the conditions set out above. However, the main disadvantage of the test is that it requires complicated testing equipment. If one wishes to simulate accurately in the laboratory the in-situ conditions of grading and stress, cyclic load triaxial equipment with a large specimen size and with variable confining pressure is required. Furthermore, much testing time is needed to cover all possible stress paths occurring in-situ. Such testing clearly is only suited for research purposes.

The first approach to circumvent the necessity of such complicated testing techniques has been to try to obtain correlations between the fundamental material parameters required and the results from standard tests like the CBR-test. As will be discussed later, this approach is of limited, if any, use. A second approach to the problem of the cyclic load triaxial test being too complicated for routine application has been to make some simplifications to the test itself, without losing its fundamental character. The main simplifications applied are reducing the required specimen size by scaling down the grading and the use of a constant confining pressure. The effect of these simplifications has been discussed in Chapter 2 and will be dealt with further in this chapter.

Although a major simplification of the required equipment can be obtained by scaling down gradings and using constant confining pressure tests, the cyclic load triaxial test even in its simplified form still is too cumbersome for routine application. The equipment for applying cyclic loading and measuring transient deformations is too complicated to allow for the test in its present form to be used on a routine basis in laboratories with standard equipment. What is really needed

for implementation in practice of a fundamentally sound manner of unbound granular material testing is a further simplified triaxial testing technique, that uses static rather than cyclic loading on a specimen that can be compacted with standard laboratory equipment. Such a testing technique will be described in this chapter and its performance in determining fundamentally sound material parameters will be investigated.

This chapter will deal with standard and fundamentally sound tests performed on the granular base course materials (Groups C and R) and the sands (Group S) mentioned in Chapter 4. Testing of the laterites (Group L) will be dealt with in Chapter 6, because of the pronounced dependency of their material parameters on water content. Paragraph 5-.2 will describe the standard tests performed for material characterization purposes and for determining mechanical parameters like resistance to degradation and CBR. Paragraph 5.3 then will deal with cyclic load triaxial testing of the wide range of materials. Next, in Paragraph 5.4 correlations between the results of standard tests and cyclic load triaxial tests will be checked for their validity. In Paragraph 5.5, a repeated static load triaxial test procedure will be suggested that allows for an accurate determination of resilient properties. Furthermore, the influence of reducing the size of the triaxial specimen on the resilient properties will be investigated. Paragraph 5.6 will focus on permanent strain properties, investigating the possibility of estimating these properties from tests which are simple to perform.

5.2 STANDARD TESTS

5.2.1 Introduction

Three groups of standard tests were performed:

- index tests
- compaction tests
- California Bearing Ratio tests.

The index tests carried out for characterization purposes involved determination of the particle size distribution, material composition, specific gravity and resistance to degradation. Proctor and Vibrating Hammer Compaction Tests were performed to obtain reference values for the density of the triaxial specimens. The California Bearing Ratio tests were carried out for checking E - CBR relationships. The whole range of tests was carried out on the conventional and recycled base course materials (Groups C and R) only; for the sands (Group S) certain tests were omitted since they pertain especially to granular base course materials. The testing of the laterites of Group L was limited to particle size distribution and specific gravity determination because of the limited quantity of sample material available. The individual standard tests will be described in some detail in this paragraph, with reference to the test standard, if available. Individual test data are given on the Material Information Sheets of Appendix 2. Here only correlations between the results of the various tests will be presented.

The standard tests performed on the granular base course materials of Groups C and R formed part of a parallel research project focussing on the repeatability of these tests. The standard testing of these materials was therefore very extensive, involving a number of repetitions of each test. Documenting of all the individual test results clearly lies beyond the scope of this dissertation. Therefore, only the average results of each series of tests will be given here.

5.2.2 Material characterization

5.2.2.1 PARTICLE SIZE DISTRIBUTION

Groups C and R (conventional and recycled materials)

Part of the materials in Groups C and R were tested at laboratory-made gradings, while the rest of the materials was tested at commercial gradings. Therefore, two separate procedures are distinguished for the determination of the particle size distribution of the materials from Groups C and R.

The laboratory-made gradings were recombined from fractions d > 45 mm, 45 - 31.5 mm, 31.5 - 22.4 mm, 22.4 - 16 mm, 16 - 8 mm, 8 - 4 mm, 4 - 2 mm and d < 2 mm (see also Paragraph 4.2.2). Therefore, for the determination of the particle size distribution, only the fraction d < 2 mm had to be analysed. The procedure followed for this analysis was equal to that followed for the commercial gradings, as discussed hereafter.

The particle size distribution of the materials with a commercial grading was determined in accordance with the Dutch standards Eisen 1978 [7]. The procedure followed involved three steps:

1: Dry sieving of the total sample material.
2: Wet sieving of the fraction with d < 2 mm, obtained from step 1.
3: Ultrasonic sieving of the fraction with d < 2 mm, obtained from step 1.

For materials having a large fraction with d < 0.020 mm (as determined in step 3), this fraction was further analysed using the hydrometer test to obtain the percentage of material with d < 0.002 mm. In general terms, the procedure followed for determination of the particle size distribution was as follows. About 5 kg of sample material was oven-dried and subsequently sieved using ISO-standard sieves (NEN 2560 [104]) of 2, 4, 8, 16. 31.5 and 45 mm aperture size. 200 g of the material passing the 2 mm sieve was mixed with a peptizing agent (a solution of 0.5 N sodiumoxalate and 0.5 H sodiumsilicate) and subsequently subjected to wet sieving using 1.0, 0.500, 0.250, 0.125 and 0.063 mm sieves, discarding the material passing the 0.063 mm sieve. To obtain the percentage of material with d < 0.020 mm, about 20 g of material passing the 2 mm sieve was mixed with the peptizing agent and subjected to wet ultrasonic sieving, followed by oven-drying of the residu passing the 0.020 mm sieve. The percentage of material with d < 0.002 mm was determined by performing hydrometer analysis on material passing the 2 mm sieve, mixed with the peptizing agent.

The results of the particle size analysis are given on the Material Information Sheets of Appendix 2, both in the form of a table and a graph indicating the grading of the material relative to the Dutch specifications for granular base course materials 0/40 mm.

Group S (sands)

For determination of the particle size distribution of the sands, 100 g of sample material was mixed with 25 ml of peptizing agent (35 g sodiumhexametaphosphate and 7 g sodiumcarbonate in 1 liter of water). Subsequently, the sample was washed with distilled water through a 75 µm sieve. The fraction retained was sieved dry, whereas the fraction passing the 75 µm sieve was subjected to hydrometer analysis. The resulting particle size distribution is shown in the Material Information Sheets of Appendix 2. Based on the particle size distribution, the sands were classified according to the Extended Unified Soil Classification System; the resulting classification is shown on the Material Information Sheets.

5.2.2.2 COMPOSITION

Ten of the 14 crushed rubble materials were tested at laboratory-made compositions, while the remaining four materials were tested at their commercial composition, that is as produced by the crusher plants. These plants normally process rubble directly from the demolition site and therefore the end-product crushed material will contain some wood, plastic and the like. To cope with the almost equal supply of concrete-rubble and masonry-rubble, the crusher is often fed with equal volumetric quantities of these materials, the end product then being a mixture of crushed concrete and crushed masonry

Materials B2C (crushed concrete 2) and K1C, K2C and K3C (crushed rubble 1, 2 and 3, respectively) were tested at their commercial composition, B2C having been produced from concrete rubble only and K1C, K2C and k3C from equal batches of concrete rubble and masonry rubble. To determine the composition of these materials, the fractions with particle diameter d > 8 mm obtained from the particle size distribution determination were analysed. Material B2C was thereby shown to consist of over 95% crushed concrete, whereas materials K1C, K2C and K3C consisted of roughly 60% crushed concrete and 40% crushed masonry (by weight). The contents of wood, plastic and the like was limited to only a few percent for all four materials.

Materials R1 through R10 were tested at recipe compositions. Two specially selected batches of masonry, one special batch of concrete and one special batch of clinker were processed by a crusher plant to obtain the "pure" materials MG, M2, BG and KG. These materials were then sieved into fractions to allow for later recombination to the desired gradings. Material FF (crushed masonry/concrete) was obtained by mixing equal quantities by weight of M2 and BG in each fraction.

The remaining material AVC (waste incineration slag) of Group R was not analysed for composition, since this was virtually impossible because of the fine grading: AVC consisted of over 50% of non-recognizable fine material.

5.2.2.3 SPECIFIC GRAVITY

Groups C and R (conventional and recycled materials)

Groups C and R cover a wide range of materials, from crushed rock with a high specific gravity (porphyry, limestone) to porous materials with a low specific gravity (lava, crushed masonry). The specific gravity of the materials in Groups C and R was determined for the fractions 4 - 8, 8 - 16 and 16 - 31.5 mm separately and also for the combined fraction 4 - 31.5 mm. This determination was done according to the Dutch "Ontwerp NEN 3543 - 7.1", which involves determination of the sample volume using pycnometers after which the specific gravity is calculated by dividing dry sample mass by sample volume. The test results are given on the Material Information Sheets of Appendix 2.

5.2.2.4 RESISTANCE TO DEGRADATION

Groups C and R (conventional and recycled materials)

As stated, the materials in Groups C and R range from hard, crushed rock materials to friable, porous materials. To obtain a characterization of the resistance to degradation, the standardized Dutch crushing test ("Verbrijzelingsfactor van steen", [7]) was performed on a number of fractions of each material. The test procedure has been described in Paragraph 2.5.2.3. The test standard prescribes testing of one

specified fraction of the material only; to cope with the heterogeneous nature of some of the materials involved here, the Verbrijzelingsfactor was determined for a range of fractions. For sake of consistency, this was done for all materials in Groups C and R. The test results are given on the Material Information Sheets of Appendix 2.

5.2.3 Compaction properties

Three types of compaction tests were performed on the various materials: the Modified Proctor Compaction Test, the Single Point Proctor Compaction Test and the Vibrating Hammer Test.

The Modified Proctor Compaction Test

The Modified Proctor Compaction Test was performed on all the materials of Groups C, R and S. The test was carried out in accordance with the Dutch test standard (7). The procedure followed is similar to that of AASHTO T180-74, Method C (Modified Proctor Test in 101.6 mm mould), the main difference being that the Dutch standards prescribe testing of material with particle diameter $d < 22.4$ mm, whereas AASHTO prescribes testing of material with $d < 19$ mm. The discarded material with $d > 22.4$ mm was replaced by material with $4 < d < 22.4$ mm.

The Proctor Tests were carried out at five different water contents per material/grading, each of these tests being repeated five times. The Maximum Modified Proctor Density MMPD, as given in the Material Information Sheets of Appendix 2, was obtained as the average value of the five test results at the water content giving the highest dry density, without water being expelled from the specimen during compaction.

The Single Point Proctor Compaction Test

The Single Point Proctor Compaction Test (105) is used in the Netherlands as part of the compaction control of granular base courses. This control involves digging a hole in the compacted base

layer and determining the volume of the hole using the Sand Replacement Method. The density thus obtained is expressed as a percentage of the density resulting from the Single Point Proctor Compaction Test. This test is performed on the material dug from the base layer at its full 0/40 mm grading and is, for lack of sample material, performed at one moisture content only. This moisture content is chosen rather subjectively by gradually adding water to the ovendried sample material until after thorough mixing all grains have been wetted and a "plastic" grains/water mixture is obtained. The resulting moisture content is denoted as the "plastic moisture content" w_{pl}. The compaction procedure is similar to that of AASHTO T99-74, method D (normal Proctor Test in 152.4 mm mould), the main difference being that the test is performed on the full 0/40 mm grading.

The Single Point Proctor Compaction Test was performed on the materials from Group C and R, and repeated five times per material/grading. The value for the Single Point Proctor Density SPPD given in the Material Information Sheets of Appendix 2 is the average of the five density-values obtained per material/grading.

The Vibrating Hammer Test

Vibrating Hammer Tests were performed on the granular base course materials of Groups C and R. The tests were carried out in accordance with the preliminary Dutch test standard [106], which is an adaptation of the UK-standard for the test (BS 5835, [33]). The main adaptation is that the Dutch test is performed on material with $d < 45$ mm, whereas BS 5835 prescribes testing of material with $d < 37.5$ mm. For each material/grading, the test was performed at five different moisture contents, again with five repetitions at each moisture content. The Maximum Vibrating Hammer Density given in the Material Information Sheets of Appendix 2 is the average value of the five test results at the water content giving the highest dry density, without water being expelled from the specimen during compaction.

Correlations between compaction test results

As discussed, the Maximum Modified Proctor Density MMPD, the Single Point Proctor Density SPPD and the Maximum Vibrating Hammer Density MVHD were determined for all materials of groups C and R. In all, 25 material/grading combinations were tested, 18 of which were recipe-made materials (laboratory-made composition and grading) and the remaining seven commercial materials (composition and grading as supplied). For the recipe-materials, each sample for each individual compaction test was composed separately, thereby ensuring that all tests per material/grading were performed on exactly the same material with respect to grading and composition. For the commercial materials, the material for the tests was sampled from the supply.

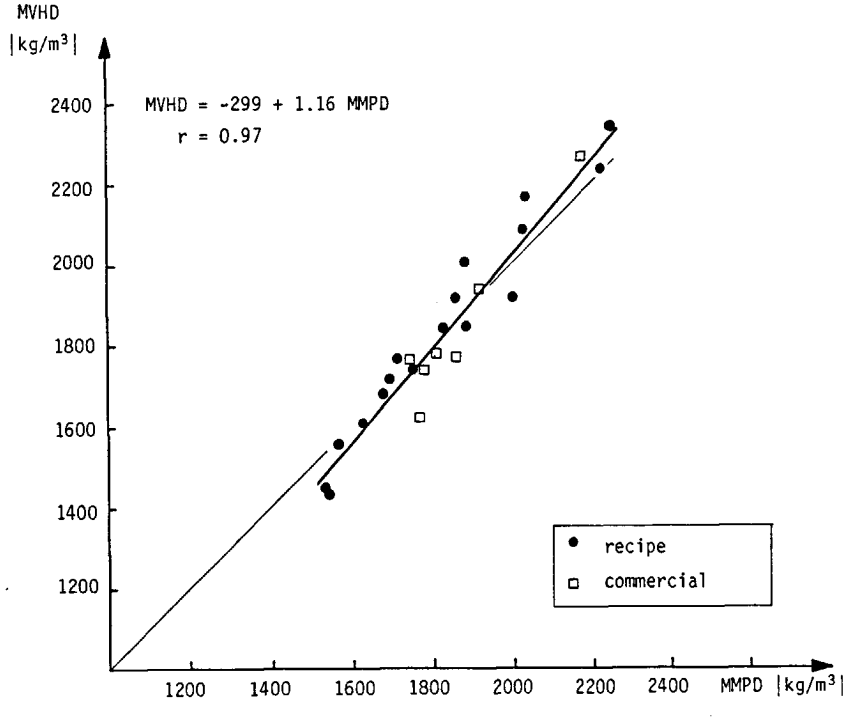

Figure 5.1: Maximum Vibrating Hammer Density MVHD versus Maximum Modified Proctor Density MMPD, for materials from Groups C and R.

Figures 5.1 through 5.3 show correlations between the results of the three types of compaction test. Different symbols are used to denote the recipe-materials and the commercial materials. The straight lines

shown were determined using linear regression; the formula of the lines and the correlation coefficient r are given in the figures. The lines pertain to all the 25 data points. Linear regression was also performed using only the data for the recipe-materials, resulting in no significant changes in the correlation coefficient r (see Table 5-.1). From this, it can be concluded that the limited scatter in the data point results from the test procedures themselves and not from errors made in sampling from the supplies of commercial materials. The scatter in the data points is indeed limited; a high correlation coefficient was found for all comparisons made.

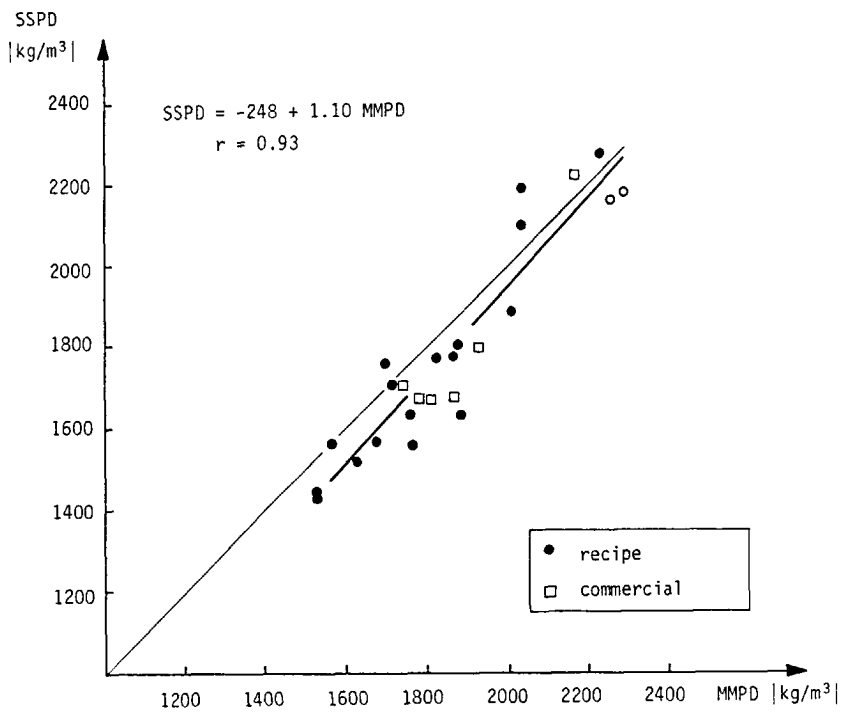

Figure 5.2: Single Point Proctor Density SPPD versus Maximum Modified Proctor Density MMPD, for materials from Groups C and R.

It should be noted here that the Modified Proctor Compaction Test was performed on a scaled-down 0-22.4 mm material, whereas the two other compaction tests were performed on effectively the full 0/40 mm grading. To check for the influence of scaling down the grading on the dry density obtained, Figures 5.1 through 5.3 also show 45° lines of equality. From Figure 5.1, it can be seen that the MVHD (0-45 mm) versus MMPD (0-22.4 mm) relationship is indeed quite close to the line of

equality. Noting that the compaction effort applied in the Vibrating Hammer Test and the Modified Proctor Compaction Test is similar, the influence of scaling down the grading on the dry density obtained appears to be small. This conclusion is consistent with results found at Nottingham University. Donbovand [44] used the same compaction effort to prepare triaxial specimens for a limestone with maximum particle sizes ranging from 40 mm to 12 mm and found little change in the dry density of the specimens.

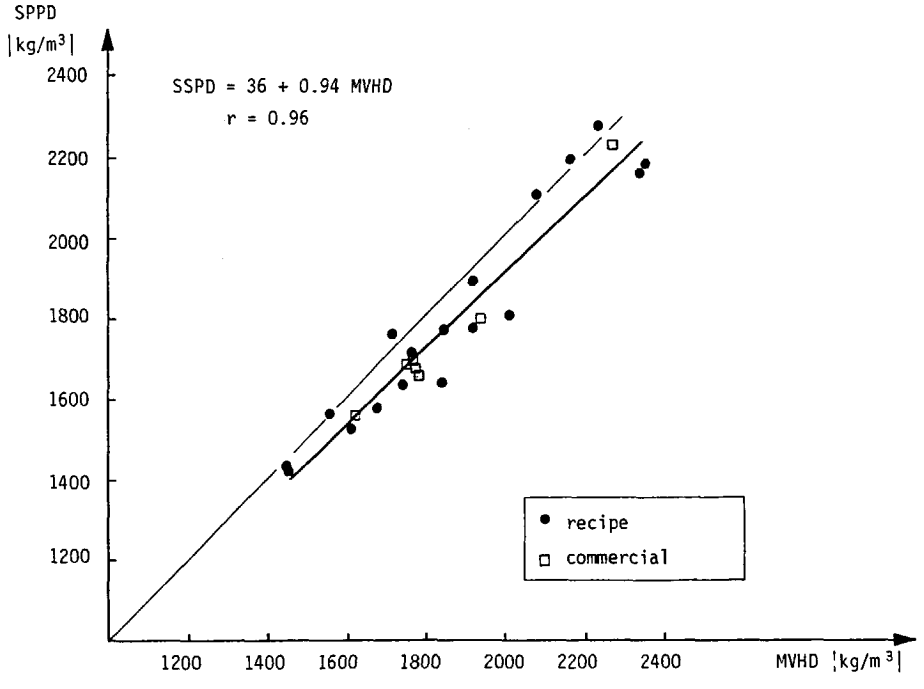

Figure 5.3: Single Point Proctor Density SPPD versus Maximum Vibrating Hammer Density MVHD, for materials from Groups C and R.

Looking at Figures 5.2 and 5.3, the influence of compaction energy can be recognized from the test results. In Figure 5.2, the SSPD (nominal 0/40 mm) versus MMPD (0-22.4 mm) relationship plots below the line of equality, indicating that SSPD values are - in general - lower than MMPD-values. The same holds for Figure 5.3: SPPD-values (nominal 0/40 mm) are - in general - lower than MVHD-values (0-45 mm). Since the compaction energy applied in the Single Point Proctor Compaction Test is significantly lower than the energy applied in the two other tests, the conclusion can be drawn that the influence of compaction energy

appears to dominate the influence of scaling down the grading. This conclusion is only tentative: a more detailed investigation involving, for instance, the same compaction test on different gradings would be required to substantiate it. Such detailed studies of standard tests and their results however clearly lie outside the scope of this dissertation.

Table 5.1: Correlations coefficients for linear regression between compaction test results

	correlation coefficient r	
correlation	all materials	recipe-materials only
MVHD vs MMPD	0,97	0,98
SPPD vs MMPD	0,93	0,95
SPPD vs MVHD	0,96	0,94

5.2.4 California Bearing Ratio

Although the Dutch standards for road building materials [7] incorporate the CBR-test for determination of "Bearing capacity of embankment and granular base course material", the test standard itself prescribes the test to be carried out on material with particle diameter d < 4 mm. For granular materials with a nominal 0/40 mm grading such testing does not make much sense. On the other hand, testing of the full 0/40 mm grading in the 152.4 mm diameter CBR-mould also is of little use. Therefore, in testing the 0/40 mm materials of Groups C and R, a grading scaled down to 0-22.4 mm (as used in the Maximum Modified Proctor Compaction Tests) was used. The sands of Group S were - of course - tested at their full grading.

Material samples were brought to the Optimum Moisture Content as determined in the Maximum Modified Proctor Compaction Test and subsequently compacted in the 152.4 mm diameter CBR-mould, using the modified Proctor compaction level. The CBR test was carried out directly after compaction. The CBR-values obtained are given in the Material Information Sheets of Appendix 2; each number given is the

average value of three CBR determinations. Values are given for both 0.1 inch (2.54 mm) and 0.2 inch (5.08 mm) penetration.

5.3 CYCLIC LOAD TRIAXIAL TESTS

5.3.1 Introduction

As noted in Paragraph 2.5.3.1, the cyclic load triaxial test nowadays is the test most widely used for the determination of resilient and permanent strain characteristics of unbound road building materials. The purpose of the test is to simulate in the laboratory as closely as possible the situation in the pavement with respect to grading, moisture content, density and stresses. The strains resulting from the application of stresses are measured and fundamental material parameters are determined from the values of stresses and strains.

For the research described in this dissertation, initially two cyclic load triaxial apparatus were built. For the coarse graded conventional and recycled base course materials (Groups C and R), a triaxial apparatus with a specimen size of 400 mm diameter by 800 mm height was built, while for the finer graded sands and laterites (Groups S and L) a cyclic load triaxial apparatus with a specimen size of 100 mm diameter by 200 mm height was built. Later, a scaled-down version of the large 400 mm apparatus was developed, having a specimen size of 150 mm diameter by 300 mm height. In this paragraph, the 400 and 100 mm specimen diameter equipment will be dealt with. The 150 mm specimen diameter apparatus will be dealt with separately in Paragraph 5.5.3, investigating the applicability of this scaled-down apparatus for testing of coarse graded unbound granular materials.

This paragraph will deal with testing of materials from Group C and R in the 400 mm specimen diameter apparatus and of the materials from Group S in the 100 mm specimen diameter apparatus. Testing of the laterites (Group L) will be dealt with separately in Chapter 6, investigating stiffness - water content relationships. Only simple material models relating stresses to strains will be used in this paragraph to

describe the test results; the more complex models will be dealt with in Chapter 7.

5.3.2 Cyclic load triaxial tests Groups C and R

5.3.2.1 INTRODUCTION

The conventional and recycled road base materials of Groups C and R had nominal 0/40 mm gradings, complying with the Dutch specifications for such materials (see Paragraph 3.2). These specifications allow for maximum 10% of the material to have a particle diameter of $d > 45$ mm; the actual maximum particle size is not specified. To allow for testing of these materials at their full grading, a large cyclic load triaxial apparatus was developed. To avoid specimen size effect, a specimen diameter of 400 mm was chosen, being ten times the nominal maximum particle size. A ratio of specimen height to specimen diameter of two was chosen, resulting in a specimen height of 800 mm. The resulting specimen volume thereby is a convenient number: 0.1005 m^3.

It was realized from the start that testing of specimens of such size would involve many practical problems, such as a specimen weight of approximately 200 kg. Large servo-hydraulic equipment would be required to perform cyclic load triaxial tests on such specimens, which in turn would require a large frame for the triaxial apparatus. Certainly, such triaxial testing would not be suited for application on a routine basis. Notwithstanding all these objections, the large specimen size was judged essential to be able to test the materials without scaling down their grading and to exclude specimen size effects. From the start, the decision was taken to later explore the possibilities of scaling-down the large triaxial apparatus to a more "user-friendly" size, which would allow the test to be carried out by other less well equiped laboratories.

Having opted for the large specimen size, the decision was taken to try to circumvent the need for a triaxial cell by using the vacuum-triaxial principle. By applying a sub-atmospheric pressure to the inside of the triaxial specimen an all around confining stress can be simulated. The advantage of the vacuum-principle is clear; no triaxial cell is required, which is a major advantage at this specimen size and

the transducers mounted on the triaxial specimen remain directly accessible during the performance of the test. This too is a major advantage; it allows for small range displacement transducers to be used, since adjustment of these transducers can be done at any time during the test. The use of these small range transducers increases the accuracy of the test results.

The use of the vacuum-principle has disadvantages too. Firstly, only CCP (constant confining pressure) triaxial tests can be performed, since a variation of the internal sub-atmospheric pressure in the specimen is not feasible at the required frequency of, for instance, 1 Hz. This certainly limits the applicability of the apparatus developed to relatively simple stress paths. However, since the main emphasis of the research described in this dissertation lies with testing of a large number of materials rather than with an extremely detailed analysis of a few materials only, the limitation in stress paths was judged not to be a major disadvantage. As discussed in Paragraph 2.5.3.2, CCP-triaxial tests yield the same material parameters as VCP (variable confining pressure) triaxial tests, provided the proper material models are used. Therefore, the simulation in the laboratory of the in-situ stress condition in CCP-triaxial tests was considered accurate enough.

A second disadvantage of the vacuum-principle is that the confining stress σ_3 can be varied over a limited range only. Theoretically, σ_3 is limited to 100 kPa (absolute vacuum) but in practice it is limited to around 90 kPa. This too is not a problem in testing unbound road base materials, since these materials are applied in the upper pavement layers only and the confining stress resulting from overburden is therefore low. Transient traffic stresses do add to the confining stress but the total confining stress stays well below 90 kPa.

A third disadvantage of the vacuum-principle lies with the fact that saturation of the triaxial specimen is not possible. The sub-atmospheric pressure inside the triaxial specimen clearly eliminates the use of a back-pressure required to fully saturate the specimen. This too was judged not to be a problem since construction practice in the Netherlands involves application of thick layers of sand underneath the unbound granular base. Together with the controlled water

table this prevents granular base courses of properly constructed pavements from becoming saturated.

5.3.2.2 THE 400 MM SPECIMEN DIAMETER APPARATUS

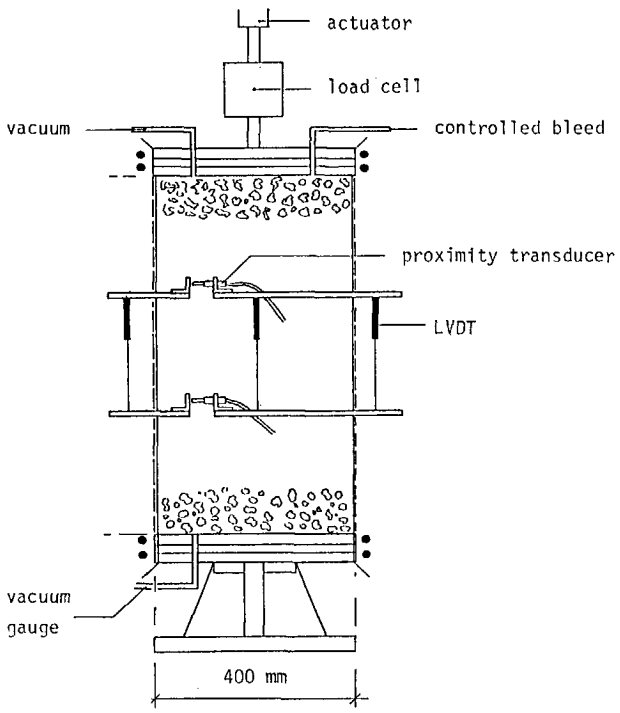

Figure 5.4: Schematics of the 400 mm specimen diameter cyclic load triaxial apparatus.

Figure 5.4 shows the schematics of the 400 mm specimen diameter apparatus. The triaxial specimen is enclosed by a double membrane, which has an air-tight connection to the bottom- and top-platen of the triaxial apparatus using grease and O-rings. A constant vacuum is applied to the specimen through a bore in the top-platen, while another bore in the top-platen is connected to a vacuum reducer providing a controlled bleed. The resulting sub-atmospheric pressure inside the specimen is measured by a vacuum Bourdon gauge connected to a bore in the bottom-platen. To the top-platen a 100 kN MTS hydraulic actuator is connected through a load cell. The hydraulic system used itself is capable of applying cyclic 100 kN loading at frequencies up to 10 Hz

but inertia effects in the triaxial specimen limit the actual frequency of this apparatus to a maximum of 5 Hz.

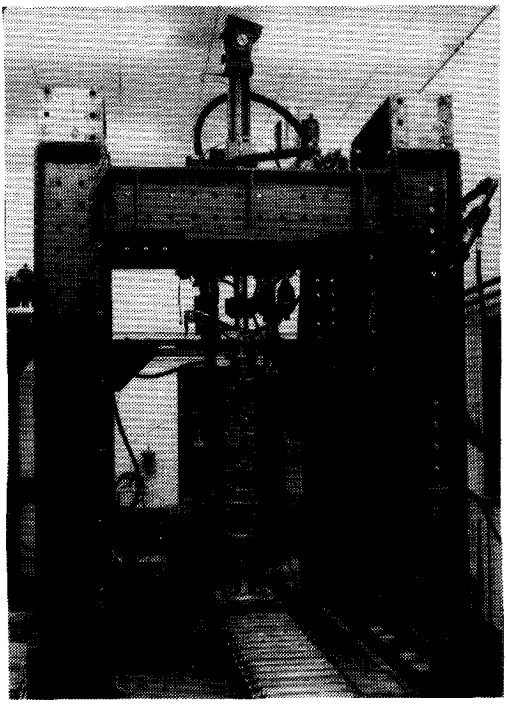

Figure 5.5: Cyclic load triaxial apparatus (400 mm specimen diameter apparatus).

Axial and radial deformations of the triaxial specimen are measured by displacement transducers mounted on two plexiglass rings surrounding the specimen at 1/3 and 2/3 of specimen height, respectively. The rings are supported by small plastic blocks glued to the triaxial membrane. Axial deformations are measured by four vertically mounted LVDT's (Linear Variable Differential Transformers), while two horizontally mounted so-called "proximity transducers" are used to measure the radial deformations of the triaxial specimen. The operating range of the displacement transducers used depends on the type of test. For measurement of resilient properties, small range transducers are used, whereas for permanent strain properties large range transducers are applied. As can be seen from Figure 5.4, deformations are only measured on the middle part of the triaxial specimen, thereby avoiding

end constraint effects at the top- and bottom-platen. Figures 5.5 and 5.6 show the triaxial apparatus and the triaxial specimen, respectively.

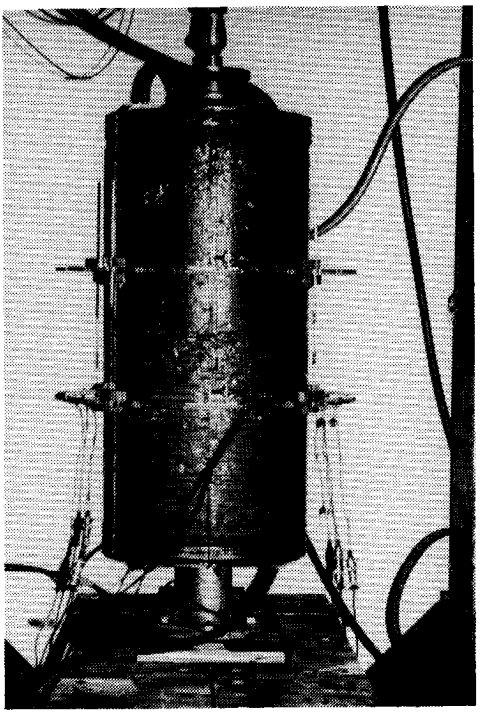

Figure 5.6: Triaxial specimen (400 mm specimen diameter apparatus).

The 400 mm specimen diameter apparatus is computer operated. An HP computer system generates the digital cyclic load signal, which is converted to an analogue signal by an HP Multiprogrammer. This signal is fed to the hydraulic loading system, which then applies the required load. The resulting specimen deformations are measured by the displacement transducers and their analogue output together with that of the load cell of the hydraulic system are converted to digital information by the Multiprogrammer and subsequently stored by the computer. Specially developed software allows for interpretation of test data and plotting of ready-made graphs of, for instance, resilient modulus M_r versus sum of principal stresses θ.

5.3.2.3 THE MATERIALS INVESTIGATED

The 400 mm specimen diameter apparatus was used to test nominal 0/40 mm unbound road base materials of Group C (conventional materials) and Group R (recycled materials). These materials have been discussed in detail in Chapter 4 (see Tables 4.1 and 4.3, respectively). All of the materials in these two groups were tested for resilient properties, whereas only a selection of the materials was also tested for permanent deformation properties. The latter type of testing was limited to a selection of materials only since permanent strain testing is very time-consuming indeed. Furthermore, permanent deformation in unbound granular base courses is of less importance under present Dutch pavement design practice.

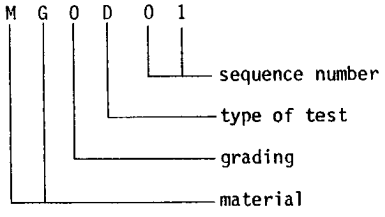

Figure 5.7: Principle of test-code.

For determination of the resilient properties one triaxial specimen per material/grading was built, whereas for permanent strain properties three specimens per material/grading were tested. To distinguish between all these tests, a coding-system was introduced, in which each test is denominated by a six character code. Figure 5.7 illustrates the coding system. The first two characters in the code indicate the material tested and the third character the grading of the material tested. These codes have been discussed earlier in Chapter 4 and are summarized in Appendix 1. Since both cyclic and static load triaxial tests were performed, the test-code contains information on that aspect too. The fourth character in the code being a D indicates a cyclic load triaxial test, while an S as the fourth character indicates a static load test. The last two characters of the test-code are numbers indicating the sequence number of the particular test.

5.3.2.4 SPECIMEN PREPARATION PROCEDURE

The specimens for the 400 mm diameter triaxial apparatus were compacted in a split mould lined with a triaxial membrane. The membranes used were home-made from P.V.C. of 0.4 mm thickness. To avoid extra support to the triaxial specimen by stretching of the membrane on deformation of the specimen, the membranes were made barrel-shaped, thereby having the shape of an already deformed specimen (see Figure 5.8). The required sheets of PVC were cut from commercially available rolls and "heat-welded" using an appropriate electric device.

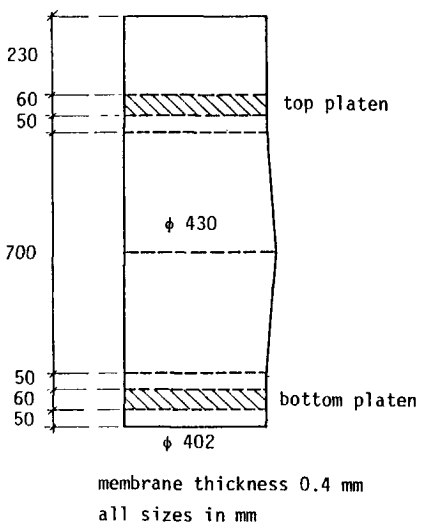

Figure 5.8: Dimensions of triaxial membrane.

As discussed earlier, the materials at the required composition and grading were obtained either by recombining various fractions of sieved material, or directly from the crusher plant. The moisture content of the bulk material thus obtained was determined and the required quantity of water to bring the material to optimum moisture content was added. It proved to be impossible to bring about 200 kg of material to exactly the required optimum moisture content; deviations of one or two percent from the target moisture content were inevitable. Sources of error are sampling from the bulk material for the determination of the initial moisture content, loss of water in the drum-mixer used to mix sample material with water and sampling from the ready made material for determination of the final water content.

Having obtained the sample material at the final moisture content, the triaxial specimen was then built in the split mould. The required quantity of sample material, calculated from the specimen volume and the wet density from the Modified Proctor Compaction Test, was divided into eight equal portions. Each portion was poured into the split mould/membrane assembly and precompacted with a heavy tamper. After each two of such layers, a full face compaction plate attached to the hydraulic actuator of the triaxial apparatus was used to further compacted the material in the mould. This compaction was performed for 30 minutes, using a halve sine load signal of 7 Hz frequency and 40 kN amplitude, superposed on 10 kN static load. After this, the top of the finished layers was roughened and two more portions of the sample material were added. Each individual layer was again compacted with the heavy tamper, followed by compaction with the hydraulic actuator on each set of two layers.

It should be stressed here that the density from the modified Proctor test was used as a reference value only and not as a target value. In the Proctor test, material particles are crushed severely by the action of the drop-hammer, which in the case of porous materials such as lava leads to an increase of density to a value not obtainable with material at the intact grading. Using the modified Proctor density value as a target in the compaction of the triaxial specimens would, therefore, mean that the sample material would have to be crushed during compaction, which clearly conflicts with the aim of testing materials at specified, laboratory-made gradings. Therefore, the triaxial compaction procedure as described above was used, thereby in fact having an oversized version of the Vibrating Hammer compaction procedure described in Paragraph 2.5.2.1. This procedure leads to far less particle crushing and is believed to better represent in-situ compaction.

Appendix 3 shows the triaxial specimen data with respect to moisture content and density. As discussed earlier, the moisture content shows some deviation relative to the target moisture content, being the optimum moisture content from the Modified Proctor Test. The dry density of the triaxial specimens also shows some scatter. Since the determination of the dry density involves determination of the moisture content of the sample material, some scatter in the calculated dry

density may be attributable to errors in moisture content determination due to sampling. The specimen volume and the wet specimen weight were determined accurately, thereby precluding sources of error in these parameters. Some actual scatter in the dry density of the triaxial specimens is bound to exist. The differences in moisture content of the sample material certainly will lead to differences in obtained density, while the triaxial compaction procedure itself will also cause some scatter.

Table 5.2: Triaxial specimen data

test code	w [%]	ρ_d [kg/m^3]
MGBD 08	24.5	1530
09	24.5	1530
BGOD 01	7.8	1878
04	7.9	1879
KGBD 01	7.6	1803
05	7.5	1743
KGOD 01	5.3	1695
03	5.4	1695

From the specimen data given in Appendix 3, the scatter in the moisture content can be concluded to be the main source of scatter in the dry density. Specimens built at the same moisture content generally show only a very small scatter in dry density. For evidence, Table 5.2 shows the triaxial specimen data for those specimens compacted at moisture contents deviating 0.1% or less. Differences in obtained dry density are very small indeed, with the exception of material KGB, which shows a difference of approximately 3% in dry density.

In summary, even with strict adherence to the triaxial compaction procedure and with years of experience a certain limited scatter in the moisture content and dry density of the 400 mm diameter triaxial specimens cannot be avoided. The main source of scatter lies in the

problem of mixing around 200 kg of granular material with water to obtain material at the target moisture content. As will be shown later, the accuracy in preparing triaxial specimens of smaller dimensions is significantly higher.

5.3.2.5 RESILIENT DEFORMATION

Material Groups C and R (conventional and recycled granular base course materials) in total incorporate 25 different material/grading combinations. For each combination, one 400 mm diameter triaxial specimen was tested for resilient properties. Resilient deformations were measured at a large number of combinations of the static confining stress and the cyclic deviator stress. Figure 5.9 shows the stresses applied on the triaxial specimen.

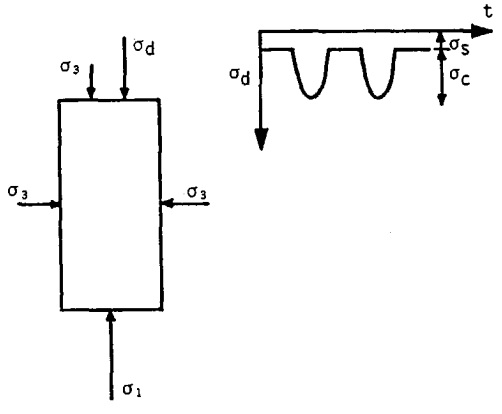

Figure 5.9: Stresses applied on triaxial specimen.

The all-around confining stress σ_3 is applied through a sub-atmospheric pressure inside the triaxial specimen. The deviator stress σ_d is applied by the hydraulic actuator of the triaxial apparatus. σ_d consists of a small static part σ_s and a large cyclic part σ_c having the form of a half sine wave with a frequency of 1 Hz. The small static stress σ_s is required to ensure a continuous contact between the hydraulic actuator and the top-platen of the triaxial specimen. It should be noted that the large height of the triaxial specimen also creates a constant vertical stress. At mid specimen height the vertical stress due to overburden is about 10 kPa. This built-in overburden stress certainly is not negligible in relation to the relatively low

deviator stress applied and will therefore be taken into account in calculation of the total axial stress in the triaxial specimen. Table 5.3 shows the values of the stresses applied in the determination of the resilient properties.

Table 5.3: Stresses applied in determination of resilient properties

stress component	value	
σ_3	12, 24, 36, 48	[kPa]
σ_s	1.5, 6, 12	[kPa]
σ_c/σ_3	1 , 2, 3, 4, 5, 6, 7	[-]

For lack of better alternatives, the horizontal stresses in unbound base courses were estimated using Boussinesq's and Odemark's theory, resulting in values around 10 to 20 kPa (107). The four values of σ_3 were then selected so as to certainly cover in-situ conditions. The cyclic part σ_c of the deviator stress was chosen as fixed ratios to the confining stress σ_3. For the weaker materials ratios of 1 to 6 were applied, for the stronger materials ratios of 2 to 7. These stress ratios ensure that only very limited permanent deformation of the triaxial specimen occurs, thereby allowing all cyclic load tests for the determination of resilient properties to be carried out on one triaxial specimen per material/grading. The static part σ_s of the deviator stress was chosen at the lowest value practically feasible: σ_s = 1.5 kPa. Tests were also carried out at σ_s = 6 kPa and σ_s = 12 kPa to investigate the influence of σ_s on resilient properties. In total, each material/grading was thus tested at four levels of the confining stress σ_3, three levels of static deviator stress σ_s and six levels of the cyclic deviator stress σ_c, resulting in a total of 72 tests per material/grading. This number of 72 tests was adhered to strictly for all resiliency testing since the interpretation software used to calculate resilient moduli and other parameters requires a fixed number of 72 data sets for input.

At each combination of stresses, 100 applications of the cyclic deviator stress were executed and resilient deformations were measured during cycle number 100. In all, the automated system measures the applied cyclic load, the output of the four vertical LVDT's measuring

axial deformation and of the two horizontal gap sensors measuring radial deformations. In this chapter the test results will be presented in the form of the resilient modulus only; the more complex material models will be dealt with in Chapter 7. For each combination of stresses applied, the resilient modulus M_r is calculated from the applied cyclic deviator stress σ_c and the resulting axial strain according to:

$$M_r = \frac{\sigma_c}{\varepsilon_{a,r}} \tag{5.1}$$

where

M_r = resilient modulus [MPa]
σ_c = cyclic deviator stress [kPa]
$\varepsilon_{a,r}$ = axial resilient strain [10^{-3}]

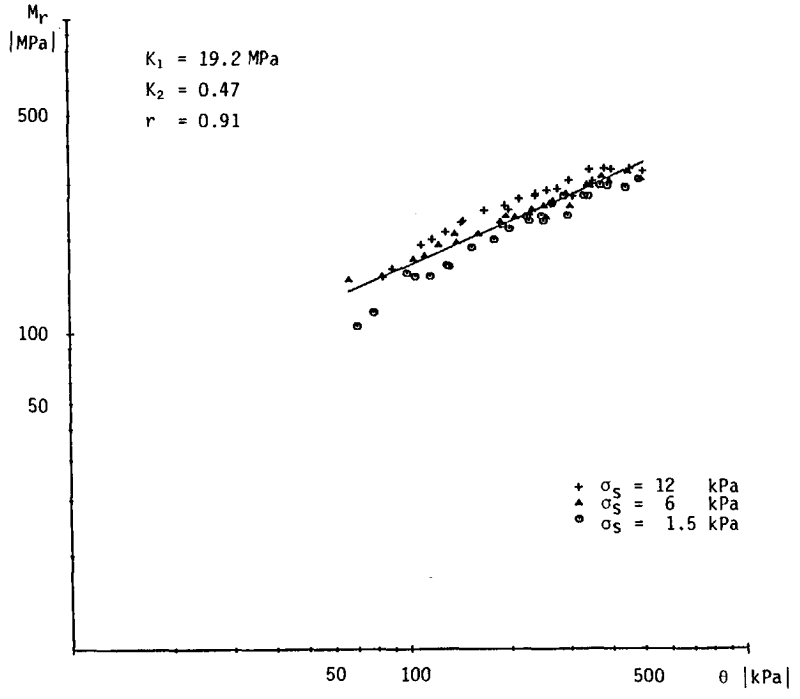

Figure 5.10: Resilient modulus M_r versus sum of principal stresses θ, for material LA0 (lava, coarse grading).

The units used for stiffness (MPa) and stress (kPa) in Equation 5.1 were chosen as such for conformity with pavement engineering practice. Figure 5.10 shows an example of the 72 test results obtained for one

material/grading. The resilient modulus M_r has been plotted on a log-log scale against the sum of principal stresses θ, calculated according to:

$$\begin{aligned}\theta &= \sigma_1 + \sigma_2 + \sigma_3 \\ &= (\sigma_3 + \sigma_d + \sigma_c) + \sigma_3 + \sigma_3 + 10 \text{ kPa} \\ &= \sigma_c + \sigma_s + 3\sigma_3 + 10 \text{ kPa}\end{aligned} \qquad (5.2)$$

The value of θ has been raised by 10 kPa to incorporate the built-in overburden stress at half specimen height discussed earlier. The data points from the 72 cyclic load tests plot along a straight line on the log-log scale. The three levels of the static deviator stress σ_s used are indicated by different symbols in Figure 5.10. Although small, the influence of σ_s on the resilient modulus M_r can be clearly recognized; higher values of σ_s lead to somewhat higher values of M_r.
The straight line depicted in Figure 5.10 can be described by the well known K-θ model:

$$M_r = K_1 \left(\frac{\theta}{\theta_0}\right)^{K_2} \qquad (5.3)$$

where

M_r	= resilient modulus	[MPa]
θ	= sum of principal stresses	[kPa]
θ_0	= 1 kPa = reference stress	[kPa]
K_1	= material parameter	[MPa]
K_2	= material parameter	[-]

Table 5.4 summarizes the values for K_1 and K_2 for the 25 combinations of materials and gradings tested. Also shown in the table are the values of M_r for values of θ of 50 kPa and 500 kPa, calculated from K_1 and K_2 using Equation 5.3. These values of M_r have been included in the the table since they allow for a direct comparison of resilient properties expressed in every-day engineering units. θ = 50 kPa and θ = 500 kPa are the rounded-off boundaries of the values of θ applied in the resiliency testing.

Table 5.4: Material parameters K_1 and K_2

material number	test code	K_1 |MPa|	K_2 |-|	M_r θ = 50 kPa |MPa|	M_r θ = 500 kPa |MPa|
C01	LABD 05	26.9	.35	106	237
C02	LAOD 07	19.2	.47	121	356
C03	POBD 03	29.2	.32	102	213
C04	POOD 01	22.9	.43	123	331
C05	GGBD 01	40.9	.23	101	171
C06	GGOD 01	47.2	.31	159	324
C07	KABD 02	156.8	.14	271	374
C08	KAOD 01	37.7	.45	219	618
C09	STND 01	157.8	.05	192	215
C10	SMCD 01	43.5	.34	164	360
R01	MGBD 07	6.3	.49	43	132
R02	MGOD 10	4.0	.65	50	227
R03	M2BD 01	27.5	.30	89	177
R04	M2OD 02	18.3	.43	98	265
R05	BGBD 01	21.1	.48	138	417
R06	BGOD 01	11.2	.59	113	438
R07	KGBD 01	41.8	.28	125	238
R08	KGOD 01	18.6	.45	108	305
R09	FFBD 01	77.3	.17	150	222
R10	FFOD 01	22.6	.44	126	348
R11	B2CD 01	71.8	.21	163	265
R12	K1CD 01	34.8	.35	137	306
R13	K2CD 01	36.1	.34	137	299
R14	K3CD 01	30.1	.36	124	282
R15	AVCD 01	39.9	.23	98	167

A comparison of the resilient properties of all the materials investigated lies beyond the scope of this dissertation. For individual comparisons, reference is made to the relevant research reports [108, 109, 110]. Here, only general conclusions with respect to the test results will be drawn:

1. The value of the material parameter K_2 indicating the slope of the M_r-θ line is consistently higher for the coarse O-gradings as compared to the finer B-grading. This is consistent with theory since stress-dependency is more pronounced for the coarse graded materials.

2. The higher value of K_2 causes all the M_r values for θ = 500 kPa of the coarse graded materials (O-grading) to be higher than those of the fine graded materials (B-grading). The M_r values for θ = 50 kPa do not show a clear pattern.

3. In general terms, the recycled base course materials (Group R) show resilient properties of the same order of magnitude as the conventional materials (Group C). The materials exhibiting the highest elastic stiffness are the crushed concrete BG and the limestone KA. The lowest elastic stiffness were found for crushed masonry 1 (MG) and for the waste incineration slag (AVC).

4. A remarkably good agreement is found between the three lots of commercial crushed rubble (K1C, K2C and K3C). Although obtained from three different crusher plants and tested at as-delivered gradings, these materials show an almost equal resilient stiffness. Furthermore, the M_r-θ lines for these commercial materials plot between the lines obtained for the laboratory made materials FFB and FFO (the laboratory-made 50%/50% mixtures of crushed masonry and crushed concrete).

5. It should be noted that all tests were performed directly after specimen preparation. Therefore, a possible self-cementing potential of the materials tested is not reflected in the resilient properties shown in Table 5.4. The investigation of the self-cementing potential of certain materials is dealt with in Chapter 8.

5.3.2.6 PERMANENT DEFORMATION

A selection of the 25 material/grading combinations tested for resilient properties was also tested for permanent deformation properties. From the conventional materials of Group C lava LA was

tested at two laboratory made gradings. From the recycled materials of Group R four materials (crushed masonry 1 MG, crushed concrete BG, crushed clincker KG and crushed masonry/concrete FF) were tested at two laboratory-made gradings. In all, 10 material/grading combinations were, therefore, tested for permanent deformation properties.

For each material/grading combination, three triaxial specimens were built. Each specimen was subjected to 10^6 applications of the cyclic deviator stress σ_c, at fixed levels of the confining stress σ_3 and the static deviator stress σ_s. Tests were performed at a loading frequency of 5 Hz, up to 10^6 load applications or up to failure, which in this case means excessive permanent deformation. The constant confining stress was set at σ_3 = 12 kPa and the static deviator stress at σ_s = 3 kPa. The cyclic deviator stress was chosen at ratios of σ_c/σ_3 = 4 up to 12, depending on material quality. Testing of all material/grading combinations at the same stress ratios was not useful since this would lead to premature failure of the weaker materials and/or no permanent deformation at all for the stronger materials. Axial and radial deformations of the triaxial specimens were monitored by the computer system as a function of the number of load applications.

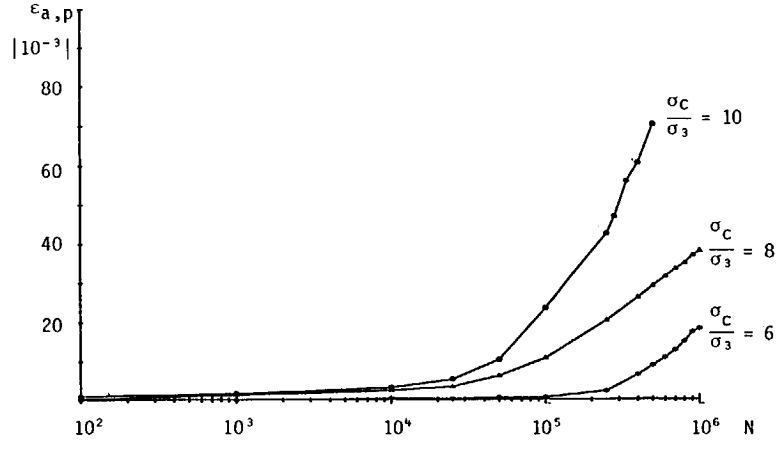

Figure 5.11: Permanent axial strain versus number of load applications, for material LA0 (lava, coarse grading).

Figure 5.11 shows an example of the test results for the material LA0 (lava, coarse grading). The tests performed at stress ratios of

σ_c/σ_3 = 6 and 8 were carried up to 10^6 load applications, resulting in limited permanent deformation only. The test performed at σ_c/σ_3 = 10 was stopped at 5×10^5 applications when a permanent axial strain $\varepsilon_{a,p} = 703 \times 10^{-4}$ had been reached (equivalent to a "rut" of 21 mm in a granular base course of 30 cm thickness).

Table 5.5: Permanent axial strain $\varepsilon_{a,p}$ at 10^6 load applications.

material number	test code	density $\lvert kg/m^3 \rvert$	σ_c/σ_3 $\lvert - \rvert$	$\varepsilon_{a,p}$ $\lvert 10^{-3} \rvert$
C01	LABD 07	1742	8	3
	LABD 08	1802	9	6
	LABD 06	1745	10	F
C02	LAOD 05	1739	6	18
	LAOD 04	1689	7	40
	LAOD 03	1665	8	F
R01	MGBD 09	1530	8	48
	MGBD 10	1460	9	F
	MGBD 06	1578	10	F
R02	MGOD 14	1499	4	1
	MGOD 13	1481	6	F
	MGOD 11	1475	8	F
R05	BGBD 05	1797	8	10
	BGBD 03	1830	10	40
	BGBD 04	1815	12	F
R06	BGOD 03	1856	10	30
	BGOD 04	1879	11	38
	BGOD 05	1811	12	F
R07	KGBD 03	1790	9	3
	KGBD 05	1743	10	34
	KGBD 04	1768	11	52
R08	KGOD 06	1722	7	- *
	KGOD 04	1704	8	47
	KGOD 03	1695	9	67
R09	FFBD 02	1644	10	10
	FFBD 04	1613	11	F
	FFBD 03	1633	12	F
R10	FFOD 02	1698	8	5
	FFOD 04	1688	9	84
	FFOD 03	1669	10	F

* Test stopped at N = 250 000 for technical reasons

As for the resilient deformations dealt with in the previous paragraph, modelling of the permanent deformations as a function of the number of load applications will be dealt with in Chapter 7. Here, the results from the permanent deformation tests will be presented in the simplest form only. Table 5.5 shows the permanent strain after 10^6 load applications for all the triaxial specimens tested. Tests that were cut off because of excessive permanent deformation are indicated in the table by a letter F ("Failure").

As was done for the resilient deformation properties, a detailed comparison of the permanent deformation properties of the materials will be omitted here. For that comparison, reference is made to the relevant research reports (108, 109). The general conclusions with respect to the permanent deformation properties of the investigated material are:

1: The effect of the applied stress ratio on the development of permanent axial strain appears to be larger than the effect of the limited variation in specimen density. Specimens of the same material/grading tested at lower stress ratios and lower densities show a smaller permanent strain than do specimens tested at higher stress ratios and densities. Since the effect of stress ratio and density on permanent deformation development are opposite (higher stress ratio leads to more permanent strain, higher density to less), it can be concluded that the effect of stress ratio dominates that of density (within the range of densities of the triaxial specimens).

2: In general, materials are more resistant to permanent deformation development at the fine B-grading than at the coarse O-grading. The crushed concrete BG deviates from this pattern: here BGO is somewhat more resistant to permanent deformation than BGB (compare tests BGOD 03 and BGBD 03).

3: The material showing the highest resistance to permanent deformation is coarse graded crushed concrete BGO. This material also showed a high resistance to resilient deformation (see Table 5.4, Paragraph 5.3.2.5), which would at first glance indicate a possible correlation between resistance to permanent and resilient deformations as suggested by Veverka (49) and Descornet (50). Fine

graded crushed masonry MGB however couples an intermediate resistance to permanent deformation to the lowest resistance to resilient deformation of all materials tested. Comparing the test results for the two gradings at which material MG was tested, Table 5.5 shows the fine grading MGB to have a higher resistance to permanent deformation than the coarse grading MGO. For resistance to resilient deformation (Table 5.4), the order is reverse. Apparently, straightforward relationships between resistance to permanent and resilient deformation do not exist. This conclusion is consistent with the results of cyclic load triaxial testing carried out at Nottingham University. Thom and Brown [111] reported on the mechanical properties of unbound granular materials from various sources. They showed that a ranking of the materials investigated with respect to resilient deformation was quite different from a ranking based on resistance to permanent deformation. The topic of possible correlations between resilient and permanent strain is dealt with further in Paragraph 5.6.2.

5.3.3 Cyclic load triaxial tests Group S

5.3.3.1 INTRODUCTION

The six sands of Group S were tested in a cyclic load triaxial apparatus with a specimen size of 100 mm diameter by 200 mm height. Although for testing of only sands a smaller specimen size would have been possible, the particular 100 × 200 mm size was chosen to allow for testing of coarser graded materials like the laterites of Group L in the same apparatus. For the specimen size of 100 × 200 mm, standard triaxial cells are commercially available. The triaxial cell used was developed from such a standard cell, with modifications for performance of cyclic load tests and measurements of radial strain.

The use of a triaxial cell with an internal pressure providing the confining stress rather than the vacuum principle used in the 400 mm specimen diameter apparatus allows for the use of back-pressure for setting the degree of saturation of the triaxial specimen at any required level. For the sands and the laterites to be tested in the 100 mm specimen diameter apparatus this is a main advantage, if not a prerequisite. These materials are applied at greater depth in the

pavement structure or, in the case of laterites, even in unpaved roads and may therefore very well be saturated in-situ. Furthermore, the use of a triaxial cell allows for confining stresses over 100 kPa to be applied, which is required for testing materials applied at greater depth.

All six sands from Group S were tested for resilient properties, while a selection of three sands was also tested for permanent strain properties. The test procedures and the results of the test will be detailed in this paragraph.

5.3.3.2 THE 100 MM SPECIMEN DIAMETER APPARATUS

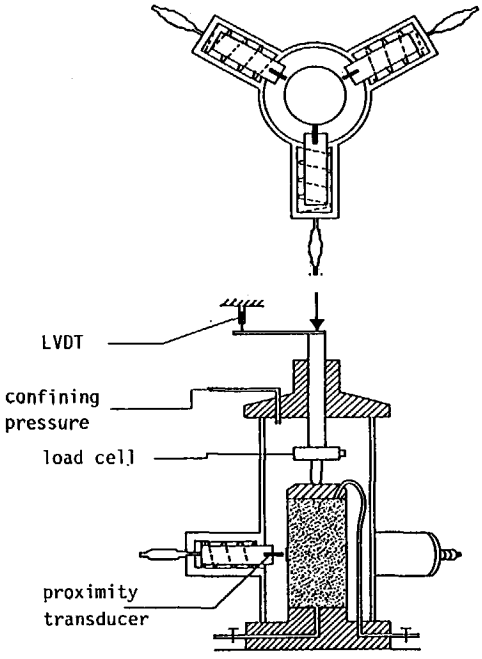

Figure 5.12: Schematics of the 100 mm specimen diameter cyclic load triaxial apparatus.

Fig. 5.12 shows the schematics of the 100 mm specimen diameter triaxial apparatus. The triaxial specimen is situated between the pedestal and the top platen of triaxial cell. The specimen is enclosed by a latex membrane, which is sealed with grease and O-rings to the pedestal and the top platen. The original standard cell was replaced

by an elongated plexiglass cylinder, thereby allowing the load cell of the servo-hydraulic loading equipment to be incorporated inside the triaxial cell. This eliminates errors in the applied load due to friction between the loading piston and the top cap.

The confining stress σ_3 is applied to the triaxial specimen by setting the internal pressure in the triaxial cell to the required level. Axial stress is applied by means of a 5 kN MTS servo-hydraulic actuator connected to the loading piston. The frequency range of the triaxial equipment is from static loading up to 10 Hz. The axial deformation of the specimen is measured by an LVDT mounted outside the triaxial cell between the loading piston and the frame of the apparatus. Radial deformation of the specimen is measured by a set of three proximity transducers, mounted through the plexiglass cell in a horizontal plane at half the specimen height. These transducers are connected to micrometers, which allow for adjustment and measurement of the position of the sensor relative to the triaxial cell wall.

The measuring system described above clearly deviates from the system suggested in AASHTO T 274-82, which involves the use of a set of two clamps mounted on the triaxial specimen supporting the displacement transducers (similar to the system used in the 400 mm specimen diameter apparatus described in the previous paragraph). The AASHTO-system has the advantage of eliminating errors in measurement of axial specimen deformations caused by deformation of the triaxial equipment itself. Furthermore, the effect of end-cap restraint (prevention of radial movement of the material tested due to friction at bottom- and top-platen) is virtually eliminated by measuring only the deformations of the middle third part of the triaxial specimen. The disadvantage of such a system is that the displacement transducers are out of reach while the test is in progress. They therefore cannot be re-adjusted into their working range if permanent deformation of the specimen occurs without stopping the test, releasing the confining stress and removing the triaxial cell. Therefore, displacement transducers with a larger working range and hence a reduced accuracy have to be used. Secondly, measurement of the axial deformation of only the middle third part of the triaxial specimen reduces the deformations measured by a factor of three, which in the case of a small sample height again has a negative effect on the accuracy of the deformation measurement. A third disadvantage of the AASHTO-system is that it is indeed quite

cumbersome since very accurate placement of the clamp/LVDT assembly is required to ensure reliable deformation measurements.

For ease of handling, the AASHTO-system of deformation measurement was rejected and the system described above was chosen. To eliminate errors in deformation measurement caused by deformation of the triaxial equipment, the apparatus is calibrated at regular intervals using a steel triaxial "specimen". By performing cyclic load triaxial test on the calibration specimen at the same axial stresses as those applied to regular specimens, the stress-dependent equipment-deformations can be determined since the deformation of the steel specimen itself is negligible. The radial deformation system was calibrated by performing tests on fully saturated specimens. For resilient deformation measurements, undrained triaxial tests were performed ensuring no volume change, while for the large-deformation permanent strain measurements drained tests were carried out with measurement of the volume of the water expelled from the triaxial specimen. Knowing the volume change in both cases and knowing the axial deformation of the specimen, the radial deformation of a specimen deforming theoretically from a true cylinder in the unloaded case to a shorter and thicker true cylinder in the loaded case could be obtained.

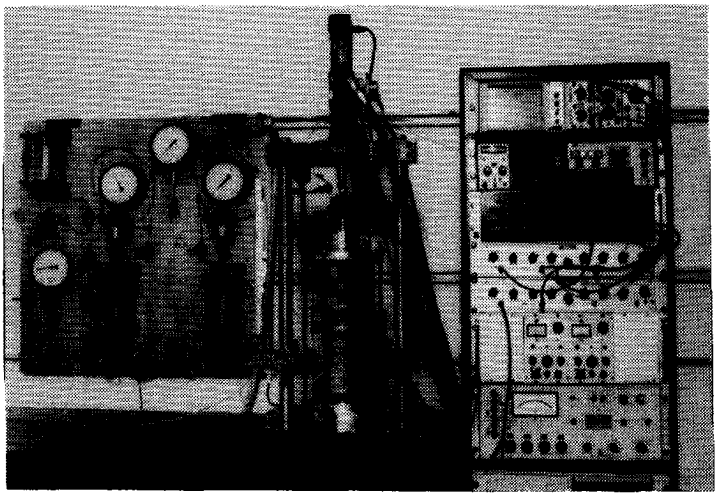

Figure 5.13: Overall view 100 mm specimen diameter triaxial equipment.

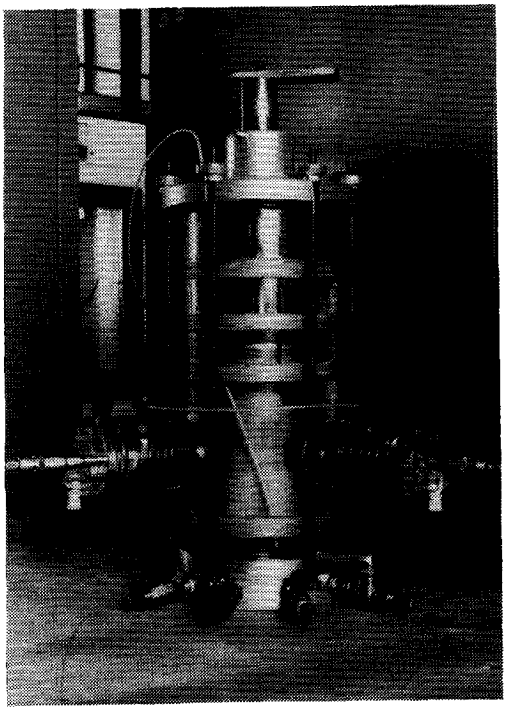

Figure 5.14: 100 mm specimen diameter triaxial cell.

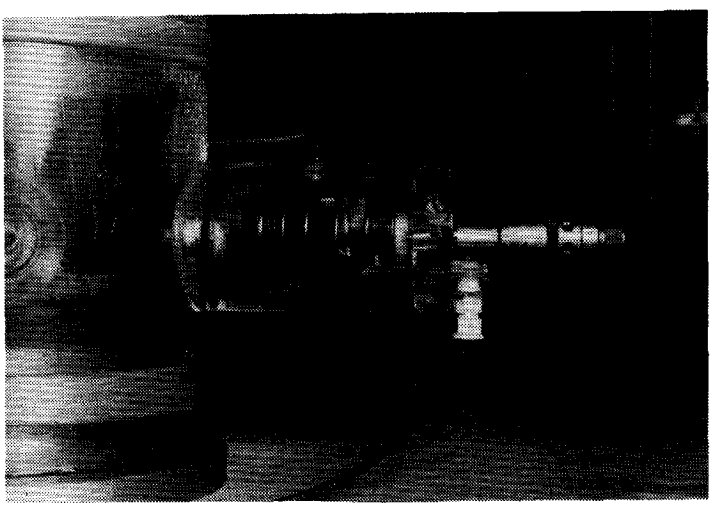

Figure 5.15: Proximity transducer for measurement of radial strain.

Through the valves in the triaxial cell pedestal the specimen is connected to an assembly of reducing valves and Bourdon-gauges, which allow for control and read-out of cell pressure, back-pressure and volume change. An electronic pressure transducer allows for high-accuracy pressure measurements. In contrast to the digitally-operated 400 mm specimen diameter apparatus, the 100 mm specimen diameter apparatus is controlled by an analogue system. All stresses applied are set by hand and deformations are read from an oscilloscope and strip-chart recorders. Figures 5.13 through 5.15 show an overall view and details of the 100 mm specimen diameter apparatus.

5.3.3.3 THE MATERIALS INVESTIGATED

Six different sands used widely in pavement construction in the Netherlands were tested. The materials have been described in Paragraph 4.4 (see Tables 4.4 and 4.5). All sands were tested for resilient properties, while one very coarse sand (Echten sand EN), one very fine sand (Eastern Scheldt sand OS) and one extremely fine sand (Zeijen sand ZE) were also tested for permanent strain properties. To denote the various tests, the coding system given in Figure 5.7 will again be used. For the material codes used reference is made to Chapter 4 (Table 4.5) and Appendix 1.

5.3.3.4 SPECIMEN PREPARATION PROCEDURE

The target values for the density and moisture content of the triaxial specimen are the Maximum Modified Proctor Density MMPD and the optimum moisture content of each of the sands, as shown in the Material Information Sheets of Appendix 2. A sample of a few kilograms of the sand to be investigated was taken and the moisture content of the sand was adjusted to optimum moisture content. The procedure for preparation of the specimens is as follows:

1. A rubber membrane is sealed with grease and O-rings to the bottom platen of the triaxial apparatus.

2. A porous disk and a filter paper are placed on the bottom platen. Subsequently, a split mould is placed over the bottom platen and

the membrane is stretched inside the mould. By applying vacuum to the space between mould and membrane the membrane is pressed against the inner side of the mould.

3. A special tamping compaction device is then placed on the pedestal of the triaxial cell, as shown in Figure 5.16.

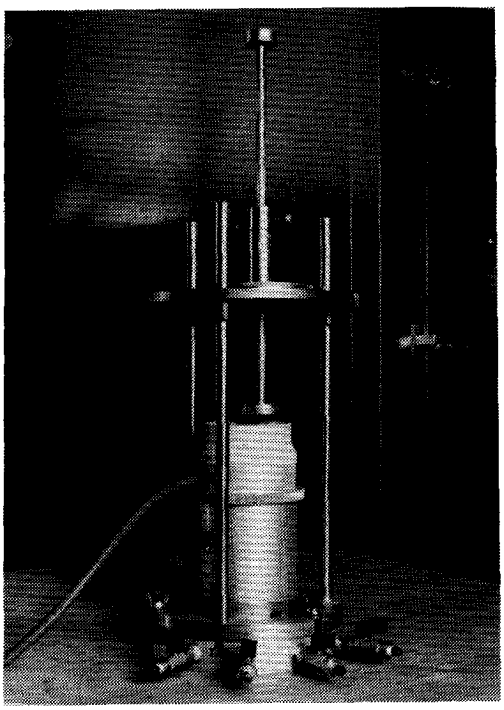

Figure 5.16: Compaction tamping device mounted on pedestal.

4. The specimen is built up in six layers of equal mass. Each layer is compacted to the required height using the compaction device with the guided tamper. After compaction of each layer, the surface of that layer is roughened to ensure a smooth transition between two adjacent layers.

5. After compaction of the sixth layer, the upper side of the specimen is trimmed horizontally to provide a smooth surface. After placement of filter paper, porous disk and top platen, the membrane is sealed to the top platen with grease and O-rings.

6. Subsequently, vacuum is applied to the inside of the specimen, after which the split mould can be removed. Figure 5.17 shows the triaxial specimen after removal of the split mould.

7. Next, the triaxial cell is placed over the specimen/pedestal assembly and air pressure is applied inside the cell. The vacuum inside the specimen can then be removed and the specimen is ready for testing.

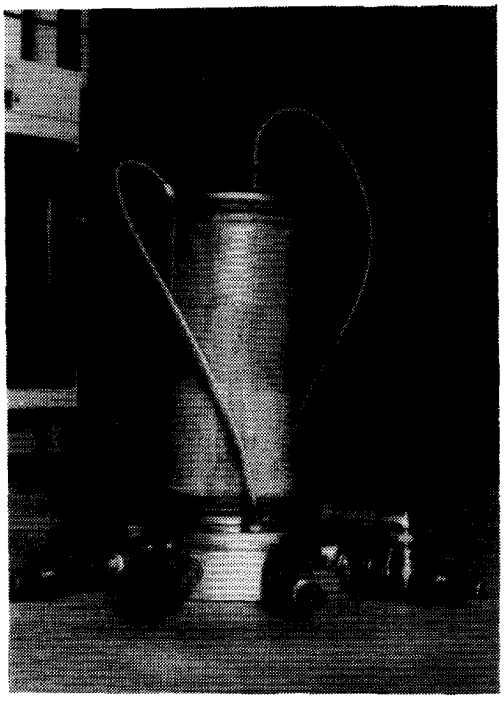

Figure 5.17: Triaxial specimen on pedestal.

It should be noted that each of the six layers in which the specimen was built was compacted to the same height. Since each layer was compacted using the same mass of sand, the target density for each layer was the same. Ladd [112] suggested a system of "undercompaction" for the preparation of remoulded triaxial specimens. The reasoning behind this system is that, after compaction of the first layer, the density of that layer will further increase due to the compaction energy exerted on the second and all other layers. Hence, the lowest layer

should initially be compacted to a somewhat lower density. The same reasoning goes for all other layers except of course the upper layer. Ladd suggested a method for calculating to which density each of the layers should initially be compacted in order to eventually ensure a constant density over the specimen height. In Ladd's method, the correction on the initial density of each layer is dependent on the target value of the density of the triaxial specimen (expressed as relative density). In this particular case of the target density being the Maximum Modified Proctor Density, the correction factors for of each of the layers turned out to be almost unity. Hence, no "undercompaction" was required and each layer was compacted to the same density.

5.3.3.5 RESILIENT DEFORMATION

For each of the six sands, one triaxial specimen was prepared and tested for resilient properties at a large number of combinations of stresses. Figure 5.18 shows the stresses applied in the resilient property tests; the levels used are given in Table 5.6.

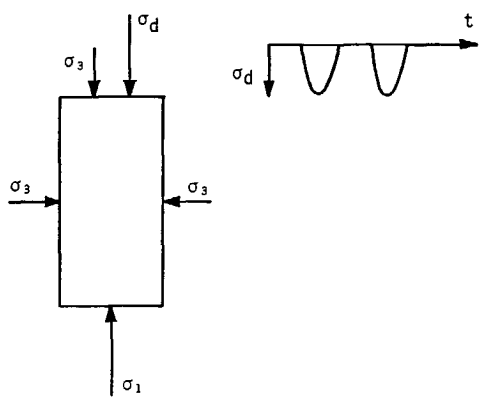

Figure 5.18: Stresses applied on triaxial specimen.

As can be seen from Table 5.6, quite a large range of confining stresses σ_3 was used in the testing of the sands, as compared to the stresses applied when testing the granular base course materials of Groups C and R (see Table 5.3, Paragraph 5.3.2.5). This was done because sands are applied in the deeper pavement layers and are thus subjected to higher overburden stresses. The stress ratios σ_c/σ_3 were

limited as compared to those applied for the granular base course materials because of the lower stress ratio at failure of the sands. Due to the apparent cohesion in the sand, higher stress ratios can be applied at the lower confining stresses.

Table 5.6: Stress levels applied in resilient properties tests.

σ_3 |kPa|	σ_c |kPa|					σ_c/σ_3 |-|
10	10	20	30	40	50	1 - 5
20	20	40	60	80		1 - 4
30	30	60	90	120		1 - 4
40	40	80	120	160		1 - 4
60	60	120	180			1 - 3
80	80	160	240			1 - 3
100	100	200	300			1 - 3
200	200	400				1 - 2
300	300					1

As can be seen from Figure 5.18, the deviator stress σ_d consisted of the cyclic part σ_c only; the static deviator stress σ_s used when testing with the 400 mm specimen diameter apparatus (see Figure 5.9, paragraph 5.3.2.5) was omitted here. The 100 mm specimen diameter apparatus allows for resiliency testing with σ_s at a negligible value. To limit the number of tests with this hand-operated apparatus σ_s was, therefore, not varied in the tests. The determination of resilient properties was further similar the procedure described for the 400 mm specimen diameter apparatus; Table 5.7 shows the resulting values of the material parameters K_1 and K_2.

Comparison of the resilient properties of the six sands can most readily be done by observing the values of the resilient modulus for θ = 50 kPa and θ = 500 kPa. Doing so, Echteld and Echten sand (EL and EN) are shown to have identical resilient properties; Eems, Eastern Scheldt and Winterswijk sand (EE, OS and WI) have almost identical resilient properties, while the properties of Zeijen sand (ZE) deviate from those of the other two groups. Figure 5.19 shows the grading curves of the six sands investigated. The same distinction in three

groups can be recognized. Echteld and Echten sand have almost identical gradings; the gradings of Eems, Eastern Scheldt and Winterswijk sand are almost identical and Zeijen sand again stands on its own. The influence of grading on resilient properties is apparent from these results.

Table 5.7: Material parameters K_1 and K_2

material number	test code	K_1 |MPa|	K_2 |-|	M_r θ = 50 kPa |MPa|	M_r θ = 500 kPa |MPa|
S01	ELND 01	8.1	.56	72	263
S02	ENND 01	7.6	.57	71	261
S03	EEND 01	8.9	.56	80	289
S04	OSND 01	9.8	.54	81	281
S05	WIND 01	10.5	.53	83	283
S06	ZEND 01	9.7	.52	74	246

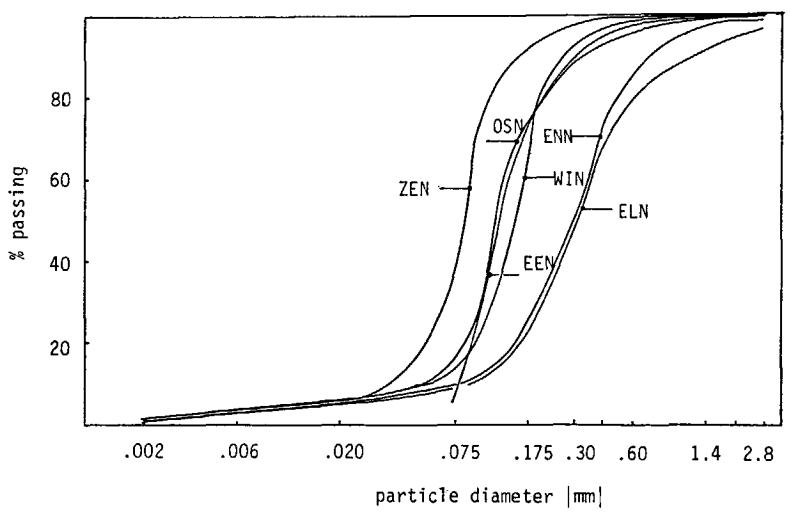

Figure 5.19: Particle size distribution of sands investigated.

5.3.3.6 PERMANENT DEFORMATION

The six sands investigated for resilient properties can be divided into three groups on the basis of their grading (see Figure 5.19):

very coarse sands (materials ELN and ENN), very fine sands (ENN, OSN and WIN) and one extremely fine sand (ZEN). One sand from each of these groups was tested for permanent strain properties.

For each sand, three triaxial specimens were built. Each specimen was subjected to 10^6 applications of the cyclic deviator stress σ_c, at a fixed level of the confining stress σ_3 = 10 kPa. As was done in the resiliency testing of the sands, the static part of the deviator stress was negligible. The permanent strain tests were performed at a loading frequency of 5 Hz, as was done in the permanent strain testing of the granular base coarse materials. The cyclic deviator stress σ_c was chosen at ratios of σ_c/σ_3 = 3 up to 6, depending on material quality. Figures 5.20, 5.21 and 5.22 show the development of permanent axial strain $\epsilon_{a,p}$ with the number of load applications N for the three sands tested.

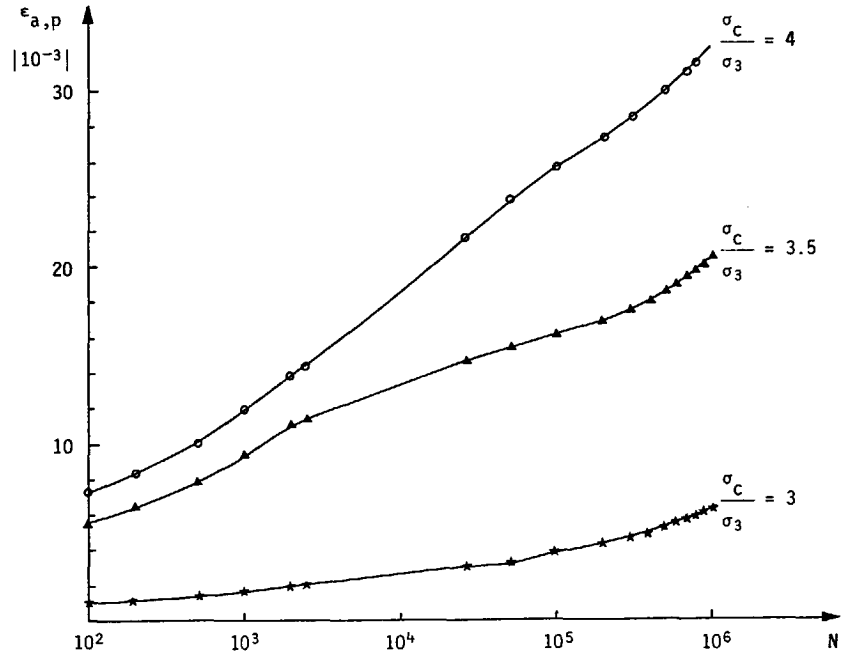

Figure 5.20: Permanent axial strain $\epsilon_{a,p}$ versus number of load applications N, for Echten sand ENN.

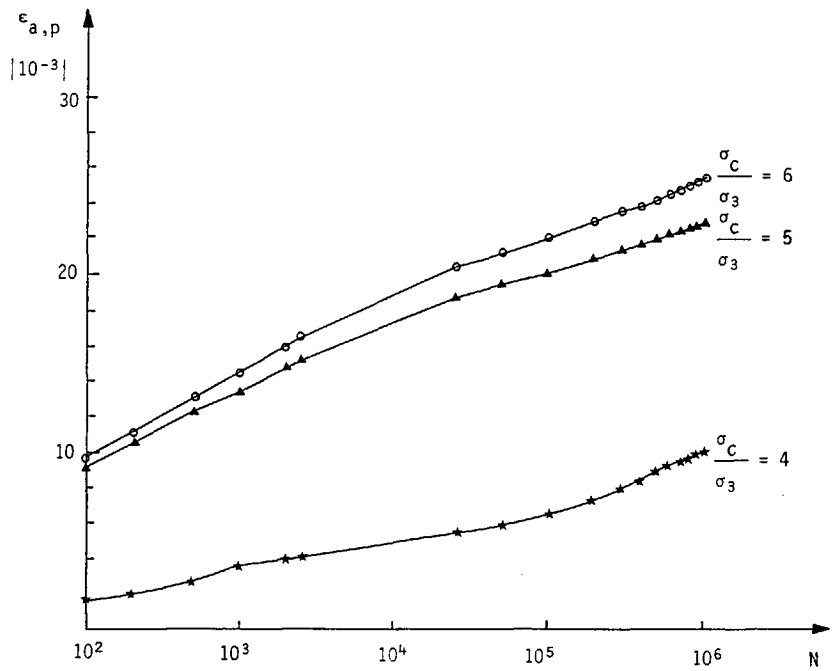

Figure 5.21: Permanent axial strain $\epsilon_{a,p}$ versus number of load applications N, for Eastern Scheldt sand OSN.

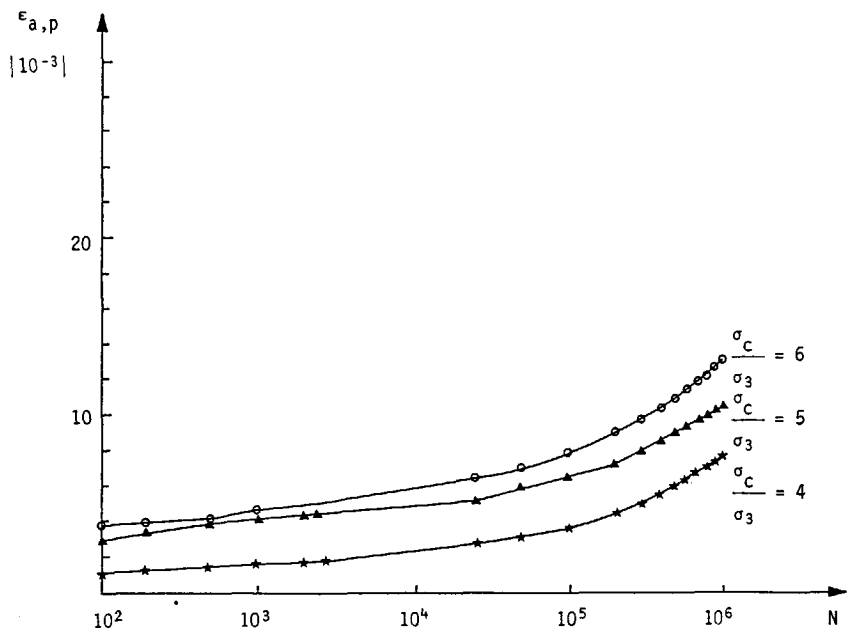

Figure 5.22: Permanent axial strain $\epsilon_{a,p}$ versus number of load applications N, for Zeijen sand ZEN.

Table 5.8 summarizes the test results and shows the initial density of each individual triaxial specimen. As was done in the resiliency testing, the Maximum Modified Proctor Density was used as target value in specimen preparation. As can be seen from the density values in the table, the 100 mm diameter specimens could be built almost exactly at the target dry density. In building the 400 mm diameter specimens the problem was encountered of not being able to bring the required 200 kg of sample material to exactly the target moisture content, which subsequently resulted in deviations in dry density (see Paragraph 5.3.2.4). This problem does not occur in preparing the small specimens, since the total batch of sample material can be easily dried prior to the addition of the required quantity of water.

Table 5.8: Permanent axial strain $\varepsilon_{a,p}$ of triaxial specimens after 10^6 load applications

material number	test code	density $\lvert kg/m^3 \rvert$	σ_c/σ_3 $\lvert - \rvert$	$\varepsilon_{a,p}(10^6)$ $\lvert 10^{-3} \rvert$
S 02	ENND 03	1713	3	6
	04	1712	3.5	21
	02	1712	4	33
S 04	OSND 02	1668	4	10
	03	1668	5	23
	04	1668	6	25
S 06	ZEND 02	1593	4	8
	03	1593	5	10
	04	1593	6	13

The modelling of the permanent strain behaviour of the sands will be dealt with in Chapter 7, together with that of the granular base course materials. Here, only general conclusions with respect to permanent strain behaviour will be drawn:

1. The test results indicate an influence of grading on the permanent strain properties of the sands; a finer grading results in a larger resistance to permanent deformation.

2. As was found when testing the granular base course materials, again no relationship exists between permanent strain properties and resilient properties. The extremely fine Zeijen sand, for instance, shows the highest resistance to permanent deformation while showing the lowest resilient moduli (see Table 5.7). As stated earlier, possible correlations between resilient and permanent strain properties will be checked numerically in Paragraph 5.6.

3. Comparing the permanent strain properties of the sands (Table 5.8) to those of the granular base course materials (Table 5.5), the sands clearly show a much lower resistance to permanent deformation.

5.3.4 Repeatability cyclic load triaxial tests

To check the repeatability of the determination of resilient properties, tests B2CD 01 (M_r-determination crushed concrete 2 in 400 mm specimen diameter apparatus) and OSND 01 (M_r-determination Eastern Scheldt sand in 100 mm specimen diameter apparatus) were repeated [113]. New material samples were taken from the stock for preparation of new triaxial specimens. Table 5.9 shows the triaxial specimen data of all tests, and the material parameters K_1 and K_2 resulting from the tests.

Table 5.9: Repeatability M_r-determination

test code	w [%]	ρ_d [kg/m^3]	K_1 [MPa]	K_2 [-]
B2CD 01	10.6	1858	71.8	.21
B2CD 02	7.4	1821	65.1	.23
OSND 01	15.7	1668	9.8	.54
OSND 05	15.7	1668	11.0	.51

The triaxial specimen data of test B2CD 02 deviate somewhat from those of test B2CD 01. As stated earlier, mixing of some 200 kg of granular

material with water to exactly the same target moisture content is not feasible. The use of the same standard compactive effort for both specimens then results in some deviation in specimen dry density. The much smaller sand specimens can easily be reproduced to the same target moisture content and density.

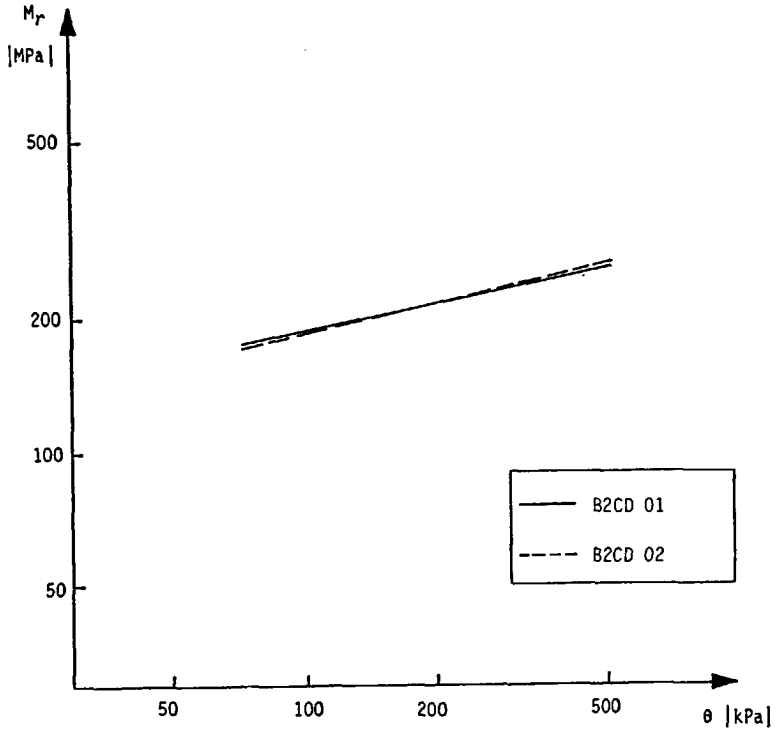

Figure 5.23: Repeatability M_r-determination in 400 mm specimen diameter apparatus.

The material parameters K_1 and K_2 too show some deviation. When plotted in M_r-θ graphs, the deviation in the test results is shown to be very small (see Figures 5.23 and 5.24). Only the regression lines through the individual data points from the cyclic load triaxial tests are given in Figures 5.23 and 5.24, since the results of the two groups of data per figure almost coincide.

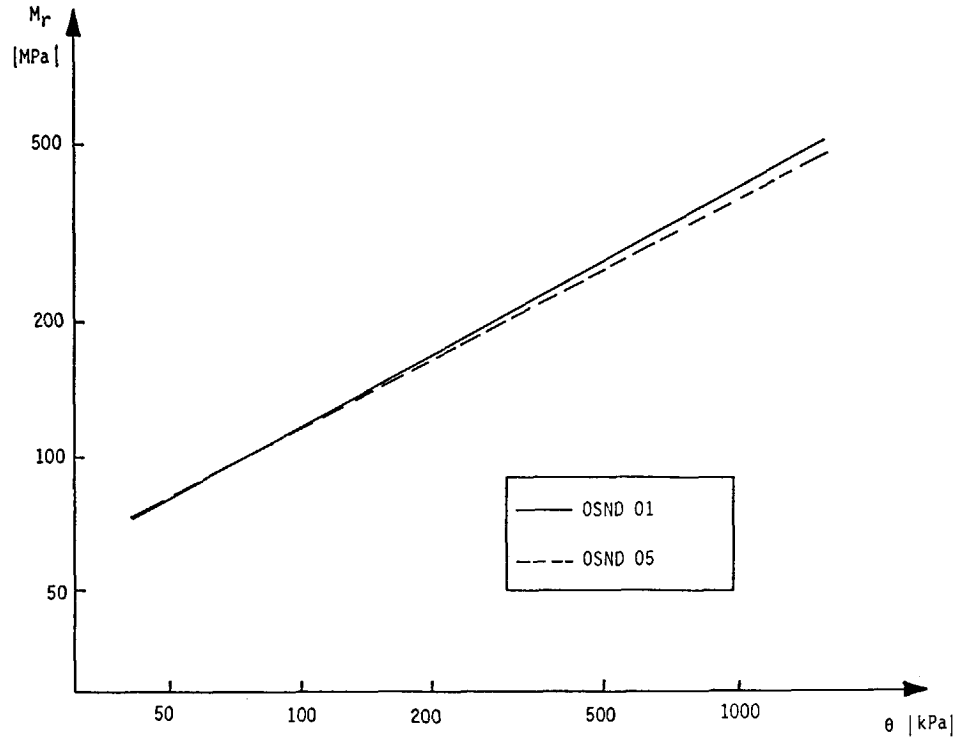

Figure 5.24: Repeatability M_r-determination in 100 mm specimen diameter apparatus.

5.4 CORRELATIONS BETWEEN FUNDAMENTAL AND EMPIRICAL MATERIAL PARAMETERS

Cyclic load triaxial tests require complicated equipment for applying the cyclic deviator stress and for readout of specimen deformations. The tests are therefore today mainly carried out for research purposes. Yet, for pavement design using mechanistic methods such as the Shell Pavement Design Manual, fundamental material parameters describing the stress/strain relationship of the materials applied in the pavement are required. To circumvent the need for cyclic load triaxial testing for determination of these fundamental material parameters, correlations have been sought between fundamental and empirical material parameters. The most well known of such correlations is the E-CBR relationship discussed earlier in Paragraph 2.7.2. As shown in that paragraph, the CBR-value of soils can only be a rough indication

of the soil stiffness expressed in Young's E-modulus. The whole concept of characterizing the resilient stress-strain properties of soils and unbound materials by one single E-value is, in fact, not correct, since such materials show a stress-dependent resilient stiffness.

For the research described in this dissertation, the stress-dependent resilient stress-strain properties of 25 granular base course materials and of six sands were determined in cyclic load triaxial tests. CBR-tests were performed on the same materials, as described in Paragraph 5.2.3.2. To underline the invalidity of E - CBR relationships, Figures 5.25 and 5.26 show plots of CBR versus the resilient modulus M_r, calculated from the M_r-θ relationship for a stress level of θ = 50 kPa.

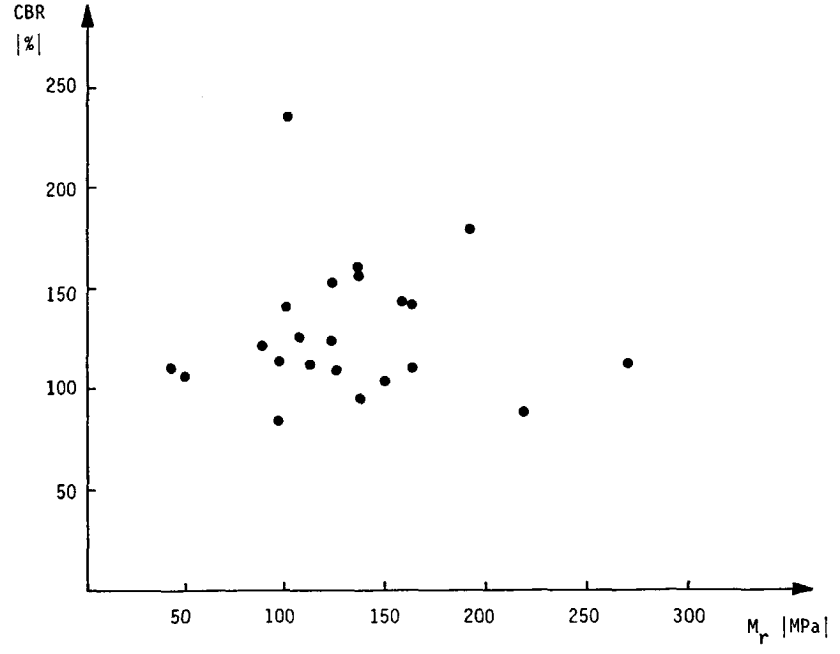

Figure 5.25: California Bearing Ratio CBR versus resilient modulus M_r (at a sum of principal stresses of θ = 50 kPa), for the granular base course materials of Groups C and R.

Figure 5.25 pertains to the 25 material/ grading combinations of the granular base course materials of Groups C and R, while Figure 5.26 pertains to the six sands of Group S. As can be seen from the figures, no correlation exists between CBR and M_r. For the granular base course materials (Figure 5.25) the data points scatter all over. For these

materials, an increase in CBR does not correlate with an increase in M_r. For the sands (Figure 5.26) the scatter is somewhat smaller, but only six materials were tested here.

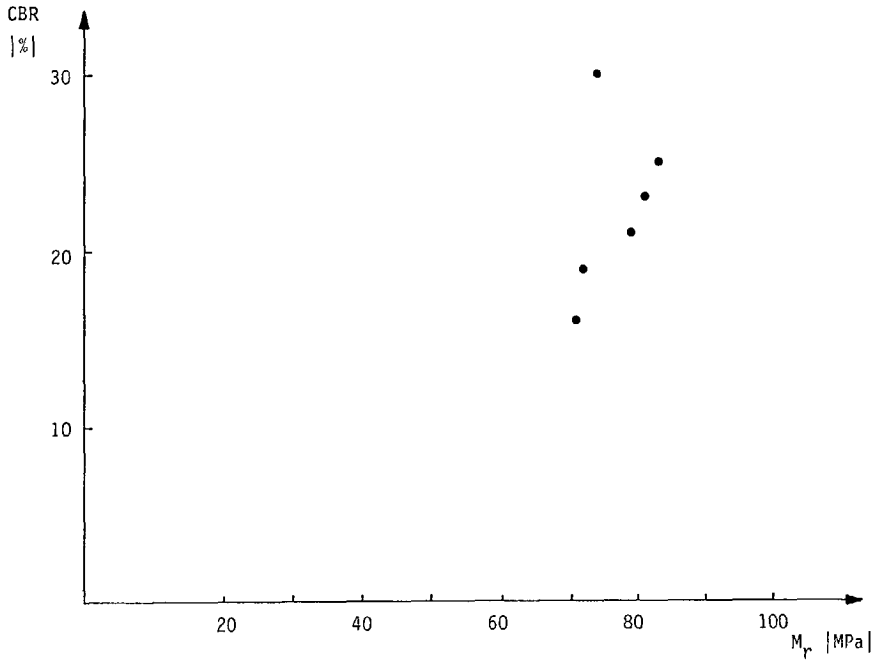

Figure 5.26: California Bearing Ratio CBR versus resilient modulus M_r (at a sum of principal stresses of θ = 50 kPa), for the sands of Group S.

From Figure 5.25 it can be observed that the CBR-values found for the granular base course materials are quite high. Almost all materials show CBR-values of over 100 %. As noted in Paragraph 5.2.3.2, the CBR tests were performed on material passing the 22.4 mm sieve. Compaction of this fraction at optimum moisture content using modified proctor compaction energy yielded for most materials CBR specimens which were solid cylinders of material rather than an arrangement of loose grains, hence the high CBR-values.

The check on possible M_r-CBR relationships was carried out here for M_r-values pertaining to a sum of principal stresses θ = 50 kPa. As noted when discussing the resiliency testing of the granular base course materials (Paragraph 5.3.3.5), θ = 50 kPa is the lower boundary of the range of θ applied in this testing. M_r-CBR plots were also made for the upper boundary of θ = 500 kPa, again showing no correlation.

In all, no relationship exists between M_r and CBR. Such a relationship is unlikely, since the deformation measured in the CBR-test is a combination of elastic and plastic deformation. Since the ratio of elastic to plastic deformation may be different for the materials tested and since the deformation in the CBR test in mainly plastic, the CBR-value can never be a proper measure of a purely elastic parameter like M_r.

5.5 SIMPLIFIED TEST PROCEDURES FOR RESILIENT PROPERTIES

5.5.1 Introduction

The fundamental stress-strain properties of unbound granular materials and soils needed for input to today's mechanistic pavement design procedures should be determined in fundamentally sound tests like the cyclic load triaxial test. Specimens with a grading, density and moisture content similar to those in-situ should be subjected to stresses representative of those in-situ while measuring the resulting deformations. The fundamental stress-strain parameters can then be calculated from the applied stresses and the resulting strains.

This fundamentally sound testing of soils and unbound materials involves two complicating factors. Firstly, application of the cyclic stresses to the triaxial specimen requires sophisticated pneumatic or servo-hydraulic loading equipment and complex electronic hardware for read-out of the cyclic specimen deformations. Secondly, testing of materials at a realistic grading requires, in the case of coarse graded granular materials, triaxial specimens of large dimensions such as the 400 by 800 mm specimens described earlier. Preparation of specimens of that size to in-situ densities again requires large servo-hydraulic loading equipment.

The requirement of complex loading and deformation measuring equipment strongly inhibits application of cyclic load triaxial tests on a routine basis. If the need for such equipment could be circumvented, a major step towards implementation of fundamentally sound testing of granular materials and soils in every-day engineering practice could

be made. In this paragraph, the applicability of simplified test procedures will be investigated. On the one hand these should circumvent the requirement of complex loading and read-out equipment and, on the other hand, meet the requirements of fundamentally sound testing techniques. First, a repeated static load triaxial test procedure will be presented that allows for accurate determination of resilient properties of granular materials using relatively simple equipment. Secondly, the effect of scaling down triaxial specimens towards sizes that allow for hand-compaction while keeping the grading of the granular material intact will be investigated.

5.5.2 Repeated static load triaxial tests

5.5.2.1 INTRODUCTION

As described in Paragraph 2.5.3.3, Kalcheff and Hicks [46] showed that load duration has no quantifiable effect on the resilient deformations of granular materials. Determination of the resilient modulus using load pulses of 0.1 second and 30 minutes showed no substantial differences in test results. Based on this information, Kalcheff and Hicks suggested a "static triaxial creep test" for determination of resilient properties of granular materials. The procedure involved, for each given stress level, a number of five minute load-on/five minute load-off periods for specimen preconditioning, followed by a load-on period of 30 minutes and a load-off period of 30 minutes. The resilient deformation upon the last unloading was then used to calculate the resilient modulus M_r. The whole loading-unloading sequence was suggested to be repeated twice at each stress level.

The main disadvantage of this procedure is the time required to obtain the resilient modulus of the material investigated as a function of stress. For each stress level, determination of the resilient modulus following the Kalcheff and Hicks procedure requires over two hours. Since the resilient modulus has to be determined at a number of different stress levels to obtain the relationship between resilient modulus and stress, the testing of one material for resilient properties may take several days. Although the suggested procedure allows for the determination of resilient properties using simple static

load equipment, the time required for it strongly inhibits routine application.

This paragraph describes an investigation into the possibility of determining resilient properties of granular materials in repeated static load triaxial tests that require far less time than the Kalcheff and Hicks procedure. Part of the base course materials of Groups C and R were tested following that procedure, with the addition of also measuring the resilient deformation upon unloading after the last five minute load-on period. After obtaining satisfactory results, the 30 minute load-on periods were omitted in testing other materials from Groups C and R. Finally, in testing the sands from Group S the possibility of omitting a separate specimen preconditioning at each stress level and only measuring resilient deformation after a single five minute load-on period was investigated, again finding satisfactory results.

5.5.2.2 REPEATED STATIC LOAD TESTING OF GRANULAR BASE COURSE MATERIALS

Repeated static load triaxial tests were performed on part of the granular base course materials of Groups C and R [114]. The tests were carried out on the specimens used for determination of resilient properties in cyclic load tests, as described in Paragraph 5.3.2.5. To exclude possible effects of self-cementing (increasing stiffness with time) of the investigated materials on the comparison of repeated static load and cyclic load test results, each repeated static load test was immediately followed by a cyclic load test at the same stress level.

The first group of materials tested involved porphyry (at two gradings, material codes POB and POO), limestone (at two gradings, material codes KAB and KAO) and waste incineration slag (material code AVC). Figure 5.27 shows the "cyclic" stress applied in the tests and the resulting axial deformation. Resilient deformations were measured after the 30 minute load-on period (according to the Kalcheff and Hicks procedure), but also after the third five minute load-on period. Since determination of the resilient modulus M_r following this repeated static load procedure requires one hour per stress level, only a limited number of combinations of confining stress σ_3 and

"cyclic" stress σ_c was used in the repeated static load tests. Table 5.10 shows the stress combinations applied.

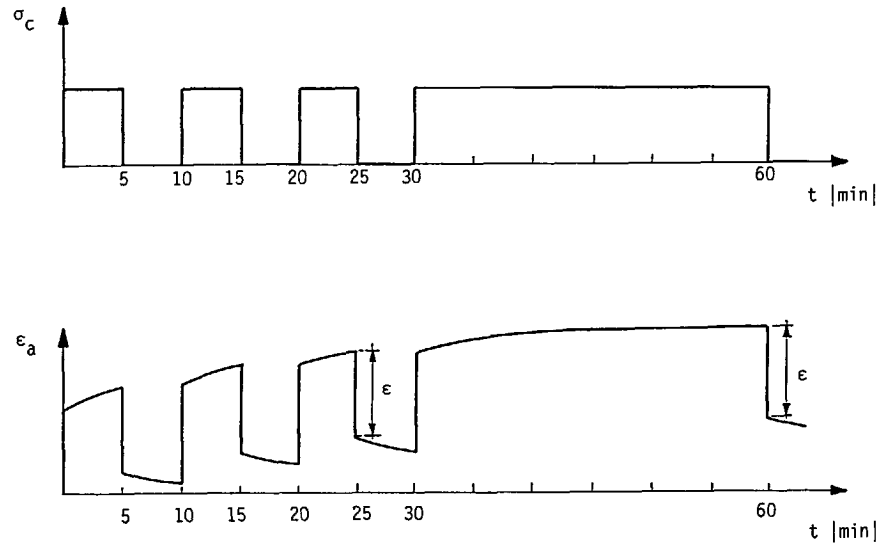

Figure 5.27: "Cyclic" stress σ_c and axial strain ε_a versus time, for repeated static load triaxial test.

Table 5.10: Stresses applied in repeated static load tests

stress component	value	
σ_3	12, 48	|kPa|
σ_s	1.5	|kPa|
σ_c/σ_3	2 , 4 , 6	| - |

From the repeated static load tests two resilient modulus values were obtained: one from the resilient deformation measured after the 30 minute load-on period (denoted as $M_{r,s}$ (30)) and one from the resilient deformation after the last five minute load-on period (denoted as $M_{r,s}$ (5)). Figure 5.28 and 5.29 show plots of the $M_{r,s}$ (30) and $M_{r,s}$ (5) values obtained versus the resilient modulus determined in the cyclic load tests, for all the materials tested. The straight lines in the figures were determined using linear regression; the formula describing the straight line relationship and the correlation coefficient r are given in the figures.

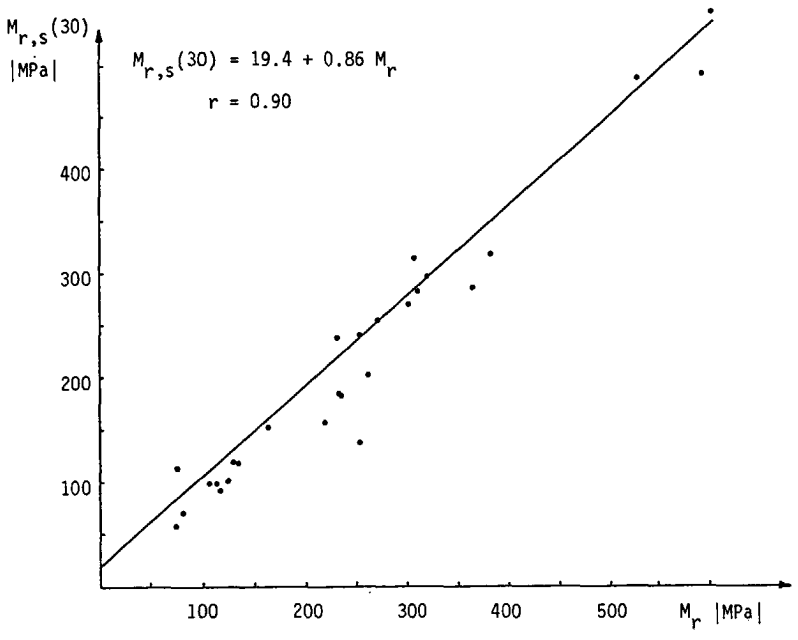

Figure 5.28: Resilient modulus from repeated static load test $M_{r,s}(30)$ versus resilient modulus from cyclic load test M_r.

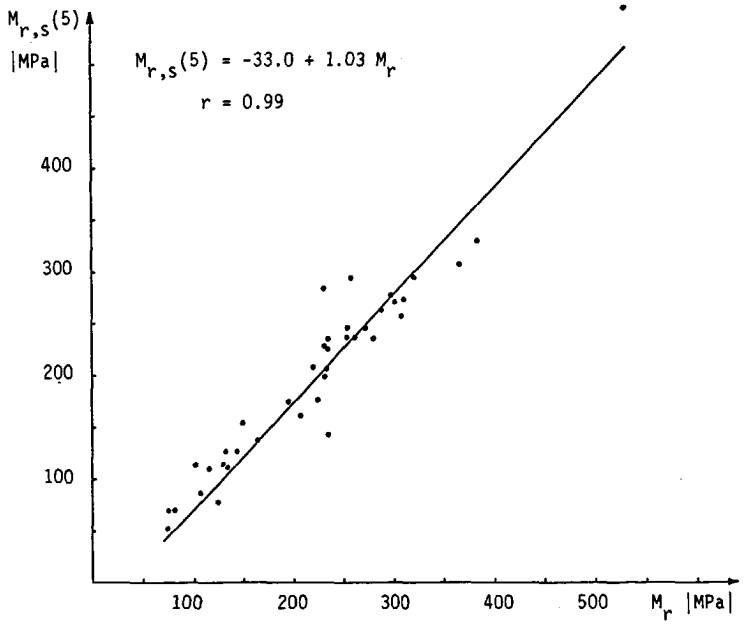

Figure 5.29: Resilient modulus from repeated static load test $M_{r,s}(5)$ versus resilient modulus from cyclic load test M_r.

As can be seen from Figures 5.28 and 5.29, the correlation between the resilient moduli determined in the repeated static load tests and those from the cyclic load tests is very good. Since the correlation between $M_{r,s}$ (5) and M_r is even better than that between $M_{r,s}$ (30) and M_r, the cumbersome 30-minute loading/unloading period was omitted in further testing of the granular base course materials. The materials stol (material code STN), crushed clincker (at two gradings, material codes KGB and KGO) and crushed concrete 2 (material code B2C) were tested using only the three five minute load-on/load-off periods. Because of the reduced testing-time per stress level, more combinations of stresses were used in testing these materials. In addition to the stress levels given in Table 5.10, also confining stresses of σ_3 = 24 kPa and σ_3 = 36 kPa were used (combined with the same σ_s = 1.5 kPa and σ_c/σ_3 = 2, 4 and 6). Again, each repeated static load triaxial test was immediately followed by a cyclic load triaxial test at the same stress combination.

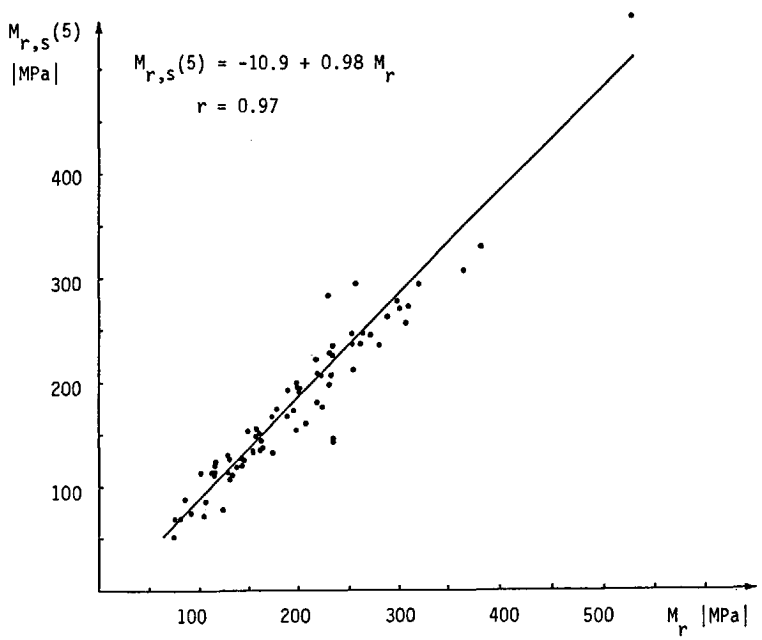

Figure 5.30: Resilient modulus from repeated load triaxial tests $M_{r,s}$ (5) versus resilient modulus from cyclic load tests M_r, for all materials tested.

Figure 5.30 shows a plot of all the $M_{r,s}$ (5) values obtained versus the resilient modulus from the cyclic load tests M_r, inclusive of the

data shown earlier in Figure 5.29, for all the granular materials tested in repeated static load triaxial tests. As can be seen from the figure and the equation and correlation coefficient given in it, the correlation between the resilient moduli obtained from the two types of tests is very good and the data points plot close to a 45° line of equality.

5.5.2.3 REPEATED STATIC LOAD TESTING OF SANDS

Repeated static load triaxial tests for the determination of resilient properties were performed on all six sands of Group S [115, 116]. For the tests the same triaxial specimens were used as for the determination of resilient properties in cyclic load tests (see Paragraph 5.3.3.5). Since the sands show no self-cementing effect, the time-consuming repeated static load tests could be performed alternately with the cyclic load tests and the results of the two types of tests could be compared directly. Figure 5.31 shows the "cyclic" stress applied in the repeated static load triaxial tests and the resulting axial deformation of the triaxial specimen.

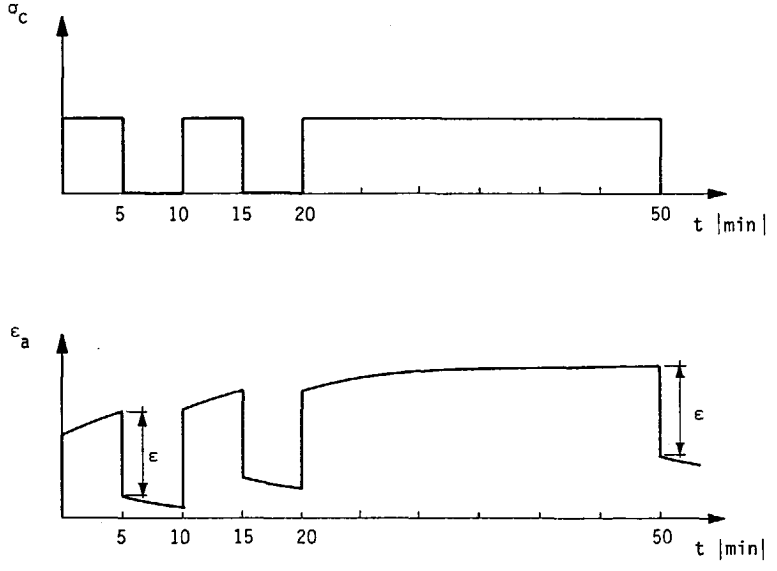

Figure 5.31: "Cyclic" stress σ_c and axial ϵ_a versus time, for repeated static load triaxial test.

Resilient deformations were measured upon unloading after the 30 minute load-on period (following the Kalcheff and Hicks procedure), but also upon unloading after the first five minute load-on period. The latter measurement was done to check whether or not a separate specimen preconditioning at each stress combination could be omitted. It should be noted that the specimens were preconditioned in a standard way at the beginning of the test sequence by applying several hundreds of load applications at a low stress ratio.

As done in testing of the granular base course materials, repeated static load tests were again only carried out at a limited number of stress combinations. Where the cyclic load triaxial tests for determination of resilient properties were performed at 29 stress combinations (see Paragraph 5.3.3.5), the repeated static load triaxial tests were, because of their time-consuming nature, only carried out at ten stress combinations. Table 5.11 shows the stresses applied in the repeated static load triaxial tests.

Table 5.11: Stresses applied in repeated static load tests.

σ_3 |kPa|	σ_c |kPa|		σ_c/σ_3 | - |	
10	20	30	2	3
30	60	90	2	3
60	120	180	2	3
100	200	300	2	3
200	200	400	1	2

As was done in the cyclic load tests, higher stress ratios σ_c/σ_3 were applied at the lower confining stresses in the repeated static load tests because of the apparent cohesion in the sand specimens. At each level of the confining stress σ_3 first the repeated static load tests were performed, followed by the cyclic load tests at that confining stress. Figures 5.32 and 5.33 show plots of the resilient moduli obtained from the repeated static load tests $M_{r,s}$ (30) and $M_{r,s}$ (5) versus the resilient modulus obtained from the cyclic load tests, for all the sands tested. Also given in the figures are the best-fit

straight lines through the data points, determined with linear regression, and the equation and correlation coefficient pertaining to that line.

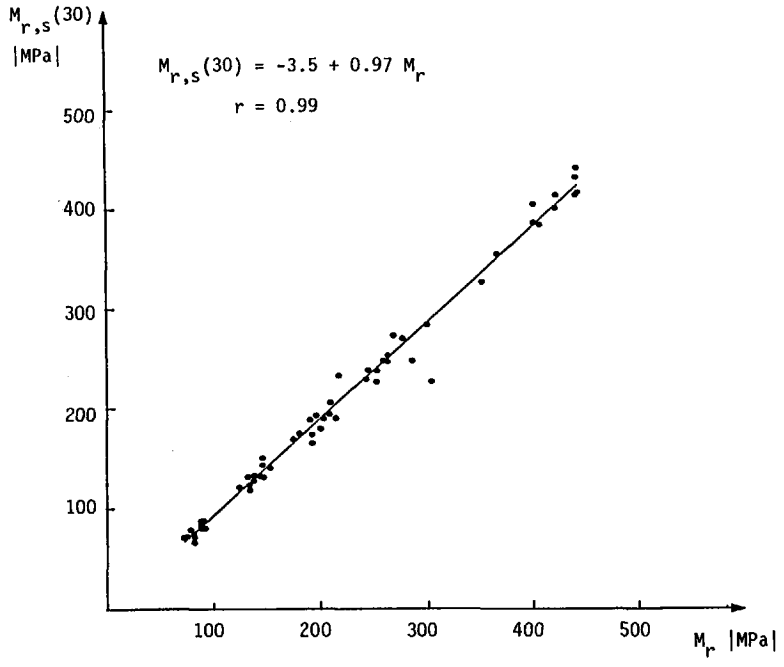

Figure 5.32: Resilient modulus from repeated static load triaxial tests $M_{r,s}$ (30) versus resilient modulus from cyclic load tests M_r, for all sands tested.

Both for $M_{r,s}$ (30) and $M_{r,s}$ (5) a very good correlation with the M_r from cyclic load tests is found. In both cases the best-fit line through the data points almost coincides with a 45° line of equality through the origin. The conclusion is that, for the wide variety of sands tested, the resilient modulus can be determined accurately using the relatively simple repeated static load triaxial test. Per stress combination to be investigated, a single, short load-on period of five minutes can be used for determination of the resilient modulus. To ensure a proper seating between the loading caps and the triaxial specimen, it is suggested to perform a few load-on periods of short duration at a high confining stress and a low stress ratio at the beginning of the test series.

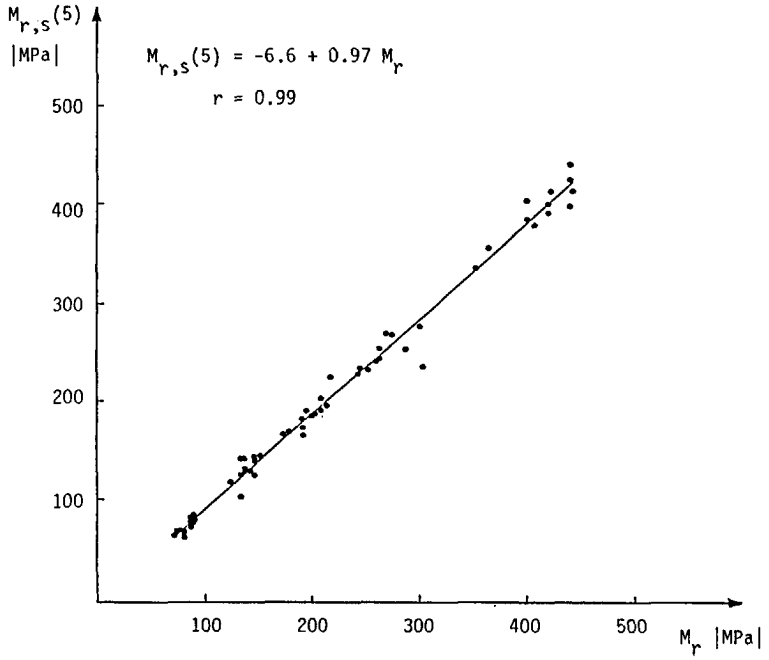

Figure 5.33: Resilient modulus from repeated static load triaxial tests $M_{r,s}$ (5) versus resilient modulus from cyclic load tests M_r, for all sands tested.

5.5.3 Specimen size reduction

5.5.3.1 INTRODUCTION

As stated in Paragraph 5.5.1, routine application of the cyclic load triaxial test in every-day practice of pavement engineering is hindered by two main problems. The first problem lies in the cyclic nature of the test. As shown in the previous paragraph, this problem can be circumvented by using repeated static load triaxial test rather than cyclic load tests. With that, the problem of not being able to determine fundamentally sound stress/strain parameters with standard equipment is solved for fine grained materials like sands.

For coarse grained granular materials, a second difficulty arises in the determination of fundamentally sound stress/strain parameters. For testing of a coarse grained granular material of say a 0/40 mm grading in a triaxial test (cyclic load or repeated static load), a specimen

size like the 400 mm diameter by 800 mm height described earlier is required to ensure a reasonable relationship between maximum grain size and specimen diameter. As stated, however, compaction of such size specimens to realistic densities requires large cyclic loading hydraulic equipment, which hinders routine application of fundamentally sound testing.

Obviously, the solution to this second problem is reducing the size of the triaxial specimen. To keep the ratio of maximum grain size to specimen diameter at or above the generally used values of 4 to 6 (see Paragraph 2.5.3.1), many researchers have scaled down the grading of the material to be tested when working with relatively small triaxial specimen diameters like for instance 150 mm. This approach is quite classical: in standard test procedures like the CBR-test the grading of the material to be tested is also adjusted to the relatively small specimen size. AASHTO T193-72 for instance prescribes the scaling down of the grading of a granular material to 0-19 mm before CBR-testing in the 152.4 mm cylindrical mould.

It should be noted that when the grading is scaled down, another material is in fact tested. As discussed in Paragraph 2.5.3.1, scaling down the grading of a granular material has been shown to result in a decrease in elastic stiffness. The resilient properties for instance of a 0-19 mm material can therefore only be indicative of the same properties of the original 0/40 mm material. Although often necessitated by the limitation of the available testing equipment, the scaling down of the material grading is in fact incompatible with one of the requirements of fundamentally sound testing, being that the material should be tested at the same grading as applied in-situ.

In this paragraph, the effect of reducing the size of the triaxial specimen while keeping the grading of 0/40 mm materials intact will be discussed. A scaled down version of the 400 mm specimen diameter triaxial apparatus discussed in Paragraph 5.3.2 was built, having a specimen size of 150 mm diameter by 300 mm height. The 150 mm specimen diameter was chosen since it "equals" the diameter of the large size Proctor compaction mould (152.4 mm) and, hence, allows for hand-operated compaction of material specimens to in-situ densities. Since the final goal of this investigation was to develop a test procedure

suitable for standardly equipped laboratories, the new 150 mm ϕ triaxial apparatus was kept relatively simple. The vacuum-triaxial principle was again used and deformation measurement was limited to axial deformations only. This allowed for easy to install measuring equipment to be used instead of the rather complicated system used in the 400 mm ϕ apparatus. Part of the materials tested earlier in the 400 mm ϕ apparatus was tested again in the 150 mm ϕ apparatus, under equal conditions of density, moisture content and stress.

5.5.3.2 THE 150 MM SPECIMEN DIAMETER APPARATUS

Figure 5.34 shows the schematics of the 150 mm specimens diameter triaxial apparatus. The 150 × 300 mm triaxial specimen is enclosed in a double membrane, connected to top- and bottom-platen with grease and O-rings. A partial vacuum inside the triaxial specimen is used to apply the confining stress σ_3. Axial loading of the triaxial specimen is provided by a 50 kN MTS hydraulic actuator.

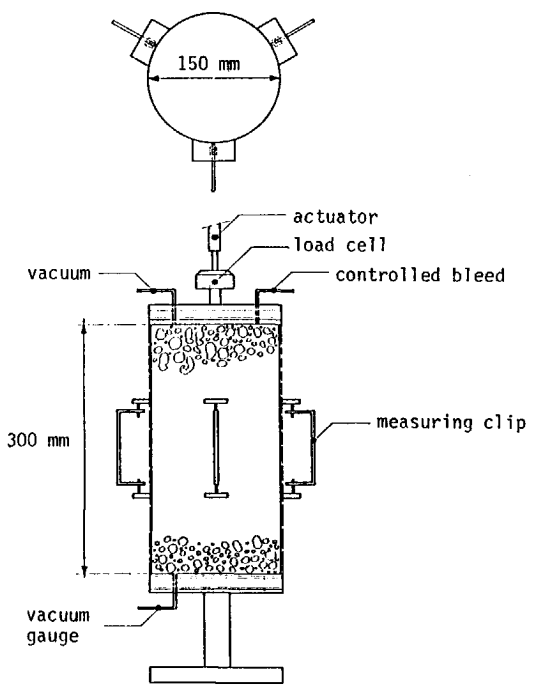

Figure 5.34: Schematics of the 150 mm specimen diameter apparatus

The apparatus is equiped with instrumentation for measurement of axial strains only. This instrumentation consists of three so-called "measuring clips", which are home-made devices made of spring-steel and equiped with a full-bridge strain gauge. Each measuring clip is supported by two plastic blocks glued to the triaxial membrane at 1/3 and 2/3 of the specimen height, respectively. The three measuring clips are mounted on the triaxial specimen at equal angles of 120° on the circumference. The measuring principle is based on bending. When the distance between two plastic blocks changes, the measuring clip (clamped between the blocks at a small pre-stressing) is bent, and the strain gauges on either side of the measuring clip change their resistance. Connected to a strain gauge amplifier the measuring clips are calibrated individually prior to the test in a calibration bench.

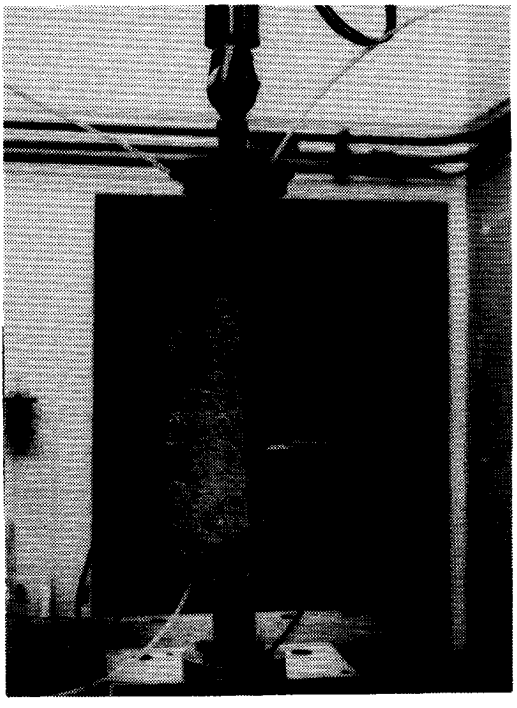

Figure 5.35: 150 mm specimen diameter triaxial specimen.

The system of using measuring clips rather than LVDT's was chosen mainly because of the required higher accuracy in working with the 150

mm ϕ apparatus. The gauge length over which to measure axial deformations of the triaxial specimen was reduced from 270 mm with the 400 mm ϕ apparatus to 100 mm with the 150 mm ϕ apparatus. The system turned out to be an accurate, easy to handle and cheap way of measuring axial resilient deformations. Figures 5.35 and 5.36 show the 150 mm ϕ triaxial apparatus.

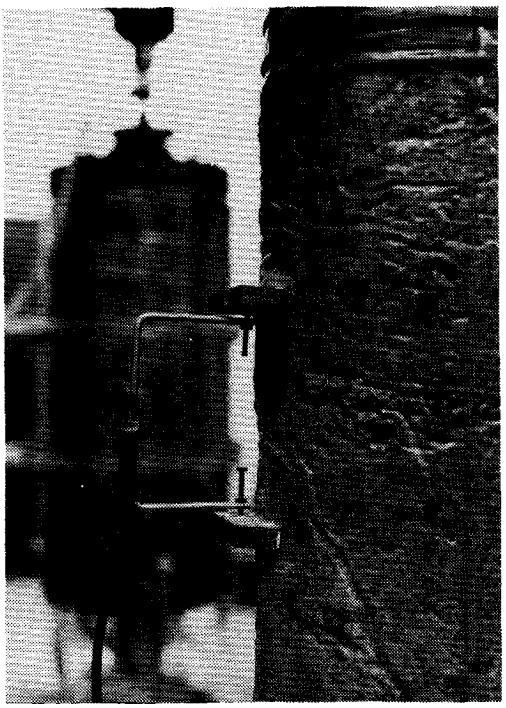

Figure 5.36: Details of measuring clip on triaxial specimen.

5.5.3.3 RESILIENCY TESTING

To investigate the influence of scaling down the specimen size while keeping the grading of the coarse grained granular materials intact, materials tested earlier in the 400 mm ϕ apparatus were tested in the 150 mm ϕ apparatus. As was done in the 400 mm ϕ apparatus, each material was tested at two 0/40 mm gradings, being one grading in conformity with the upper limit of the Dutch specifications for unbound granular materials 0/40 mm and one grading in conformity with the

lower limit of those specifications (the "B"- and "O"-grading, see Figure 4.1, Paragraph 4.2.2). For each triaxial specimen, new sample material was recipe-made to the required B- or O-grading, thereby ensuring that the grading of the materials tested in the 150 mm ϕ apparatus was equal to that of the same materials tested in the 400 mm ϕ apparatus. Two materials were tested in the 150 mm ϕ apparatus, being crushed masonry 2 and crushed concrete 1. The codes of the materials tested hence were M2B, M2O, BGB and BGO.

Since the aim of the testing described in this paragraph was to investigate the influence of the reduction in specimen size on resilient properties, effort was made to duplicate the specimen conditions of the 400 mm ϕ apparatus in the 150 mm ϕ apparatus. As noted above, the gradings were made equal by testing recipe-made materials. In preparation of the triaxial specimens, the actual values of moisture content and dry density obtained earlier in the respective tests with the 400 mm ϕ apparatus were used. Table 5.12 shows the target data from the 400 mm ϕ tests and the obtained specimen data from the 150 mm ϕ tests.

Table 5.12: Specimen data 400 mm ϕ and 150 mm ϕ tests

ϕ 400 mm			ϕ 150 mm		
test code	w |%|	ρ_d |kg/m^3|	test code	w |%|	ρ_d |kg/m^3|
M2BD 01	16.0	1585	M2BD ϕ150	15.5	1584
M2OD 02	13.7	1516	M2OD ϕ150	14.0	1511
BGBD 01	13.5	1863	BGBD ϕ150	13.4	1861
BGOD 01	7.8	1878	BGOD ϕ150	8.1	1870

As can be seen from Table 5.12, the specimen preparation procedure of the 150 mm ϕ apparatus allows for accurately building triaxial specimens to a target moisture content and dry density. The good agreement between target- and specimen-values of moisture content and dry density illustrates one of the advantages of working with a relatively small specimen size. As noted when describing the specimen preparation procedure of the 400 mm ϕ triaxial tests (Paragraph 5-.3.2.4), preparing the required 200 kg of sample material at a given

target moisture content proved to be quite difficult. For the 150 mm ϕ triaxial specimens, this difficulty does not occur. The total required quantity of 10-15 kg of sample material was ovendried, weighed directly upon removal from the oven and later after cooling down of the sample material water was added to bring the total weight of sample material plus water to the required value. From the target wet density of the triaxial specimen and the specimen volume, the quantity of the sample material to be compacted in the split mould of the triaxial apparatus could then be calculated. Compaction was then performed in three layers, using a hand-operated Marshall compaction hammer.

5.5.3.4 SPECIMEN SIZE EFFECTS

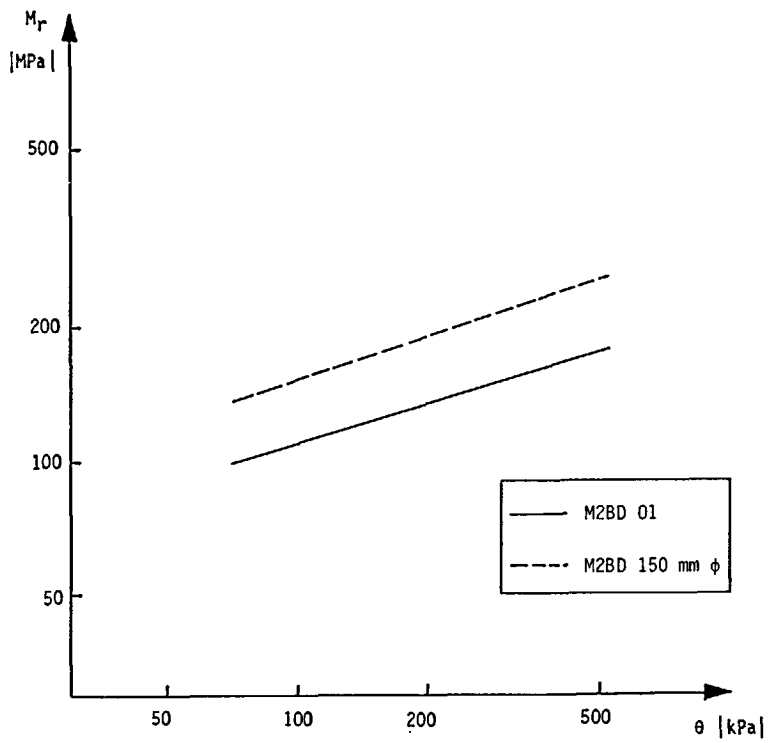

Figure 5.37: Resilient modulus M_r versus sum of principal stresses θ, as measured in 400 mm ϕ and 150 mm ϕ apparatus, for material M2B.

Figures 5.37 through 5.40 show the M_r-θ relationships obtained from the testing with the 150 mm ϕ apparatus, together with those obtained from the 400 mm ϕ apparatus. As can be seen from the figures, the test results are not consistent with respect to specimen size effects. For the crushed masonry (materials M2B and M20) higher resilient moduli were found with the 150 mm ϕ apparatus as compared to the 400 mm ϕ apparatus. This result was expected: testing of a 0/40 mm material in a 150-300 mm triaxial specimen would lead to relatively large end-constraint effects, rendering the material stiffness higher. If however this reasoning was valid, then the influence of end constraint should be larger when testing the coarse grained 0/40 mm material (M20) as compared to the fine grained 0/40 mm material (M2B), taking into account that material M2B contained as much as 50% material 0-2 mm (see Figure 4.1, Paragraph 4.2.2). This expected difference because of grading is however not substantiated by the test results for materials M2B and M20.

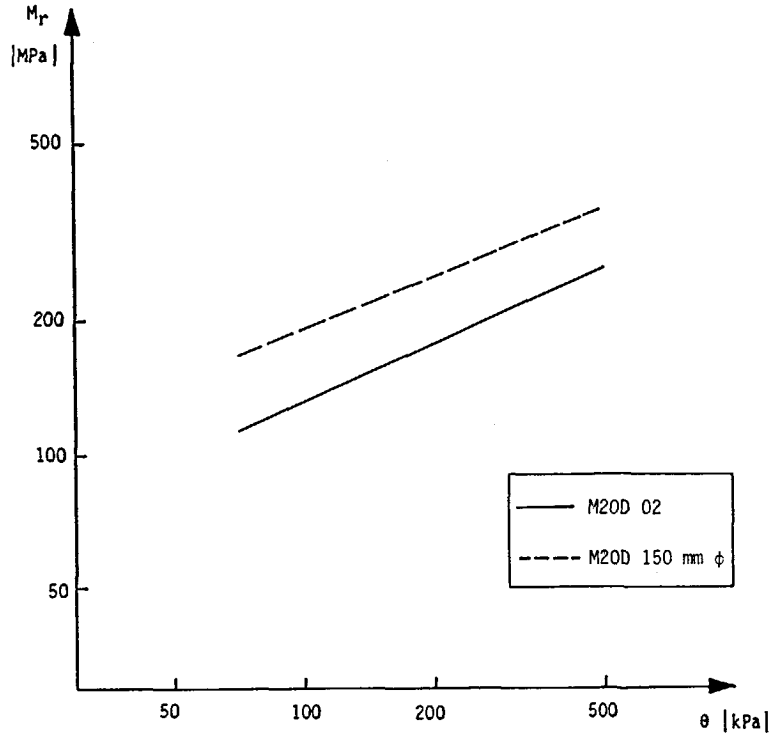

Figure 5.38: Resilient modulus M_r versus sum of principal stresses θ, as measured in 400 mm ϕ and 150 mm ϕ apparatus, for material M20.

The test results become even less consistent when also the testing of the crushed concrete is taken into account. As can be seen from Figures 5.39 and 5.40, specimen size has little effect on the resilient moduli obtained. For both the fine (BGB) and the coarse grading (BGO) of the crushed concrete the 400 mm ϕ apparatus and the 150 mm ϕ apparatus yield almost identical results.

From the results depicted in Figures 5.37 through 5.40, the conclusion can be drawn that specimen size does have an influence on the resilient properties measured, although this influence is not consistent. Reasoning that the resilient moduli values measured in the 400 mm ϕ apparatus are the correct values thanks to the large enough specimen size, it follows from the test results that the 150 mm ϕ apparatus cannot be used without further preface to determine resilient moduli of 0/40 mm granular materials.

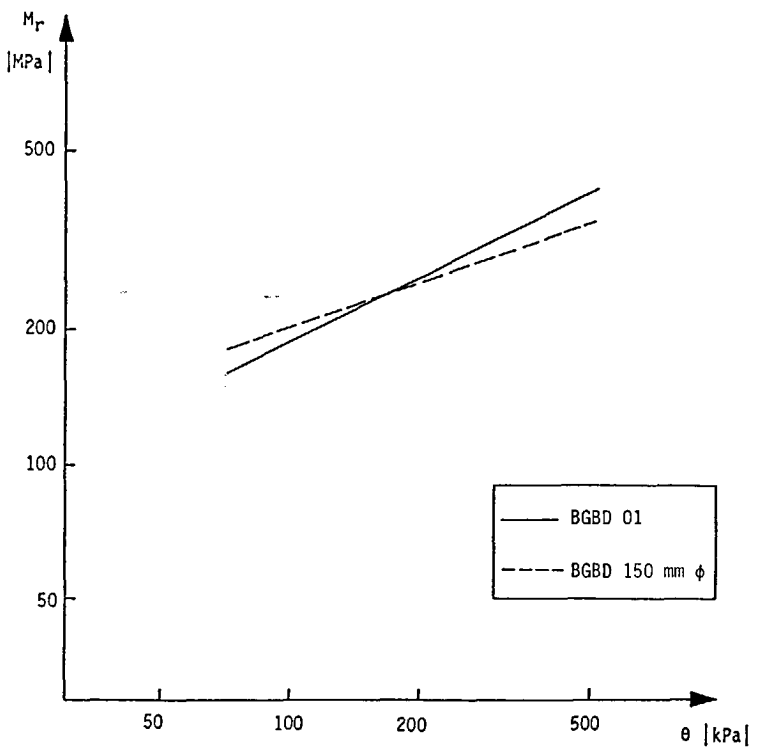

Figure 5.39: Resilient modulus M_r versus sum of principal stresses θ, as measured in 400 mm ϕ and 150 mm ϕ apparatus, for material BGB.

The fact that for the crushed masonry higher moduli values were found in the 150 mm ϕ apparatus while the crushed concrete showed approximately the same moduli in the 150 mm ϕ and the 400 mm ϕ apparatus rules out that end-constraint effects lead to a higher stiffness, since the test-gradings of the crushed masonry and the crushed concrete were equal. The most probable source of the differences in stiffness found is the packing-arrangement of the grains in the triaxial specimen. Having the same grading and specimen density does not necessarily imply that the packing-arrangement of the grains is equal. Whether the coarse grains in the triaxial specimen are stacked in a vertical column or nicely distributed throughout the specimen is bound to make a difference in measured resilient stiffness. Already during compaction of the 150 mm ϕ triaxial specimen such differences in packing-arrangement were observed from the response of the material in the split mould to the impact of the compaction hammer.

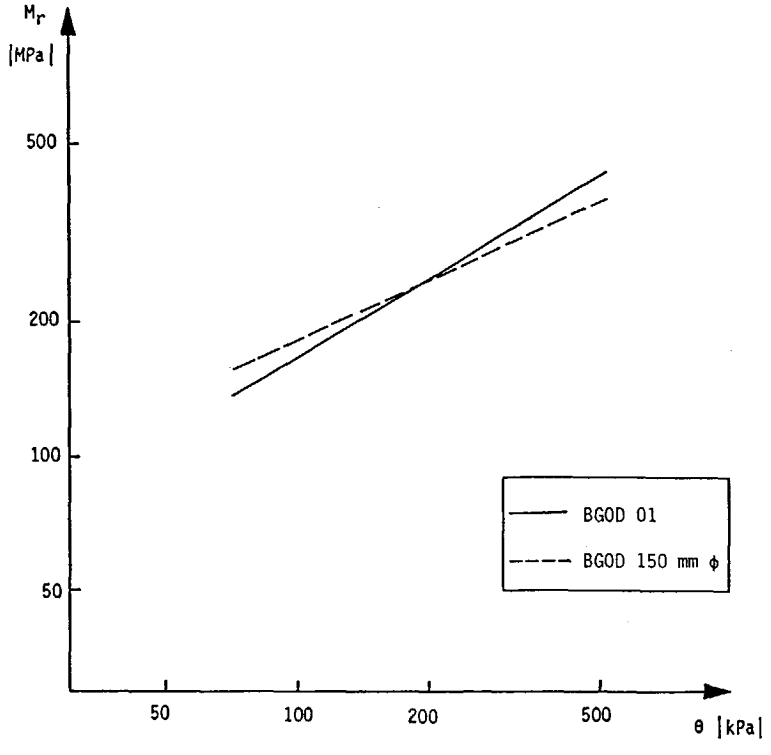

Figure 5.40: Resilient modulus M_r versus sum of principal stresses θ, as measured in 400 mm ϕ and 150 mm ϕ apparatus, for material BGO.

In the large 400 mm ϕ triaxial specimens, possible differences in packing-arrangement are compensated for by the large specimen size. Locally occurring differences in packing-arrangement do not have sufficient influence on the overall specimen behaviour to be of any significance. Packing-arrangement may therefore influence the moduli values obtained from the 150 mm ϕ apparatus and not those from the 400 mm ϕ apparatus. Since packing-arrangement cannot be standardized, unlike for instance grading and density, the 150 mm ϕ triaxial specimen is too small relative to the 0/40 mm grading to allow for an accurate determination of resilient moduli.

Having observed the above, no further effort was put into testing with the 150 mm ϕ apparatus. It is believed that the apparatus is suited for classification of materials into categories of resilient stiffness. For this, either cyclic or repeated static loading can be used. Thanks to its simplicity, such testing could be performed by standardly equiped laboratories. However, for a detailed study of the stress/strain properties of granular materials with gradings like the 0/40 mm discussed here large triaxial specimens should be used.

5.6 SIMPLIFIED TEST PROCEDURES FOR PERMANENT STRAIN PROPERTIES

5.6.1 Introduction

As stated in the literature review (Paragraph 2.5.3.3) the determination of the permanent strain properties of granular materials in cyclic load triaxial tests is quite cumbersome. Application of say 10^6 load applications in the test requires at least several days. Furthermore, permanent strain testing requires a new triaxial specimen for each set of stress conditions investigated, since permanent strain testing by definition involves changes in specimen geometry and density.

Permanent strain testing being this cumbersome has on the one hand led to only limited permanent strain data being available in the literature, certainly in comparison to the abundance of resilient strain data. On the other hand, it has led to several attempts published to

assess permanent strain properties from simpler and/or faster to perform tests. Two approaches will be discussed here, being assessment of permanent strain properties from resilient strain properties and predicting permanent strain under cyclic loading from the results of static load triaxial tests. The validity of these approaches will be checked here using the available data for the granular base course materials and the sands.

5.6.2 Correlations between permanent and resilient strain

Veverka [49] published a straightforward correlation between the permanent and resilient strain properties of granular materials of the form:

$$\varepsilon_p (N) = \varepsilon_r \cdot a\, N^b \qquad (5.4)$$

where

$\varepsilon_p (N)$ = permanent deformation after N load applications
ε_r = resilient deformation
N = number of load applications
a, b = material constants

Equation 5.4 suggests a linear relationship between permanent and resilient strain. For the granular base course materials and the sands tested for this dissertation, certainly no such relationship exists per group of materials. Discussing the permanent strain properties of the granular base course materials (Paragraph 5.3.2.6) and those of the sands (Paragraph 5.3.3.6) it was noted that the materials showing a low resistance to resilient deformation often showed a high resistance to permanent deformation. This was observed for both the group of granular base course materials (Groups C and R) and for the group of sands (Group S).

Equation 5.4 not being valid per group of materials, the next question is whether it is valid per individual material. By adjusting the material constants individually per material, the discrepancy between permanent and resilient strain within each group of materials might be dealt with. If Equation 5.4 were to be valid per individual material, then only one cyclic load permanent strain test at a certain stress

condition would be required per material to determine the parameters a and b and permanent strains at another stress condition could then be deduced from the fixed parameters a and b and the resilient strain at that particular stress condition.

Table 5.13 shows the permanent axial strain after 10^6 load applications $\varepsilon_{a,p}$ (10^6), resulting from the 3 × 3 permanent strain tests on the sands of Group S (taken from Table 5.8, Paragraph 5.3.3.6), and the K_1 and K_2 values from the resiliency testing of the same sands (taken from Table 5.7, Paragraph 5.3.3.5). With the K_1 and K_2 parameters and the stresses applied in the permanent strain test the axial resilient strain $\varepsilon_{a,r}$ at the particular stress level can be calculated. If Equation 5.4 is valid per individual material (meaning that per material the constants a and b have fixed values), then the ratio of $\varepsilon_{a,p}$ (10^6) to $\varepsilon_{a,r}$ should be constant. As can be seen from the results given in Table 5.13, the ratio of permanent strain to resilient strain is far from constant per individual material. Hence, Equation 5.4 is not valid, not even per individual material.

Table 5.13: Comparison of permanent and resilient strain properties for sands

test code	$\frac{\sigma_c}{\sigma_3}$ |-|	$\varepsilon_{a,p}$ (10^6) $\|10^{-3}\|$	K_1 |MPa|	K_2 |-|	$\varepsilon_{a,r}$ $\|10^{-3}\|$	$\frac{\varepsilon_{a,p}\ (10^6)}{\varepsilon_{a,r}}$ |-|
ENND 03	3	6			0.383	16
ENND 04	3.5	21			0.426	49
ENND 02	4	33			0.467	71
ENND 01			7.6	.57		
OSND 02	4	10			0.412	24
OSND 03	5	23			0.479	48
OSND 04	6	25			0.539	46
OSND 01			9.8	.54		
ZEND 02	4	8			0.627	13
ZEND 03	5	10			0.683	15
ZEND 04	6	13			0.737	18
ZEND 01			9.7	.52		

The check on the validity of Equation 5.4 in Table 5.13 was done for the sands of Group S only, since the triaxial specimens of the sands

showed the smallest variation - if any - per material. It might be reasoned that the resilient strain properties were determined on a different triaxial specimen than the permanent strain properties and that this might account for deviations from Equation 5.4. However, given the fact that the triaxial specimens were per material tested almost - if not completely - identical with respect to grading, moisture content and density and given the good repeatability of the cyclic loading triaxial tests (see Paragraph 5.3.4), the deviations in the ratio $\varepsilon_{a,p}(10^6)/\varepsilon_{a,r}$ given in Table 5.13 are simply too large to stem from specimen variability and/or test inaccuracies and, hence, must stem from Equation 5.4 being not valid for the materials tested here.

Table 5.14 shows a check on the validity of Equation 5.4 for a granular base course material. The permanent strain data given were taken from Table 5.5 (Paragraph 5.3.2.6) and the resilient strain data from Table 5.4 (Paragraph 5.3.2.5). The particular material KGB was chosen since it is the only material for which three permanent strain tests were run up to 10^6 load applications; of all other granular base course materials tested for permanent strain properties at least one specimen failed before the 10^6 load applications could be completed. Although specimen variability with respect to density and moisture content is somewhat larger (see Appendix 3) as compared to the variability of the sand specimens, the variations in the ratio $\varepsilon_{a,p}(10^6)/\varepsilon_{a,r}$ are again far too large to be accounted for by specimen variability and/or test inaccuracies. Again, Equation 5.4 proves to be not valid.

Table 5.14: Comparison of permanent and resilient strain properties for a granular base course material

test code	$\frac{\sigma_c}{\sigma_3}$ |-|	$\varepsilon_{a,p}$ (10^6) $\|10^{-3}\|$	K_1 |MPa|	K_2 |-|	$\varepsilon_{a,r}$ $\|10^{-3}\|$	$\frac{\varepsilon_{a,p}\ (10^6)}{\varepsilon_{a,r}}$ |-|
KGBD 03	9	3			0.627	4
KGBD 05	10	34			0.683	50
KGBD 04	11	52			0.737	71
KGBD 01			41.8	.28		

5.6.3 Static load failure tests

Obviously, a certain relationship must exist between the stress-ratio σ_c/σ_3 that can be applied say 10^6 times in a cyclic load triaxial test without causing excessive permanent deformation and the stress-ratio at failure $\sigma_{d,f}/\sigma_3$ obtained on the same material in a classical static load failure test. To check for such a relationship, some of the materials tested for permanent strain properties in cyclic load triaxial tests (see Paragraph 5.3.2.6 and 5.3.3.6) were also subjected to static load failure tests. Because of better specimen reproducability, the sands of Group S were again tested first, followed by testing of some of the granular base course materials from Groups C and R.

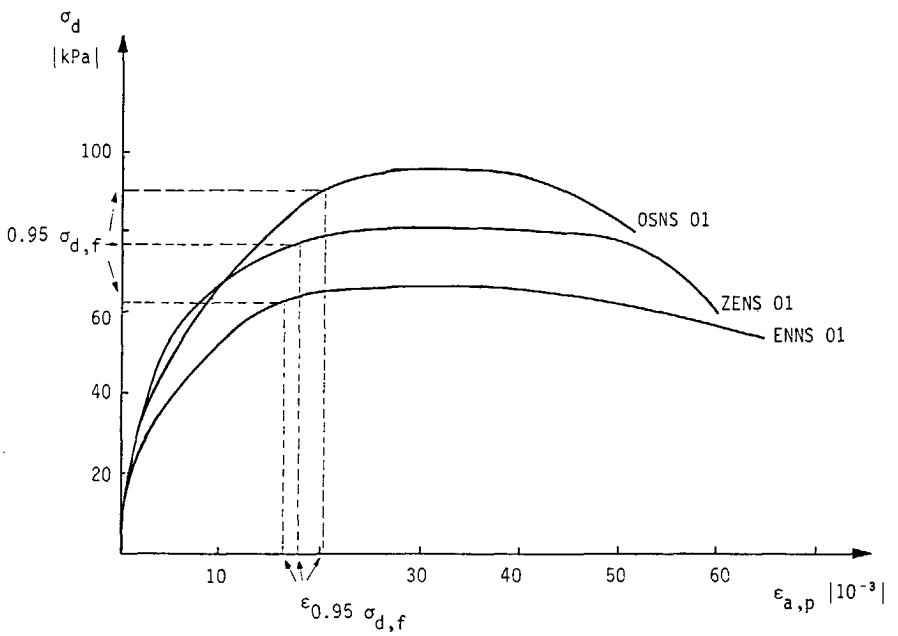

Figure 5.41: Stress-strain curves from static loading failure tests on the sands (materials ENN, OSN and ZEN).

The three sands subjected to permanent strain testing (ENN, OSN and ZEN) were tested in "consolidated"-drained strain-controlled static load failure tests (rate of strain 3% per minute). The sands were tested at a confining stress σ_3 = 10 kPa, which is equal to the value of σ_3 applied in the permanent strain tests. For the specimen data reference is made to Appendix 3 (test codes ENNS 05, OSNS 06 and ZENS

05). Figure 5.41 shows the stress-strain curves obtained, and Table 5-.15 shows the numerical results.

Table 5.15: Numerical results static loading failure tests on the sands (materials ENN, OSN and ZEN)

material number	test code	σ_3 |kPa|	$\sigma_{d,f}$ |kPa|	$\frac{\sigma_{d,f}}{\sigma_3}$ |-|	$\varepsilon_{0.95\ \sigma_{d,f}}$ $\|10^{-3}\|$
S2	ENNS 05	10	67	6.7	17
S3	OSNS 06	10	96	9.6	21
S6	ZENS 05	10	81	8.1	18

As can be seen from Figure 5.41, the maximum deviator stress at failure $\sigma_{d,f}$ is quite well defined. The axial strain at failure is however less well defined, since the stress-strain curve runs parallel to the strain axis at the failure stress $\sigma_{d,f}$. Therefore, to characterize the axial strain from the static failure test, the strain at a deviator stress of 0.95 $\sigma_{d,f}$ is better suited since the stress-strain curve still rises significantly at that level of σ_d.

Comparing the static load test results (Figure 5.41) to the permanent strain results obtained from the cyclic load tests (Figures 5.20 through 5.22, Paragraph 5.3.3.6), Echten sand ENN performs most poorly in both types of tests: it shows the lowest stress ratio at failure and the lowest resistance to permanent deformation. The agreement between static and cyclic load test results however is less for the other two sands: Eastern Scheldt sand OSN shows a higher stress ratio at failure than does Zeijen sand ZEN, whereas the resistance to permanent deformation is less for OSN as compared to ZEN.

Lentz and Baladi [47] correlated both stress and strain from static load failure tests to permanent strain results from cyclic load tests. They tested one sand in both static and cyclic load tests, at three levels of confining stress and at two levels of density. Cyclic load permanent strain tests were run to 10^4 load applications. By normalizing both the cyclic deviator stress and the permanent strain from the cyclic load tests with stress and strain parameters from the static

load failure test, Lentz and Baladi obtained a very good correlation between the results of the two types of tests. Figure 5.42 shows their results. The cyclic stress from the permanent strain test divided by the deviator stress at failure from the static load failure tests is plotted on the vertical axis versus the permanent strain after 10^4 load applications divided by the strain at 0.95 $\sigma_{d,f}$ from the static load tests on the horizontal axis.

Realizing that the data points shown in Figure 5.42 pertain to one material tested at three levels of confining stress and at two levels of density, the agreement between cyclic load and static load test results found is indeed remarkable. Lentz and Baladi checked this relationship for another sand and the data points obtained plotted right among the results given in Figure 5.42 for the first sand tested. Having obtained this agreement, Lentz and Baladi concluded that once a curve like the one depicted in Figure 5.42 has been established for a certain group of materials like, for instance, sands, permanent strain properties of materials from that group at other levels of confining stress and density could be obtained by performing just a static load failure tests at those conditions.

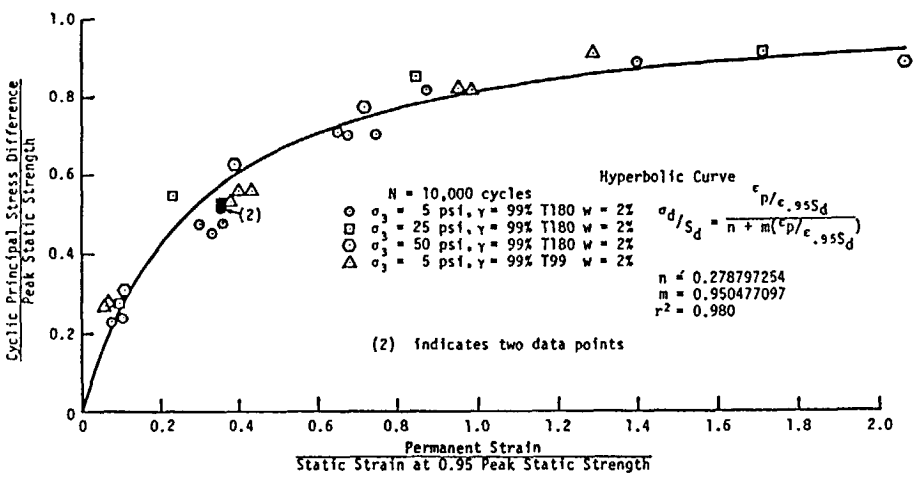

Figure 5.42: Normalized cyclic stress versus normalized permanent strain (source: [47]).

To check the validity of the Lentz-Baladi approach for the sands of Group S, the permanent strain results from the cyclic load tests (Table 5.8, Paragraph 5.3.3.6) and the results from the static load

failure tests (Table 5.15) are combined in Table 5.16. Figure 5.43 shows the normalized cyclic deviator stress versus the normalized permanent axial strain.

Table 5.16: Results from cyclic load permanent strain tests and static load failure tests, for the sands ENN, OSN and ZEN

test code	σ_c |kPa|	$\varepsilon_{a,p}(10^6)$ $\|10^{-3}\|$	$\sigma_{d,f}$ |kPa|	$\varepsilon_{0.95\ \sigma_{d,f}}$ $\|10^{-3}\|$	$\frac{\sigma_c}{\sigma_{d,f}}$ |-|	$\frac{\varepsilon_{a,p}(10^6)}{\varepsilon_{0.95\ \sigma_{d,f}}}$ |-|
ENND 03	30	6			0.45	0.35
04	35	21			0.52	1.24
02	40	33			0.60	1.94
ENNS 05			67	17		
OSND 02	40	10			0.42	0.48
03	50	23			0.52	1.10
04	60	25			0.63	1.19
OSNS 06			96	21		
ZEND 02	40	8			0.49	0.44
03	50	10			0.62	0.56
04	60	13			0.74	0.72
ZENS 05			81	18		

As can be seen from Figure 5.43, the agreement between cyclic and static load triaxial test results is far less for the materials tested here as compared to the Lentz-Baladi results. It should be noted here that two of the Lentz-Baladi "variables" were omitted here; all specimens were tested at the same confining stress and at the same density (per sand). Included here is one extra variable: Figure 5.43 pertains to three different sands, whereas Figure 5.42 pertains to one sand only. Furthermore, Figure 5.43 pertains to permanent strains after 10^6 load applications, whereas Figure 5.42 pertains to permanent strains after only 10^4 load applications.

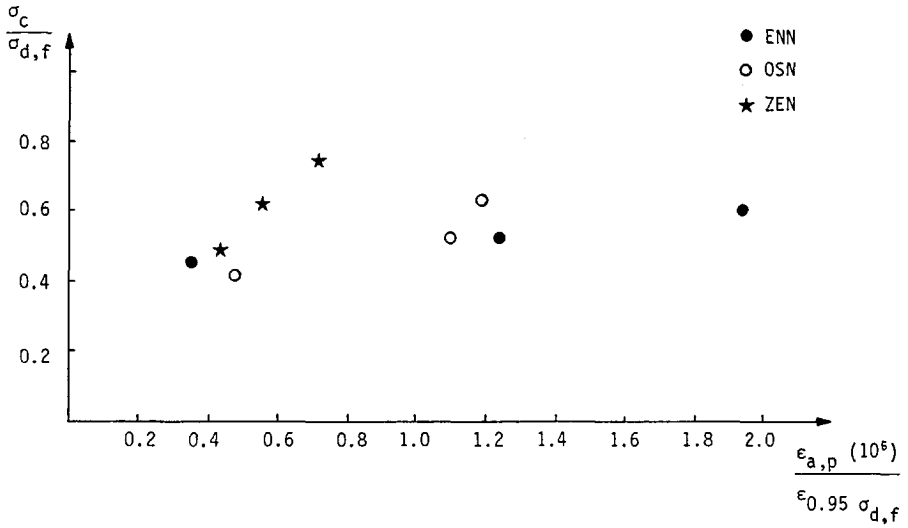

Figure 5.43: Normalized cyclic stress versus normalized permanent strain, for sands ENN, OSN and ZEN.

Figure 5.43 indicates that possibly hyperbolic relationships as suggested by Lentz and Baladi exist per individual sand; too few tests were however run per sand to establish such a relationship. A general relationship pertaining to the whole group of sands however does not exist.

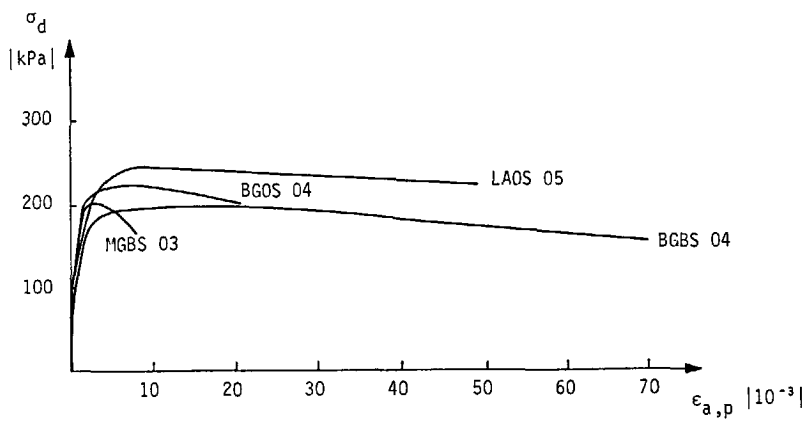

Figure 5.44: Stress-strain curves from static load failure tests on granular base course materials (materials LAO, MGB, BGB and BGO).

Table 5.17: Results from cyclic load permanent strain tests and static load failure tests, for the granular base course materials LAO, MGB, BGB and BGO

test code	σ_c |kPa|	$\varepsilon_{a,p}(10^6)$ $\|10^{-3}\|$	$\sigma_{d,f}$ |kPa|	$\varepsilon_{0.95\ \sigma_{d,f}}$ $\|10^{-3}\|$	$\frac{\sigma_c}{\sigma_{d,f}}$ |-|	$\frac{\varepsilon_{a,p}(10^6)}{\varepsilon_{0.95\ \sigma_{d,f}}}$ |-|
LAOD 05	72	18			0.29	3.7
04	96	40			0.39	8.2
03	120	-			0.49	-
LAOS 05			247	4.9		
MGBD 09	96	48			0.48	22.9
10	108	-			0.55	-
06	120	-			0.61	-
MGBS 03			198	2.1		
BGBD 05	96	10			0.51	2.0
04	120	40			0.63	8.2
03	144	-			0.76	-
BGBS 04			190	4.9		
BGOD 03	120	30			0.54	8.3
04	132	38			0.60	10.6
05	144	-			0.65	-
BGOS 04			221	3.6		

To check the validity of the Lentz-Baladi approach for granular base course materials, some of the materials of Groups C and R tested for permanent strain properties (see Paragraph 5.3.2.6) were also tested in static load failure tests [117]. For reasons of availability, materials LAO, MGB, BGB and BGO were chosen. The static load failure tests were performed using the 400 mm specimen diameter apparatus, in the strain-controlled mode (rate of strain 0.4 % per minute). The confining stress was set at σ_3 = 12 kPa, which is equal to the value of σ_3 used in the cyclic load permanent strain tests. Figure 5.44 shows the stress-strain curves obtained. Comparing the stress-strain behaviour of the granular base course materials (Figure 5.44) to that of

the sands (Figure 5.42), it can be seen that the stress ratio at failure $\sigma_{d,f}/\sigma_3$ is much higher for the granular base course materials, while the axial strain at failure is much less.

Table 5.17 summarizes the results of the cyclic load permanent strain tests (taken from Table 5.4, Paragraph 5.3.2.6) and of the static load failure tests. The stress and strain data from the cyclic permanent strain test were again normalized by the stress and strain from the static failure tests. Figure 5.45 shows the normalized cyclic stress plotted against the normalized permanent strain. As was the case with the sands from Group S (Figure 5.43) the data points do not plot on a single curve, as was found by Lentz and Baladi (Figure 5.42). It should be noted here that for the granular base course materials specimen reproducability is not as good as for the sands of Group S and that, therefore, specimen variability may account for some of the scatter found in Figure 5.45. However, the data-points from the permanent strain tests LAOD 04, BGBD 03 and BGOD 04 do not plot on a hyperbolic line, while the specimens used for these cyclic load tests were almost identical to those used in the static load failure tests.

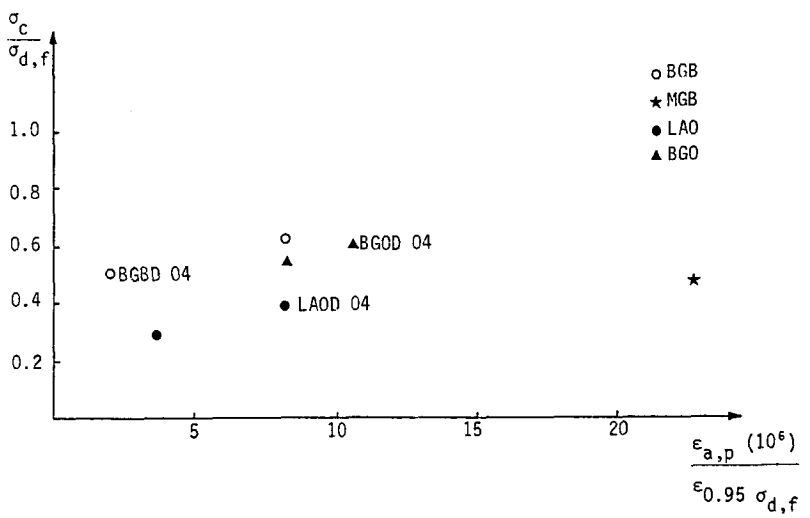

Figure 5.45: Normalized cyclic stress versus normalized permanent strain, for granular base course materials LAO, MGB, BGB and BGO.

In summary, the conclusion can be drawn that for the sands and the granular base course materials tested here, the Lentz-Baladi approach

to normalizing stress and strain data from cyclic load permanent strain tests with stress and strain data from static load failure tests cannot be used to derive the permanent strain behaviour of a particular material/density/stress combination from that of another such combination. Hence, cyclic load triaxial tests remain indispensable for establishing permanent strain properties of granular materials in the laboratory.

5.7 CONCLUSION

This chapter has dealt with the laboratory testing of a wide range of granular base course materials and sands. The granular base course materials ranged from porous, friable materials like lava to solid crushed stone materials like porphyry. A number of these materials was tested at two gradings in conformity with the upper and lower boundary of the Dutch specifications for granular base course materials with a 0/40 mm grading. The grading of the sands tested ranged from extremely fine to very coarse. In all, 25 material/grading combinations for the granular base course materials and 6 sands were tested.

A range of standard tests was performed on all the materials. The resilient properties of all materials were determined in cyclic load triaxial tests. A selection of 10 granular material/grading combinations and 3 sands was tested for permanent deformation properties in cyclic load triaxial tests with 10^6 load applications. From the test results obtained the following conclusions can be drawn:

1. The results of the Modified Proctor Compaction Test, the Single Point Proctor Compaction Test and the Vibrating Hammer Test showed a good mutual correlation. The test results indicated the influence of scaling down the grading of a granular material on density to be small. Compaction energy obviously had a large influence on density.

2. The resilient modulus M_r determined in cyclic load triaxial tests showed no correlation with the California Bearing Ratio, either for the granular materials or for the sands. Apparently, E - CBR relationships do not exist for these materials. Such relationships

are unlikely since the deformation in the CBR-test is mainly plastic, while E is a purely elastic parameter.

3. The resilient modulus of granular base course materials and sands was shown to be affected by grading. For materials with the same maximum particle size, those with the coarse"O"-grading showed a larger stress-dependency than those with the fine "B"-grading. For the sands, the subdivision into three groups based on their grading was reflected in the resilient stiffness.

4. The resistance to permanent deformation too was shown to be dependent on grading. Both for the granular base coarse materials and for the sands a finer grading was shown to result in a larger resistance to permanent deformation.

5. The resistance to permanent deformation of the granular materials was shown to be much higher than that of the sands. The difference in resilient stiffness between the two groups of materials was less pronounced.

6. In the search for simplified test procedures for determination of resilient properties the repeated static load triaxial test was shown to yield the same results as the far more complicated cyclic load triaxial test. The time-consuming "static triaxial creep test" procedure suggested by Kalcheff and Hicks [46] can be replaced by the far more user-friendly procedure suggested in Paragraph 5.5.2, without loss of accuracy.

7. Scaling down the triaxial specimen while keeping the grading intact yielded inconsistent results. Apparently, a 0/40 mm material cannot be tested for resilient properties with sufficient accuracy in a 150 mm specimen diameter triaxial apparatus.

8. The relationship between permanent strain and resilient strain as suggested by Veverka [49] was shown to be not applicable to the range of materials tested here in cyclic load permanent strain tests. The approach of Lentz and Baladi [47] of coupling permanent strain to the results of static load failure tests was also shown to be not valid for the materials tested here. Apparently, cyclic load triaxial tests with large numbers of load applications are the

only means of establishing the permanent strain properties of granular materials in the laboratory.

6 BEHAVIOUR RELATED TO WATER CONTENT

6.1 INTRODUCTION

Basic engineering practice aims at designing pavement structures in such a way that the granular base remains unsaturated throughout the life of the pavement. The problems of saturated bases such as development of positive pore water pressures and fine material from the lower pavement layers migrating upward with water into the granular base are well appreciated by practicing engineers. In the Netherlands, for instance, construction of major roads involves application of a thick layer of sand that in addition to a load-spreading function has a significant drainage function.

In unsaturated unbound materials, the negative pore water pressure or suction contributes to the strength and the stiffness of the material. As discussed in the literature review (Paragraph 2.6), suction may reach very high levels in case of the presence of clayey material, leading to a large increase in material strength and stiffness. Even when no clay is present suction may still significantly influence material behaviour: even children building sand castles know that they should use wet sand rather than dry, thereby unknowingly creating suction and hence a higher shearing resistance in their construction material.

Although pavement engineers aim at keeping granular bases unsaturated throughout the life of the pavement, this by no means guarantees that this favourable material condition will indeed prevail throughout the life of the pavement. Water may enter the granular base of the completed pavement structure both from below through capillary action or from above through cracks in the impervious pavement layers. In tropical areas, the impervious cover which is almost standard in the temperate zones is often omitted altogether. Then, the granular layers built mainly of lateritic material are exposed directly to the action of traffic and climate. In the dry seasons, the laterites then become dessicated and form a very hard riding surface. Although relatively rough and extremely dusty, such pavements may perform very well their

main function of merely providing a connection between one place and another, since both traffic speed and traffic volume are limited in such areas. In the rainy seasons, however, the top layers of the pavement are bound to become saturated and the hard pavement of the dry season becomes a muddy dirt road trafficable only by special vehicles like jeeps. For this type of roads, suction is one of the major factors influencing the performance of the pavement.

The theoretical background of soil-water and granular material-water interaction has been described in the literature review (Paragraph 2-.6). In this chapter, the effects of suction on material stiffness will be examined using data from cyclic load triaxial testing on specimens at different water contents. The effect will be studied first on the laterites of Group L, since the stiffness of these materials because of their grading is most susceptible to changes in water content. After illustrating the dramatic effect of soil suction on the elastic stiffness of the laterites, the same effect will be studied for a number of materials from Group S (sands) and Group C (conventional granular base course materials).

6.2 SUCTION GENERATION

6.2.1 Introduction

In the literature review (Paragraph 2.6) soil suction has been defined as the force exerted by the soil to take in water. Suction, however, does not only occur in soils. As will be shown in this chapter, suction may also contribute to the stiffness of granular materials. To deal with this properly, the more general term "suction" (without the addition "soil") will be used throughout this chapter.

As discussed in Paragraph 2.6, the total suction in an unbound material is made up of various components. The "matric suction" is the main component, comprising suction generated by capillary effects and suction caused by the surface forces in clays. In addition to matric suction, other components may also contribute to the total suction, such as osmotic suction. This latter component arises from differences

in concentration of, for instance, salts between the water present in the soil and the free water. Nature will balance this concentration difference by drawing water into the soil, and thus create suction. Although such concentration differences may occur in pavements (for instance when a granular base is penetrated from the top by salt used in winter time to reduce slipperiness), the main interest here lies with the matric suction. Generation of both components of this matric suction (capillary and swelling forces) will be dealt with separately in this paragraph.

6.2.2 Suction caused by capillary effects

When a capillary stands in a free pool of water (see Figure 6.1), water is drawn into the capillary by the surface tension at the curved water/air interface.

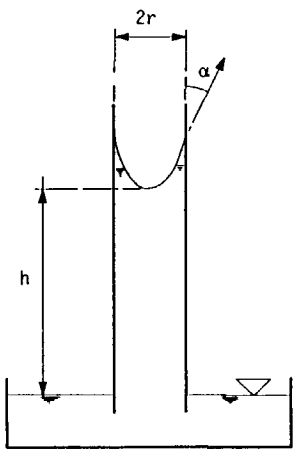

Figure 6.1: Rise of water in a capillary.

The surface tension T acting around the circumference of the water/air interface is in equilibrium with the gravitational force drawing the water from the tube according to:

$$2 \pi r T \cos \alpha = \pi r^2 h \gamma_w \qquad (6.1)$$

where

r = radius of capillary

T = surface tension

α = angle between water surface and capillary wall

h = height of water column

γ_w = density of water

The voids in a soil certainly are not straight capillaries like the one depicted in Figure 6.1. The voids are more cellular, connected by openings of various sizes. Nevertheless, curved water-air interfaces exist in soils and give rise to capillary forces drawing water into the soil and hence to suction. Figure 6.2 shows a schematization of a cellular void in, for instance, a sand. The void consists of a spherical part with a large diameter connected to other voids through narrow connections of smaller diameter.

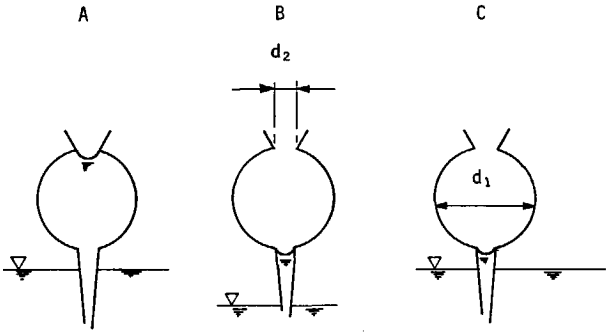

Figure 6.2: Schematization of a void in a granular material.

The varying diameter of the pores causes a hysteresis effect in the relationship between suction and water content [118]. Upon drying of the soil (lowering of the free water table, Figure 6.2A), the pore will not drain past the narrow connection at the top of the pore until the height of water in the pore corresponds with the small diameter d_2. Upon further lowering of the water table the pore will drain (Figure 6.2B). Once the pore has drained, it will not fill beyond the lower narrow connection upon a rise of the water table to the original level (Figure 6.2C), because the larger diameter d_1 of the pore corresponds with a relatively low capillary rise. In other words, the soil will have a higher water content upon drying as compared to wetting. This hysteresis effect is a major complicating factor in dealing with suction. No unique relationship exists between suction and water content and, therefore, suction cannot be deduced directly from the easy to determine water content. The relationship between suction and water content for a given soil therefore has to be determined twice,

namely on reduction and on increase of the water content. This multiplies the time needed for establishing suction-water content relationships by a factor of two. Even then, only the two extreme values of suction at a given water content are obtained. Compaction of for instance a triaxial specimen at a given water content will yield a suction somewhere in between the two values. Taking into consideration that establishing the full suction-water content relationship (drying and wetting) may take more than a year, a direct approach to measuring suction in the triaxial specimen is much more practical.

Since capillary suction originates from the curved air-water interfaces in the voids of the material, both air and water are needed to create capillary suction. Both in a fully saturated (no air in the voids) and in a fully dry (no water in the voids) material capillary suction cannot occur. Therefore, in a pure quartz sand (without any clay and hence without suction due to surface forces) suction will be zero both in the fully saturated and in the fully dry case. As discussed in Paragraph 2.6, this is a major convenience in triaxial testing of sands. For the fully saturated condition Terzaghi's effective stress principle can be used to calculate effective stresses from the measured total stresses and pore water pressure, whereas in the fully dry condition effective stresses equal total stresses since the pore water pressure is zero.

6.2.3 Suction caused by swelling forces

In general, clay particles show a net negative charge, caused by deficiencies in the mineral structure of the clay lattices. These deficiencies mainly stem from the so-called "isomorphous substitution". Silicon and aluminium atoms have been replaced in the clay mineral structure by atoms of similar size ("isomorphous") like magnesium, but of lower valence. The net effect is a shortage of positive charges and hence an overall negative charge of the clay particle. This negative charge is balanced by attracting cations to the clay particle surface [119]. This in turn causes the concentration of cations to be higher at the surface of the clay particle as compared to the general pore fluid. Nature wants to balance this concentration difference and since the positive charges cannot be pulled away from the clay-particle surface, the reverse balancing of

concentration takes place: water is pulled in between the clay particles to lower the concentration at that point.

In saturated clays, this migration of water to the places in between the clay particles causes swelling of the clays. The clay particles are pushed further apart by the migrating water, resulting in an increase in void content of the soil and in an overall volume increase. The swell pressure and volume increase involved in this are indeed tremendous. Janssen and Galjaard (120), for instance, tested a "black-cotton" montmorillonite clay from Sudan, obtaining a swell-pressure of 615 kPa (which would lift some 30 m of embankment) and a volume increase due to swelling of 33%.

The fact that water is pulled in between the clay particles to balance the concentration difference of the cations results in suction. It should be well noted that even in a "saturated" clay (saturated by the definition of all voids being filled with water) suction can still occur. A swelling soil may very well have all its pores filled with water, but when given access to free water more water may be pulled into the soil to further balance the concentration difference of the cations. This means that the simple rule given in the previous paragraph for a pure sand "suction is zero in the saturated condition" does not hold for clays. Pure sand consists of non-charged SiO_2-crystals, attracting no cations and, therefore, suction in pure sand originates from capillary effects only and is thus zero at saturation. In a saturated clay, suction due to capillary effects will also be zero, but suction due to surface forces may still exist.

From the above it follows that when the water content of a saturated soil is reduced by decreasing the void content of the soil (for instance in a consolidation test in an oedometer), suction in the clay will increase. On removal of the external loading in the oedometer, water will be pulled into the soil against gravity by suction. When drying a clay soil to below saturation (air entering the voids in the soil) suction will further increase. Again, the situation is completely different for clay as compared to sand. Starting from saturation, in a pure sand suction will increase from zero upon air entering the pores up to a maximum somewhere in the unsaturated region and then upon further drying decrease back to zero in the fully dry condition. In a clay, suction is not necessarily zero at saturation

and will keep or increasing or reduction of the water content in the unsaturated region towards the extremely high values of pF = 7 (suction equals 10^7 cm H_2O or 10^6 kPa) in the "dry" condition.

The marked difference in suction behaviour between a pure sand and a clay should at all times be borne in mind when testing unsaturated soils. The simple rule of suction being zero in the saturated or dry condition only applies to pure quartz-sands. When dealing with soils in general, which are bound to contain some clay, suction may very well be substantial in the saturated and the dry condition. The simple approach of testing the material in the dry condition and interpreting total stresses as being effective stresses is then no longer allowed, since the pore water pressure is not zero but has a significant negative value.

6.3 SUCTION-DEPENDENCY OF THE STIFFNESS OF LATERITES

6.3.1 Introduction

Suction is predominantly controlled by the amount and type of clay present in a given material. Prior to discussing the suction-dependency of the stiffness of sands and granular base course materials which contain little or no clay, this paragraph will deal with the testing of laterites containing various amounts of clay. As discussed in Paragraph 2.4.5, laterites in general are materials that may contain substantial amounts of clay. Often these materials have a so-called "gap-graded" particle size distribution. They consist of a coarse and a fine fraction only, while the intermediate sand-sized fraction is lacking. Continuously graded laterites also occur, again often having a substantially large clay fraction.

The behaviour of such materials is strongly dependent on suction. For the gap-graded materials, Figure 6.3 shows two possible soil structures. Structure A is a skeleton of coarse particles, the voids of which are filled with clay. Structure B is a matrix of clay, with coarse grained particles "floating" in it.

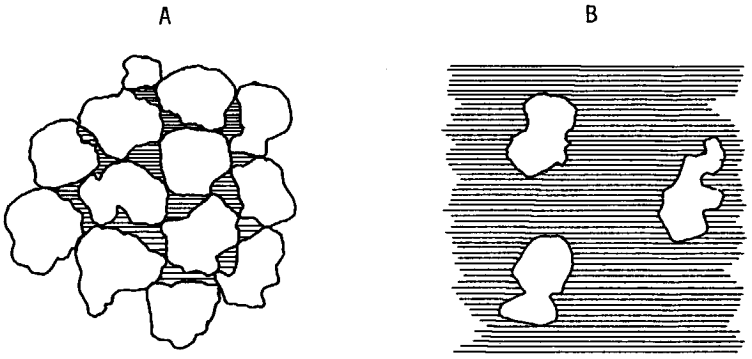

Figure 6.3: Two possible soil-structures for gap-graded laterites. A: Skeleton structure. B: Matrix structure.

The main load-bearing capacity of structure A is generated by the skeleton of coarse particles, as in a normal properly graded granular base course material. In the dry condition, the clay in the voids of the skeleton generates high levels of suction, thereby substantially increasing the overall shear strength and stiffness of the material. Upon wetting, the suction is reduced and the stiffness of the material is reduced to that of the skeleton of coarse particles. For structure B, the coarse grained particles do not interlock and hence they do not contribute to the overall stiffness of the material. This stiffness is wholly dependent on that of the clay matrix, which in the dry case may be quite substantial thanks to the high level of suction in the clay. Upon wetting, however, the stiffness of the material will be reduced to that of a wet clay.

For continuously graded materials, Fuller and Thompson (121) have shown that to obtain a maximum number of intergrain contact points, the material should have a particle size distribution represented by the formula:

$$p = 100 \sqrt{\frac{d}{d_{max}}} \qquad (6.2)$$

where

p = percentage smaller than particle diameter d

d_{max} = maximum particle diameter in the material.

Equation 6.2 yields low percentages of fine material. In a 0-19 mm material, which is quite a common particle size range for laterites, Equation 6.2 for instance yields 6% material passing the 75 μm sieve.

Most laterites found in nature have a higher percentage of fines. Then, the same reasoning as for gap-graded materials is valid. The material is "over-filled" with fines and the coarse graines are more or less floating in a matrix of fine material. When the material is dry, a high stiffness can be obtained thanks to the high level of suction in the fine material. Upon wetting, however, a drastic drop in stiffness may occur because of reduction of suction. In conclusion, both gap-graded and continuously graded laterites often show a stiffness which is strongly dependent on suction.

6.3.2 The laterites investigated

As described in Paragraph 4.5, the six laterites investigated were obtained from borrowpits alongside the road Moengo-Albina in Suriname, South America. Details on the materials are given in that paragraph, and in the Material Information Sheets of Appendix 2. The grading of the individual materials is given in Appendix 2; Figures 6.4 through 6.7 summarize the gradings, grouping the materials per horizon from which they were taken. Also shown in these figures are the Fuller-curves calculated from the maximum particle diameter in the various materials using Equation 6.2.

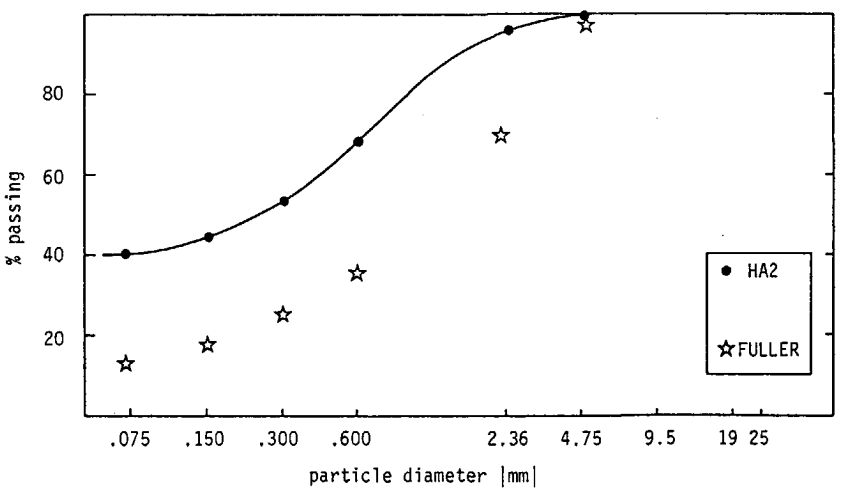

Figure 6.4: Particle size distribution of material HA2.

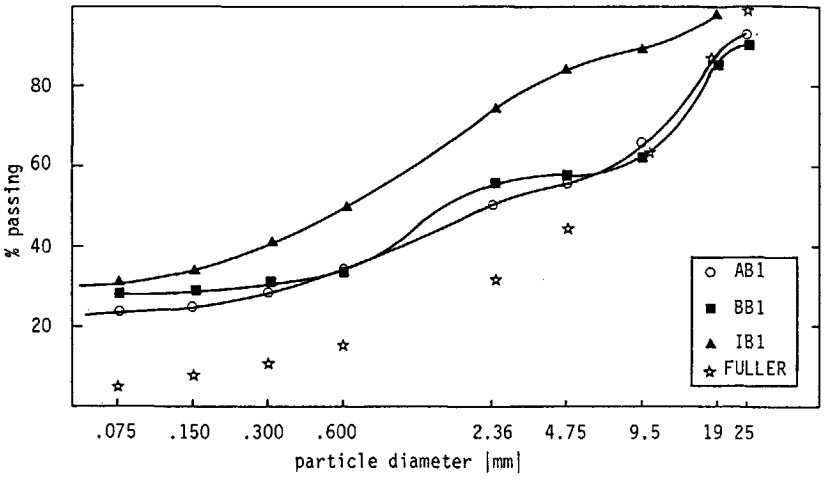

Figure 6.5: Particle size distribution of materials AB1, BB1 and IB1.

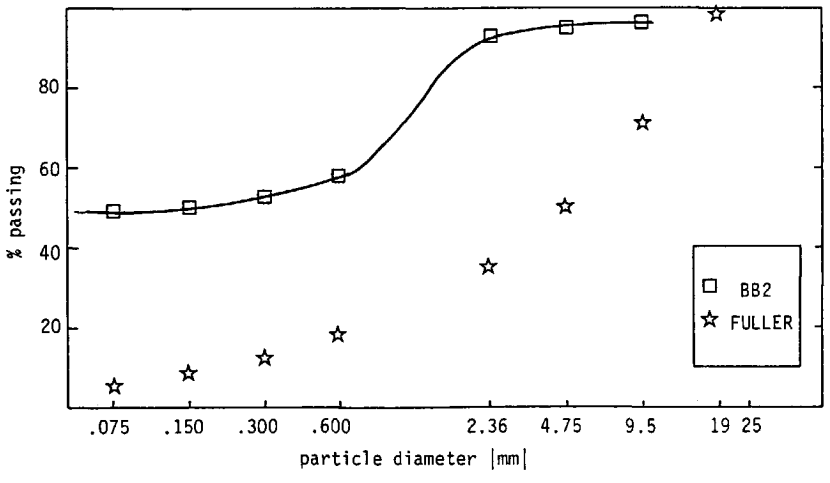

Figure 6.6: Particle distribution of material BB2.

As can be seen from Figures 6.4, 6.6 and 6.7, the materials from the A2, B2 and C horizons (HA2, BB2 and AC) have particle size distributions that deviate substantially from the Fuller-curve. These materials show a substantial shortage of coarse particles and a clear surplus of fines. Although these materials do contain some gravel sized particles, the percentage of these particles is quite low. Practically speaking, these materials are therefore mixtures of sand-sized particles and fines.

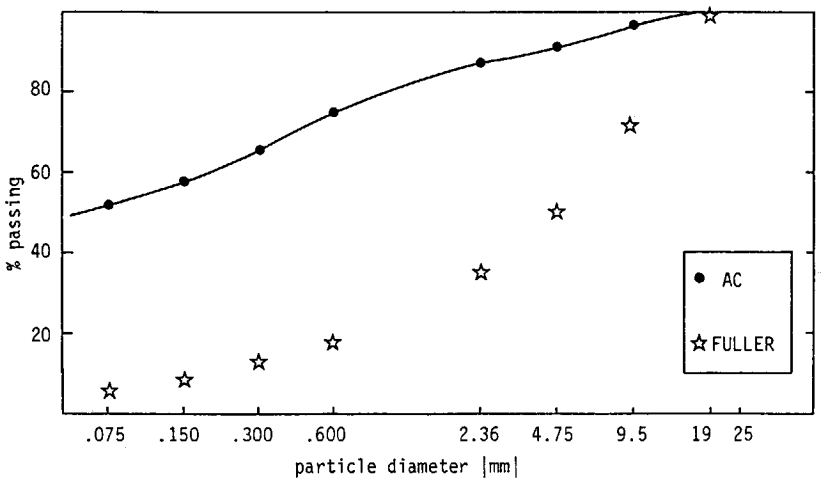

Figure 6.7: Particle size distribution of material AC.

Figure 6.5 shows that the materials from the B1 horizon (AB1, BB1 and IB1) contain a substantial percentage of gravel-sized particles. The materials AB1 and BB1 have particle size distributions that lie relatively close to the Fuller-curve. The material IB1 deviates substantially from the Fuller-curve. As the materials from the other horizons, this material too shows a shortage of gravel sized particles, while the percentage of fines (material < 0.075 mm) is similar to that of the other two materials from the B1 horizon.

6.3.3 Cyclic load triaxial tests with measurement of suction

6.3.3.1 INTRODUCTION

For each of the six laterites, one triaxial specimen was prepared and subsequently tested for resilient properties at two different moisture contents. The resiliency testing was carried out using the 100 mm specimen diameter triaxial apparatus described in Paragraph 5.3.3.2. As can be seen from Figure 6.5, the materials from the B1 horizon contained small amounts of particles with a diameter d > 19 mm. In view of the limited specimen diameter, these particles were crushed to d < 19 mm and then re-added to the sample material.

6.3.3.2 MEASUREMENT OF SUCTION

Since the main interest in the testing of the laterites lies with their suction-dependent stiffness, an addition was made to the 100 mm specimen diameter triaxial apparatus to allow for direct measurement of suction in the triaxial specimen during the test. Figure 6.8 shows the schematics of the so-called "tensiometer" that was used for measurement of suction. The tensiometer consists of a high air-entry ceramic stone, connected through a double plastic hose to the plastic body tube. The tensiometer is standardly equiped with a vacuum Bourdon gauge, that was for this purpose replaced by an electronic pressure transducer.

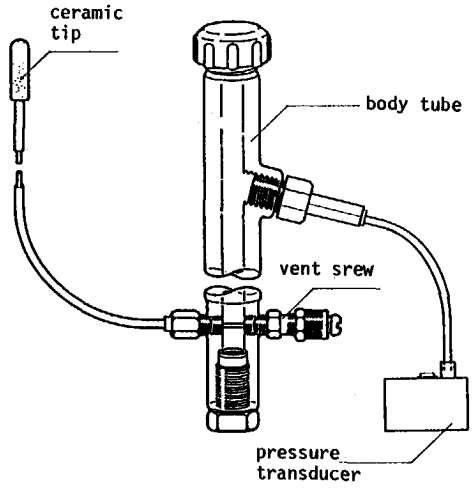

Figure 6.8: Schematics of tensiometer.

The principle of the tensiometer is relatively simple. Prior to installment, the whole device is saturated, including the ceramic tip. Then, the ceramic tip is placed into the material of which the suction has to be measured. Water is then pulled by suction into the material from the tensiometer, creating a sub-atmospheric pressure in it. Water movement goes on until the negative pressure in the tensiometer equals that in the material to be tested. The equilibrium pressure can then be read from the pressure gauge. It should be well noted that the working range of the tensiometer because of its principle is limited to theoretically suction values up to 100 kPa (pF 3).

As noted, the tensiometer is standardly equiped with a Bourdon-type vacuum gauge, which has the disadvantage of needing a relatively large volume change in order to measure the negative pressure. This has two drawbacks. Firstly, the movement of a substantial quantity of water from the tensiometer into the triaxial specimen influences (reduces) the suction in the specimen and thus the measuring device itself influences the parameter to be measured. Secondly, the movement of water into low permeability soil takes time, causing the response time to changes in suction to be several days. Both these disadvantages only play a minor role in field testing for agricultural purposes, for which the tensiometer was developed. However, when testing a relatively small quantity of soil in a triaxial test for relatively fast changing suction, the two disadvantages are indeed a problem. This was solved by replacing the Bourdon-gauge by an electronic pressure transducer requiring only negligible volume change to measure changes in pressure.

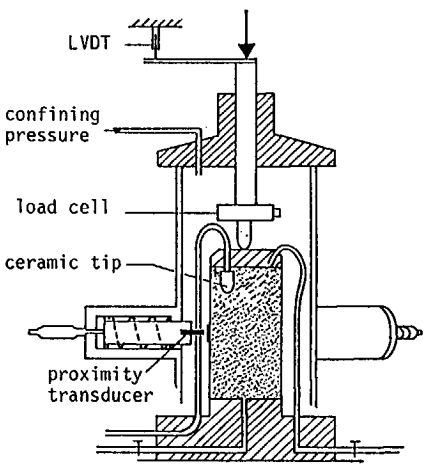

Figure 6.9: 100 mm specimen diameter triaxial cell with ceramic tip in triaxial specimen.

Figure 6.9 shows the schematics of the 100 mm specimen diameter triaxial apparatus with the ceramic tip of the tensiometer placed in the top of the triaxial specimen. The plastic hose connecting the ceramic tip to the body of the tensiometer passes through the top-platen and the pedestal of the triaxial cell. This double hose allows for flushing of water into the ceramic tip and back to remove any entrapped

air. The body of the tensiometer is mounted on the outside of the triaxial cell (see Figure 6.10).

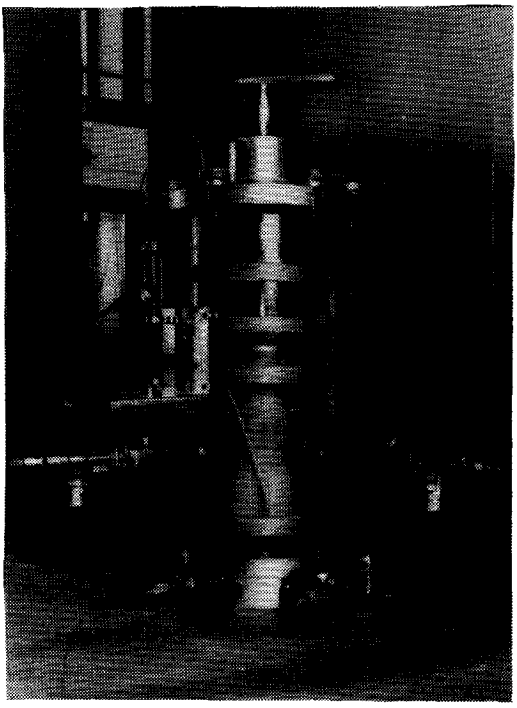

Figure 6.10: Tensiometer mounted on triaxial cell.

6.3.3.3 SPECIMEN PREPARATION AND TEST PROCEDURES

The triaxial specimens were compacted in a 100 mm diameter steel mould in five layers, using a full-faced compaction drop-hammer. Per layer, ten blows of the hammer were applied, resulting in a compaction energy equal to that of AASHTO T99-74 standard Proctor compaction. To obtain a smooth transition between the successive compaction layers, each layer was duly roughened after compaction prior to admission of the material of the following layer. After completion of the compaction procedure, the specimen was extruded from the steel mould and placed in the triaxial cell.

The resiliency testing was carried out at two material conditions, namely a relatively dry condition (degree of saturation S_r = 70%) and a wet condition (degree of saturation approximately S_r = 90%). After compaction, the triaxial specimens were first brought to the specified degree of saturation of S_r = 70%, either by drying or wetting of the specimen, depending on the initial degree of saturation after compaction. The degree of saturation of the triaxial specimen during drying or wetting was determined by continuously weighing the whole specimen/triaxial pedestal assembly. The amount of water lost or taken in by the specimen could thus be measured and the degree of saturation S_r could be calculated from the known initial moisture content, the moisture loss or intake and the specific gravity of the material at hand.

After the required degree of saturation S_r = 70% for the "dry" condition was reached, the triaxial specimen was tested for resilient properties. After completion of the tests, the specimen was allowed to take in water under a hydraulic head of 150 kPa for a period of approximately one week, again with continuous weighing of the specimen/pedestal assembly. After this wetting procedure, the triaxial specimens were again tested for resilient properties. Table 6.1 shows the specimen characteristics after compaction and in the "dry" and the "wet" testing conditions.

Also shown in Table 6.1 is the suction in the triaxial specimens as measured with the tensiometer. The materials from the A2, B2 and C horizons (HA2, BB2 and AC) containing a large amount of fine material show in the dry condition suction values beyond the practical working range of the tensiometer (pF > 2.9). The coarse graded materials from the B1 horizon (AB1 and BB1) show modest suction values in the dry condition, whereas the more finely grained material IB1 from the same horizon again has a suction of pF > 2.9 in the dry condition. After wetting, all specimens have suction values within the measuring range of the tensiometer. The materials from the A2, B2 and C horizons and material IB1 show a substantial decrease in suction, while the suction in materials AB1 and BB1 is practically speaking constant. The measured small increase in suction upon wetting of material IB1 indicates the accuracy of this way of measuring suction, since in reality suction cannot increase upon wetting in a material containing a substantial amount of clayey material.

Table 6.1: Triaxial specimen characteristics

	compaction			dry			wet		
material	ρ_d |kg/m³|	w |%|	S_r |%|	w |%|	S_r |%|	pF |-|	w |%|	S_r |%|	pF |-|
HA2	1694	21.3	90.4	16.5	70.0	>2.9	21.6	91.8	2.3
AB1	1890	10.2	57.0	12.5	70.0	1.9	15.5	87.1	1.8
BB1	1851	11.9	55.3	15.1	70.0	1.7	18.8	87.3	1.8
IB1	1599	24.4	86.9	19.6	70.0	>2.9	25.1	89.5	1.9
BB2	1860	17.1	91.1	13.2	70.0	>2.9	17.3	92.2	2.2
AC	1560	25.7	90.6	19.8	70.0	>2.9	25.1	88.4	2.2

The procedure for the resiliency testing itself was quite similar to the one used for the "standard" resiliency testing of the sands of Group S, as described in Paragraph 5.3.3.5. The main difference lies in the stresses applied in the resiliency testing. Since the laterites tested were applied as a base course material at shallow depth in the road Moengo-Albina, the confining stress applied in the resiliency testing were limited to maximum σ_3 = 50 kPa. Table 6.2 shows the stresses applied in the resiliency testing.

Table 6.2: Stresses applied in resiliency testing

σ_3 |kPa|	σ_c |kPa|					σ_c/σ_3 |-|
10	10	20	30	40	50	1 - 5
20	20	40	60	80		1 - 4
30	30	60	90	120		1 - 4
40	40	80	120	160		1 - 4
50	50	100	150			1 - 3

As was done when testing the sands, higher stress ratios were omitted at the higher values of the confining stress σ_3, since at those values of σ_3 the stress ratio at failure is lower because of the cohesion in the material. It should be noted that all stresses given here are total stresses. No attempt was made to interpret test results in terms of effective stresses, since for the unsaturated materials dealt with here the pore pressures are negative and hence Terzaghi's effective stress principle cannot be applied.

6.3.3.4 TEST RESULTS

Table 6.3 shows the parameters K_1 and K_2 from the K-θ model, describing the resilient modulus M_r as a function of the sum of principal stresses θ. Two sets of parameters are given per material tested, namely one for the dry and one for the wet condition of the triaxial specimen.

Table 6.3: Material parameters K_1 and K_2 for the dry and the wet specimen condition

	dry			wet		
material number	test code	K_1 |MPa|	K_2 |-|	test code	K_1 |MPa|	K_2 |-|
L01	HA2D 01	26.0	.46	HA2D 02	60.8	0.03
L02	AB1D 01	15.6	.51	AB1D 02	15.9	0.50
L03	BB1D 01	92.6	.15	BB1D 02	28.9	0.36
L04	IB1D 01	76.1	.26	IB1D 02	17.4	0.22
L05	BB2D 01	18.8	.53	BB2D 02	15.7	0.32
L06	ACD 01	16.7	.45	ACD 02	135.3	-0.24

Figure 6.11 shows the M_r-θ relationships for the materials from the A2, B2 and C horizons, both for the dry and the wet specimen condition. For both conditions, materials BB2 and HA2 show a higher resilient modulus than does material AC. All three materials show a substantial drop in resilient modulus upon wetting. This decrease in

stiffness is attributable to the decrease in suction in the material upon wetting, as shown in Table 6.2. As noted above, all three materials contain a surplus of fine material, and therefore their stiffness is strongly dependent on that of the fine fraction. In the dry specimen condition, this fine material shows a high stiffness thanks to suction, which is readily lost upon wetting.

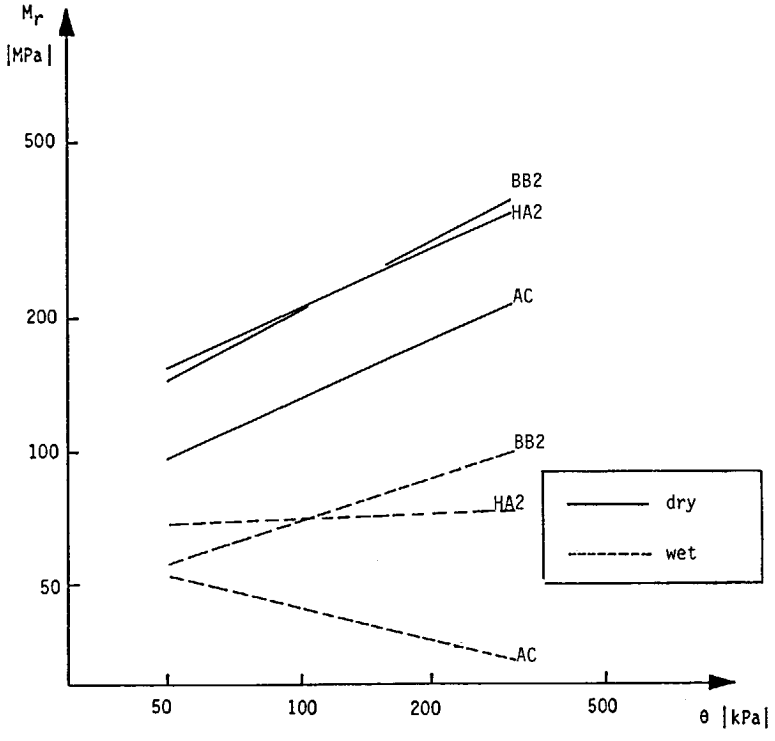

Figure 6.11: M_r-θ relationships for materials HA2, BB2 and AC, for the dry and the wet specimen condition.

The behaviour of material AC is typical. In the dry condition, it shows an increasing stiffness with increasing stress, which after wetting turns into a soil-like behaviour of decreasing stiffness with increasing stress. Figure 6.12 shows the individual resilient moduli measured in the cyclic load tests of materials AC in the dry and the wet condition. This time, the resilient modulus has been plotted on a linear scale as a function of the cyclic deviator stress σ_c on a linear scale, which is the standard way of relating the resilient stiffness of soils to deviator stress. For the dry specimen condition, material AC behaves like a granular material. The influence of the

confining stress σ_3 is larger than that of the cyclic deviator stress σ_c. For the wet specimen condition, the material shows a soil-like behaviour. In this case, the influence of the confining stress is small relative to that of the cyclic deviator stress.

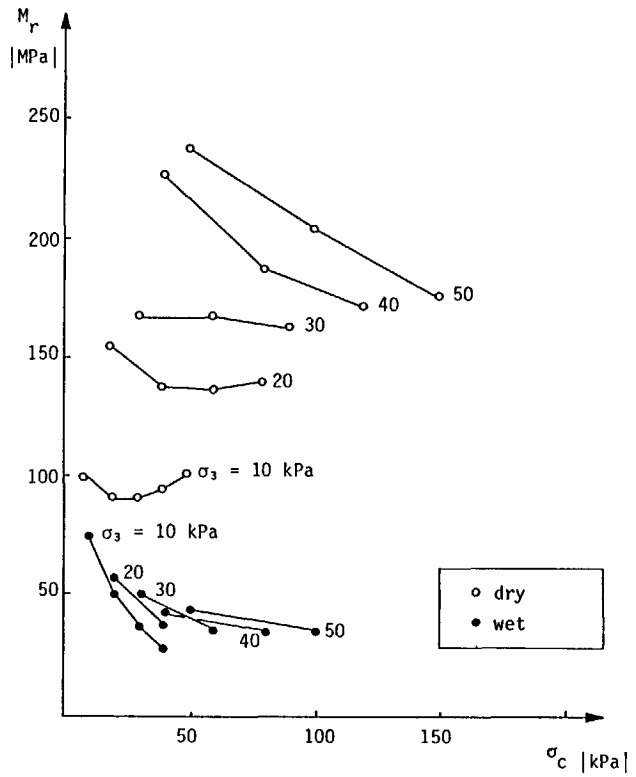

Figure 6.12: Resilient modulus M_r versus cyclic deviator stress σ_c for material AC.

Figure 6.13 shows M_r-θ relationships for the materials from the B1 horizon, again for the dry and the wet specimen condition. For material AB1, the resilient modulus remains constant upon wetting, whereas for material BB1 the resilient modulus shows a decrease in the low stress region and remains constant in the high stress region. The behaviour of material IB1 is quite distinct from that of AB1 and BB1: IB1 shows a drastic drop in resilient modulus upon wetting, as did the materials from the other horizons (see Figure 6.11). Looking back at Table 6.1, the change in stiffness of the materials upon wetting is again consistent with the change in suction. Material AB1 and BB1 show a more or less constant suction and stiffness upon wetting, whereas

material IB1 shows a drastic drop in suction upon wetting which causes the drastic drop in stiffness.

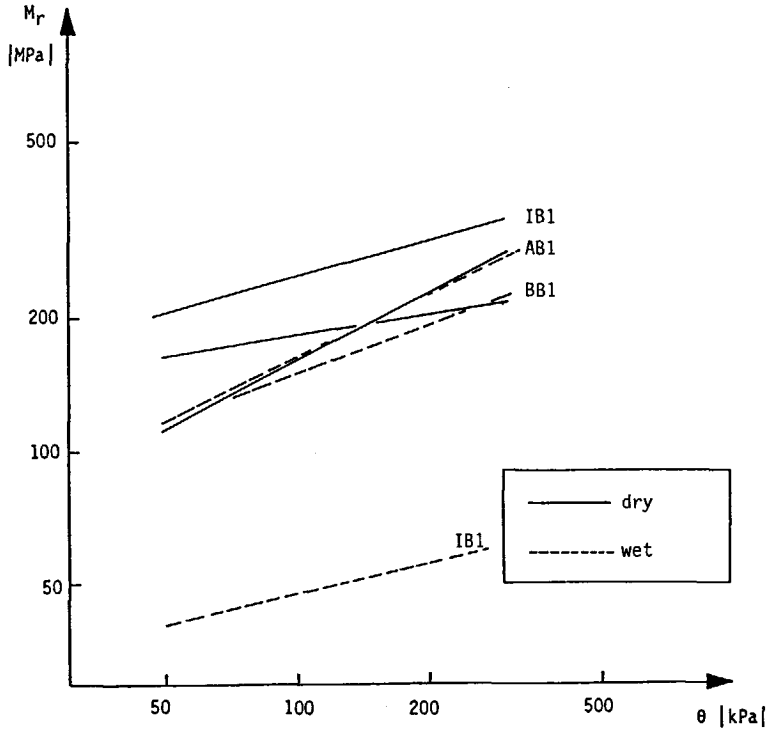

Figure 6.13: M_r-θ relationships for materials AB1, BB1 and IB1, for the dry and the wet specimen condition.

6.4 SUCTION DEPENDENCY OF THE STIFFNESS OF SANDS

6.4.1 Introduction

In the previous paragraph, some of the laterites tested were shown to have a stiffness strongly dependent on suction, while other laterites showed little or no change in stiffness between the dry and the wet material condition. The first group of laterites had an abundance of fines, which controlled their stiffness-suction relationship. The second group of laterites had a more skeleton-type of soil structure,

the stiffness of which is derived from the skeleton and is therefore less dependent on suction.

The stiffness of the sands of Group S can be expected to be far less dependent on suction than that of the fine grained laterites, since all of the sands have a skeleton-type of soil structure. Table 6.4 shows the maximum particle size d_{max} of each of the six sands from Group S (taken from Appendix 2 as the sieve opening through which more then 95 % of sample material passed), the percentage of material passing the 0.075 mm sieve and the percentage smaller then 0.075 mm calculated from the Fuller-equation (Equation 6.2). All six sands contain less material passing the 0.075 mm sieve then "allowed for" by the Fuller-equation and hence do not have a matrix-type soil structure like the fine grained laterites.

Table 6.4: Comparison of actual percentage and theoretical Fuller-percentage passing the 0.075 mm sieve, for the six sands of Group S

material code	d_{max} |mm|	% <0.075 mm	$100\sqrt{\frac{0.075}{d_{max}}}$
ELN	2.8	9	16
ENN	2.8	9	16
EEN	.600	6	35
OSN	.600	12	35
WIN	.600	12	35
ZEN	.420	34	42

To check whether the stiffness of the sands is indeed less dependent on soil suction, the materials ENN, OSN and ZEN (Echten sand, Eastern Scheldt sand and Zeijen sand) were tested for resilient properties at two different water contents, using a procedure quite similar to the one used for the laterites. The sands tested are the same materials as those tested earlier for permanent strain properties. As noted in Paragraph 5.3.3.6, they were selected from the total of six sands in Group S in such a way that each sub-group (very coarse sands, fine sands and extremely fine sands) is represented.

6.4.2 Resiliency testing and results

To establish the suction dependency of the stiffness of the sands, the same procedure was followed as for the laterites (Paragraph 6.3.3). For each of the three sands one triaxial specimen was built and tested for resilient properties in a "wet" and a "dry" condition, with measurement of the suction in the triaxial specimen using the tensiometer. The wet condition was in case of the sands chosen at the optimum moisture content w_{opt} from the modified Proctor compaction test, since this water content is close to the maximum water content that can be retained by the sand under conditions of free drainage. The dry condition was chosen at a degree of saturation of S_r = 30%. The triaxial specimens were prepared at optimum moisture content, tested for resilient properties, then dried to S_r = 30% and tested again for resilient properties. The specimen preparation procedure was equal to that used for the earlier cyclic load triaxial testing of the sands (see Paragraph 5.3.3.4), with the addition of incorporating the ceramic tip of the tensiometer in the top of the triaxial specimen.

Table 6.5: Triaxial specimen characteristics

		wet			dry		
test number	ρ_d [kg/m^3]	w [%]	S_r [%]	pF [-]	w [%]	S_r [%]	pF [-]
ENND 05	1713	13.6	66	1.5			
ENND 06	1713				6.2	30	2.0
OSND 06	1669	15.6	68	1.9			
OSND 07	1669				6.9	30	2.2
ZEND 05	1594	14.9	59	1.9			
ZEND 06	1594				7.5	30	2.5

Table 6.5 shows the triaxial specimen characteristics for both the wet and the dry condition. The dry density for both conditions was of course equal, since the same triaxial specimen was used for testing.

As can be seen from Table 6.5, the suction in the triaxial specimens remained well within the working range of the tensiometer for both the wet and the dry condition.

The actual resiliency testing was performed at the same confining stresses as applied earlier in the "standard" resiliency testing (see Table 5.6, Paragraph 5.3.3.5). Since two full sets of resiliency tests had to be performed on the same triaxial specimen, the maximum ratio of the cyclic deviator stress to the confining stress σ_c/σ_3 was kept somewhat lower than in the "standard" resiliency testing. Since comparison of the stiffness of each of the sands at two different levels of suction was the aim of the testing described here, it was judged essential to perform the tests in the wet and the dry condition on the same specimen at the same stresses. The stress ratios close to failure were, therefore, omitted from the test program.

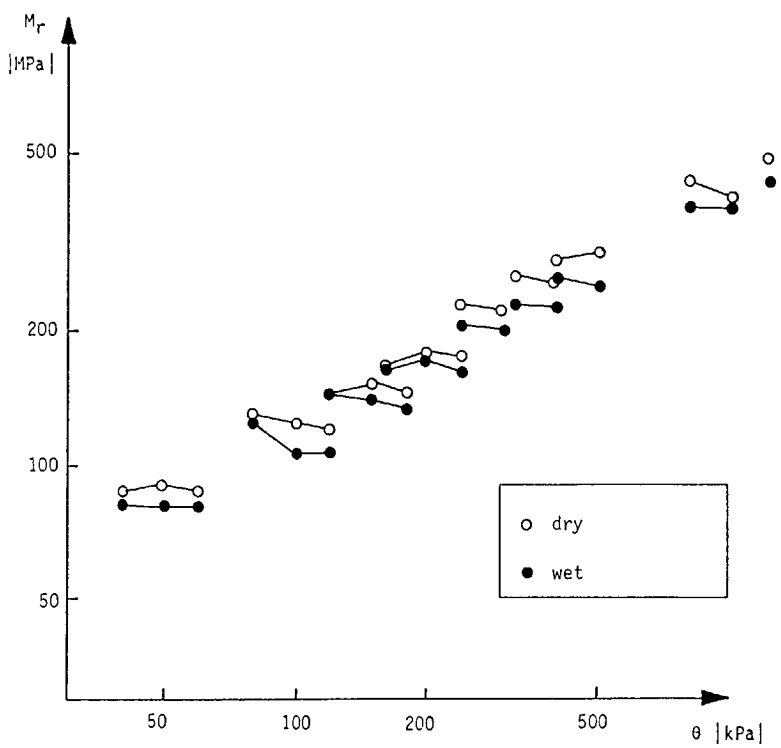

Figure 6.14: M_r-θ relationships for Echten sand ENN, for the wet and the dry specimen condition.

Figures 6.14 through 6.16 show the results of the resiliency testing at the wet and the dry specimen condition. The individual data points from all tests at the various stress combinations are given in the figures. The data points are connected in the figures per level of the confining stress σ_3. All three sands show an increase in resilient stiffness upon drying of the triaxial specimen, which is attributable to the increase in suction. As expected, the increase in resilient stiffness is small, certainly when compared to the changes in stiffness found for part of the laterites (see Figures 6.11 and 6.13). Apparently, the sands derive their stiffness from the skeleton of the sand grains. This stiffness is increased to a limited extend only upon drying of the triaxial specimens, which is consistent with the relatively small increase in suction upon drying. Table 6.6 shows the numerical results from the resiliency testing of the sands for the wet and the dry condition, being the material parameters K_1 and K_2 from the K-θ model for resilient stiffness.

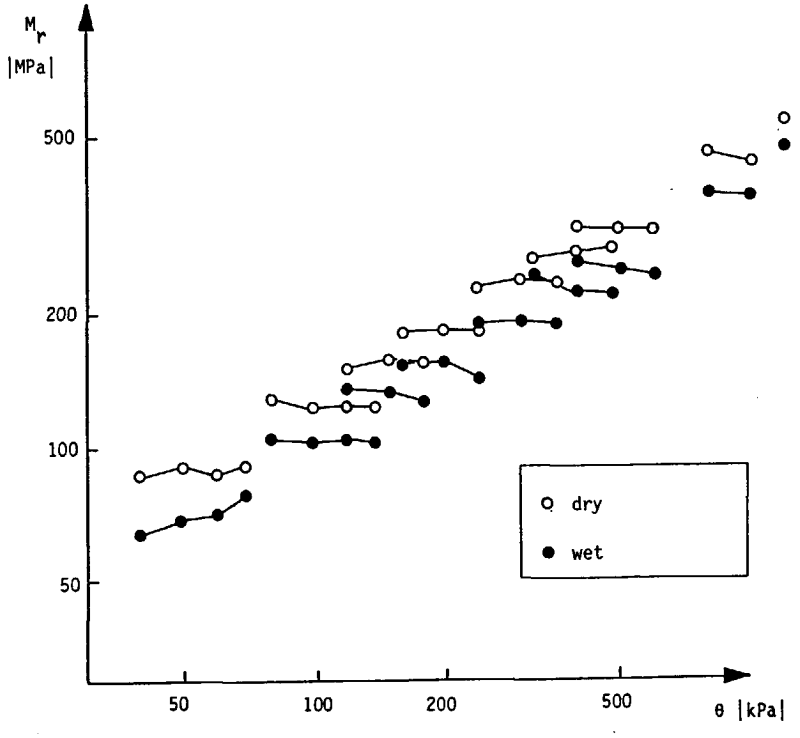

Figure 6.15: M_r-θ relationships for Eastern Scheldt sand OSN, for the wet and the dry specimen condition.

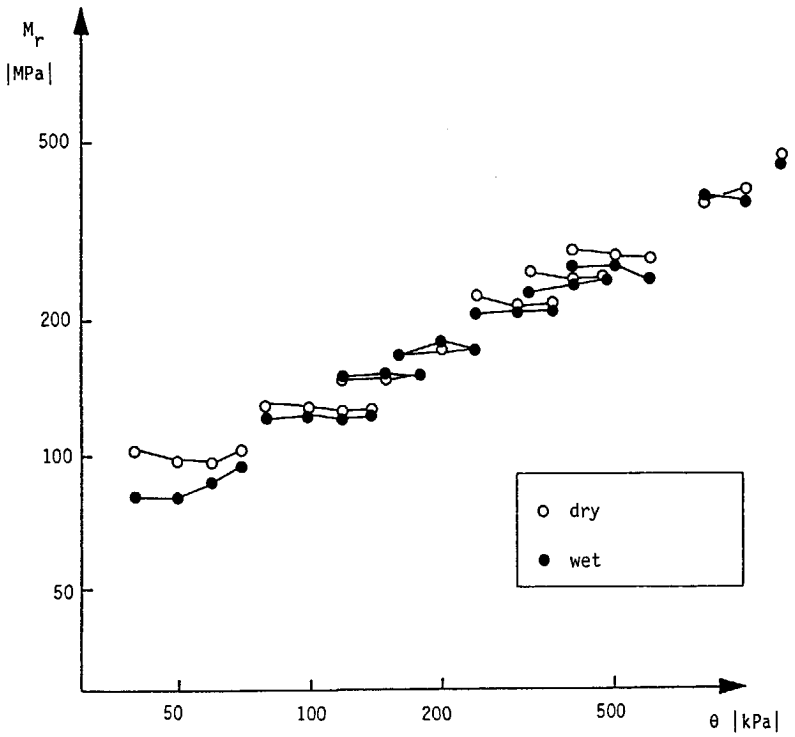

Figure 6.16: M_r-θ relationships for Zeijen sand ZEN, for the wet and the dry specimen condition.

Table 6.6: Material parameters K_1 and K_2, for the wet and the dry specimen condition

	wet			dry		
material number	test code	K_1 |MPa|	K_2 |-|	test code	K_1 |MPa|	K_2 |-|
SO2	ENND 05	10.7	.52	ENND 06	11.0	.53
SO4	OSND 06	7.6	.57	OSND 07	9.4	.56
SO6	ZEND 05	12.6	.49	ZEND 06	15.0	.47

6.5 SUCTION DEPENDENCY OF THE STIFFNESS OF GRANULAR BASE COURSE MATERIALS

6.5.1 Introduction

In Paragraph 6.3, the laterites containing a large clay fraction were shown to have a resilient stiffness which is strongly dependent on suction. For the laterites containing a relatively small clay fraction and for the sands containing almost no clay, the resilient stiffness was shown to be far less dependent on suction. To study the effect of clay on the suction dependent stiffness of granular base course materials, one such material containing clay and one straightforward crushed rock material were tested at two different water contents. The material containing clay is the gravel/loam mixture stol (material code STN), while porphyry (material code PO) was selected for testing as a straightforward crushed rock material since this material had the lowest optimum moisture content. To study the effect of grading the porphyry was tested at the B- and the O-grading (material codes POB and POO).

6.5.2 Resiliency testing and results

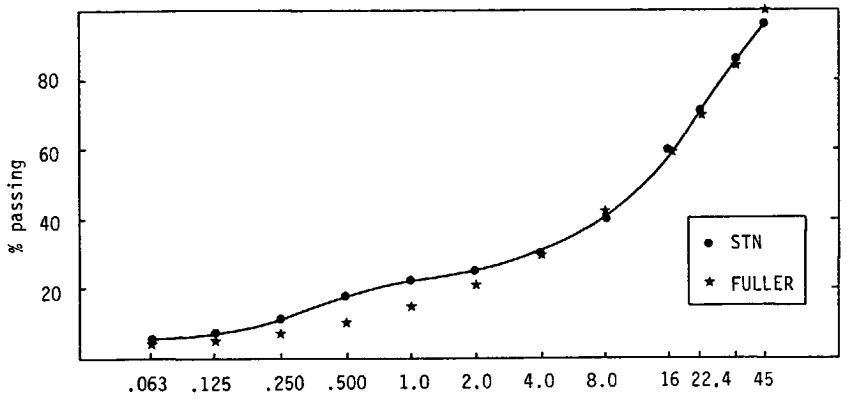

Figure 6.17: Particle size distribution of material STN and Fuller-curve.

Figure 6.17 shows the grading of material STN, together with the Fuller-curve calculated using Equation 6.2 with a maximum particle

diameter of d_{max} = 45 mm. As can be seen from Figure 6.17, the naturally occurring material STN has a grading almost in conformity with the Fuller curve. Figure 6.18 shows the gradings of materials POB and POO, again with the same Fuller-curve. Material POO has a grading on the Fuller-curve, since it was made to comply with the lower boundary of the Dutch specifications for a 0/40 mm granular base course material, which boundary is the Fuller-curve. Material POB was made in conformity with the upper boundary of the 0/40 mm specifications, which is well above the Fuller-curve.

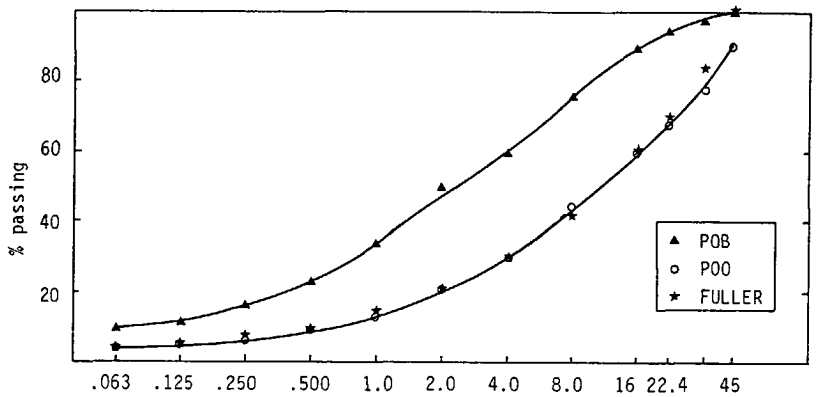

Figure 6.18: Particle size distribution of materials POB and POO and Fuller-curve.

Material STN was tested in the large 400 mm specimen diameter triaxial apparatus. The specimen built at optimum moisture content for the standard-package of resiliency testing (test STND 01, see Paragraph 5-.3.2.5) was dried after this testing by flushing air through the specimen. To do this, vacuum was applied to the top of the triaxial specimen and holes were punctured in the triaxial membrane at the bottom of the specimen. It took considerable time to reduce the moisture content of the large specimen in this way. Six weeks of flushing air were required to reduce the moisture content from the initial 4.9% down to 1.6%. To reduce the time required for drying when testing materials POB and POO, these materials were tested in the 150 mm specimen diameter triaxial apparatus discussed in Paragraph 5.5.3.2. Triaxial specimens were prepared for both materials at optimum moisture content, tested for resilient properties, dried by flushing air through the specimen and tested again.

Thanks to the use of a smaller specimen size, the time required for drying of the triaxial specimen was reduced to one week. As discussed in Paragraph 5.5.3.4, testing of a 0/40 mm graded material in a 150 mm specimen diameter triaxial apparatus may yield too high resilient moduli values, dependent on the packing arrangement of the coarse grains in the relatively small triaxial specimen. This was judged not to be a problem here, since the tests in the wet and the dry specimen condition were performed on the same specimen and only the shift in resilient modulus upon drying was of interest here, not the absolute value of it. Table 6.7 shows the triaxial specimen characteristics for the materials STN, POB and POO, for the "wet" and the "dry" specimen condition. As can be seen from Table 6.7, the degree of saturation S_r for the wet specimen condition is quite low for materials POB and POO, although the wet specimen condition corresponds to the optimum moisture content from the Proctor test. Evidently, the material porphyry is not capable of retaining much water.

Table 6.7: Triaxial specimen characteristics.

			wet		dry	
material code	test number	ρ_d [kg/m^3]	w [%]	S_r [%]	w [%]	S_r [%]
STN	STND 01	2121	4.9	67		
	STND 02	2121			1.6	22
POB	POBD 04	2072	4.5	42		
	POBD 05	2072			1.4	13
POO	POOD 02	2117	1.8	18		
	POOD 03	2117			0.7	7

Figure 6.19 shows the results of the resiliency testing of material STN in the wet and the dry specimen condition. As stated, the test in the wet specimen condition (test number STND 01) formed part of the standard resiliency testing program described in Paragraph 5.3.2.5.

For the test in the dry specimen condition (test number STND 02), the same stresses were used as for the wet specimen condition.

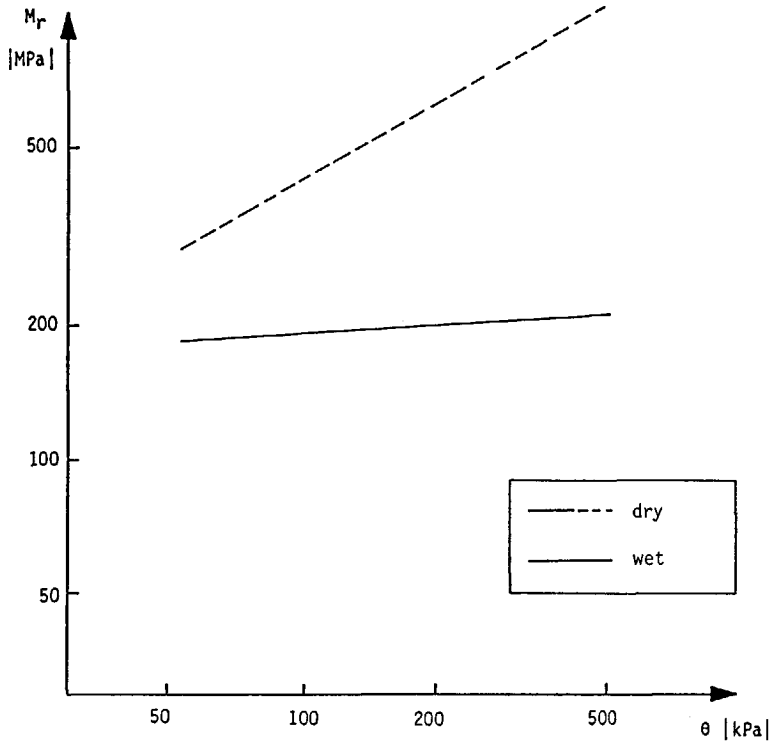

Figure 6.19: M_r-θ relationship for material stol (STN), for the wet and the dry specimen condition.

As can be seen from Figure 6.19, the gravel/loam mixture stol shows a considerable increase in resilient modulus upon drying of the material. Furthermore, the material shows more stress-dependency in the dry condition as compared to the wet condition.

Figures 6.20 and 6.21 show the M_r-θ plots obtained from the testing of materials POO and POB in the wet and the dry specimen condition. As noted, these materials were tested for practical reasons in the 150 mm specimen diameter triaxial apparatus. The stresses applied in the resiliency testing were equal to those applied in the standard resiliency testing with the 400 mm specimen diameter triaxial apparatus (see Table 5.3, Paragraph 5.3.2.5), with the exception that for practical reasons only one of the levels of the static deviator

stress σ_s was applied. By testing only at σ_s = 6 kPa, the number of tests to be performed reduced from 72 to 24 for each of the specimen conditions.

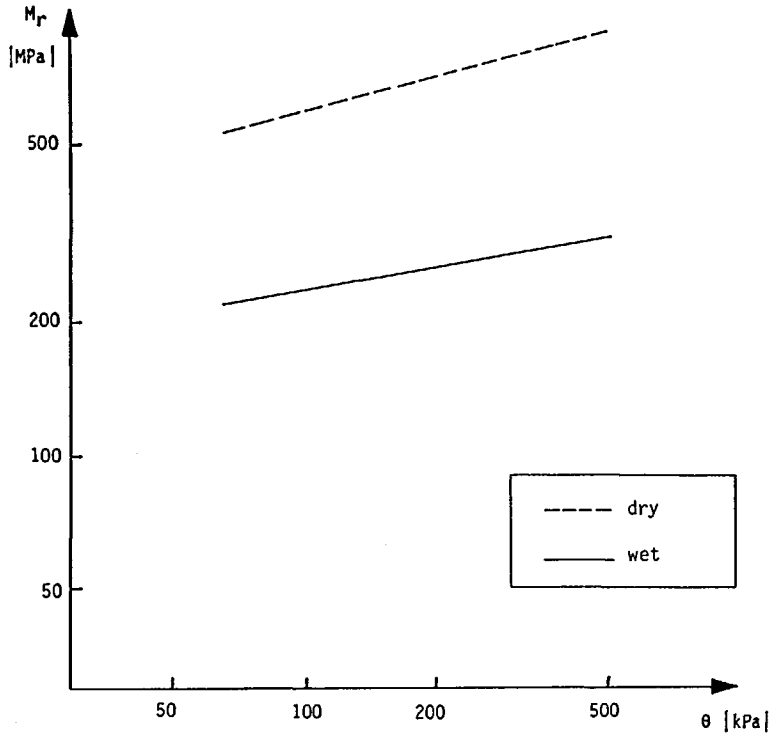

Figure 6.20: M_r-θ relationship for porphyry, fine grading (material code P0B), for the wet and the dry specimen condition.

The increase in resilient modulus upon drying as shown in Figures 6.20 and 6.21 is unexpectedly large. As can be seen from Figure 6.18, the material P00 has a grading in conformity with the Fuller curve. Assuming this crushed rock materials contains little or no clay, the suction in the material is caused by capillary effects only and should, therefore, be limited. The overall stiffness of the material should mainly originate from the Fuller-skeleton of coarse particles and be less dependent on suction. Yet, upon drying a substantial increase in material stiffness is observed for P00. Comparing the results of materials P00 and STN (Figure 6.21 and 6.19), it can be seen that the increase in stiffness of P00 upon drying is almost as large as that of STN. The two materials both have gradings along the Fuller curve, but STN contains clay in its fine fraction. From this,

STN could be expected to have a more suction-dependent stiffness, which is only partly reflected in the test results. Comparing the two porphyry-gradings (materials POB and POO, Figures 6.20 and 6.21), it can be observed that the fine grained material POB shows a larger increase in stiffness than does the coarse graded material POO. This result is consistent with expectation. Material POB has a grading which is considerably finer than the Fuller grading, therefore lacks sufficient coarse particles to form a true skeleton structure and, hence, the stiffness of the fine fraction controls the overall stiffness of the material. Since the stiffness of the fine fraction is dominated by suction, material POB should show a larger suction-dependency than material POO. The overall increase in stiffness of both materials POB and POO, however, remains unexpectedly large for a material considered to contain no clay.

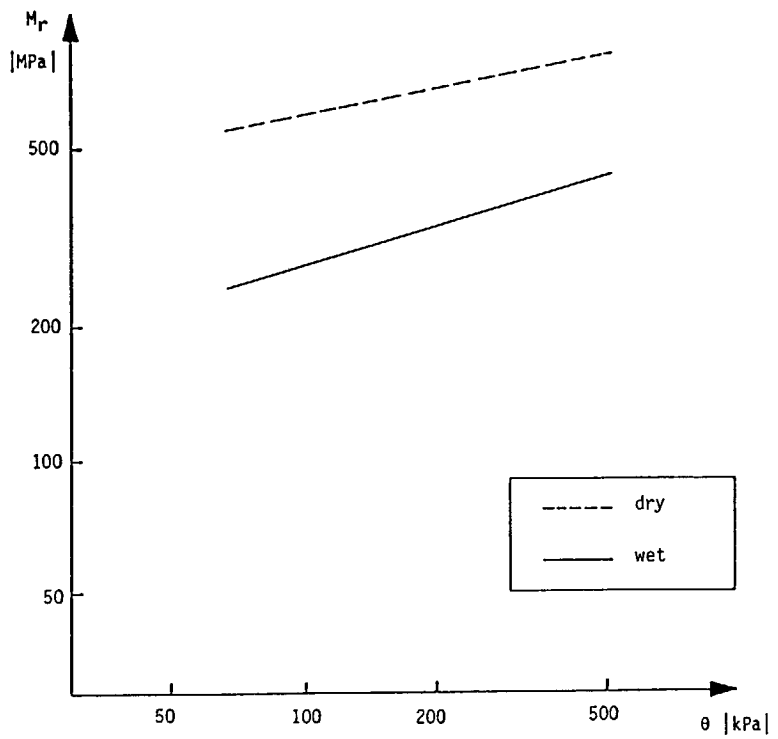

Figure 6.21: M_r-θ relationship for porphyry, coarse grading (material code POO), for the wet and the dry specimen condition.

6.5.3 Discussion

The results found in the suction-dependent stiffness testing for the porphyry were not in agreement with expectation. To further explore the suction-dependency of the stiffness of granular base course materials, Figures 6.22 and 6.23 show results taken from the limited literature available on the subject. Rada and Witczak [122, 123] developed typical M_r-θ relationships for a number of groups of unbound granular road base materials complying with the Maryland State Highway Authority (MSHA) specifications. Figure 6.22 shows their typical M_r-θ relationships for two types of limestone (denoted DGA-limestone-1 and DGA-limestone-2, DGA being short for Dense Graded Aggregate), while Figure 6.23 shows their M_r-θ relationship for a CR-6-crushed stone (CR being short for Crushed Rock).

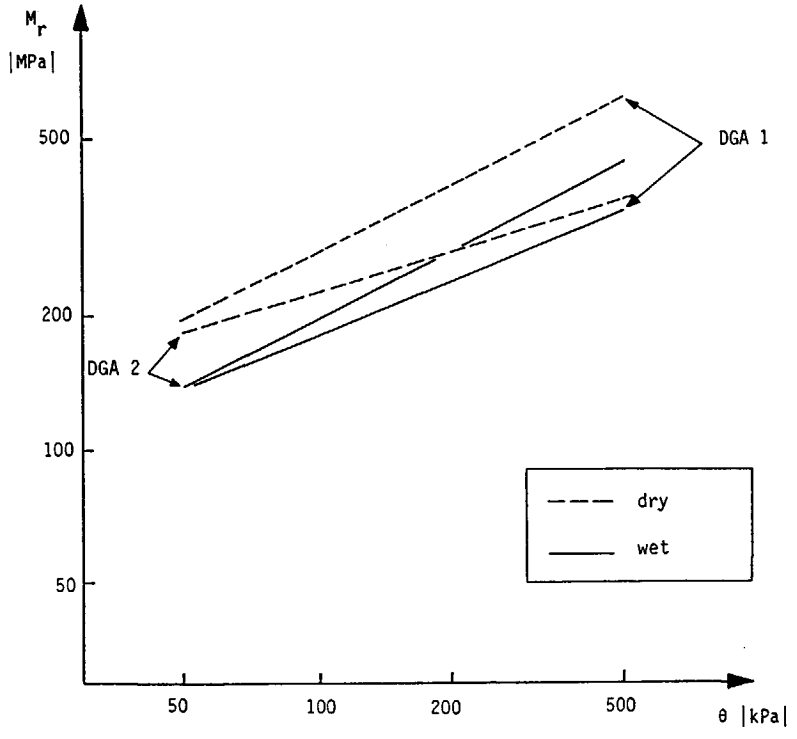

Figure 6.22: M_r-θ relationships for two types of limestone [124].

As can be seen from Figures 6.22 and 6.23, the results summarized by Rada and Witczak are not consistent. One material (DGA-limestone-1) shows a substantial increase in resilient modulus upon drying (as did

materials P0B and P00), while for the other two materials the resilient modulus is more or less constant upon drying of the material (as was the case for the sands discussed in Paragraph 6.4).

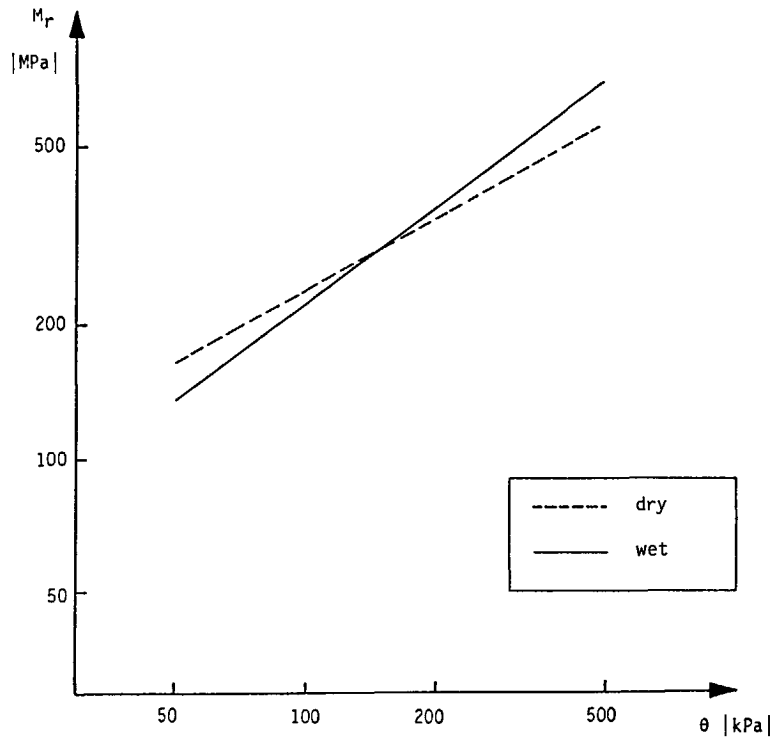

Figure 6.23: M_r-θ relationship for a crushed stone (124).

Based on the results found for the materials P0B and P00 and on the Rada and Witczak results for the DGA-limestone-1, the conclusion can be drawn that crushed stone materials can very well show a strong suction-dependency in their elastic stiffness. The cause of this dependency must lie in the nature of the fine fraction of the material. The Rada and Witczak paper does not go into detail on this. A closer examination of the porphyry tested here first of all learned that its fine fraction was a "rock-flower" rather than a sandy type of material. The pores in such a rock-flower can be expected to be substantially smaller than those in a sandy material, which would cause the capillary suction to be higher. Secondly, although the material porphyry was produced as a straightforward crushed rock, this does not necessarily mean that the material contains no clay. Dependent on the state of weathering of the bedrock material, a certain amount of clay

may be released upon crushing. Furthermore, the crushed material may have been contaminated with clay from the overburden in the quarry. A detailed investigation of the fraction 0-2 mm of the porphyry using the Methylene Blue Adsorption test indeed indicated clay to be present.

The overall conclusion of the suction-dependent stiffness determination of the granular base course materials is that the straightforward assumption that crushed rock materials do not show a strong suction-dependency is not valid. A close examination of the fine fraction of such crushed rock materials is required to assess the possibility of large changes in stiffness upon wetting and drying. Such an examination could be done using the Atterberg limits tests or the Methylene Blue Adsorbtion test. To limit suction-dependency, maximum Atterberg limits could be prescribed for the fine fraction of granular materials together with the grading specifications prescribing the amount of fine material. As discussed in Paragraph 2.3, the UK-specifications and the tropical Road Note 31 specifications do contain such limits for the plasticity of the fine fraction of granular base course materials.

6.6 CONCLUSION

This chapter has dealt with the suction-dependency of the stiffness of three groups of materials: laterites, sands and granular base course materials. The test results lead to the following conclusions:

1. Some of the laterites tested showed a distinct suction-dependent behaviour, whereas the other laterites showed little change in elastic stiffness with changes in the moisture content. The behaviour of the laterites could be clearly traced back to their grading and composition. The materials containing a surplus of fines and, therefore, having a structure of a matrix of fines with coarse particles floating in it were shown to have a suction-dependent stiffness. The laterites with a grading close to the Fuller-curve and thus consisting of a skeleton of coarse particles

were shown to be far less suction-dependent with respect to their stiffness.

2. Three sands were tested for suction-dependent stiffness, representing the three sub-groups of the sands of Group S (very coarse sands, fine sands and extremely fine sands). Comparing the grading of the sands tested to the Fuller curve, all three were shown to have a skeleton-type of structure, the stiffness of which is mainly derived from the skeleton itself. The behaviour of the sands upon changes in the water content was consistent with the skeleton-type of structure. Little increase in resilient stiffness was observed upon drying of the triaxial specimens.

3. Two granular materials were tested for suction-dependent stiffness. One of these two materials was known to contain clay (the gravel/loam mixture stol STN), whereas the other material was a straightforward crushed rock (the porphyry PO). The latter material was tested at two gradings (material codes POO and POB). The elastic stiffness of material STN containing clay showed the expected dependency on suction. Surprisingly, the crushed rock materials POO and POB too showed a marked suction-dependent stiffness. The stiffness of the fine grained POB was shown to be more dependent on suction than that of the coarse graded POO, which is consistent with expectation. Analysis of the fine fraction of the porphyry showed it to contain clay, which explains for the suction dependency.

4. Ideally, granular materials should be tested for resilient properties at various suction levels to establish their stiffness-suction relationship. Such testing is, however, very cumbersome indeed. For design purposes, therefore, granular materials should be tested for resilient properties in cyclic load triaxial tests at the highest moisture content likely to occur in the particular layer.

5. If proper drainage is provided to the granular base, the optimum moisture content from the modified Proctor test appears to be a reasonable estimate of that highest in-situ moisture content. For the bulk of the granular materials tested here, the optimum moisture content was obtained from the Proctor tests at that moisture

content above which water was expelled from the Proctor specimen. Compaction of the 400 mm diameter triaxial specimens too proved the optimum moisture content to be very close to the maximum moisture content of the materials at hand under conditions of free drainage, since often some water was expelled from the specimen under compaction.

6. Testing of granular materials at optimum moisture content and using the values obtained for design, however, does imply that free drainage should indeed be provided in the pavement structure. The practice of using thick draining sub-bases of sands in the Netherlands is a good example of paying proper attention to drainage of the granular base. If such drainage is neglected, however, serious problems may occur when the base becomes saturated by water travelling downward or upward through the pavement structure.

7. The finding that straightforward crushed rock materials may show a marked suction-dependent stiffness due to the nature of their fine fraction indicates the necessity of checking that fine fraction for its composition. Maximum values for the Atterberg limits or for the results of the Methylene Blue Adsorption test should be set in the material specifications.

7. MODELLING OF MATERIAL STIFFNESS FOR PAVEMENT DESIGN

7.1 INTRODUCTION

Chapter 5 of this dissertation has dealt extensively with laboratory testing of unbound granular materials. The major part of the testing described in Chapter 5 involved determination of the resilient and permanent strain properties of a wide range of materials as a function of the applied stresses. The results of the testing were presented in Chapter 5 in the simplest form. The resilient strain properties were expressed in the stress dependent resilient modulus M_r, while permanent strain properties were presented in graphs plotting permanent axial strain as a function of the number of load applications and the applied ratio of cyclic deviator stress to confining stress.

The way in which resilient and permanent strain properties of unbound granular materials were presented in Chapter 5 has become the standard way in pavement engineering. The main advantage of this approach lies in its simplicity. The resilient modulus M_r is regarded by practicing engineers as the stress-dependent equivalent of Young's E-modulus, expressed in well-known units as MPa or N/mm^2. Straightforward plots of permanent strain versus number of load applications too can be easily understood in practice.

This simplest form of presenting resilient and permanent strain properties of granular materials, however, has major drawbacks. The stress-dependent resilient modulus M_r is mostly used together with a constant value of Poisson's ratio ν. In doing so, the stress-dependent nature of Poisson's ratio for granular materials is ignored and, in fact, half of the information obtained from the cyclic load triaxial test is not used. For permanent strains the situation is the same: only the axial deformation of the triaxial specimen is used for analysis. The data obtained from the test on radial deformation and hence on specimen volume change is set aside.

The shortcomings of this approach will be discussed in detail in this chapter and improvements in modelling of material stiffness will be

dealt with. Over the years, a vast number of constitutive relationships relating strain to stress for granular materials has been developed, the majority of the relationships dealing with resilient strains. The applicability of a selection of these material models will be investigated in this chapter, using cyclic load triaxial test data for one granular base course material and one sand to visualize the ability of the model at hand to predict the actually measured specimen deformations. For reasons given later, no attempt will be made to develop yet another material model. Resilient and permanent strains will be dealt with separately in Paragraph 7.2 and 7.3, respectively.

Before dealing with the various material models, one point should be clearly stressed here. The material properties dealt with in this chapter were determined in the laboratory on specimens of the investigated material by itself, isolated from the other materials in the pavement. The properties given are therefore truly material properties, pertaining only to the particular material. The material parameters discussed here are therefore quite distinct from the "structure parameters" dealt with in Chapter 8. These structure parameters were obtained from in-situ testing and, therefore, from testing of a combination of materials in layers of different thicknesses. Parameters pertaining to individual materials can from such in-situ testing of completed pavement constructions only be obtained by back-analysing the behaviour of the pavement structure. Falling Weight Deflectometer measurements, for instance, determine the response of a complete pavement structure to external loading. The parameters obtained for the various pavement materials from a back-analysis of the measured response are structure parameters, pertaining to the behaviour of the material at hand in the combination of materials and layer thicknesses that constitutes the particular pavement. These structure parameters cannot without further preface be used to design a completely different combination of materials and layer thicknesses.

To link the material parameters determined in the laboratory on isolated materials to structure parameters as measured on complete pavement structures a mechanical/mathematical pavement model is required that can accurately calculate stresses and strains in pavement

structures. Where unbound granular materials with their stress-dependent stiffness are concerned, the linear elastic pavement models used today cannot do so. Finite element pavement models that are presently being developed can make an accurate calculation of stresses and strains in a pavement structure, but they are far from implemented in every day practice of pavement design and evaluation.

The use of finite element pavement models involves the prerequisite of a material model that accurately links material deformations to the applied stresses. As will be discussed in this chapter, some of the material models presently available are truly elastic, but do not accurately predict material deformations. The remainder of the models available are mere curve-fitting models that do accurately predict material deformations as a function of applied stresses, but are not elastic and may therefore involve problems on implementation in finite element computer programs based on elasticity.

7.2 RESILIENT DEFORMATION

7.2.1 Introduction

The simplest form of modelling resilient deformations of unbound granular materials as measured in cyclic load triaxial tests is in terms of as-applied stresses and as-measured strains. To the triaxial specimen, axial and radial stresses are applied, which by nature of the test are also the principal stresses. Axial and radial strains are measured, which again are principal strains. The classical and still most widely used material models interpret material behaviour in terms of these axial and radial stresses and strains.

The model most widely used for resilient deformations of unbound granular materials is the so-called K-θ model, which expresses the resilient modulus M_r as a function of the sum of principal stresses θ. The resilient modulus M_r is simply the ratio of the applied cyclic axial deviator stress over the resulting axial resilient deformation. To deal with radial deformations, the K-θ model is often used in conjunction with a constant value of Poisson's ratio ν, being the ratio

of resilient radial strain over axial resilient strain. For granular materials, the constant value of Poisson's ratio is usually taken at $\nu = 0.35$. The accuracy of the K-θ model in conjunction with a constant Poisson's ratio will be discussed in Paragraph 7.2.2.

The ratio of radial to axial strains for granular materials is not constant. At high ratios of axial over radial stress granular materials often exhibit dilation, which means that the volume of the triaxial specimen increases under the application of the compressive stresses. In terms of Poisson's ratio, dilation leads to values of $\nu > 0.5$. At lower ratios of axial to radial stress dilation does not occur, hence $\nu < 0.5$. In all, the ratio of radial to axial strain for granular materials is clearly dependent on the ratio of axial to radial stress. Paragraph 7.2.3 will discuss the accuracy of a material model incorporating a stress-ratio dependent ν, in conjunction with the K-θ model.

As discussed in Paragraph 2.7, a better description of the mechanical behaviour of granular materials can be obtained by separating stresses and strains into volumetric and shear components. The theoretical background of this approach has been described in Paragraph 2.7.4. For convenience, the main relationships pertaining to triaxial conditions will be repeated here. The volumetric component p and shear component q of the applied stresses and the volumetric component ε_v and shear component ε_s of the resulting strains can be obtained from the principal stresses and strains using:

$$p = \frac{1}{3}(\sigma_1 + 2\sigma_3) \tag{7.1}$$

$$q = \sigma_1 - \sigma_3 \tag{7.2}$$

$$\varepsilon_v = \varepsilon_1 + 2\,\varepsilon_3 \tag{7.3}$$

$$\varepsilon_s = \frac{2}{3}(\varepsilon_1 - \varepsilon_3) \tag{7.4}$$

The so-called "G-K model" developed by Boyce to describe resilient deformations of granular materials (see Paragraph 2.7.5) uses this approach of separating volumetric and shear components of stress and strain. The accuracy of this model will be discussed in Paragraph 7-.2.5. The advantage of Boyce's model is that it is purely elastic,

since it meets the first law of thermodynamics. However, as will be shown in Paragraph 7.2.5, the model results in a poor fit between the volumetric strains predicted by the model and the measured values.

A far better fit between model-predicted and measured values of volumetric strains can be obtained using a kind of curve-fitting approach, as is done in the contour-model developed at Nottingham University (see Paragraph 2.7.6). The equations used in this model are quite similar to the ones from Boyce's model. The inclusion of extra parameters on the one hand leads to a better agreement between model-predicted and measured values of strain, but on the other hand the model then no longer meets the strict requirements set by thermodynamics for the elastic behaviour of granular materials. Paragraph 7.2.6 will deal with the advantages and shortcomings of the curve-fitting type of approach.

The accuracy of the various models mentioned above will be illustrated in this chapter by plotting the model-predicted values of the volumetric and shear components of strain versus the measured values. This comparison will be made for one granular base course material (BGO: crushed concrete 1, coarse grading) and one sand (OSN: Eastern Scheldt sand).

7.2.2 The K-θ model with constant ν

Figures 7.1 and 7.2 show plots of the resilient modulus M_r versus the sum of principal stresses θ for the materials BGO (crushed concrete 1, coarse grading) and OSN (Eastern Scheldt sand). The parameters K_1 and K_2 from the K-θ model are given in the figures, together with the correlation coefficient r. As can be seen from the figures and from the value of the correlation coefficient, the K-θ model provides an almost perfect fit between the measured value of M_r and its model-predicted value. In other words, the axial resilient strain of the triaxial specimen is modelled with great accuracy by the K-θ model and the search for more accurate models to predict axial resilient strains is of little use.

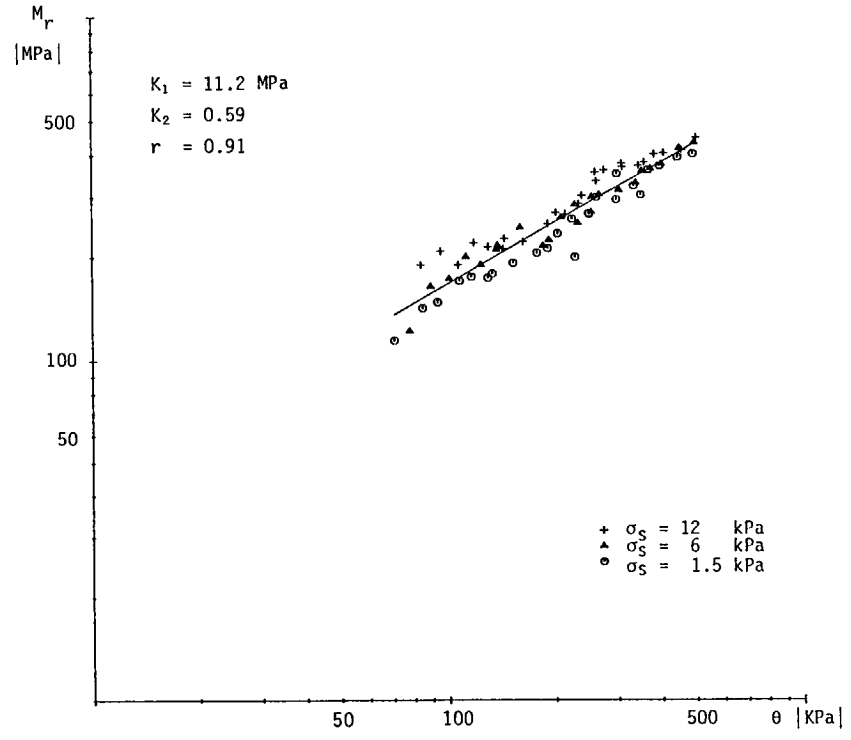

Figure 7.1: Resilient modulus M_r versus sum of principal stresses θ, for material BGO.

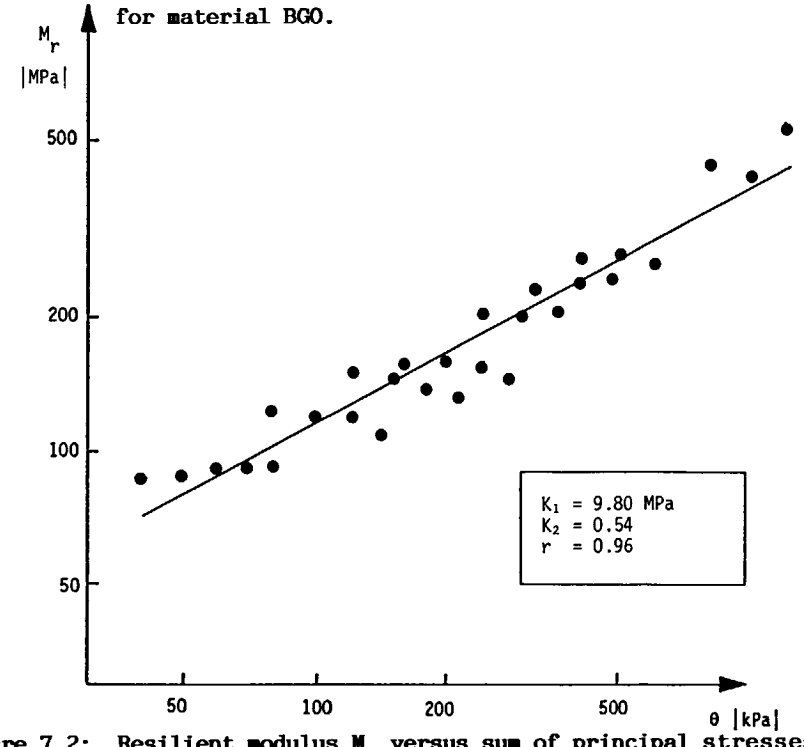

Figure 7.2: Resilient modulus M_r versus sum of principal stresses θ, for material OSN.

The accurate K-θ model for axial resilient strains of the triaxial specimen is often used in conjunction with quite a crude approach to modelling radial resilient strains. The ratio of radial to axial strains expressed in Poisson's ratio ν is often taken as a constant, thereby ignoring the dependency of ν on the stress ratio σ_c/σ_3. To illustrate the inadequacy of this approach, Figures 7.3 and 7.4 show plots of model predicted versus measured values of the volumetric and shear components of the strains obtained from the cyclic load triaxial testing of material BGO, using ν = 0.35.

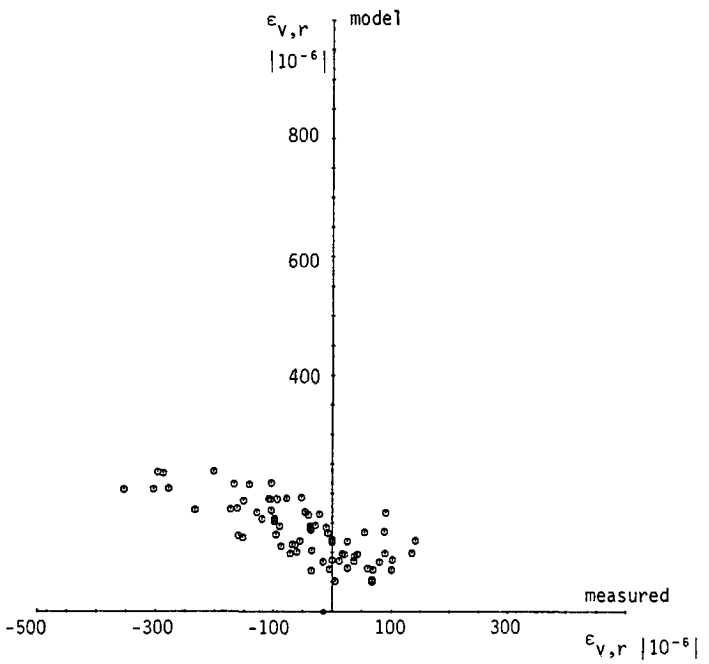

Figure 7.3: Model-predicted versus measured values of volumetric strain for material BGO (K-θ model with constant ν).

As can be seen from Figure 7.3, the approach of modelling the resilient deformations using the K-θ model in conjunction with a constant value of Poisson's ratio is quite inadequate with respect to the volumetric component of strain. In the cyclic load triaxial tests on material BGO, positive volumetric strains (indicating specimen compression) were measured at low ratios of cyclic deviator stress over confining stress, whereas negative volumetric strains (indicating specimen dilation) were measured at higher stress ratios. Clearly, the use of a constant Poisson's ratio cannot deal with these test results.

For $\nu < 0.5$, the model only predicts specimen compression ($\varepsilon_{v,r} > 0$) and for $\nu > 0.5$ only specimen dilation ($\varepsilon_{v,r} < 0$) is obtained from the model, irrespective of the stress ratio applied.

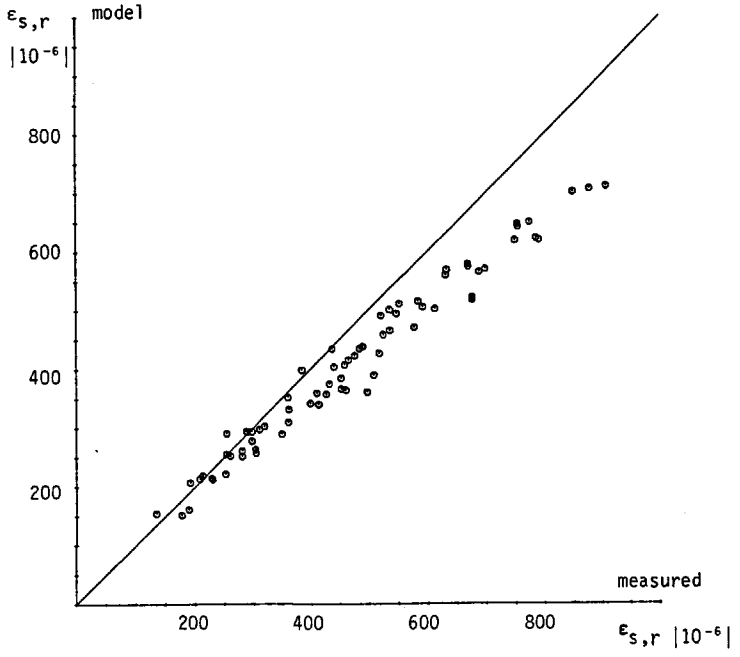

Figure 7.4: Model-predicted versus measured values of shear strain for material BGO (K-θ model with constant ν).

Looking at the shear component of strain (Figure 7.4), the agreement between model predicted and measured values of resilient strains is far better. The data points, each representing a cyclic load triaxial test at a given combination of stresses, plot quite closely to the 45° line of equality in Figure 7.4. Hence, for the material BGO discussed here, even the crude approach of using the K-θ model in conjunction with a constant value of Poisson's ratio is quite adequate to predict specimen shear strains.

Figures 7.5 and 7.6 show plots of model-predicted versus measured values of volumetric and shear strains respectively for the material Eastern Scheldt sand (OSN). Again, large deviations in volumetric strain are found, whereas the deviations in shear strain are much smaller. The difference in performance of the K-θ model with constant ν in predicting volumetric strains on the one hand and shear strains on the other can be explained by looking at Equations 7.3 and 7.4.

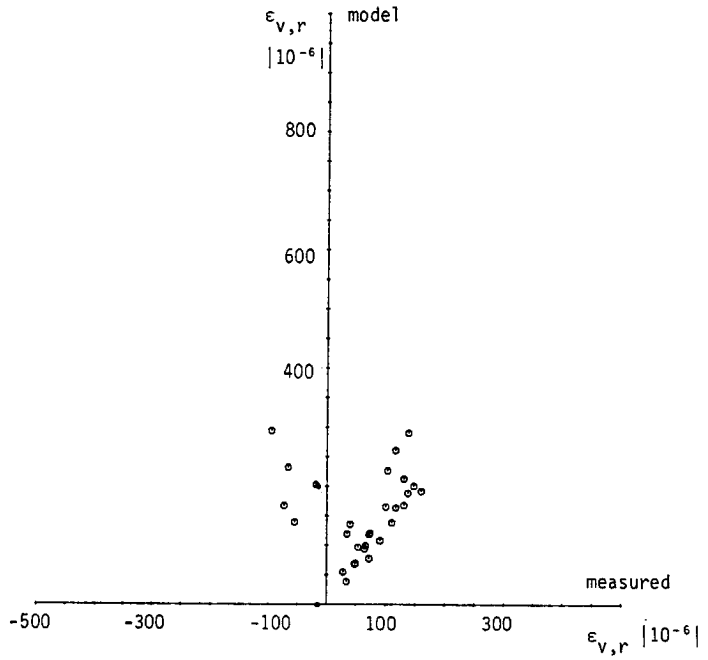

Figure 7.5: Model-predicted versus measured values of volumetric strain for material OSN (K-θ model with constant ν).

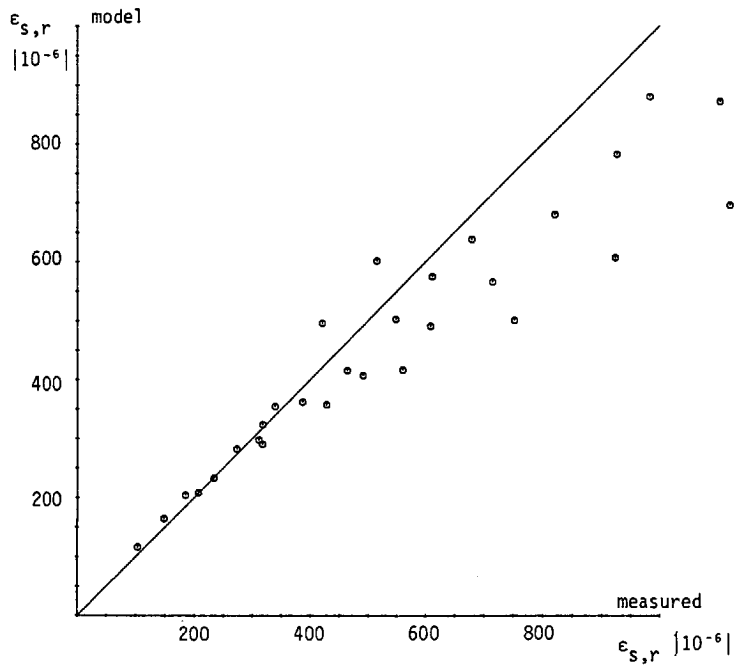

Figure 7.6: Model-predicted versus measured values of shear strain for material OSN (K-θ model with constant ν).

The volumetric component of strain is calculated from axial and radial resilient strains according to $\varepsilon_v = \varepsilon_{a,r} + 2\,\varepsilon_{r,r}$, whereas the shear component of strain is calculated from $\varepsilon_s = \frac{2}{3}(\varepsilon_{a,r} - \varepsilon_{r,r})$. As shown in Figures 7.1 and 7.2, the resilient modulus M_r and, hence, the resilient strain $\varepsilon_{a,r}$ ($= \varepsilon_1$) is predicted with great accuracy by the K-θ model. The poor performance of the K-θ model with constant ν stems from the inadequate approach of modelling the radial resilient deformation of the triaxial specimen. In fact, the data obtained on this parameter from the triaxial test is not used at all. Taking Poisson's ratio at a constant value of for instance $\nu = 0.35$ clearly ignores the stress-dependent nature of the radial deformations, and thus leads to a very poor prediction of the radial resilient strain $\varepsilon_{r,r}$ ($= \varepsilon_3$). Since this strain contributes more to the volumetric strain than it does to the shear strain, the assumption of a constant ν leads to larger deviations in model-predicted values of volumetric strain than of shear strain.

7.2.3 The K-θ model with variable ν

The main drawback of the model discussed in the previous paragraph is its poor prediction of radial resilient strain and, hence, of volumetric strain. From cyclic load triaxial tests on unbound granular materials the dependency of ν on the ratio of cyclic deviator stress over confining stress is obvious. Figures 7.7 and 7.8 show plots of Poisson's ratio ν versus stress ratio σ_c/σ_3 for the materials BG0 and OSN, respectively. Different symbols are used to check the influence of the various levels of the confining stress σ_3.

The increase of Poisson's ratio ν with stress ratio σ_c/σ_3 is clear from both figures. The material crushed concrete BG0 moves from compression ($\nu < 0.5$) for low stress ratios to dilation ($\nu > 0.5$) at higher stress ratios, reaching a maximum Poisson's ratio of $\nu = 0.78$. For Eastern Scheldt sand OSN the increase of ν with σ_c/σ_3 is somewhat less pronounced; the maximum value of ν attained for this material is $\nu = 0.54$. The straight lines through the data points of Figure 7.7 and 7.8 were drawn using linear regression. The equations obtained are:

for material BG0: $\nu = 0.28 + 0.06\,(\sigma_c/\sigma_3)$ $\quad r = 0.91$ (7.5)

for material OSN: $\nu = 0.33 + 0.04\,(\sigma_c/\sigma_3)$ $\quad r = 0.79$ (7.6)

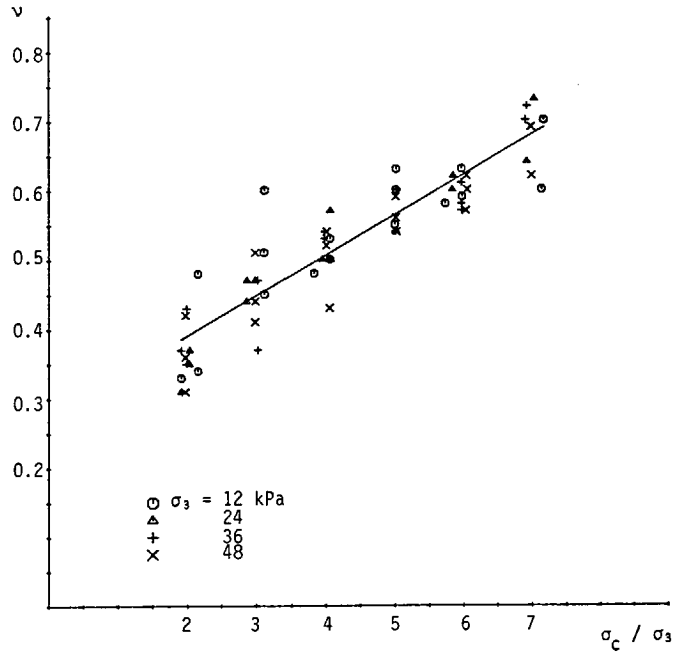

Figure 7.7: Poisson's ratio ν versus ratio of cyclic deviator stress over confining stress σ_c/σ_3, for material BGO.

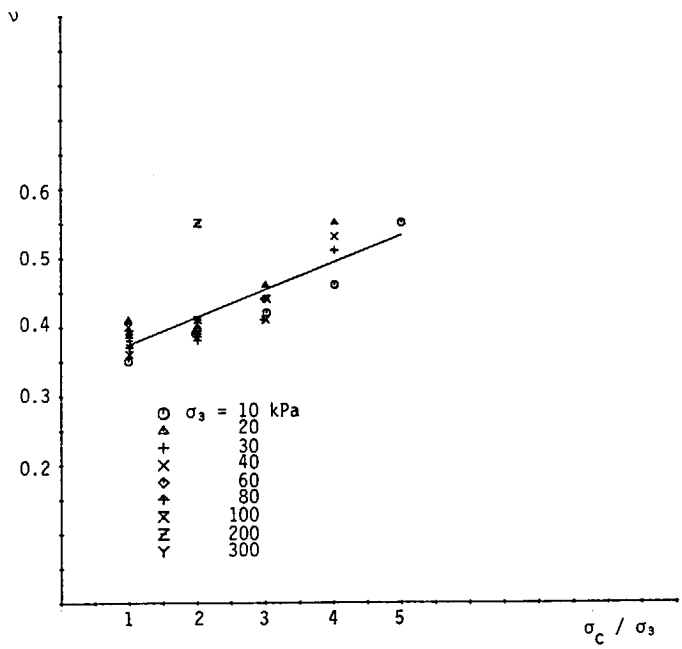

Figure 7.8: Poisson's ratio ν versus ratio of cyclic deviator stress over confining stress σ_c/σ_3, for material OSN.

From Figures 7.7 and 7.8 no separate influence of the confining stress σ_3 by itself is recognizable. Hence, no attempt was made to further increase the correlation coefficient r of Equations 7.5 and 7.6 by adding σ_3 as a separate entry into the equations. Using Equations 7.5 and 7.6 to estimate Poisson's ratio ν for materials BGO and OSN respectively in conjunction with the K-θ model for these materials, an improved prediction of volumetric and shear strain can be obtained. Figures 7.9 and 7.10 show plots of the volumetric and shear strain, respectively, predicted by such a combined model versus the measured values of volumetric and shear strain, for material BGO.

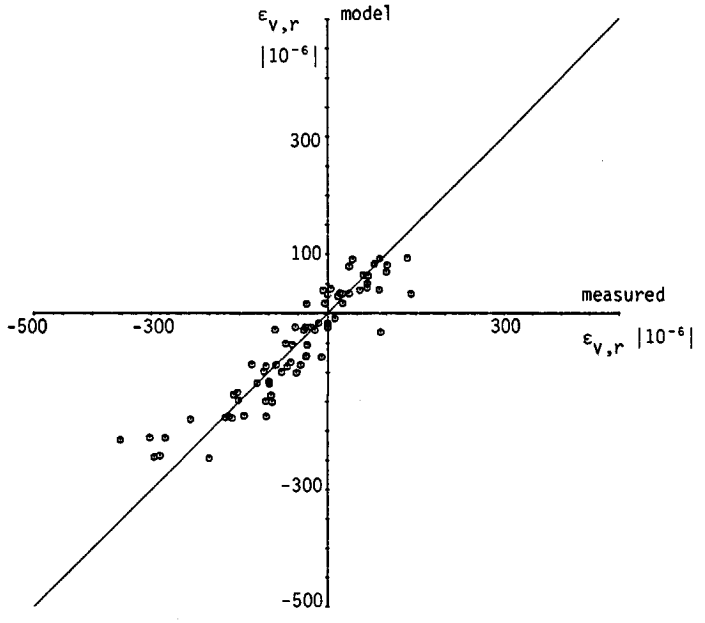

Figure 7.9: Model-predicted versus measured values of volumetric strain for material BGO (K-θ model with variable ν).

Comparing Figure 7.9 (K-θ model with variable ν) to Figure 7.3 (K-θ model with constant ν), the gain in agreement between model predicted and measured values of volumetric strain thanks to inclusion of a stress dependent ν is obvious. Although still some scatter of data points around the 45° line of equality occurs, the K-θ model with stress dependent ν is capable of describing accurately the effects of specimen compression and dilation that occurred in the cyclic load triaxial testing of the coarse graded material BGO. The prediction of shear strain by the K-θ model with variable ν (Figure 7.10) is also

improved relative to the K-θ model with constant ν (Figure 7.4). Starting from the already good performance of the K-θ model with constant ν the gain in accuracy is, however, relatively small.

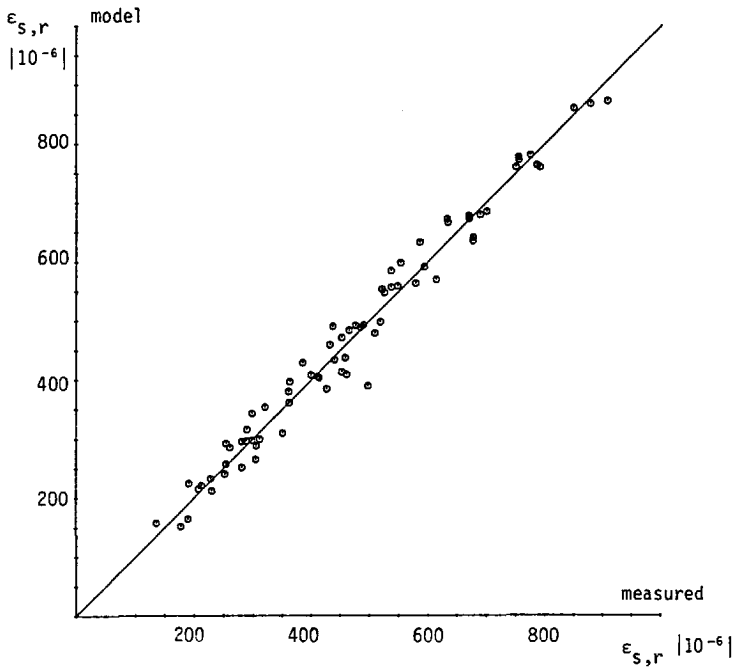

Figure 7.10: Model-predicted versus measured values of shear strain for material BGO (K-θ model with variable n).

Figures 7.11 and 7.12 show plots of volumetric and shear strain respectively as predicted by the K-θ model with variable ν versus the measured values of volumetric and shear strain for Eastern Scheldt sand OSN. Comparing Figures 7.11 and 7.12 to 7.5 and 7.6, again a better performance of the K-θ model with variable ν is observed. The gain in accuracy thanks to introduction of the stress-dependent ν is, however, limited simply because of the limited variation in Poisson's ratio as measured in the cyclic load triaxial testing of material OSN (see Figure 7.8). In fact, for the maximum stress ratio of $\sigma_c/\sigma_3 = 5$ applied in testing of OSN (see Paragraph 5.3.3.5), Equation 7.6 predicts a maximum value of $\nu = 0.496$. Hence, no dilation is predicted by the K-θ model with variable ν for material OSN.

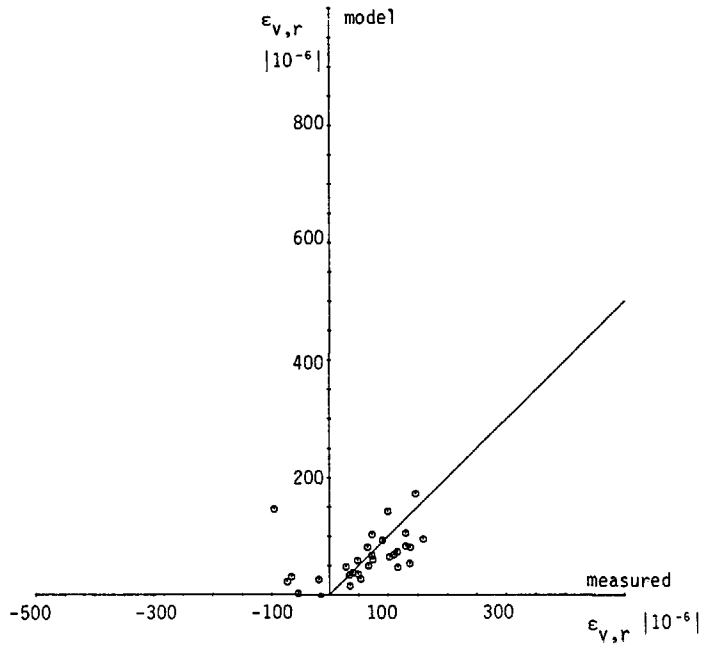

Figure 7.11: Model-predicted versus measured values of volumetric strain for material OSN (K-θ model with variable ν).

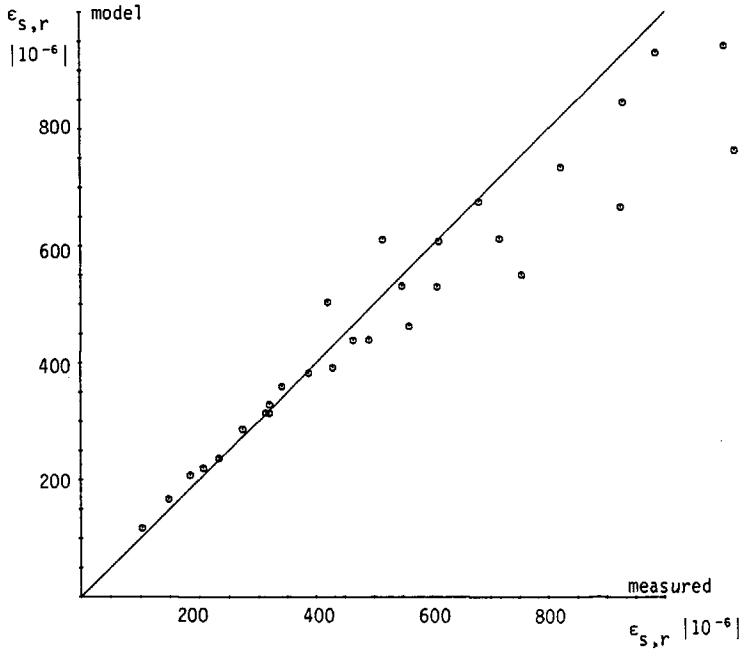

Figure 7.12: Model-predicted versus measured values of shear strain for material OSN (K-θ model with variable ν).

7.2.4 Theoretical considerations

7.2.4.1 HOOKE'S LAW

Hooke's law describes the linear relationship between stress and strain for a uniaxial stress condition (see Figure 7.13) as:

$$\varepsilon_z = \frac{\sigma_z}{E} \tag{7.7}$$

where:

ε_z = strain in z-direction
σ_z = stress in z-direction
E = Young's modulus

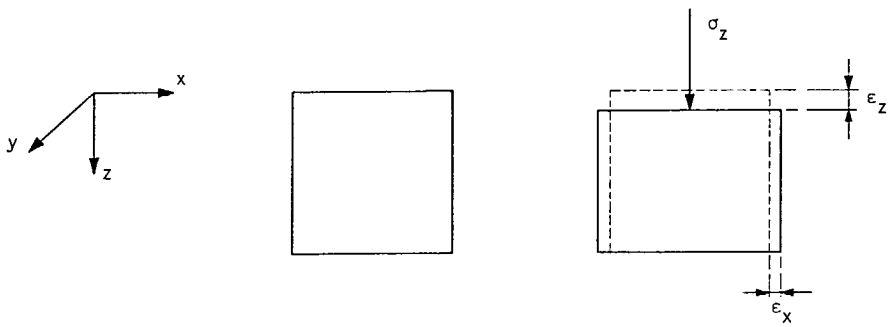

Figure 7.13: Uniaxial stress condition Hooke's law.

The compression in z-direction is accompanied by expansions in x- and y-directions according to:

$$\varepsilon_x = - \nu \cdot \varepsilon_z \tag{7.8}$$

$$\varepsilon_y = - \nu \cdot \varepsilon_z \tag{7.9}$$

Cyclic load triaxial tests with constant confining pressure (CCP-tests) are usually interpreted using Equations 7.7 and 7.8/7.9, with adaptations for the subscripts, the axisymetric condition and the

sign-convention of compressive stresses being positive (see Figure 7-.14). The equations used are:

$$\varepsilon_{a,r} = \frac{\sigma_{a,c}}{M_r} \tag{7.10}$$

$$\varepsilon_{r,r} = - \nu \cdot \varepsilon_{a,r} \tag{7.11}$$

where

$\varepsilon_{a,r}$ = axial resilient strain
$\varepsilon_{r,r}$ = radial resilient strain
$\sigma_{a,c}$ = axial cyclic stress
M_r = resilient modulus
ν = Poisson's ratio

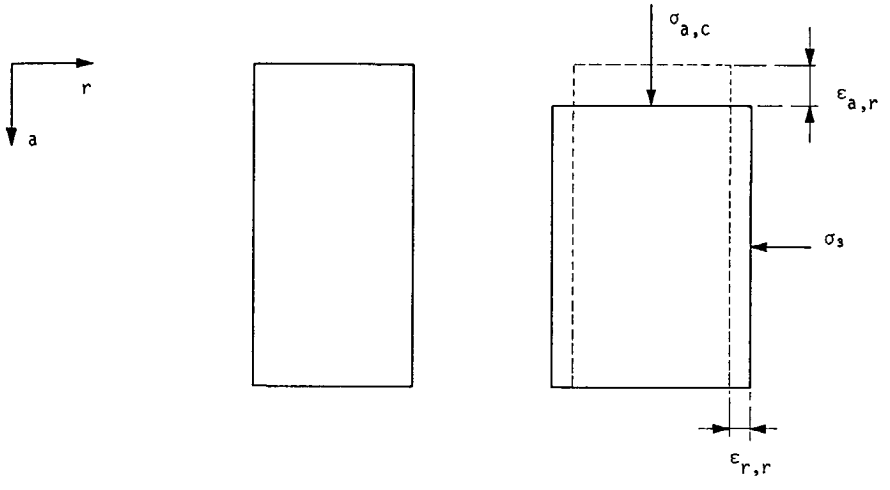

Figure 7.14: Stress condition cyclic load triaxial test.

Clearly, the stress condition of the specimen in the cyclic load triaxial test is not a uniaxial one. In addition to the major principal stress σ_1, also the minor principal stresses $\sigma_2 = \sigma_3$ act on the triaxial specimen. Hence, the major principal strain ε_1 is for the triaxial case smaller than for the uniaxial case assumed in Hooke's law, as depicted in Figure 7.13. Thus, at first glance, the use of

Equations 7.10 and 7.11 to interpret cyclic load triaxial test results is not correct.

Hooke's law for the uniaxial case (Equation 7.7) can be expanded to cope with a triaxial stress condition where normal stresses act in x, y and z direction by superposing the strains obtained from Equations 7.7 through 7.9. One then obtains the "generalized Hooke's law":

$$\varepsilon_x = \frac{1}{E} \{\sigma_x - \nu(\sigma_y + \sigma_z)\} \tag{7.12}$$

$$\varepsilon_y = \frac{1}{E} \{\sigma_y - \nu(\sigma_x + \sigma_z)\} \tag{7.13}$$

$$\varepsilon_z = \frac{1}{E} \{\sigma_z - \nu(\sigma_x + \sigma_y)\} \tag{7.14}$$

where

σ_x, σ_y, σ_z = normal stresses
ε_x, ε_y, ε_z = normal strains

For the axisymetric stress condition of the cyclic load triaxial test, stresses and strains in x- and y-direction are equal and Equations 7-.12 through 7.14 reduce to:

$$\varepsilon_1 = \frac{1}{E} \{\sigma_1 - 2\nu\sigma_3\} \tag{7.15}$$

$$\varepsilon_3 = \frac{1}{E} \{-\nu\sigma_1 + (1-\nu)\sigma_3\} \tag{7.16}$$

These are the equations that should be used to interpreted cyclic load triaxial test results. As can be seen from Equations 7.15 and 7.16, the confining stress σ_3 reduces the major principal strain ε_1 and increases (makes it a smaller negative number) the minor principal strain ε_3. As can be seen from Equations 7.10 and 7.11, the usual interpretation of cyclic load triaxial test results seems to ignore the action of σ_3: this parameter does not occur in these equations. Once again, the use of Equations 7.10 and 7.11 to interpret the cyclic load triaxial test results looks at first glance incorrect.

The case of the constant confining pressure cyclic load triaxial test (CCP-test), however, is a special one. The triaxial specimen is built and subsequently the confining stress σ_3 is applied. The strains

caused by this all-around confining stress are completely ignored; σ_3 is in fact no more than a boundary condition applied before the actual cyclic load testing. On application of the cyclic deviator stress, only the strains caused by this stress are measured and only this strain is used for further analysis. Hence, the cyclic stress condition in the CCP-test can be considered to be a uniaxial one, beit with a boundary condition of a constant σ_3. Hence, application of Equations 7.10 and 7.11 to determine E and ν from the major and minor principal strains measured in the CCP-test is allowed. It should, however, be well noted that the values of E and ν obtained are so-called "chord" values: they refer to the stress/strain behaviour of the material in the transition from one particular state of stress to another. Figure 7.15 graphically shows the meaning of the word "chord" and its complementary concept "secant" for a general stress - strain relationship.

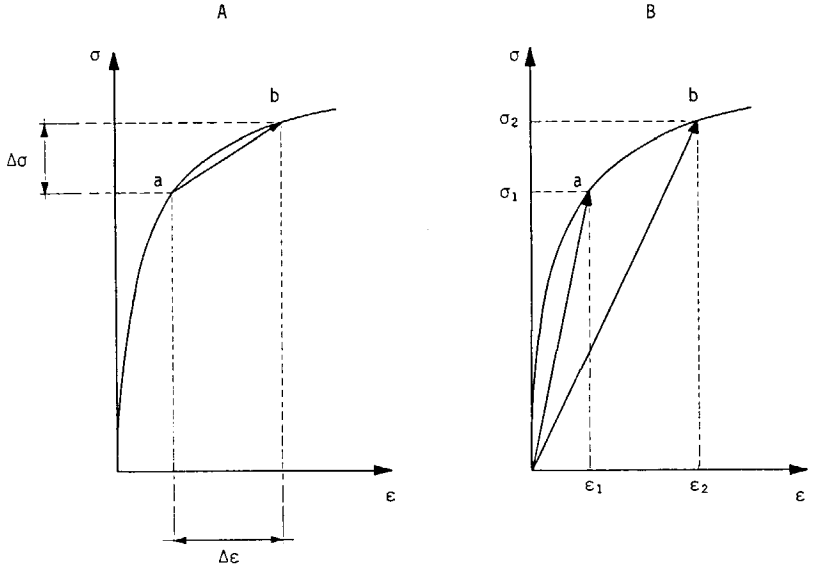

Figure 7.15: Definition of chord and secant approach to stress/strain relationships.
A: Chord approach. B: Secant approach.

In the chord approach of relating strain to stress (Figure 7.15A) the chord E-modulus is calculated directly from the increments of stress $\Delta\sigma$ and strain $\Delta\varepsilon$ according to:

$$E_{chord} = \frac{\Delta\sigma}{\Delta\varepsilon} \tag{7.17}$$

In the secant approach, two separate moduli for the points a and b on the stress-strain curve are determined:

$$E_{secans,\ a} = \frac{\sigma_1}{\varepsilon_1} \tag{7.18}$$

$$E_{secans,\ b} = \frac{\sigma_2}{\varepsilon_2} \tag{7.19}$$

The increment in strain due to transition in stress from point a to b can then in later analysis be calculated as the difference in strain in points A and B:

$$\Delta\varepsilon = \varepsilon_2 - \varepsilon_1 = \frac{\sigma_2}{E_{secans,\ b}} - \frac{\sigma_1}{E_{secans,\ a}} \tag{7.20}$$

Obviously, in the linear-elastic case of having a constant E modulus over the whole stress range, the two approaches give the same result. However, since unbound granular materials certainly do not have a constant E-modulus, a clear distinction between a chord and a secant approach should be made.

As stated, the resilient modulus and Poisson's ratio determined in CCP cyclic load triaxial tests using the standard approach of Equations 7-.10 and 7.11 yields chord values for both parameters. To cope with stress dependency, the values of M_r and ν are related to the peak stresses in the particular test. The resilient modulus M_r is expressed as a function of the sum of principal stresses θ, including the cyclic deviator stress. Poisson's ratio ν is either taken constant (Paragraph 7.2.2) or expressed as a function of cyclic deviator stress over confining stress σ_c/σ_3 (Paragraph 7.2.3).

Since the resilient modulus M_r and Poisson's ratio ν are determined in CCP cyclic load triaxial tests as chord values, they can indeed be

calculated using the simple approach of Equations 7.10 and 7.11. Chord values are calculated from increments of stress $\Delta\sigma$ and strain $\Delta\varepsilon$ only, which on substitution into generalized Hooke's law for triaxial test conditions (Equations 7.15 and 7.16) renders for CCP-test conditions ($\Delta\sigma_3 = 0$):

$$\Delta\varepsilon_1 = \frac{1}{E}\{\Delta\sigma_1 - 2\nu\Delta\sigma_3\} = \frac{\Delta\sigma_1}{E} \tag{7.21}$$

$$\Delta\varepsilon_3 = \frac{1}{E}\{-\nu\Delta\sigma_1 + (1-\nu)\Delta\sigma_3\} = \frac{-\nu\sigma_1}{E} = -\nu\Delta\varepsilon_1 \tag{7.22}$$

Since in the CCP triaxial test the increment in the major principal stress $\Delta\sigma_1$ is the applied axial cyclic stress $\sigma_{a,c}$ and the increments in major and minor principal strains are the measured resilient strains $\varepsilon_{a,r}$ and $\varepsilon_{r,r}$, Equations 7.21 and 7.22 can be rewritten as:

$$\varepsilon_{a,r} = \frac{\sigma_{a,c}}{M_r} \quad \text{or} \quad M_r = \frac{\sigma_{a,c}}{\varepsilon_{a,r}} \tag{7.23}$$

$$\varepsilon_{r,r} = -\nu\,\varepsilon_{a,r} \quad \text{or} \quad \nu = -\frac{\varepsilon_{r,r}}{\varepsilon_{a,r}} \tag{7.24}$$

which are the standard equations for determination of M_r and ν from CCP-test results.

7.2.4.2 CCP VERSUS VCP TRIAXIAL TEST

The chord approach to calculate the resilient modulus M_r and Poisson's ratio ν used in interpreting CCP-test results also explains part of the differences in M_r and ν values obtained from those tests as compared to the values of M_r and ν obtained from VCP (variable confining pressure) tests. As discussed in Paragraph 2.5.3.2, Allen and Thompson [41] performed both CCP and VCP triaxial tests on granular materials, finding somewhat higher M_r values and much higher ν-values from the

CCP-tests as compared to the values obtained from the VCP-tests. In their VCP-tests, both the deviator and the confining stress were cycled from zero to a given maximum value and, consequently, the strains used to determine M_r and ν were calculated from the deformations occurring between the wholly unloaded and the wholly loaded condition. The M_r and ν values obtained from these tests were therefore secant values, whereas the CCP-tests yielded chord values. Figure 7.16 shows the stages in which the stresses are applied in the two types of tests.

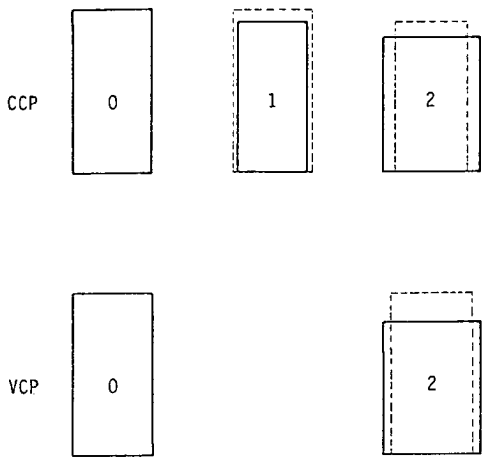

Figure 7.16: Stages of stresses applied in CCP and VCP triaxial tests.

0 : No stress.

1 : Confining stress only.

2 : Confining stress + deviator stress.

The main difference between the two types of test with respect to deformations is that in the CCP-test the deformations caused by the confining stress (going from situation 0 to situation 1 in Figure 7-.16) are not measured and, hence, not taken into account in calculating M_r and ν. In the VCP-test situation 1 does not occur and M_r and ν are calculated from the strains occurring between situation 0 and situation 2. In the CCP-test, the triaxial specimen "consolidates" under the influence of the confining stress and all deformations are measured relative to the "consolidated" size of the specimen (situation 1). In the VCP-test, all deformations are measured relative to the completely unloaded (situation 0) condition. Hence, the axial deformation measured in the CCP-test is smaller, resulting in a higher

value of the resilient modulus M_r. The radial deformation measured in the CCP-test is larger, resulting in a higher value of ν.

If the materials tested were linear elastic, then superposition of stresses and resulting strains would be allowed since all deformations are small and do not affect the exerted stresses. Then, the difference between the values for M_r (or rather E) and ν could be examined numerically. However, since for granular materials both M_r and ν are stress-dependent, the deformations measured in the CCP-test between situations 1 and 2 (Figure 7.16) cannot be extrapolated numerically back to situation 0, using the M_r and ν values pertaining to transition from situation 1 to 2. The M_r and ν values obtained from the CCP-test are chord values, pertaining to transition from the situation of confining stress only to the situation of confining stress plûs cyclic deviator stress. This fact should at all times be well taken into account. It is not necessarily a drawback of the CCP test, since in pavement analysis the interesting part of the calculations is a chord one too, going from one loaded condition (overburden stress only) to another loaded condition (overburden stress plus traffic stress).

Figure 7.17 shows two exemplary stress situations for a triaxial specimen in the CCP-test. The two stress conditions are identical, with the exception of the confining stress, which in situation A equals σ_3 = 10 kPa and in situation B equals σ_3 = 40 kPa.

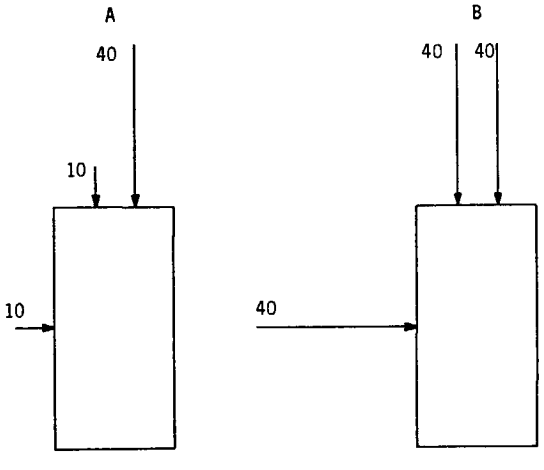

Figure 7.17: Two exemplary stress conditions for CCP-triaxial test.
A: σ_3 = 10 kPa B: σ_3 = 40 kPa

In case of testing of a granular material, the higher confining stress of situation B clearly leads to lower values for axial and radial resilient strain $\varepsilon_{a,r}$ and $\varepsilon_{r,r}$. To model this properly, generalized Hooke's law for triaxial test conditions (Equations 7.15 and 7.16) should be used. To do so, however, the strains caused by the confining stress σ_3 are needed and, as stated, these strains are not measured in the chord approach of the CCP-test. In the CCP-test, only the deformations caused by the cyclic deviator stress of $\sigma_{a,c}$ = 40 kPa are measured. The resilient modulus M_r and Poisson's ratio ν are calculated using the standard equations for the CCP-test (Equations 7.10 and 7.11) from the cyclic deviator stress (which is equal for situations A and B) and the resulting strains (which are smaller in situation B as compared to situation A). Hence, the smaller axial strains occurring in situation B result in a higher value of the resilient modulus M_r and a lower value of Poisson's ratio ν. The K-θ model discussed earlier (Paragraphs 7.2.2 and 7.2.3) deals with this increased M_r through the increase in the value of the sum of principal stresses θ, caused by the increase in confining stress σ_3. If a constant value of Poisson's ratio ν is used (Paragraph 7.2.2), the model predicts a smaller radial resilient strain simply because also a smaller axial resilient strain is predicted. When using a model with a stress-dependent ν (Paragraph 7.2.3), the extra reduction in radial resilient strain due to the decreased ratio of σ_c/σ_3 can also be dealt with by the model.

The example of Figure 7.17 is given here only to show, on the one hand, that the standard chord approach of the CCP-test combined with the K-θ model can indeed cope with a wide range of stress combinations. Certainly when combined with a stress-dependent ν, the influence of the higher confining stress is dealt with properly by the material model, in the sense that axial and radial resilient strains are predicted with a reasonable accuracy by the material model (see Paragraph 7.2.3). On the other hand, it remains a drawback that the influence of the various stresses is not dealt with explicitly in the K-θ model. The influence of a higher confining stress on the resilient modulus is only dealt with through an increase of the sum of principal stresses θ, which might just as well have been caused by an increase in the cyclic deviator stress. Although a very good fit can be obtained with the K-θ model between measured and model-predicted values

of axial resilient strain $\varepsilon_{a,r}$, the influence of the various components of stress is not recognizable in the model.

7.2.4.3 VOLUMETRIC AND SHEAR COMPONENTS OF STRESS AND STRAIN

An approach to modelling of material behaviour that does allow for an accurate examination of the influence of the various components of stress on material deformations is the one suggested originally by Brown and Bush [124]. Using Equations 7.1 through 7.4 given earlier, the axial and radial stresses applied to the triaxial specimen and the resulting axial and radial strains can be separated into volumetric and shear components (see also Paragraph 2.7.4). For a linear elastic material, the mean normal stress p causes volumetric strain ε_v and the deviator stress q causes shear strain ε_s. For such a material, the ratio of p to ε_v is the bulk modulus K and the ratio of q to ε_s is the shear modulus G. The stress-strain behaviour of a linear elastic material can thus be characterized by either of two sets of parameters: Young's modulus E and Poisson's ratio ν or the bulk modulus K and the shear modulus G. The two sets of parameters are interrelated according to:

$$K = \frac{E}{3(1-2\nu)} \tag{7.25}$$

$$G = \frac{E}{2(1+\nu)} \tag{7.26}$$

The above is valid only for linear elastic materials and hence does not apply straightforwardly to granular materials, which clearly show a stress-dependent stress/strain behaviour. As discussed in detail in Paragraph 2.7.5, Boyce [75] developed the so-called "G-K model" in which the bulk modulus K is a function of the mean normal stress p and the deviator stress q, whereas the shear modulus G is a function of the mean normal stress p only (Equations 2.29 and 2.30, Paragraph 2-.7.5). Since $\varepsilon_v = p/K$ and $\varepsilon_s = q/3G$, a change in the deviator stress q at a constant mean normal stress p gives volumetric strain ε_v in the

G-K model (through the influence of q on K) and a change in mean normal stress p causes shear strain ϵ_s (through the influence of p on G). Granular materials do show such behaviour, as shown by Pappin and Brown in their detailed analysis of the stress-strain behaviour of a crushed rock [76].

The G-K model developed by Boyce is an elastic model, meaning that all strain is entirely recoverable, the state of strain is uniquely related to the state of stress, and the net energy absorbed when the material is cycled from one stress condition to another and back is zero. From this it follows that the stress/strain behaviour of an elastic model has to meet the theorem of reciprocity which states that:

$$\frac{\partial \epsilon_v}{\partial q} = \frac{\partial \epsilon_s}{\partial p} \qquad (7.27)$$

This prerequisite limits the number of material parameters in the functions K = f(p,q) and G = f(p), since it imposes a certain relationship between K and G. Boyce's G-K model therefore contains only three material parameters (denoted K_1, G_1 and n) to relate K and G to stress. Since the G-K model is purely elastic, it can by definition not cope with any inelastic stress/strain behaviour. If, therefore, a granular material exhibits some form of inelastic behaviour such as hysteresis in a cyclic load triaxial test, the values of volumetric and shear strain predicted by the G-K model are bound to deviate from the measured values. It will be shown in Paragraph 7.2.5 that, when applied to the test results of the two exemplary materials BGO and OSN, Boyce's G-K model indeed yields values of strain deviating substantially from the measured values. Paragraph 7.2.6 will describe a model quite similar to Boyce's G-K model, but incorporating five material parameters relating G and K to stress rather than the three material parameters incorporated in Boyce's model. Thanks to the inclusion of more material parameters, the model discussed in Paragraph 7.2.6 predicts volumetric and shear strains from the applied stresses better than does Boyce's model. However, it no longer meets the theorem of reciprocity (Equation 7.27) and is therefore not elastic.

7.2.5 The G-K model

As discussed in Paragraph 2.7.5, Boyce's G-K model involves separation of stresses and strains into volumetric and shear components using the equations given earlier in this chapter (Equations 7.1 through 7.4). The stresses applied to the triaxial specimen are separated into the mean normal stress $p = \frac{1}{3}(\sigma_1 + 2\sigma_3)$ and the shear stress $q = \sigma_1 - \sigma_3$. Having done this, the stresses applied to the triaxial specimen can be plotted in p-q stress space, as shown in Figures 7.18 and 7.19. Figure 7.18 pertains to the standard set of stress-combinations applied in determination of the resilient properties of the granular base course materials (see Table 5.3, Paragraph 5.3.2.5). Only the stress paths pertaining to the level σ_s = 3 kPa of the static part of the deviator stress are shown in the figure; the stress paths for the other two levels of σ_s almost coincide with the stress paths shown. Figure 7.19 pertains to the standard set of stress combinations for resiliency testing of the sands (see Table 5.6, Paragraph 5.3.3.5).

Due to the nature of the CCP-test, all stress paths are at the same angle ($\Delta q/\Delta p = \frac{1}{3}$), since the change in shear stress between beginning and end of stress path Δq equals $\Delta\sigma_1$ in the triaxial test and the change in mean normal stress Δp equals $\frac{1}{3}\Delta\sigma_1$. The stress paths being at fixed angles to the p-q axes illustrates one of the limitations of the CCP-triaxial test; rotation of the stress paths is not feasible in such tests. The levels of confining stress (four in Figure 7.18 and eight in Figure 7.19) can be clearly recognized from the p-q plots. At each given level of confining stress, the stress paths for all tests at that level of σ_3 plot on the same line. The stress path do not start from q=0, due to the self-weight of the specimen material and, in case of testing of the granular base course materials, the inclusion of the static part of the deviator stress σ_s (see Figure 5.9, Paragraph 5.3.2.5) in the standard set of stress combinations.

Boyce related the volumetric strain $\varepsilon_v = \varepsilon_1 + 2\varepsilon_3$ and the shear strain $\varepsilon_s = \frac{2}{3}(\varepsilon_1 - \varepsilon_3)$ to the mean normal stress p and the shear stress q using the equations given in Paragraph 2.7.5 (Equations 2.31 - 2.33). Boyce's G-K model contains only three parameters to describe the resilient deformation of the material, denominated as K_1, G_1 and n. K_1 and G_1 are the bulk and the shear modulus of the material at hand for the mean normal stress p being unity and the shear stress q being

zero, while n is a measure of stress-dependency (see Equations 2.29 and 2.30).The parameter n varies between 0 and 1; as can be seen from Equations 2.31 through 2.33, for n = 1 the linear-elastic case is obtained ($\beta = 0$, $\varepsilon_v = p/K_1$ and $\varepsilon_s = q/3G_1$).

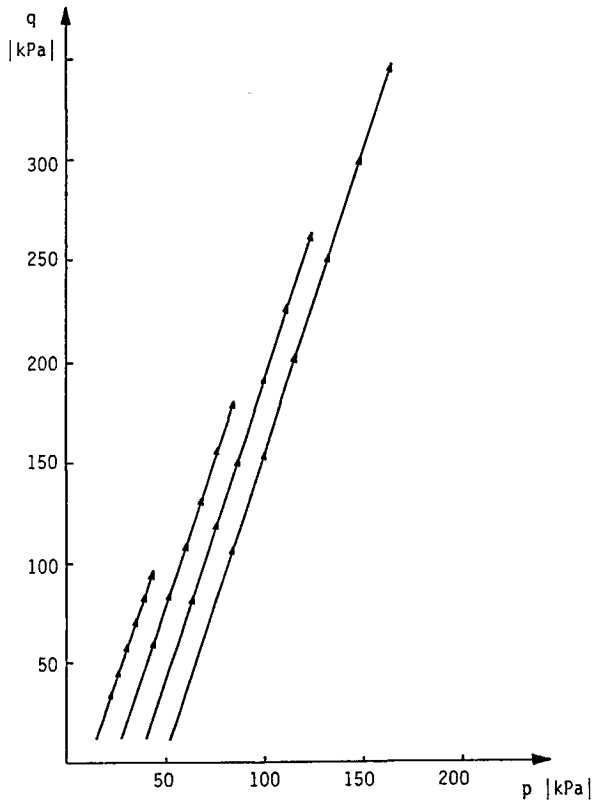

Figure 7.18: p-q stress-space representation of stresses applied in resiliency testing of granular base course materials.

The material parameters K_1, G_1 and n were determined from the results of the resiliency testing of materials BGO and OSN using regression analysis. Table 7.1 shows the values obtained. The complicated mathematical formulation of Equations 2.32 and 2.33 does not allow for allocating proper dimensions to the material parameters K_1 and G_1 in Table 7.1. The values given for K_1 and G_1 are for use with the stresses p and q in [MPa] and the strains ε_r and ε_s in [m/m]. The parameter n has no dimension.

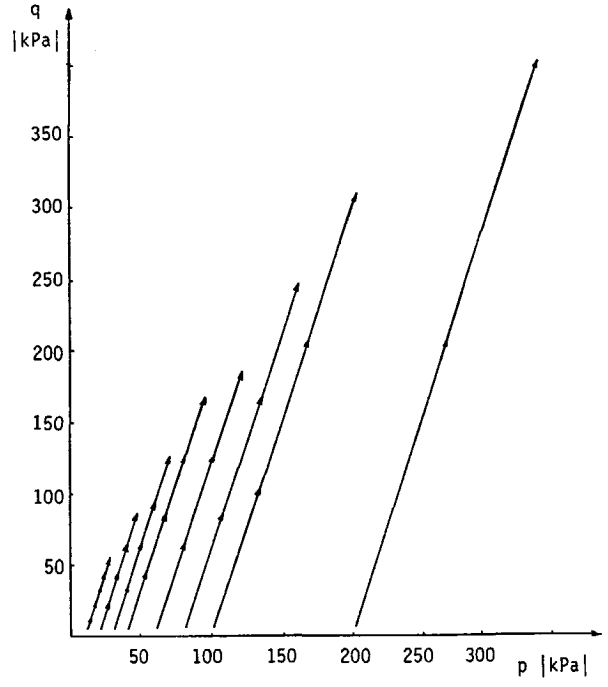

Figure 7.19: p-q stress-space representation of stresses applied in resiliency testing of sands.

Table 7.1: Values for parameters K_1, G_1 and n for materials BGO and OSN (G-K model)

material	K_1	G_1	n
BGO	306	396	0.34
OSN	196	286	0.34

Figures 7.20 and 7.21 show plots of of model-predicted versus measured values of volumetric and shear strains for material BGO. As can be seen from Figure 7.21, the prediction of shear strain by the G-K model is very good. However, the prediction of volumetric strain (Figure 7-.20) is quite poor. Although the model is capable of dealing with both positive volumetric strain (specimen volume decrease) and negative volumetric strain (specimen volume increase), the deviation between model-predicted and measured values may be well over 100%. Also, the model predicts for certain stress combinations negative volumetric strains where positive volumetric strains were measured.

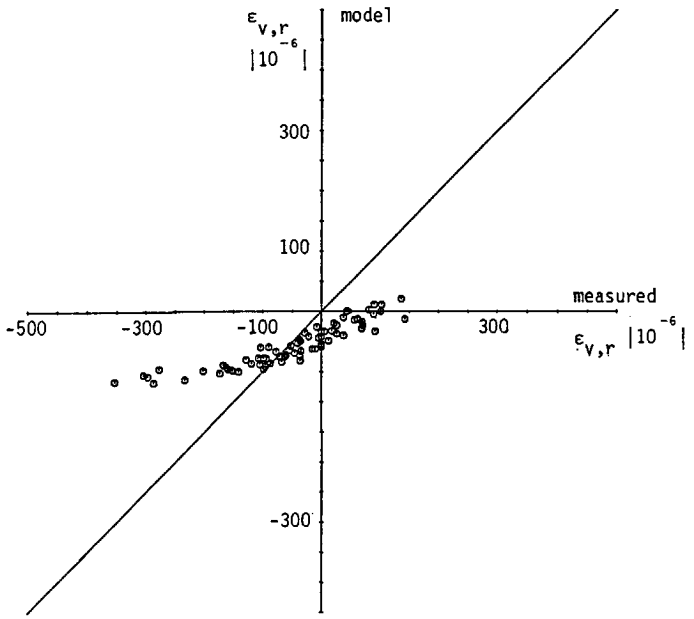

Figure 7.20: Model-predicted versus measured values of volumetric strain for material BGO (G-K model).

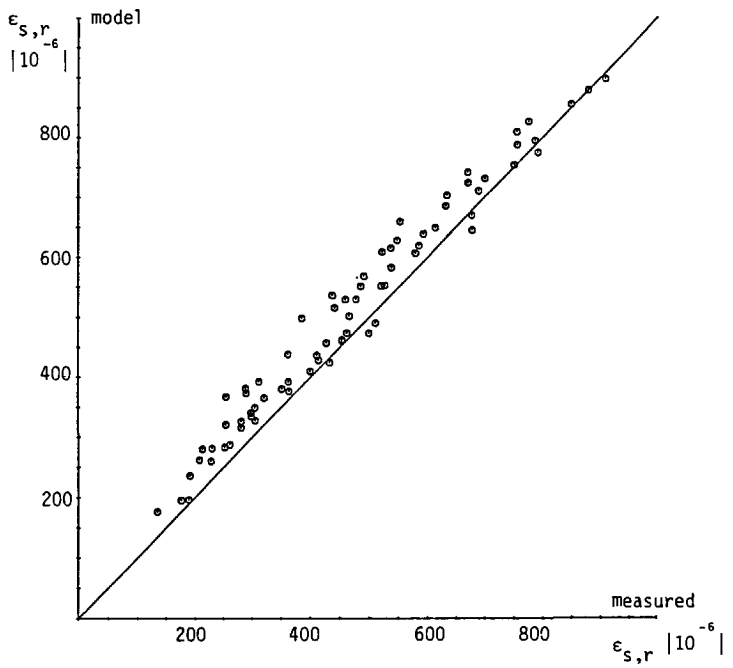

Figure 7.21: Model-predicted versus measured values of shear strain for material BGO (G-K model).

Figures 7.22 and 7.23 show plots of model-predicted versus measured values of volumetric and shear strain for the Eastern Scheldt Sand OSN. As was the case for the crushed concrete BGO, the prediction of shear strain by the G-K model is good. The prediction of volumetric strain is again poor, although the deviation from the 45° line of equality is somewhat smaller for material OSN as compared to material BGO. The somewhat better fit is attributable to the fact that almost all volumetric strains measured in the test were positive (indicating volume decrease) and almost no negative volumetric strains were measured.

The good performance of the G-K model in predicting shear strains is not surprising. As noted when discussing the K-θ model with constant ν (Paragraph 7.2.2), shear strains are easier to model than volumetric strains because of the definition of both components of strains in terms of principal strains. Even the very crude K-θ model with constant ν (Paragraph 7.2.2) gave a reasonable prediction of shear strain. The real test for a material model lies in its capability to accurately predict volumetric strains. In that respect, Boyce's G-K model performs poorly for the exemplary materials BGO and OSN.

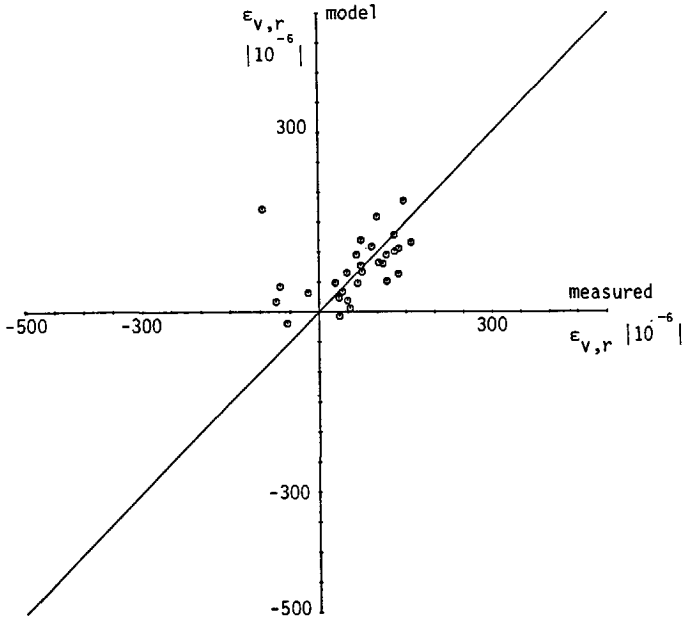

Figure 7.22: Model-predicted versus measured values of volumetric strain for material OSN (G-K model).

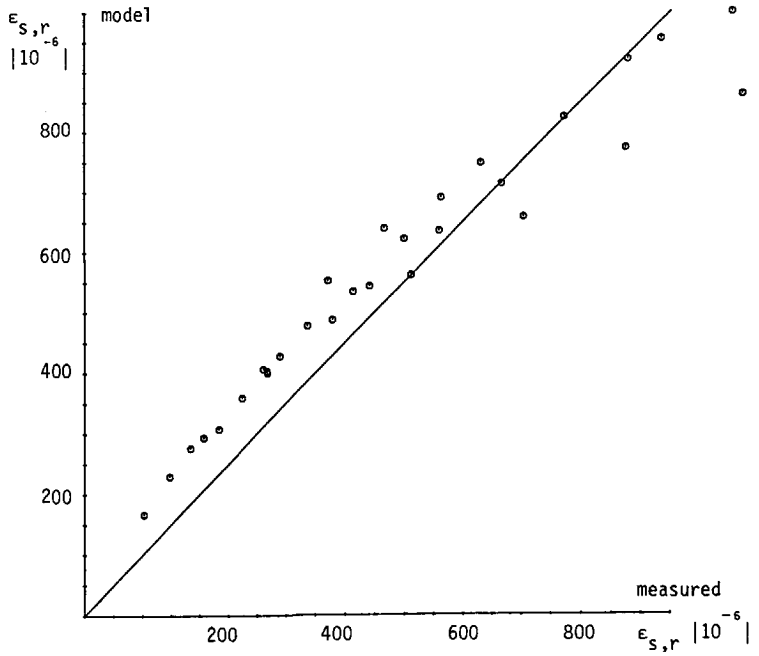

Figure 7.23: Model-predicted versus measured values of shear strain for material OSN (G-K model).

The poor performance of the G-K model in predicting volumetric strain follows from the rigid condition set by Boyce for his model to be truly elastic. As explained in Paragraph 2.7.5, this condition of being elastic implies that volumetric and shear strains have to meet the theorem of reciprocity (Equation 7.27, Paragraph 7.2.4.3). This theorem sets rigid boundaries to the parameters used in any elastic model and causes Boyce's G-K model (Equations 2.31 through 2.33) to contain only three independent material parameters. The "fourth" parameter β from Boyce's model being a direct function of the other parameters K_1, G_1 and n (Equation 2.31) follows from reciprocity.

The condition of Boyce's G-K model being elastic means, by definition, that the model cannot cope with any inelastic material behaviour. Although the deformations measured in cyclic load triaxial testing of granular materials may become entirely recoverable after a limited number of load applications, this does not necessarily imply that the deformations are also elastic. Although the stress-strain curve measured under cyclic loading ends at the same point where it began, the loading part of the curve may be quite different from the unloading part. Figure 7.24 shows two exemplary load-displacement signals

from the resiliency testing of Eastern Scheldt sand (test OSND 01, see Paragraph 5.3.3.5).

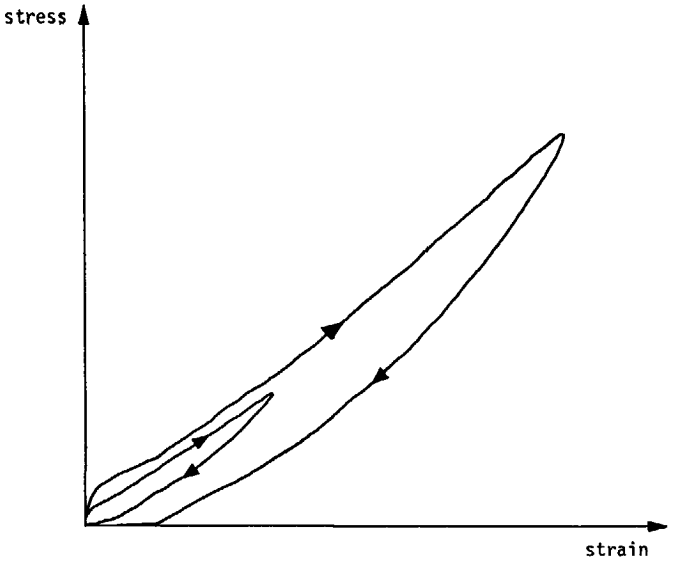

Figure 7.24: Stress-strain behaviour of Eastern Scheldt sand under cyclic loading.

Both for the small and the large stress increment, the loading and unloading part of the stress-strain curve do not coincide. Hence, no unique stress-strain relationship exists and energy is dissipated during application of the cyclic loading. The material behaviour then is, by definition, inelastic. Since such inelastic behaviour does occur in cyclic load triaxial testing of granular materials, an elastic model like Boyce's G-K model cannot be expected to accurately predict measured values of strain.

As stated, the discrepancy between model-predicted and measured values of strain is largest for the volumetric components. The solution to the problem of not being able to accurately model volumetric strains by the elastic G-K model is obvious. By removing the strict condition of the model being elastic and, hence, of the coupling of volumetric and shear strains by the theorem of reciprocity, models can be obtained that relate volumetric strains to the applied stresses (expressed in mean normal stress p and shear stress q) independently of the relationship between shear strain and stresses. The number of

possible such models is virtually infinite: in fact a straight forward curve-fitting approach relating ε_v to p and q and ε_s to p and q may be used. As many material parameters as required to obtain a sufficiently accurate agreement between model-predicted and measured values of strains may be incorporated in the model. As discussed in the literature review (Paragraph 2.7.6), a number of material models has been developed over the years using this type of approach. In the next paragraph only one of these models will be discussed as an illustration. The particular model will be shown to have a high accuracy in predicting both volumetric and shear strains from the applied stresses.

7.2.6 An inelastic G-K model

As discussed in the previous paragraph, Boyce's G-K model was developed from observations of increments in volumetric and shear strains caused by increments of the mean normal stress and the shear stress, coupled with the strict requirements of elasticity. Keeping to Boyce's observations of how strains are related to stresses, but removing the requirement of reciprocity (Equation 7.27, Paragraph 7-.2.3.4) a model containing independent relationships between ε_v and p and q on the one hand and ε_s and p and q on the other hand can be obtained. The resulting model (SW 31) then is:

$$\varepsilon_v = \frac{1}{K_1} p^n \left(1 - \beta \frac{q^2}{p^2}\right) \tag{7.28}$$

$$\varepsilon_s = \frac{1}{3G_1} p^m \frac{q}{p} \tag{7.29}$$

This model is very similar to Boyce's G-K model, but contains five rather than three independent material parameters. β is no longer a direct function of K_1, G_1 and n (as was the case in Boyce's model) and the stress-dependency factor m in the equation for shear strain ε_s is no longer equal to the stress-dependency factor n in the equation for volumetric strain ε_v. Using regression analysis, the five material parameters K_1, G_1, n, m and β from this model were determined from the resiliency testing results of the crushed concrete BGO and Eastern Scheldt sand OSN. The values obtained are shown in Table 7.2. As was the case with Boyce's G-K model, no proper dimensions can be given to

the material parameters K_1 and G_1 because of the mathematical structure of Equations 7.28 and 7.29. The values of K_1 and G_1 given in Table 7.2 are for use with the stresses p and q in [MPa] and the strains ε_v and ε_s in [m/m]. The material parameters n, m and β have no dimension.

Table 7.2: Values for parameters K_1, G_1, n, m and β for materials BGO and OSN (inelastic G-K model)

material	K_1	G_1	n	m	β
BGO	57	404	1.00	0.33	0.17
OSN	24	286	0.02	0.34	0.01

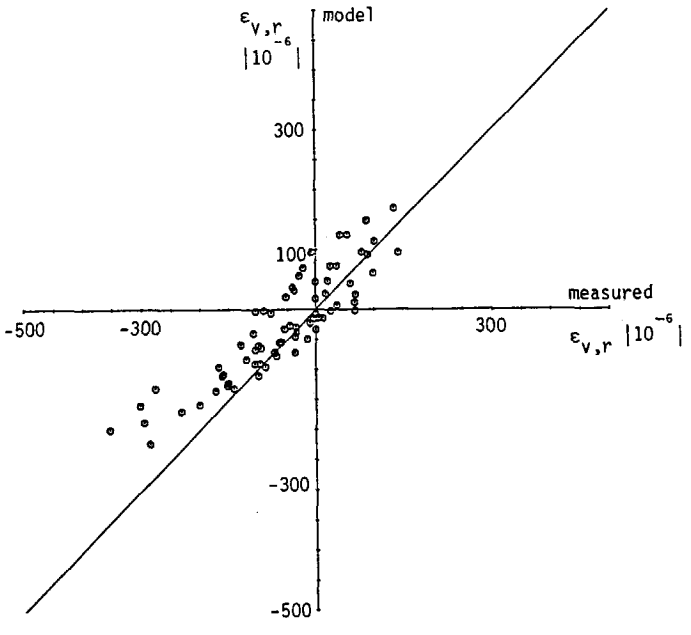

Figure 7.25: Model-predicted versus measured values of volumetric strain for material BGO (inelastic G-K model).

Figures 7.25 and 7.26 show plots of model-predicted versus measured values of volumetric strain for crushed concrete BGO and Eastern Scheldt sand OSN. Comparing the performance in predicting volumetric strain of the inelastic G-K model for BGO (Figure 7.25) to that of the elastic G-K model (Figure 7.20), the improvement due to the removal of

the strict conditions of elasticity is striking. For OSN (Figures 7.26 and 7.22) the improvement is much smaller, mainly because of the already reasonable fit obtained with the elastic G-K model. The plots of model-predicted versus measured values of shear strain have been omitted here, since the inelastic G-K model yields almost or exactly the same material parameters for predicting shear strain as does the elastic G-K model (compare parameters K_1 and m in Table 7.2 to K_1 and n in Table 7.1). The difference between the two models lies in the parameters for volumetric strain, which in the case of the inelastic G-K model can be fitted independently from those for shear strain.

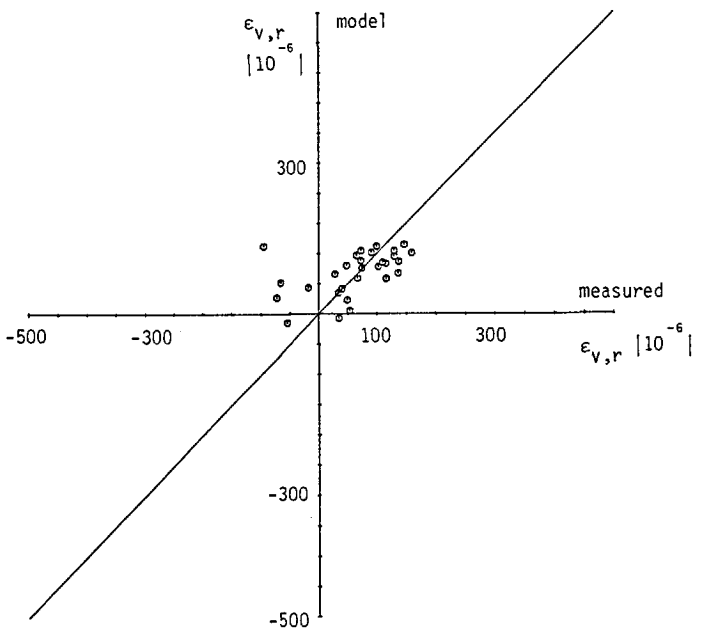

Figure 7.26: Model-predicted versus measured values of volumetric strain for material OSN (inelastic G-K model).

7.3 PERMANENT DEFORMATION

7.3.1 Introduction

Paragraphs 5.3.2.6 and 5.3.3.6 have dealt with permanent strain testing of the granular base course materials of Groups C and R and of the sands of Group S, respectively. The results of this testing were presented in Chapter 5 in the simplest form, being straightforward plots of the permanent axial strain $\varepsilon_{a,p}$ of the triaxial specimens as a function of the number of load applications N (on a logarithmic scale to deal with the extended range of N).

This paragraph deals with the modelling of permanent deformations. As compared to modelling of resilient deformation, the literature available on modelling of permanent deformation is rather scarce. Part of the available models has already been discussed in Paragraph 5.6, which deals with estimating permanent deformation from the results of tests that are relatively simple to perform. The models discussed there describe permanent deformation as a function of number of load applications, coupled to the results of resilient strain tests or static load failure tests. As shown in Paragraph 5.6, these models are inadequate to fit the experimental data obtained here for the materials from Groups C, R and S.

The modelling of permanent deformations discussed in this paragraph is, in fact, no more than a search for a sufficiently accurate mathematical description of the plots of permanent strain versus number of load applications mentioned earlier. Paragraph 7.3.2 will deal with axial and radial strains as a function of N, whereas Paragraph 7.3.3 will deal with separating stresses and strains into volumetric and shear components. As was done when discussing the modelling of resilient deformations, the applicability of the various models will be illustrated with the test results for one granular base course material and one sand.

7.3.2 Axial and radial permanent strain

Figures 7.27 and 7.28 show the standard representations of permanent strain test results for one granular base course material (lava, coarse grading LA0) and one sand (Echten sand ENN). These results were given earlier in Chapter 5 (Figure 5.11, Paragraph 5.3.2.6 and Figure 5.20, Paragraph 5.3.3.6). The axial permanent strain $\varepsilon_{a,p}$ is plotted on a linear scale against the number of load repetitions N on a logarithmic scale.

Figures 7.27 and 7.28 each contain three $\varepsilon_{a,p}$-N lines, each line pertaining to a separate cyclic load triaxial test at a different ratio of the cyclic deviator stress σ_c over the confining stress σ_3. The strains are plotted in the figures for values of N from 10^2 to 10^6; the starting values for N = 0 cannot be plotted on a log-scale, and of course all coincide at $\varepsilon_{a,r} = 0$.

Many researchers have described $\varepsilon_{a,p}$-N lines similar to those shown in Figures 7.27 and 7.28 mathematically by the equations of a straight line on a log-natural scale:

$$\varepsilon_{a,p} = a + b \log N \qquad (7.30)$$

where a and b are constants dependent on the material at hand, on the specimen conditions with respect to density and moisture content and on the stresses applied in the cyclic load test. As can be seen from Figure 7.28, the results of the permanent strain testing of the Echten sand can indeed be approximated by a straight line and, hence, by Equation 7.30. The permanent strain test results for the granular base course material LA0 (Figure 7.27), however, cannot be described accurately by Equation 7.30. Up to $N = 10^4$ the data points do plot on a straight line, but for the higher stress ratios the rate of accumulation of permanent strain increases markedly for $N > 10^4$. Therefore, for higher numbers of load applications an approximation of the test results by Equation 7.30 appears to be not valid. It should be noted here that much of the applications of Equation 7.30 given in the literature were done for permanent strain tests run only up to $N = 10^4$ or $N = 10^5$, which may account for the good fit described in literature. For actual pavement design purposes tests should be run up to at

least N = 10^6 since the design life of the pavement is bound to incorporate at least that number of load repetitions.

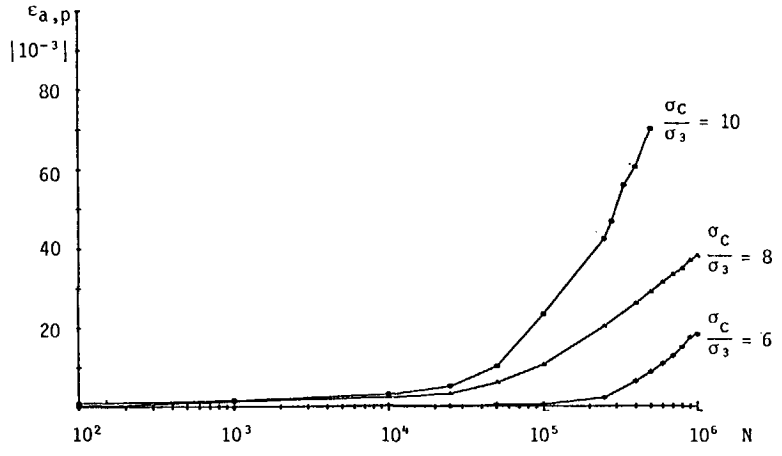

Figure 7.27: Permanent axial strain $\varepsilon_{a,p}$ versus number of load applications N, for lava LA0 (log-natural plot).

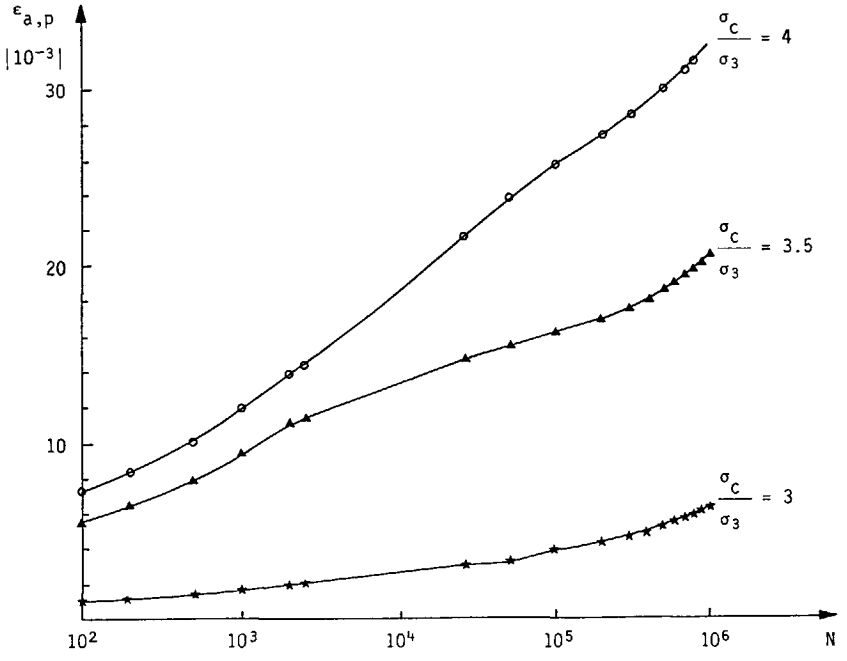

Figure 7.28: Permanent axial strain $\varepsilon_{a,p}$ versus number of load applications N, for Echten sand ENN (log-natural plot).

To check the applicability of Equation 7.30 numerically, linear regression analysis was performed on the data points given in Figure 7.27 and 7.28. The results of this analysis, being the parameters a and b from Equation 7.30 and the respective correlation coefficient r are given in Table 7.3. For the Echten sand, very high correlation coefficients are found, up to r = 0.999 for test ENND 02 which indicates an almost perfect fit. The correlation coefficients found for the permanent strain data of the lava are indeed much lower.

Table 7.3: Permanent axial strain parameters a and b and correlation coefficient r for materials LA0 and ENN (Equation $\varepsilon_{a,p} = a + b \log N$)

material number	test code	σ_c/σ_3	a	b	r
C02	LAOD 05	6	-12.96	4.08	0.687
	LAOD 04	8	-11.88	6.78	0.760
	LAOD 03	10	-51.51	17.14	0.791
S02	ENND 03	3	- 2.24	1.32	0.975
	ENND 04	3.5	- 1.45	3.59	0.997
	ENND 02	4	- 7.16	6.46	0.999

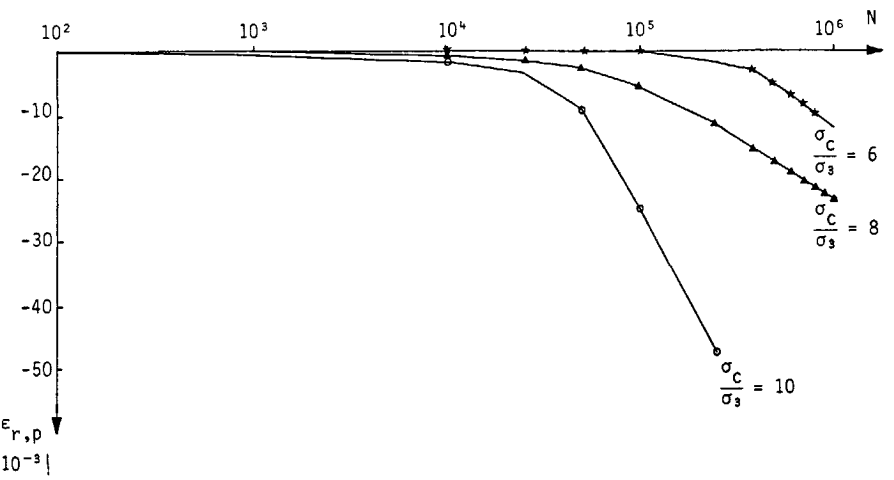

Figure 7.29: Permanent radial strain $\varepsilon_{r,p}$ versus number of load applications N, for lava LA0 (log-natural plot).

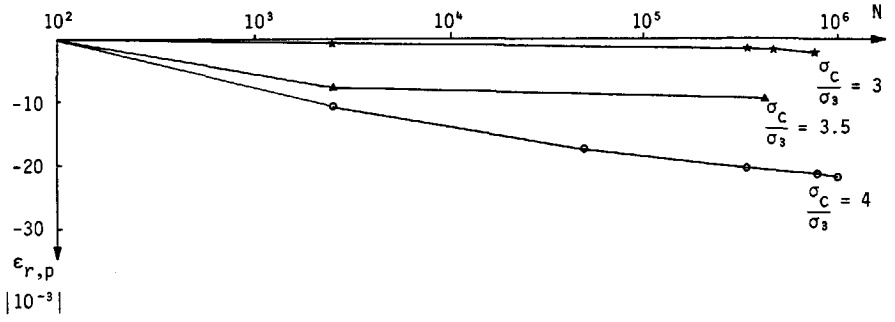

Figure 7.30: Permanent radial strain $\varepsilon_{r,p}$ versus number of load applications N, for Echten sand ENN (log-natural plot).

Figures 7.29 and 7.30 show the development of the radial permanent strain $\varepsilon_{r,p}$ with the number of load applications N. As can be seen from Figure 7.29, no data are available beyond N = 2.5 * 10^5 for test LAOD 03; the LVDT's measuring radial permanent deformation were disconnected at that point since the deformations became too large. The Echten sand ENN was tested in the 100 mm specimen diameter apparatus; only limited data points are available here since measurement of permanent radial strain with this apparatus is not automated.

With respect to modelling the permanent radial strain as a function of the number of load applications N, the same conclusion can be drawn as with the axial permanent deformations. For the Echten sand the points plot closely to a straight line on the log-natural scale, whereas for the lava the data points deviate substantially from a straight line. Again, the increase in the rate of accumulation of permanent strain for higher values of N accounts for the poor fit found for the lava. For sake of completeness, Table 7.4 shows the parameters a and b and the correlation coefficient r for a straight line through the data points of Figures 7.29 and 7.30.

The problem of not being able to deal with the marked increase in the rate of accumulation of permanent strain for higher numbers of load applications can be dealt with by plotting the permanent strains on a logarithmic scale too, as was done with the number of load applications. The equation for axial permanent strain then becomes:

$$\log \varepsilon_{a,p} = a + b \log N \qquad (7.31)$$

Table 7.4: Permanent radial strain parameters a and b and correlation coefficient r for materials LAO and ENN (Equation $\varepsilon_{r,p} = a + b \log N$)

material number	test code	σ_c/σ_3	a	b	r
CO2	LAOD 05	6	7.84	- 2.51	0.704
	LAOD 04	8	20.98	- 6.60	0.861
	LAOD 03	10	31.13	-10.70	0.722
SO2	ENND 03	3	0.86	- 0.48	0.950
	ENND 04	3.5	-5.01	- 0.77	1.000 [1]
	ENND 02	4	4.36	- 4.22	0.990

[1] only two data points available, hence a perfect correlation

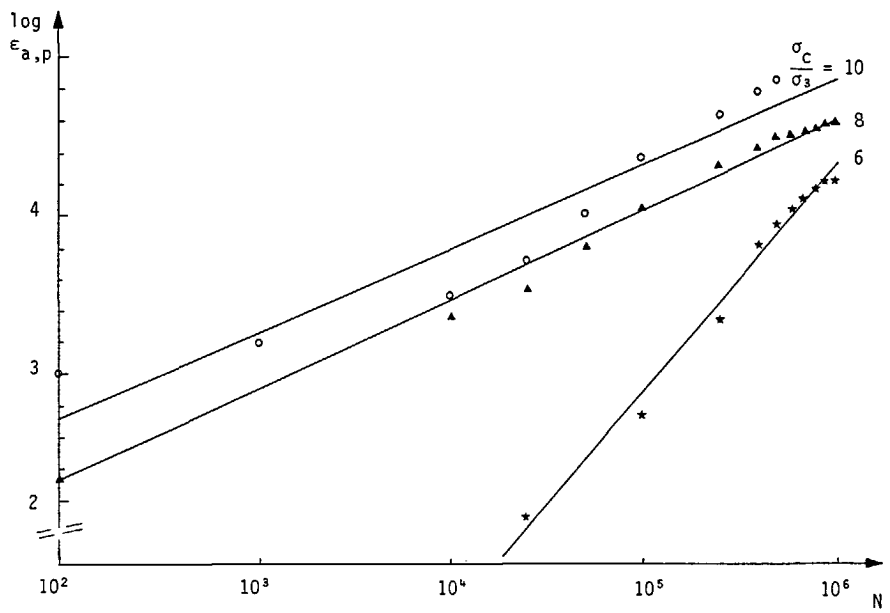

Figure 7.31: Permanent axial strain $\varepsilon_{a,p}$ versus number of load applications N, for lava LAO (log-log plot).

Figures 7.31 and 7.32 show plots of the axial permanent strain $\varepsilon_{a,p}$ versus the number of load applications N, both parameters now being on a logarithmic scale. As expected, the data points for the Echten sand

ENN (Figure 7.32) plot closely to a straight line (as they did on the log-natural plot), but also the data for lava LAO now can be described accurately by a straight line relationship.

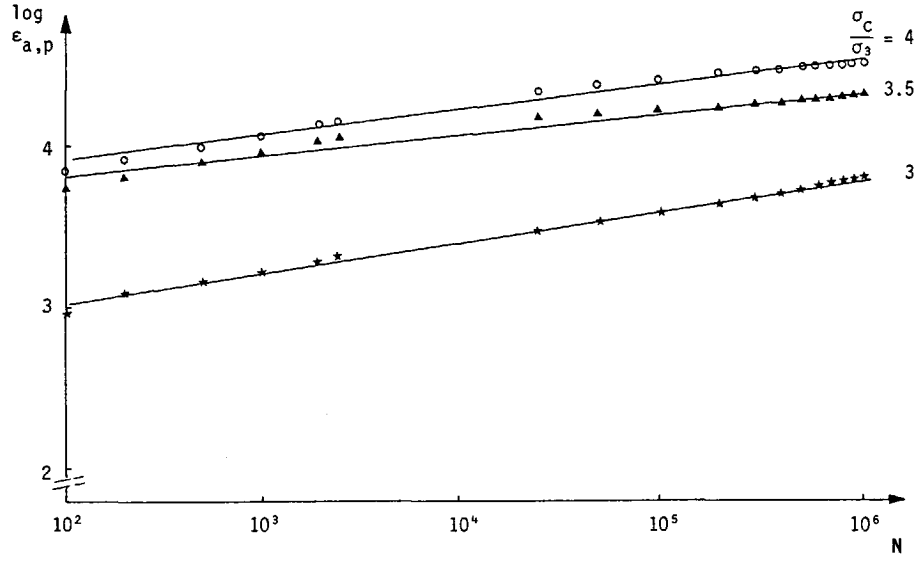

Figure 7.32: Permanent axial strain $\varepsilon_{a,p}$ versus number of load applications N, for Echten sand ENN (log-log plot).

Table 7.5: Permanent axial strain parameters a and b and correlation coefficient r for materials LAO and ENN
(Equation: $\log \varepsilon_{a,p} = a + b \log N$)

material number	test code	σ_c/σ_3	a	b	r
C02	LAOD 05	6	-4.22	1.42	0.995
	LAOD 04	8	1.23	0.56	0.994
	LAOD 03	10	1.66	0.53	0.957
S02	ENND 03	3	-0.37	0.19	0.993
	ENND 04	3.5	0.56	0.13	0.980
	ENND 02	4	0.59	0.16	0.992

Table 7.6: Permanent radial strain parameters a and b and correlation coefficient r for materials LAO and ENN
(Equation: $\log(-\varepsilon_{r,p}) = a + b \log N$)

material number	test code	σ_c/σ_3	a	b	r
C02	LAOD 05	6	0.11	0.62	0.925
	LAOD 04	8	0.49	0.65	0.989
	LAOD 03	10	0.70	0.69	0.940
S02	ENND 03	3	2.34	0.16	0.983
	ENND 04	3.5	3.74	0.04	1.000 [1]
	ENND 02	4	3.59	0.13	0.975

[1] only two data points, hence a perfect correlation.

Tables 7.5 and 7.6 show the permanent strain parameters a and b and the correlation coefficient r, for axial and radial strains respectively. The equation for radial strain was adapted to cope with the negative strain values by multiplying radial strain by -1. For sake of brevity, the figures plotting log $\varepsilon_{r,p}$ versus log N have been omitted.

All correlation coefficients found are very high, both for axial and radial permanent strains. Indeed, the values of r are so high, that a further search for even more accurate models expressing permanent strain as a function of the number of load applications is of little use. It should, however, be well noted that the log-log model described here does not contain a stress parameter. Hence, for each stress level separate permanent strain parameters a and b have to be determined from the results of a time-consuming cyclic load triaxial test. Once the test has been done, then both axial and radial permanent strain for the given stress level can be predicted with a high accuracy as a function of the number of load applications N, using the log-log approach illustrated in Figures 7.31 and 7.32.

A major improvement to permanent strain modelling could be made if some stress parameter could be incorporated in the model. A single equation per material (at a given density and moisture content) would then be enough to describe permanent strain behaviour, instead of needing a separate equation for each stress level. Determination of

the parameters of such a model would, however, require very extensive testing. For a number of stress levels, permanent strain cyclic load triaxial tests up to 10^6 load applications would have to be run, each test requiring a new triaxial specimen and several days of running time.

If, further, specimen variables as dry density and moisture content could be incorporated in the permanent strain model, then a versatile model would be obtained incorporating all factors that influence permanent strain behaviour. However, since each factor introduced into a material model multiplies the required number of tests by a factor of, say, five, the determination of the permanent strain parameters for such a model would require per material several months of laboratory testing. The limited role of permanent strain modelling in flexible pavement design does not warrant such extensive testing. The solution to this problem would be to relate permanent strain behaviour to the results of tests that are fast and simple to perform, such as resilient strains (at a given stress/density/moisture content combination) or static load failure data (at a given density/moisture content). This solution has been surveyed by other researchers, as discussed in Paragraph 5.6. As was shown there, such solutions however are limited in their applicability, working for instance only for limited numbers of load applications and/or only for a single material.

Therefore, cyclic load triaxial tests with large numbers of load applications, performed at in-situ levels of density, moisture content and stress appear to be indispensable for determination of permanent strain properties of granular materials. The log-log model relating permanent strain to number of load applications described above is by all means sufficiently accurate to describe the results of such testing.

7.3.3 Volumetric and shear components of permanent strain

The previous paragraph has dealt with modelling of as-measured permanent strains, being the axial and radial strain obtained directly from the cyclic load triaxial test. Using these as-measured strains

has the disadvantage of not being able to see directly from the permanent strain plots what type of deformation is taking place. No distinction can be made between shear deformation (a change in specimen shape without volume change) of volumetric deformation (densification or decompation of the specimen). By transferring the as-measured strains to volumetric and shear strains using Equations 7-.3 and 7.4 (Paragraph 7.2.1), the type of deformation occurring can be recognized directly. Certainly when studying, for instance, the effect of density on permanent deformation properties, the more fundamental approach of using volumetric and shear strains is preferable over the use of as-measured strains.

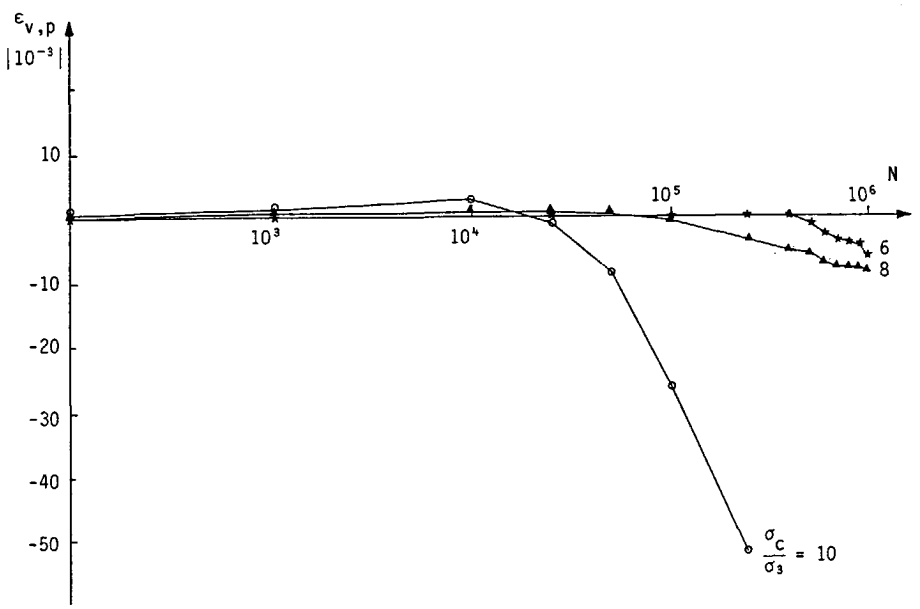

Figure 7.33: Permanent volumetric strain $\varepsilon_{v,p}$ versus number of load applications N, for lava LAO (log-natural plot).

Figures 7.33 and 7.34 show the permanent volumetric and shear strains obtained from the cyclic load testing of lava LAO plotted against the number of load repetitions. As can be seen from Figure 7.33, the triaxial specimens initially show some densification (positive volumetric strains indicating a decrease in specimen volume), but at higher numbers of load applications significant dilation (decompaction of the triaxial specimens) takes place. For the testing at stress ratio σ_c/σ_3 = 10 (test number LAOD 03) the volumetric strain at N = 2.5×10^5 is

$\varepsilon_{v,p} = 52 \times 10^{-3}$, indicating a decrease in specimen density of 5.2%. Starting at 99% of Maximum Modified Proctor Density (see Appendix 3), the eventual density of the specimen thus only is some 94% of that density. Looking at shear strain (Figure 7.34) a similar trend as for axial and radial strains can be observed. A marked increase in the rate of accumulation of permanent strain occurs at high numbers of load applications.

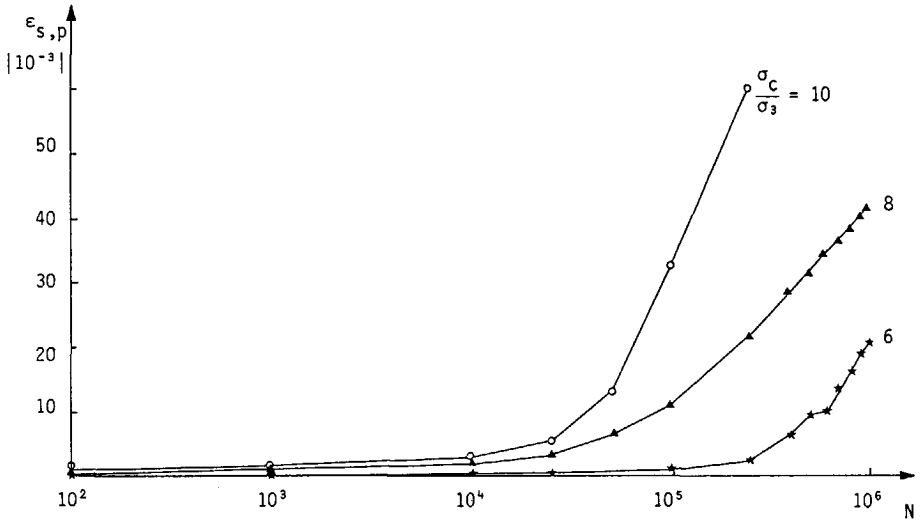

Figure 7.34: Permanent shear strain $\varepsilon_{s,p}$ versus number of load applications N, for lava LA0 (log-natural plot).

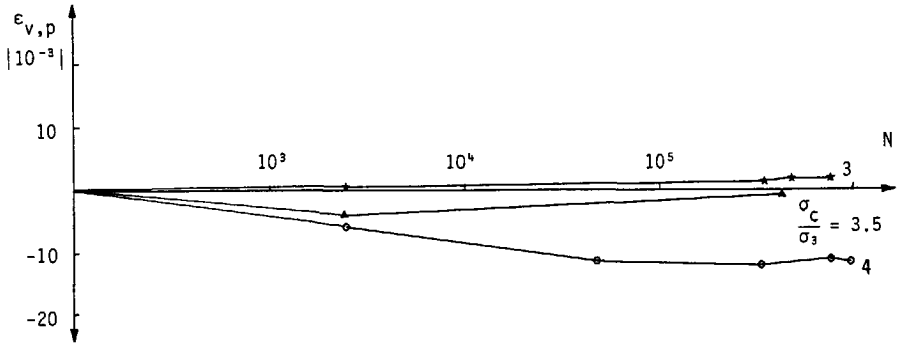

Figure 7.35: Permanent volumetric strain $\varepsilon_{v,p}$ versus number of load applications N, for Echten sand EEN (log-natural plot).

Figures 7.35 and 7.36 show the permanent volumetric and shear strains for the Echten sand, again as a function of the number of load applications. Only a limited number of data points for volumetric and shear strain is available, because of the limited number of radial measurements discussed earlier.

Figure 7.35 shows that for the stress ratios σ_c/σ_3 = 3 and σ_c/σ_3 = 3.5 (test codes ENND 03 and ENND 04) the volume change of the specimen during the test is limited. For σ_c/σ_3 = 4 (test code ENND 02) decompaction of the specimen material is observed, beit that the decrease in density is limited to about 1%. The permanent shear strain (Figure 7.36) again shows a similar trend as did permanent axial and radial strains; the data points approximate a straight line on the log-natural plot.

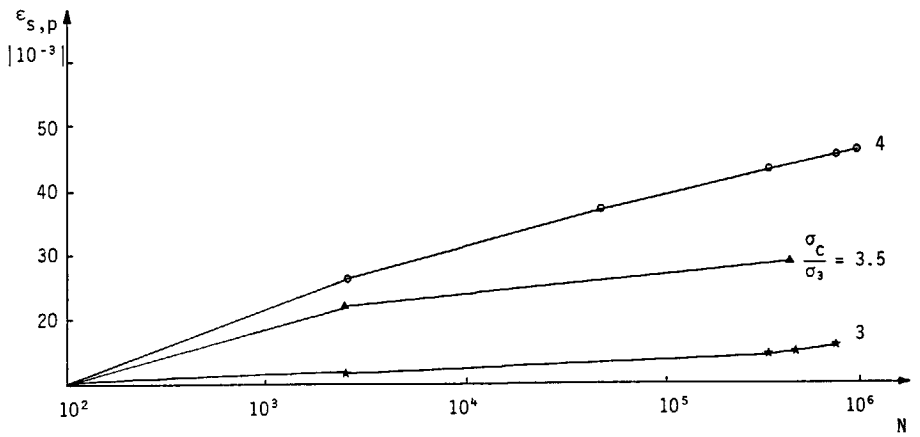

Figure 7.36: Permanent shear strain $\varepsilon_{s,p}$ versus number of load applications N, for Echten sand ENN (log-natural plot).

As was the case with the principal strains, the plots of volumetric strain and shear strain for the Echten sand can be approximated by a straight line on the log-natural scale depicted in Figures 7.35 and 7-.36. For the lava (Figures 7.33 and 7.34) such an approximation is, however, not possible because of the marked increase in rate of strain at high numbers of load applications. Plotting the results on a log-log scale to obtain a straight line relationship is not possible either, since the volumetric strain has both positive and negative values. Modelling of permanent strain as a function of the number of load applications should, therefore, preferably be done in terms of

principal strains, which yields straight line relationships on a log-log scale. For obtaining more insight into material behaviour under large numbers of load applications, the log-natural plots of volumetric and shear strain versus number of load applications should be used.

7.4 CONCLUSION

Chapter 5 of this dissertation has dealt with the testing of a large number of granular base course materials and sands for resilient and permanent strain properties. In this chapter, a selection of models expressing resilient and permanent strains as a function of the applied stresses has been discussed. The following conclusions can be drawn with respect to modelling of resilient strains:

1. The classical K - θ model expressing the resilient modulus M_r as a function of the sum of principal stresses θ gives a good prediction of the axial resilient strains as measured in the cyclic load triaxial test. Given the accuracy of this model, a further search for even more accurate models predicting axial resilient strain is of little use.

2. The K - θ model is often used in conjunction with a constant value of Poisson's ratio ν. Cyclic load triaxial tests, however, clearly indicate the ratio of radial to axial resilient strain to be stress-dependent. This crude approach of modelling radial resilient strains in the K-θ model with constant ν results in a poor prediction of volumetric strain of the triaxial specimens.

3. A far better prediction of volumetric strains can be obtained by using a stress-ratio dependent value of Poisson's ratio ν. Expressing ν as a function of the ratio of cyclic deviator stress over confining stress σ_c/σ_3 in conjunction with the K-θ model gives a good prediction of both volumetric and shear strains. This model is by all means adequate for pavement design purposes.

4. The K - θ model with stress-ratio dependent ν relates principal strains to principal stresses. Since these are the "as-applied" stresses and "as-measured" strains from the cyclic load triaxial test, the use of principal stresses and strains can be readily understood by practicing engineers. The major drawback, however, of this approach is that the influence of the various components of stress are is not dealt with explicitly. No distinction is made by the model between volumetric and shear deformation. Furthermore, the distinction between a chord and a secant approach to modelling cyclic load triaxial test results is lost using this model. The stresses applied in the cyclic load triaxial test and the resulting strains are incremental values, but the K - θ model with a stress-ratio dependent ν expresses them as a function of total stresses.

5. A better modelling of stress-strain behaviour can be obtained by separating stresses and strains into volumetric and shear components and relating the incremental strains measured to the incremental stresses applied.

6. Boyce's G-K model uses this approach under the strict conditions of elasticity. It contains only three parameters to relate volumetric strain ε_v and shear strain ε_s to mean normal stress p and shear stress q. Because of the use of only three parameters the model gives a poor prediction of volumetric strain.

7. Keeping to Boyce's approach of modelling volumetric and shear components of strain, but removing the strict requirements of elasticity, a five parameter model was obtained that gives a far better prediction of stains as a function of stresses. The accuracy of this model is such that it is by all means adequate for pavement design purposes.

8. A clear distinction should at all times be made between secant and chord values of stresses and strains. In the Constant Confining Pressure cyclic load triaxial test, increments of strain resulting from increments of stress are measured. The use of uniaxial Hooke's law to interpret the test results is therefore permitted. The situation of the granular material in-situ is a chord one too. The constant overburden stress is no more than a boundary condition, giving the material a certain initial stiffness. The increments of

stress caused by traffic loading result in increments of strain and these increments are of main interest for pavement design. The K - θ model involves a certain bias in dealing with stresses and strains since it expresses increments in strain as a function of total stresses. In the approach of using volumetric and shear components of stresses and strains, such bias is omitted.

With respect to the modelling of permanent deformation, the following conclusions can be drawn:

9. For modelling of principal permanent strains as a function of the number of load applications, the log-natural approach used widely in literature was shown to be not accurate when dealing with large numbers of load applications. Using a log-log approach, a satisfactory fit between model-predicted and measured strains can be obtained, even for tests with large numbers of load applications.

10. As was the case with the modelling of resilient strains, more insight into material behaviour under stress can be obtained by separating stresses and strains into volumetric and shear components.

11. The exemplary granular base course material LA0 and the sand EEN showed permanent dilation under a large number of load applications. In practical engineering terms, the dry density of the triaxial specimens decreased under prolonged cyclic loading. This finding raises doubt with respect to the occurrence of "post-compaction" under traffic loading, as often reported. Well compacted granular materials may exhibit shear deformation in-situ, which is mistakenly considered to be volumetric deformation.

8 IN-SITU TESTING

8.1 INTRODUCTION

Chapter 5 of this dissertation has dealt extensively with cyclic load triaxial testing of sands and granular base course materials. Resilient and permanent strain properties of these materials were determined on specimens with specified conditions of grading, moisture content and density. These laboratory tests yield the material parameters that are used as input to mechanistic pavement design.

It should be well noted that the material parameters determined in the laboratory indeed pertain to the specified conditions of grading, moisture content and density of the triaxial specimen tested only. In-situ, after construction of sand sub-base and granular bases, conditions of grading, moisture content and density may very well deviate from those of the triaxial specimen. For granular materials of say a 0/40 mm grading, segregation of the material may occur upon transportation and laying of the material, whereas for both sands and granular materials conditions of moisture and density are bound to show variations along the length and even the width of the pavement under construction. Furthermore, layer thickness may show variations of a few centimeters after compaction. Such variations are unavoidable in the practice of road construction, but when used as input to pavement design they may show to be quite significant.

For design procedures that attribute only limited structural capacity to granular base and sub-base, the approach of working with fixed design parameters for material stiffness and layer thickness may be appropriate. When actual values of stiffness and thickness are lower than those assumed for the design, this will not lead to excessive pavement distress since the design procedure underestimates the structural capacity of the granular layers anyhow. However, when the structural capacity of the granular layers is to be used in the design to its full extend, then the use of fixed values for material stiffness and layer thickness is only justified if after construction a statistically sound check of the design assumptions is made.

A first approach to checking whether the contractor's work meets the design assumptions is to determine in-situ density, moisture content, grading and layer thickness. Of these four parameters, in practice only the in-situ dry density (and with it the moisture content) is checked. In-situ grading is at best checked on sight only by looking for segregated patches. Determination of in-situ layer thickness is hardly feasible since it involves a too large inaccuracy to be of any use. Even if all four parameters (density, moisture content, grading and layer thickness) were measured in-situ, still this first approach to checking design assumptions in-situ would be an indirect one. Density and moisture content, for instance, are by themselves of limited interest only, since they are not straightforwardly correlated to the design parameter which is of real interest, being the elastic stiffness and the resistance to permanent deformation. Furthermore, determination of these parameters in-situ is too cumbersome and time-consuming to allow for a sufficient number of measurements to be performed and the measurements themselves may involve too large inaccuracies to be of practical use in acceptance control of granular layers (see also Paragraph 2.8.2).

A far better approach to checking the contractor's work in-situ is the direct approach of determining the elastic stiffness and the resistance to permanent deformation of the laid-and-compacted granular layers. As noted in the literature review (Paragraph 2.8.2.2), the Plate Bearing Test is used in a number of countries for this purpose. This test is fundamentally sound since it involves application of realistic stresses and measurement of the resulting deformations. In Germany, the Plate Bearing Test forms an essential part of the pavement design procedure (see Paragraph 2.9.2.4). The subgrade and all successive granular layers are checked for their elastic stiffness using the Plate Bearing Test. The required stiffness as measured on each of the pavement layers is specified in the German pavement design guide (86).

As noted in the literature review, the German approach to checking in-situ granular layers is a thorough one, but also a very cumbersome and time consuming one. The Plate Bearing Test according to the German procedure takes over one hour per measuring point, which in practice may mean that measuring points are spaced too far apart to obtain a statistically sound measure of the stiffness of the granular layers. A

clear need therefore exists for development of a testing procedure that combines the fundamental approach of the Plate Bearing Test with ease and especially speed of execution.

This chapter describes an investigation [125] into the possibility of checking the design assumptions with respect to the stiffness of the granular layers by means of tests that are fast and preferably simple to perform. It will focus on the elastic stiffness, since the design calculations of flexible pavements only involve assumptions on that parameter. Four types of tests for in-situ determination of the elastic stiffness were performed on a specially built test pavement. The four tests carried out were:

- The Plate Bearing Test, according to the Dutch procedure [126].

- The "Dynamic Plate Bearing Test", being a copy of the static Plate Bearing Test, using a Falling Weight Deflectometer to apply the dynamic loading.

- The Falling Weight Deflectometer Tests, with measurement of the deflection bowl and back-analysis of individual layer moduli using the BISAR-program.

- The Clegg Impact Test, which is an empirical test that is very simple and fast to perform.

The standard static Plate Bearing Test was performed mainly for reference purposes, since the drawback of being too time-consuming was judged from the start as being a major obstacle towards implementation in every day practice of quality control of granular layers. The Dynamic Plate Bearing Test was set up as a copy of the static Plate Bearing Test, with removal of the obstacle of being time-consuming. The Falling Weight Deflectometer Test was included in the test program since it is already well implemented in the practice of pavement engineering in the Netherlands. The Clegg Impact Test, finally, was performed not to check its applicability for determination of fundamental stress-strain properties, but merely to check its potential as a device suited for use by the contractor himself to check the uniformity of the laid-and-compacted granular base.

No attempt was made to couple the stiffness parameters determined in-situ to the results of cyclic load triaxial tests. For such a coupling, an analytical tool capable of accurately calculating stresses in the granular base is required to cope with the stress-dependent stiffness of the granular materials. As will be discussed in Chapter 9, the computer programs based on linear elastic theory presently available do not yield realistic stress distributions for the granular layers and are thus not suited for coupling in-situ stiffness to laboratory determined stiffness. The solution to this problem lies with finite element calculations, but development of such an analytical tool lies well beyond the scope of this dissertation. The main goal of the research described in this chapter is development of an in-situ testing procedure, that couples speed and ease of execution to a fundamental nature. Such a fundamental test would allow for an analytical assessment at the design stage of the required outcome of the test, given the assumptions on material stiffness that form the input to the overall pavement design. The analytical tool required for that purpose is being developed in a parallel research project.

8.2 THE TEST PAVEMENT

For the research described in this and the following chapter a full scale test pavement was built at the outdoor Pavement Test Facility of the Road and Railroad Research Laboratory. The test facility consists of a 50 by 20 m large area where the natural clay subgrade has been replaced to a depth of 5 m by Eastern Scheldt sand. Figure 8.1 shows the lay-out of the test pavement built. It consists of six sections of each 7.5 m long, containing different granular base course materials. The granular bases were constructed at a width of 10 m and subsequently paved with a 6 m wide layer of asphalt. This cross-section was chosen to allow for measurements directly on the granular base and on the asphalt to be repeated over a period of several months. The measurements on the asphalt will be described in Chapter 9, whereas this chapter will deal with the measurements directly on the granular bases.

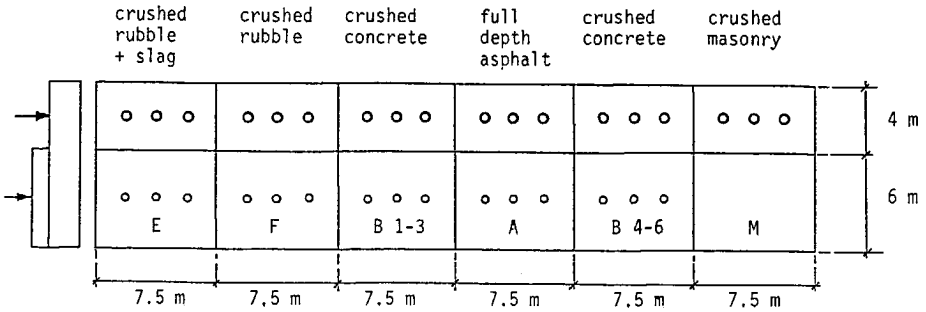

Figure 8.1: Lay-out of test pavement

The following granular base course materials were applied in the various sections of the test pavement:

- section E : crushed rubble with 10% electro-furnace slag
- section F : crushed rubble
- section B1-3: crushed concrete
- section A : no granular base, measurements performed directly on the Eastern Scheldt sand
- section B4-6: crushed concrete
- section M : crushed masonry

Sections E and F both contained the same commercial crushed rubble (a mixture of approximately 50% crushed concrete and 50% crushed masonry, by volume), the only difference being that to the material of section E 10% electro-furnace slag was added to increase its cementing potential. Sections B1-3 and B4-6 contained the same commercial crushed concrete; the only difference between these two sections was the thickness of the asphalt cover (see Chapter 9). Section A had a full-depth asphalt structure and, hence, no granular base. Section M finally had a granular base of commercial crushed masonry.

It should be noted here that the materials applied in the granular bases of the test pavement were not included in laboratory test program discussed in Chapter 5. For the construction of the test pavement, new large lots of commercially available materials were supplied. The materials applied all conformed with the specifications for recycled materials [14]. Hence, their composition and grading is similar to those of the materials tested in the laboratory progamme, within the limits of those specifications. The Eastern Scheldt sand

which forms the imported subgrade of the test pavement is the material OSN included in the laboratory test program.

As stated, the purpose of the research described in this chapter was the search for a fast and easy to perform test, capable of assessing in a fundamentally sound way the in-situ stiffness of the granular base and sand sub-base. To be able to properly judge the performance of the four types of tests carried out, three "identical" measuring points were incorporated in each section, as indicated in Figure 8.1. "Identical" here means that great care was taken in construction of the test pavement to ensure the same conditions with respect to grading, density, moisture content and layer thickness throughout each section. Although it would have been interesting to assess the capability of the various tests of observing variations in, for instance, density or layer thickness, this aspect was deliberately not investigated since the size of the various sections did not allow for building in variations in these properties.

To allow for comparison of the results of the various tests, all measurements for all four tests were performed at exactly the same locations. The three measuring points in each section were therefore duly marked and great care was taken to set the loading plate of the Plate Bearing Apparatus and the Falling Weight Deflectometer at exactly the marked position. The Clegg Hammer measurements were performed at the center of these positions. In all, each measuring point sustained three Plate Bearing Tests, three Dynamic Plate Bearing Tests, four Falling Weight Deflectometer Tests and four Clegg Hammer Tests. Although each of these tests involved application of several loads, the high density obtained in the various sections thanks to the use of full scale rolling equipment ensured no cross-influence between the various tests. Even at the end of the whole series of tests, no indentations could be observed on sight at the measuring points.

8.3 THE TEST PROGRAM

Part of the materials applied in the granular base courses of the test pavement are known to show self-cementing effects. Crushed concrete

and crushed rubble for instance were shown in cyclic load triaxial tests to have an elastic stiffness that increases considerably with time [127, 128]. The material crushed rubble with 10% electro-furnace slag shows a strong cementing effect thanks to the addition of the slag [128]. To deal with this increasing stiffness, the various tests on the granular base course were performed not only directly after compaction, but also one and three months after that. Since comparison of the results of the various tests was not by itself an aim of the research described here, no attempt was made to do all four tests on exactly the same day per measuring point.

Table 8.1 shows the time-schedule of the measurements. Rather than using calendar-dates, a day-numbering was introduced for ease of survey. "Day 0" was defined as the day on which the last layer of asphalt was built. As can be seen from Table 8.1, all four tests were performed upon completion of the test pavement and repeated approximately one and three months after that. The Falling Weight Deflectometer Tests and the Clegg Impact Tests were also performed roughly half a year after completion of the test pavement. For practical reasons, the other two tests were not performed at that time.

Table 8.1: Time-schedule of measurements on granular base.

test	day			
Plate Bearing	0	28	91	
Dynamic Plate Bearing	-7	37	111	
Falling Weight Deflectometer	14	43	87	182
Clegg Impact	-8	20	73	237

The negative day-numbering for the first series of Dynamic Plate Bearing Tests (Day -7) and the Clegg Impact Tests (Day -8) follow from the definition of Day 0 being the last day of asphalt paving. The particular series of tests were performed directly after compaction of the granular base, prior to asphalt paving. Performance of Plate Bearing Tests on all the measuring points took more than one day; the day-numbering indicated in Table 8.1 pertains to the first day of the particular series of tests.

8.4 PLATE BEARING TESTS

8.4.1 Introduction

As noted in the literature survey (Paragraph 2.8.2.2), the Plate Bearing Test dates back to the 1920's. Westergaard [84] then introduced his "modulus of subgrade reaction k" as a measure of the stiffness of the subgrade. Nowadays, the Plate Bearing Test is used in a number of countries to assess the stiffness of not only the subgrade but also of the granular layers above that. To obtain the stiffness in units on N/m^2 rather than Westergaard's k in N/m^3, the Burmister approach of interpreting Plate Bearing Test results is nowadays used. Since the test is performed on top of a finished layer and the plate bearing value is calculated from the ratio of the applied load to the resulting displacement of the plate, the test in fact measures the combined stiffness of the layer on which it is performed plus all layers below that. The test is performed at realistic stress levels, thereby dealing with the stress-dependent nature of the stiffness of the granular materials and the subgrade. Finally, the thickness of the various pavement layers is not entered into calculation of the plate bearing value, thereby avoiding interpretation problems caused by a wrong estimate of layer thickness.

From the above it follows that the plate bearing value is a fundamental parameter on the one hand and a very simple to interpret one on the other hand. The support to the asphalt structure after completion of the pavement by all layers below is expressed in a single parameter in sound engineering units. Whether a given level of poor support at a particular measuring point originates from a locally low stiffness of the granular material or from a locally insufficient layer thickness cannot be recognized from the test result of the Plate Bearing Test. However, the origin of a poor support is of minor interest only in quality control of the granular layers. It is the overall support to the asphaltic cover that is the parameter of interest. If a locally low stiffness of the granular layer itself happens to be compensated for at the same location by a greater layer thickness, the Plate Bearing Test will give the same support-value as when both stiffness and thickness were at their target values and the asphaltic cover will indeed get the target-support at the particular location.

Eventually, when finite element calculations of pavement structures will be implemented, the required plate bearing values for the top of the subgrade, the sub-base and the granular base can be calculated prior to construction, given the design-assumptions on the stiffness of the various unbound materials. By then performing Plate Bearing Test or similar, faster to perform tests on top of each layer, a simple check whether or not the design assumption of the ultimate support to the asphalt cover has indeed been achieved at, say, 95% of all measuring points can be made. If this is not the case, the contractor can be told to improve his product. If the support is significantly higher than assumed in the design, even a reduction in asphalt thickness might be considered. This is in fact the approach of the Germans in pavement design and construction (see Paragraph 2.9.2.4), beit that nowadays the basis of the acceptance procedure can become an analytical one rather than an empirical one.

8.4.2 Test procedure

The Plate Bearing Test is performed in a number of countries, each having their own procedure. These procedures differ in number of load applications and load duration. The tests described here were carried out by the Road and Hydraulic Engineering Division of Rijkswaterstaat according to their own procedure, which will be detailed here. For comparison between the various Plate Bearing Test procedures, reference is made to the literature [129].

Figure 8.2 shows the principle of the Plate Bearing Test apparatus used. It consists of a hydraulic actuator mounted on a heavy truck which provides the reaction force for the actuator. The load is applied to the unbound layer to be tested through a steel plate of 300 mm diameter. A load cell incorporated in between the actuator and the loading plate measures the applied force. The vertical displacement of the loading plate is measured by an LVDT, connected to a 4.5 m long reference beam. The length is of beam ensures that its supports at either end stand outside the influence area of the applied plate load.

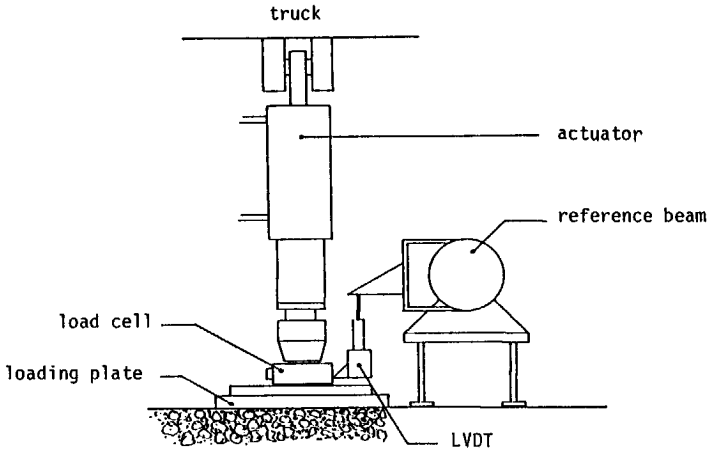

Figure 8.2: Principle of Plate Bearing Test apparatus.

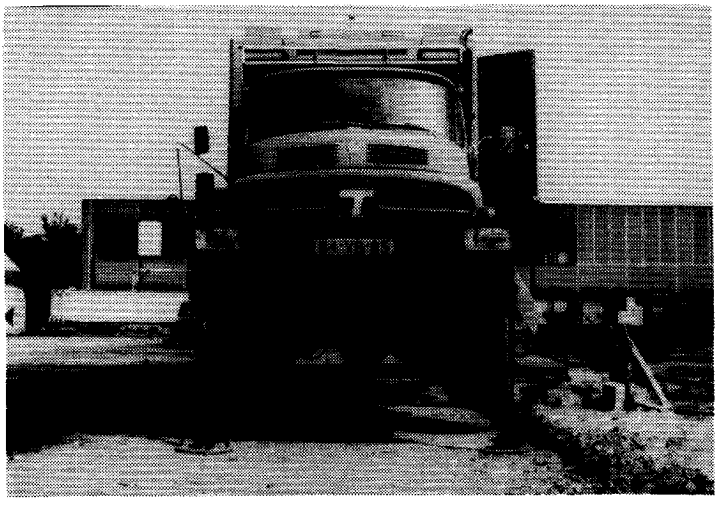

Figure 8.3: Plate Bearing Test in progress

The test procedure applied involves seven applications of a 36 kN load on the 300 mm diameter loading plate, which results in a vertical stress on the layer to be tested of 509 kPa. Certainly for the granular base course this can be seen as a realistic stress level, comparable to the vertical stress on the granular base under truck loaded asphalt. Prior to the application of the 36 kN load, a pre-load of 1 kN (vertical stress 14 kPa) is applied to exclude the effect of play within the apparatus. The 1 kN pre-load is maintained throughout

the test. The 36 kN load is then applied in one step, maintained for three minutes and then released in one step back to the 1 kN pre-load. The applied load and the resulting deformation are registered on an X-Y recorder. The whole load on-load off cycle is repeated to a total of seven load applications. Only the seventh load on-load off cycle is used for analysis, thereby excluding inelastic effects such as crushing of particles at the load plate/granular material interface from influencing the test results. Figure 8.3 shows the Plate Bearing Test being carried out on the unpaved stretch of the test pavement, while Figure 8.4 shows a detail of the loading plate.

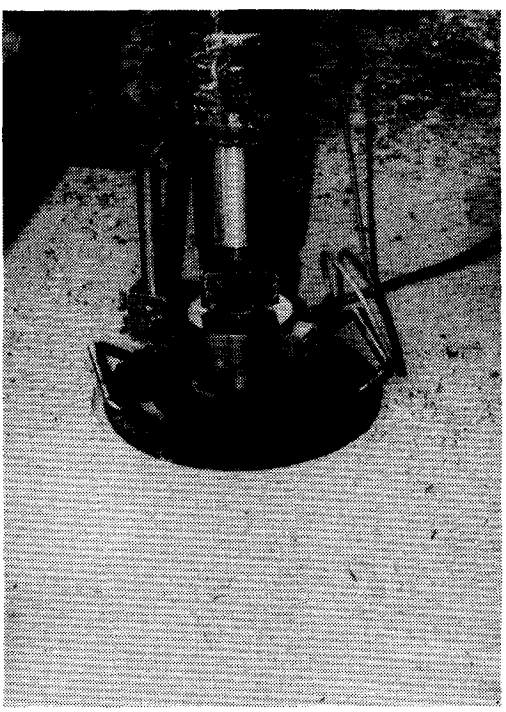

Figure 8.4: Detail of loading plate

8.4.3 Interpretation

Figure 8.5 shows a typical load-displacement diagram from the Plate Bearing Test for the seventh load application. The load-displacement

line is curved, which is consistent with the stress-dependent behaviour of the granular material. At the beginning of the loading, stresses in the material are small resulting in a low stiffness and, hence, a large displacement per unit load. On increasing the load, the material stiffness increases and the displacement per unit load decreases. In the standard interpretation of the Plate Bearing Test, a tangent is drawn to the load-displacement curve through the point of maximum load/displacement and the plate bearing value is obtained from that tangent. In other words, not the total displacement w of the plate is used for analysis, but only part of it. This "correction" is applied to deal with possible inelastic effects at the loading plate/material interface.

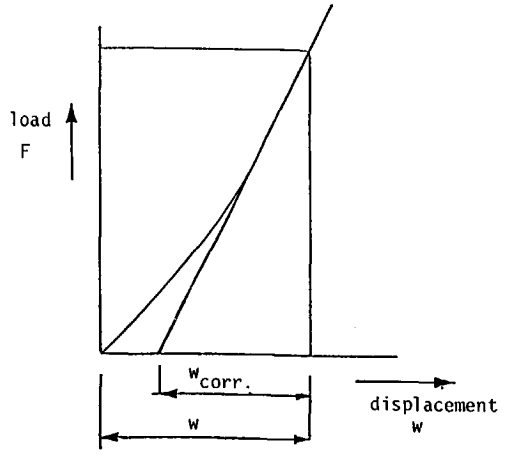

Figure 8.5: Typical load-displacement diagram for the Plate Bearing Test (seventh load application).

However, as noted earlier such inelastic effects as crushing of grains only occur in the first load applications, which are not used for analysis. On the seventh load application, significant inelastic effects will not occur and, hence, no correction for that should be applied. As stated, the curved nature of the load-displacement line originates from the non-linear stiffness properties of the granular materials and not from inelastic effects. Hence, in the analysis presented here the full displacement as measured in the test will be used.

When the Plate Bearing Test is performed on a linear elastic half-space, the displacement of the plate can be calculated from:

$$w = \frac{f\sigma_0 a}{E}(1 - \nu^2) \qquad (8.1)$$

where

- w = displacement of loading plate centre
- σ_0 = average stress on loading plate
- a = radius of loading plate
- E = Young's modulus
- ν = Poisson's ratio
- f = $\pi/2$ for rigid loading plate (peak stresses at edge loading plate)
- f = 2 for non-rigid loading plate (uniform stress distribution)

Reversing Equation 8.1, the parameter of interest being Young's modulus of the half-space can be calculated from

$$E = \frac{f\sigma_0 a}{w}(1 - \nu^2) \qquad (8.2)$$

In reality, the Plate Bearing Test is of course not performed on an elastic half-space. For the measurements performed directly on the sand in the test pavement discussed here, one might consider the 5 m thick layer of Eastern Scheldt sand to behave as a half-space. The stresses due to the plate load will have decreased at 5 m depth to a negligible level and, hence, the bulk of the displacement originates from the sand layer. Neglecting stress-dependent material behaviour, the "E-modulus" calculated from Equation 8.2 would then be the E_3 of the sand "subgrade".

The results of the tests performed on top of the granular base, however, can no longer be interpreted in terms of a half-space. Then, the test is performed on a relatively stiff layer of limited thickness, placed on the sand "half-space". The bulk of the displacement

measured still originates from the sand layer because of its low stiffness and large thickness and the main effect of the granular layer is that it reduces the stresses applied to the top of the sand "half-space". The "E-modulus" calculated from Equation 8.2 now represents the combined stiffness of the granular base and the sand "subgrade" and will therefore be denoted here as E_{2+3}. Actually, the parameter calculated from Equation 8.2 using the displacement measured on top of the granular base is no more or less than Young's E-modulus of a true elastic half-space giving the same support to the asphalt layer as does the granular base/sand combination. The advantage of this approach is that the support to the asphalt layer is characterized in a single, easy to interpret parameter. The main disadvantage is that all coupling to the reality of two combined layers with separate, stress dependent stiffness properties has been lost.

8.4.4 Back-analysis of individual layer moduli

Individual layer moduli can be obtained from the results of Plate Bearing Tests using a back-analysis procedure. Certainly when no cyclic load triaxial testing equipment is available, this seems to be quite a direct and fundamental approach to establishing the stiffness parameters of individual materials that are needed for today's mechanistic design procedures. To obtain sufficient input data for this back-analysis, Plate Bearing Tests then have to be performed on top of each subsequent granular pavement layer. In case of the test pavement discussed here, the individual stiffness of the granular base E_2 could be back-analysed from the test results obtained directly on the sand (denoted as E_3) and on the sand plus granular base structure (denoted above as E_{2+3}).

The classical approach to such a back-analysis of individual layer moduli is using a combination of Boussinesq's solution for displacements in a half-space [63] and Odemark's theory for transferring multi-layered systems into an elastic half-space [65]. Figure 8.6 shows an interpretation-graph for Plate Bearing Test results developed by Odemark, with notations adapted to the ones used here. On the vertical axis the ratio of E_3/E_{2+3} is plotted against the ratio of the thickness of the granular base h_2 to the radius of the loading plate a on the horizontal axis. Using these two ratios as input, the ratio of

the individual stiffness of the granular base E_2 to that of the subgrade E_3 can be obtained from Figure 8.6.

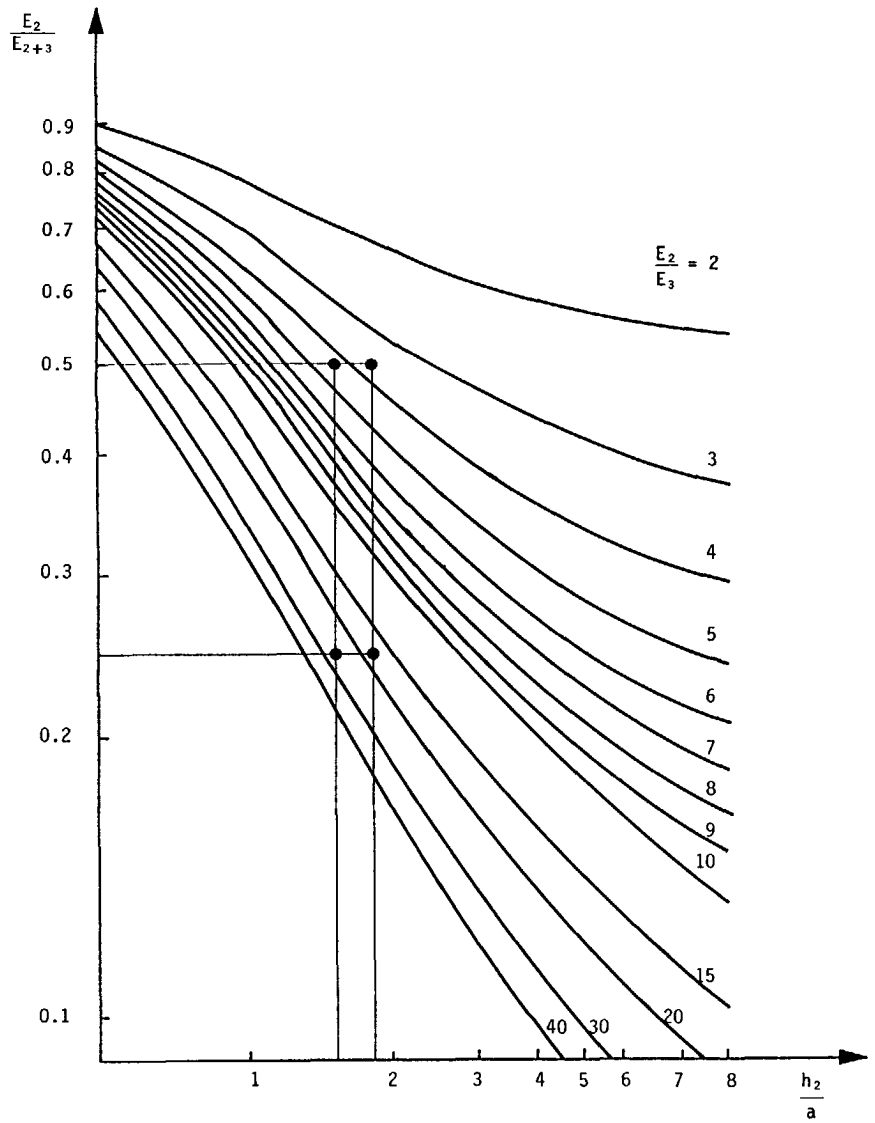

Figure 8.6: Odemark's interpretation graph for Plate Bearing Test results.

Of the four input parameters to Figure 8.6, the radius of the loading plate a is exactly known and the Plate Bearing Test results E_3 and E_{2+3} are known with sufficient accuracy, provided the proper equipment was used for the tests. Care should be taken that E_3 and E_{2+3} are

measured at the same location, if one wishes to back-analyse the individual stiffness of the granular base E_2 at that location from E_3 and E_{2+3}. The thickness of the granular base h_2, however, is known with limited accuracy only. In practice, if the contractor is supposed to construct the laid-and-compacted base to 25 cm thickness, the actual thickness is bound to vary between, say, 23 and 27 cm. Table 8.2 shows the influence of this variation in layer thickness on the outcome of back-analysing E_2 using Figure 8.6. The plate bearing value of the sand subgrade of the test pavement was taken at E_3 = 100 MPa, and the plate bearing value measured on top of the granular base was taken at E_{2+3} = 200 MPa and E_{2+3} = 400 MPa.

Table 8.2: Back-analysed stiffness of the granular base E_2 (Boussinesq/Odemark approach)

measured		back-analysed		
E_3 |MPa|	E_{2+3} |MPa|	E_2 |MPa|		
		h_2 = 230 mm	h_2 = 250 mm	h_2 = 270 mm
100	200	420	380	360
100	400	2600	2000	1750

As can be seen from Table 8.2, the influence of a wrong estimate of the thickness of the granular base h_2 has only limited influence on the back-analysed E_2 value in case of the granular base having only a limited stiffness (plate bearing value E_{2+3} = 200 MPa). When, however, the granular base has a large stiffness (plate bearing value E_{2+3} = 400 MPa), then the thickness of the base has quite a large effect indeed on the outcome of the back-analysis and the possible error due to a wrong estimate of the h_2 may be as high as 30%. A plate bearing value of E_{2+3} = 400 MPa certainly is not unrealistic; values in that order of magnitude were, for instance, measured on blast furnace slag bases on a test pavement of the Province of Zuid-Holland in the Netherlands [16].

Table 8.3 shows the same exercise as Table 8.2, this time using the BISAR-program to back-analyse the stiffness of the granular base E_2. The E_{2+3} values of 200 and 400 MPa were converted to "center-deflections" of 335 and 670 µm, respectively. E_2 was fitted until the calculated deflection matched the measured one to within 1 µm, using the plate bearing value E_3 = 100 MPa as the stiffness of the subgrade. As expected, the results are similar to those of the Boussinesq/Odemark analysis; again large deviations are found in case of high stiffness of the granular base.

Table 8.3: Back-analysed stiffness of the granular base E_2 (BISAR-approach)

measured		back-analysed		
E_3 |MPa|	E_{2+3} |MPa|	E_2 |MPa|		
		h_2 = 230 mm	h_2 = 250 mm	h_2 = 270 mm
100	200	383	355	335
100	400	2300	1935	1660

The results shown in Table 8.2 and 8.3 show that certainly in case of stiff granular bases the back-analysis of the individual stiffness of the granular base E_2 is too sensitive to a wrong estimate of the thickness of the granular base to be of practical use. One might argue here that the thickness of the granular base should be measured at each point analysed. However, in addition to being cumbersome, such a measurement is inaccurate. It is quite doubtful whether the actual thickness of the granular base can be measured with an accuracy of, say, 1 cm.

The conclusion therefore is that the Plate Bearing Test should be used for its original purpose only, being the establishment of a measure of the support given by a combination of layers to all layers above, expressed in a single, easy to interpret parameter. The stiffness of

individual materials should be determined in the laboratory on the material by itself, isolated from all other pavement materials. Such an approach is standard in other fields of civil engineering such as steel and concrete engineering, and should also be applied in pavement engineering now that analytical/mechanistic design procedures are being implemented.

8.4.5 Test results

Figure 8.7 shows the results of the Plate Bearing Tests performed on the granular bases and on the sand "subgrade" of the test pavement described in Paragraph 8.2.

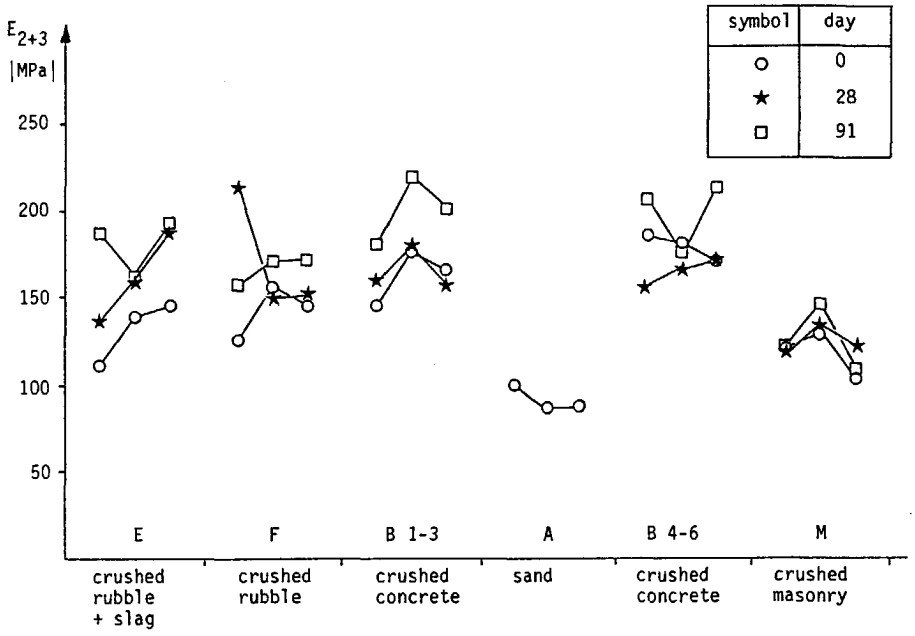

Figure 8.7: Results of Plate Bearing Test.

The measured load and displacement data were interpreted using Equation 8.2 to obtain the combined stiffness of the granular base and the sand subgrade E_{2+3}, as plotted on the vertical axis in Figure 8.7. A uniform stress distribution was assumed under the loading plate, and hence the factor f in Equation 8.2 was set at f = 2. Poisson's ratio was chosen at $\nu = 0.35$. The Plate Bearing Tests were performed on Days 0, 28 and 91 at three measuring points in each of the six sections of

the test pavement. The tests were performed on top of the granular base, with the exception of section A (full depth asphalt structure), which had no granular base. At this section, the Plate Bearing Tests were performed on the sand and thus yielded the stiffness E_3 of the "half-space" of sand. For this particular section, the vertical axis of Figure 8.7 should therefore read E_3 rather than E_{2+3}.

From the results depicted in Figure 8.7, the following conclusions can be drawn:

1. The influence of the bases is clearly reflected in the test results. All sections with a granular base show a higher value for the combined stiffness E_{2+3} than does section A for the stiffness of the sand subgrade E_3.

2. Looking at the results of the measurements on Day 0, the quality of the various granular bases is reflected in the test results. Crushed masonry shows the lowest E_{2+3}-value, and crushed concrete the highest. Crushed rubble (sections E and F) being a mixture of crushed concrete and crushed masonry shows an intermediate stiffness E_{2+3}.

3. There is some evidence of stiffening of the granular bases with time for all materials except crushed masonry. As will be discussed later in Chapter 9, the increase of stiffness of this type of (self-)cementing granular bases has a considerable influence on asphalt tensile strain. It should be noted here that the Plate Bearing Tests on the sand (section A) were only performed on Day 0, since the Eastern Scheldt sand shows no self-cementing effects.

8.5 DYNAMIC PLATE BEARING TESTS

8.5.1 Introduction

In the previous paragraph, the Static Plate Bearing Test has been discussed as a fundamental type of test that applies realistic stresses to the structure tested and measures the resulting displacement. The

support provided to all layers above is expressed in a single, easy to interpret parameter in sound engineering units. No complicated interpretation-software is required for analysing the test results; the plate bearing value is calculated straightforwardly from the ratio of the applied stress over the resulting displacement. As noted, the Static Plate Bearing Test has one major drawback. It simply requires too much time to be of practical use in a statistically sound quality control procedure.

The Dynamic Plate Bearing Test discussed in this paragraph was developed as a copy of the static Plate Bearing Test, with removal of the one major drawback of the test. Rather than using static plate loading, the Dynamic Plate Bearing Test uses impact loading, thereby drastically reducing the time required per test and eliminating the need for a heavy reaction load. Because of its widespread availability in the Netherlands, a Falling Weight Deflectometer apparatus was used to apply the impact loading for the testing of the granular bases of the test pavement described in Paragraph 8.2. Any other means of applying impact loading could, however, be used to perform the Dynamic Plate Bearing Test, provided the applied loading is of sufficient magnitude to yield realistic stresses in the granular base course.

8.5.2 Test procedure and interpretation

Figure 8.8 shows the principle of the Dynamic Plate Bearing Test. The drop-weight of the Falling Weight Deflectometer falls from an adjustable height onto the buffer/loading plate assembly. The mass of the drop-weight and the height from which it fell were adjusted in such a way that the impact load on the layer tested was similar to that of the static Plate Bearing Tests. The impact load, however, does not only depend on the mass and the drop-height, but also on the combined stiffness of the layers on which the test is performed. Bearing in mind the prerequisite of developing a test which is fast to perform, no attempt was made to obtain the same impact loading at each measuring point of the test pavement by adjusting the mass of the drop weight and the drop height for each point individually. The mass and the drop height were kept constant throughout all tests, resulting in

impact loadings between 20 and 30 kN. Figure 8.9 shows the Dynamic Plate Bearing Test in progress.

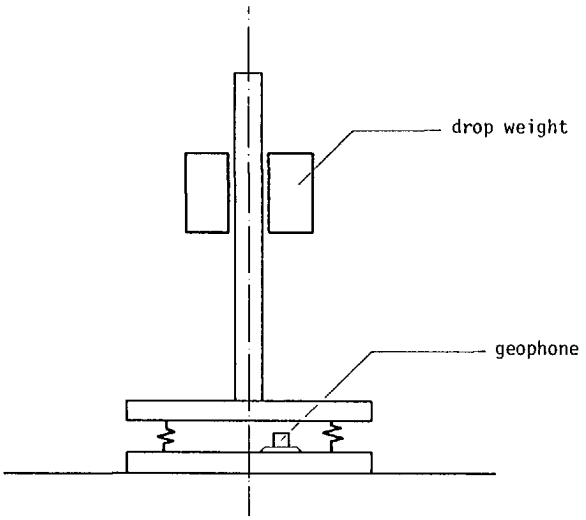

Figure 8.8: Principle of Dynamic Plate Bearing Test.

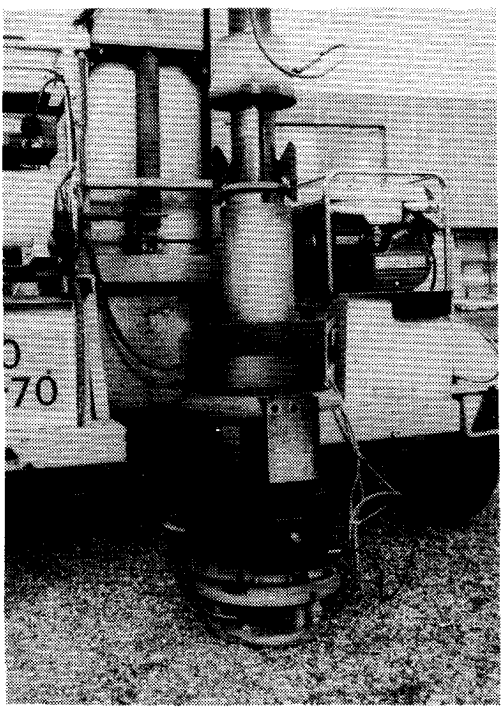

Figure 8.9: Dynamic Plate Bearing Test in progress.

Since it was the purpose to develop a dynamic copy of the static Plate Bearing Test, the measurement of the displacement was quite different from the method used in standard Falling Weight Deflectometer tests. The geophone measuring the velocity of the loading plate on impact was placed òn the loading plate, instead of on the layer tested through the hole in the loading plate. The measured velocity therefore after integration by the FWD-hardware yielded the displacement of the loading plate on impact. A second distinction with standard FWD-measurements is that the rubber plate attached to the bottom of the loading plate was removed and the loading plate was thus placed directly on the granular material in the layer to be tested. If the tests were carried out with the rubber plate, the stiffness of the rubber plate would influence the test results since the geophone was set on the loading plate. To ensure good contact between the loading plate and the granular material tested, each Dynamic Plate Bearing Test consisted of four applications of the impact loading, using only the displacement of the fourth blow for analysis. The influence of individual particles protruding from the granular layer was thereby excluded from the test results. Figure 8.10 shows a detail of the loading plate on a granular base course.

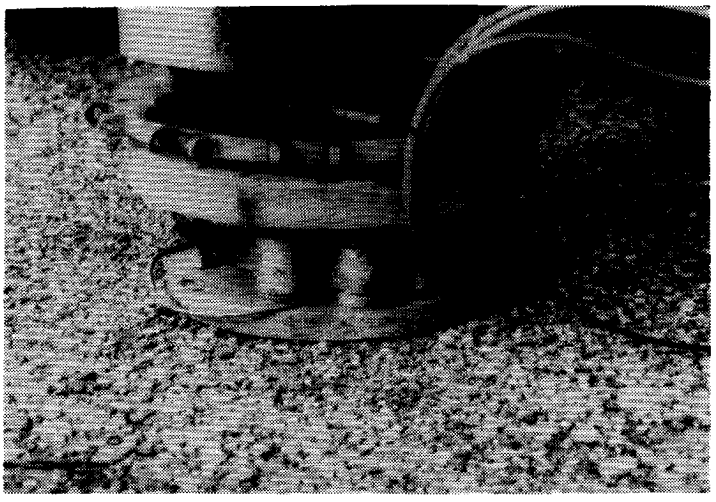

Figure 8.10: Detail of loading plate.

The interpretation of the test results was equal to that used for the static Plate Bearing Tests. Equation 8.2 (Paragraph 8.4.3) was used to

obtain a single stiffness parameter for the layer on which the test was performed plus all layers below. In case of testing on the granular base courses of the test pavement, the Dynamic Plate Bearing Test therefore yielded after interpretation the E_{2+3}-parameter discussed earlier and in case of testing on the sand the E_3-parameter of the sand "half-space" was obtained. As with the static Plate Bearing Tests, no attempt was made to back-analyse individual layer-moduli from the measured load and displacement data.

It should well noted here that the FWD-hardware used to measure the applied load and the resulting deformation does not yield a full load-displacement diagram as the one depicted in Figure 8.5 for the static Plate Bearing Test. The dynamic signals for the applied load and the resulting displacement in the Dynamic Plate Bearing Test are measured by the FWD-hardware using a so-called "peak detector", which only yields maximum load and maximum displacement. The measured data of the Dynamic Plate Bearing Test therefore consists of two numbers only, as opposed to the full load-displacement diagram measured in the static Plate Bearing Test. The interpretation of the dynamic and the static test however were completely equal, since for the static test too maximum load and maximum displacement were used for analysis (see Paragraph 8.4.3).

8.5.3 Test results

Figure 8.11 shows the results of the Dynamic Plate Bearing Tests performed on the granular bases and on the sand "subgrade" of the test pavement. The tests were performed directly after compaction of the granular bases (being seven days before asphalt paving, hence the numbering Day -7) and 37 and 111 days after paving.

From the results depicted in Figure 8.11, the following conclusions can be drawn:

1. As was the case with the static Plate Bearing Tests, the influence of the granular base is clearly reflected in the test results. All sections with a granular base show a higher value for the combined stiffness E_{2+3} than does section A for the stiffness of the sand subgrade E_3.

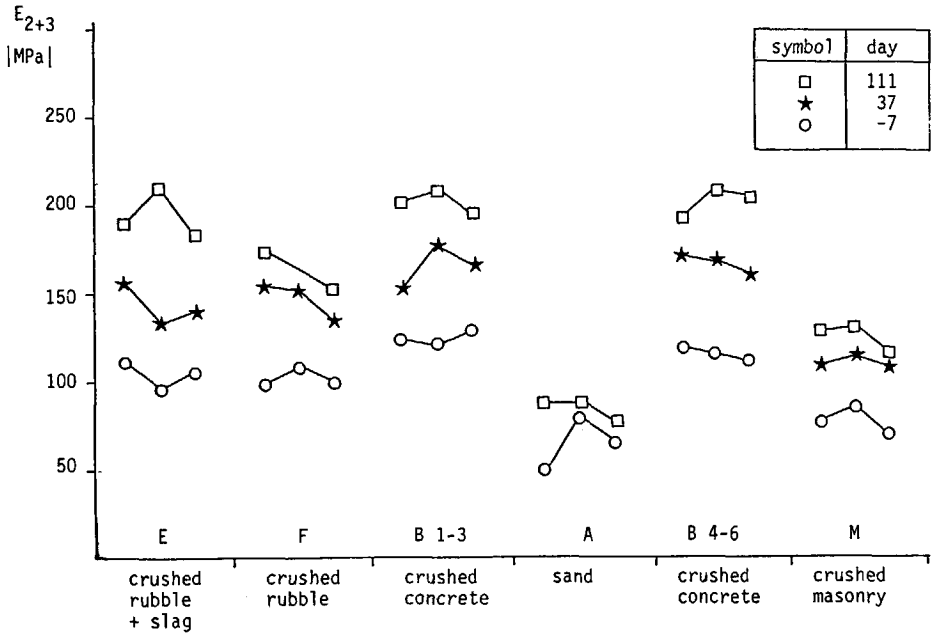

Figure 8.11: Results of Dynamic Plate Bearing Tests.

2. Looking at the results of the tests on Day -7, the quality of the various granular bases is clearly reflected. Crushed masonry shows the lowest E_{2+3}-value, and crushed concrete the highest. Crushed rubble (sections E and F) with and without the addition of the slag shows an intermediate stiffness. This difference in quality of the granular base course materials of the test pavement is consistent with expectation. The cyclic load triaxial test results for crushed masonry, crushed concrete and crushed rubble discussed in Chapter 5 (see Table 5.4, Paragraph 5.3.2.5) indicated the same ranking in elastic stiffness. Crushed masonry (section M) shows an E_{2+3}-value almost equal to the E_3-value of the sand subgrade (section A), indicating a similar stiffness for the crushed masonry and the Eastern Scheldt sand. Again, this in-situ finding is consistent with the cyclic load triaxial test results discussed in Chapter 5 (see Tables 5.4 and 5.7, Paragraph 5.3).

3. The test results indicate a substantial stiffening of the granular bases with time due to cementing effects. Crushed masonry (section M) shows some stiffening, probably due to the mortar being present in the material. Crushed rubble with slag (section E), crushed

rubble (section F) and crushed concrete (sections B1-3 and B4-6) show a large increase in stiffness. It should be noted here once again that the E_{2+3}-parameter indeed expresses the combined stiffness of the granular base and the sand subgrade. To increase E_{2+3} with the numerical values shown in Figure 8.11, the increase in stiffness of the granular base itself must indeed be quite substantial, taking into account the small layer thickness of the base (25 cm) as compared to that of the subgrade.

4. The tests on the sand subgrade (section A) were repeated on Day 111. As expected, little variation in stiffness was found.

5. The repeatability of the tests proves to be good. Scatter within the sections is small, whereas the two crushed concrete sections (B1-3 and B4-6) show almost identical results, which is consistent with the structure of both section being equal.

6. Comparing the results of the Dynamic Plate Bearing Test (Figure 8-.11) to those of the static Plate Bearing Test (Figure 8.7), it can be observed that the results from the last series of both tests indicate the same stiffness values for the various granular bases. The first series of measurements with the Dynamic Plate Bearing Test indicates a somewhat lower stiffness than the first series of the static Plate Bearing Test. This difference in stiffness can be explained by the fact that the first series of Dynamic Plate Bearing Tests was performed directly after compaction of the granular bases (Day -7), whereas the first series of static Plate Bearing Tests was performed one week later (Day 0). The rate of increase in stiffness for these materials is highest directly after compaction, which explains for the differences found here.

8.6 FALLING WEIGHT DEFLECTOMETER TESTS

8.6.1 Introduction

The Falling Weight Deflectometer Tests is used widely in the Netherlands and a number of other countries as a non-destructive means of assessing the structural condition of flexible pavements. The

principle of the test is rather straightforward: an impact loading similar in magnitude and duration to that of truck traffic is applied to the pavement and the vertical displacements of the top of the pavement (the so-called "deflections") are measured at a number of fixed positions relative to the load center. When done at regular time intervals, FWD-tests can be used to monitor the deterioration of the structural condition of the pavement and remedial measures such as construction of an asphalt overlay can be applied in time prior to the onset of major structural damage.

Falling Weight Deflectometer tests are also used to determine the stiffness parameters of the individual layers that constitute the particular pavement. In this "back-analysis" of material parameters, a computer program like BISAR capable of calculating deflections in a pavement structure is run in a trial-and-error manner until the calculated deflection bowl matches the measured one within the limits of a given accuracy. As discussed earlier, the so obtained material stiffness are "structure parameters". They are indeed no more or less than the E-moduli that should be used as input to the particular computer program to obtain the measured deflections. Great care should be taken in using the structural parameters thus obtained on one pavement for the design of another pavement. Focusing on the granular materials, back-analysis of FWD-measurements yields a single "E-modulus" for the whole granular layer, ignoring the stress-dependent behaviour of the material. For analysis of the particular pavement tested this structural parameter E may be used to characterize the elastic properties of the granular base. However, for another pavement with, for instance, a different asphalt thickness, the particular E-modulus will not do. The stresses in the granular base will be different and, hence, also the stiffness of the granular base course material.

The whole approach of obtaining individual material parameters from measurements on completed structures is quite typical for pavement engineering. In the field of structural engineering, consideration would not be given to obtaining, for instance, the E-modulus of steel by placing a heavy lorry on a steel bridge and substituting E-moduli into the design of that bridge until the calculated deflection of the bridge matches the actual deflection. Yet, in pavement engineering more and more consultants are using this type of approach to obtain

the material parameters needed for design. As stated earlier, individual material parameters should be determined in the laboratory using a suitable test on the particular material by itself, isolated from the rest of the pavement structure. Having obtained all the individual material parameters needed, the pavement structure can then be designed. In addition to calculating the main design parameters such as asphalt tensile strain and vertical compressive subgrade strain, also the deflections of the pavement under the FWD-loading can be calculated beforehand in a "forwards-analysis" type of approach. After completion of the pavement, FWD-measurements can then be used directly to check whether the design assumptions have been met by the contractor's work. By repeating the FWD-measurements at regular intervals, the structural condition of the pavement can be monitored, and remedial action can be taken before the onset of severe deterioration.

This paragraph describes the Falling Weight Deflectometer tests performed directly on the granular base of the test pavement. The main reason for including FWD-tests in the program was to investigate their suitability for use in the "forward-analysis" type of approach discussed above.

8.6.2 Test procedure

Figure 8.12 shows the principle of the Falling Weight Deflectometer Test. The drop weight of the FWD falls from an adjustable height onto the loading plate/buffer assembly. The resulting "deflections" (displacements in vertical direction) are measured by six "geophones" (velocity transducers). The first geophone stands on the layer to be tested through a hole in the loading plate, while the rest of the geophones stand at pre-selected distances from the load centre. For the tests described here, geophone distances were chosen at 0, 300, 500, 1000, 1500 and 2000 mm from the load centre. The FWD-hardware integrates the measured velocities and displays the peak value of the deflections thus obtained. The mass of the drop weight and the height from which it fell were taken constant for all tests, yielding impact loadings between 20 to 30 kN. The loading plate was standardly equiped with the rubber plate at its bottom.

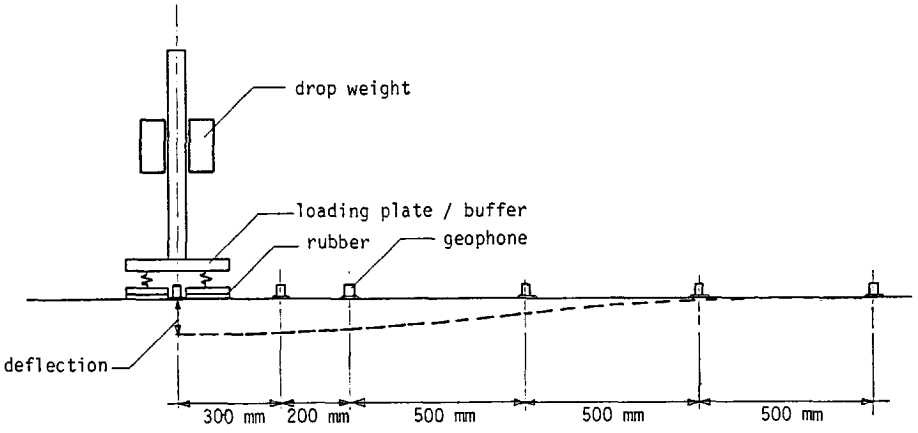

Figure 8.12: Principle of the Falling Weight Deflectometer Test.

Figure 8.13: Falling Weight Deflectometer equipment.

For sake of conformity with the Dynamic Plate Bearing Tests described in the previous paragraph, each FWD-test on a given measuring point consisted of four applications of the FWD-loading, using only the deflections measured on the fourth loading for later analysis. Great care was taken to set the geophones correctly on the uneven surface of the granular base. Figure 8.13 shows the FWD-equipment, while Figure 8.14 shows a detail of the geophones on the granular base. The FWD-tests on the granular base course were performed on Days 14, 43, 87 and 182.

Figure 8.14: Detail of geophones on granular base.

8.6.3 Interpretation

As noted above, finite element analysis of pavement structures lies beyond the scope of this dissertation. Therefore, no forward-analysis translating cyclic load triaxial test data into in-situ deflections under the FWD-loading was performed. The measured FWD-deflections were interpreted only in the standard way of back-analysing individual layer-moduli by matching BISAR-calculated deflections to the measured deflections. The computer program MISS (Moduli Information System) [130] was used for this purpose. The program uses an iterative procedure with the BISAR-program as a sub-routine to match calculated and measured deflections. The fit between calculated and measured values was judged to be sufficiently accurate when deflections matched within 2% or moduli within 0.5%, for five consecutive iterations.

In addition to the measured load and deflections also the dimensions of the structure tested are input to the back-analysis program. As stated earlier when discussing the back-analysis of individual layer moduli from Plate Bearing Test data (Paragraph 8.4.3), the layer thickness of the granular base is generally known with limited accuracy only. A similar exercise as done with the Plate Bearing Test interpretation was therefore also carried out for exemplary FWD-data.

Table 8.4 shows two deflection bowls, one for a relatively weak granular base and one for a relatively stiff granular base, interpreted for three thicknesses h_2 of the granular base (h_2 = 230, 250 and 270 mm). Deflection bowls that were actually measured on the granular base of the test pavement were used for this exercise. They were selected in such a way that the center deflection matched the vertical displacement of the loading plate of the exemplary Plate Bearing Test discussed earlier as closely as possible (see Tables 8.2 and 8.3; E_{2+3} = 200 MPa means a vertical displacement of 335 µm, and E_{2+3} = 400 means a vertical displacement of 670 µm).

Table 8.4: Back-analysed stiffness of the granular base E_2 and of the subgrade E_3, from FWD-data

measured		back-analysed		
geophone distance |mm|	deflection |µm|	h_2 |mm|	E_2 |MPa|	E_3 |MPa|
0	670	230	163	123
300	223			
500	112	250	161	123
1000	55			
1500	41	270	159	122
2000	31			
0	339	230	587	134
300	163			
500	109	250	539	134
1000	55			
1500	36	270	501	134
2000	27			

As can be seen from Table 8.4, an error of + or -20 mm in the assumed thickness of the granular base has only little effect on the back-analysed stiffness of the granular base E_2 in the case of the relatively weak granular base. As expected, however, in case of a relatively stiff granular base the thickness of the granular base does have a substantial influence on the back-analysed E_2-value. An error

of + or -20 mm in the assumed thickness of the granular base yields a wrong estimate of E_2 of 8 and 7%, respectively. Comparing this error to the one found in back-analysing individual layer moduli from Plate Bearing Test results (see Tables 8.2 and 8.3, Paragraph 8.4.4), the improvement due to measuring deflections at various distances from the load centre as well as at the centre itself is clear. Using the same exemplary data, the error in back-analysed moduli from the Plate Bearing Test was 30%, while the additional information obtained in the FWD-test reduces the error to maximum 8%. Although such an error might be considered allowable in every-day practice, the values shown in Table 8.4 do hold a warning for back-analysing individual moduli when even stiffer granular bases are involved.

8.6.4 Test results

Figure 8.15 shows stiffness of the granular base E_2, as obtained from the back-analysis of the FWD-measurements. The FWD-tests were not performed on the sand subgrade (section A), since the disturbance of the surface of the compacted sand caused by the wheels of the FWD-equipment or even by walking has too great an influence to render such measurements of practical use.

From the results depicted in Figure 8.15, the following conclusions can be drawn:

1. Looking at the results of the measurements on Day 14, the quality of the granular bases is reflected in the results. Crushed masonry (section M) shows the lowest E_2-values, crushed concrete (sections B1-3 and B4-6) the highest and the two sections with the masonry/concrete mixture (sections E and F) show an intermediate stiffness.

2. The stiffening of the base courses with time is reflected in the test results, although at some points considerable scatter occurs. This scatter may partly result from inhomogeneities in the surface of the granular base. The diameter of the footing of the geophones used is similar to the maximum grain size of the granular material. Therefore, the measured deflections may have been influenced by the location of the geophones on the base. It is

virtually impossible to set the geophones on exactly (that is: within a few mm) the same location for each FWD-measurement. A small deviation in the position of the geophone may result in a difference in the measured deflection, which is subsequently enhanced by the back-analysis procedure which is very sensitive to small variations in deflections.

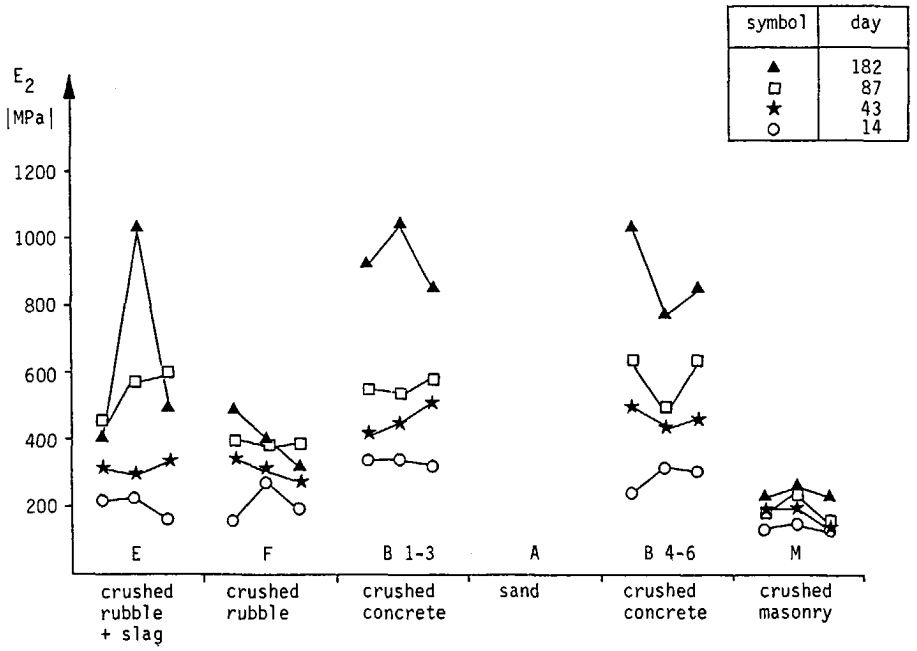

Figure 8.15: Results of FWD-tests: back-analysed stiffness of the granular base E_2.

3. Some of the stiffness values obtained from the measurements on Day 182 are quite high. E_2-values of up to 1000 MPa were obtained for certain points in the two crushed concrete sections (sections B1-3 and B4-6) and in the crushed rubble + slag section (section E). The scatter, however, in the stiffness values for Day 182 for these sections is also quite large, especially in section E. Part of this scatter may be realistic, in the sense that the actual in-situ stiffness shows a certain variation over the length of the section. If the absolute value of the stiffness increases, then the scatter in the stiffness will also increase. Other sources of scatter may be incorrect setting of the geophones on the granular base and a wrong estimate of layer thickness. As noted above, the

FWD back-analysis becomes more sensitive to layer thickness with increasing stiffness of the granular base. Table 8.5 shows the same excercise as given earlier in Table 8.4, this time for measuring point B2 on Day 182. The absolute scatter due to an error in the layer-thickness assumption of + or -20 mm is now larger; the relative scatter is 14 and 11%, respectively.

Table 8.5: Back-analysed stiffness of the granular base E_2 and of the subgrade E_3, for measuring point B2

measured		back-analysed		
geophone distance [mm]	deflection [μm]	h_2 [mm]	E_2 [MPa]	E_3 [MPa]
0	320	230	1191	136
300	174			
500	134	250	1045	136
1000	66			
1500	45	270	930	135
2000	33			

Without dwelling any further on the accuracy of Falling Weight Deflectometer Tests on granular base courses and their interpretation, it can be concluded that the straightforward approach of the Dynamic Plate Bearing Test discussed in Paragraph 8.5 involves less scatter in the test results than the more complicated FWD-tests. The two main advantages of the Dynamic Plate Bearing Test are that firstly the geophone stands on the loading plate and hence on a smooth surface. Secondly, the calculation of the E_{2+3}-value does not require the layer thickness of the granular base as input. Certainly, the Dynamic Plate Bearing Test gathers less information by using only one geophone, but in the forward-analysis discussed above the extra information obtained from the FWD-test using six geophones is not required. When Dynamic Plate Bearing Tests are performed on each of the successive layers of the pavement, sufficient information is gathered from this simple and fast to perform test to check the design assumptions on the individual stiffness properties of the materials applied.

8.7 CLEGG IMPACT TESTS

8.7.1 Introduction

Three types of test have been discussed so far in this chapter: the static Plate Bearing Test, the Dynamic Plate Bearing Test and the Falling Weight Deflectometer Test. All three tests are fundamentally sound. They apply the right level of loading on a realistic area, measure the resulting displacement and the test results are expressed in sound engineering units. All three tests are therefore suited for acceptance control by the principal of the contractor's work, beit that the static Plate Bearing Test is too cumbersome and time consuming and the FWD-test may involve inaccuracies in measurement and interpretation.

The main disadvantage of the three tests is that they require rather complicated, bulky and expensive equipment. The tests are therefore far less suited for use by the contractor himself in every-day practice of pavement construction. For this purpose, a small, portable apparatus would be required, again with the condition of giving a measure of stiffness in, say, a few minutes. The Clegg Impact Tester discussed earlier in Paragraph 2.8.3.1 is such an apparatus. As noted there, the Clegg Impact Test is in fact no more or less than a dynamic version of the CBR-test. A cylindrical drop weight having the same diameter as the CBR-piston is dropped inside a guide tube from a given height onto the layer to be tested, and the maximum deceleration on impact is measured by the electronics of the tester. The relationship between the Clegg Impact Test and the cumbersome in-situ CBR-test is therefore similar to that between the Dynamic Plate Bearing Test and the cumbersome static Plate Bearing Test. In both dynamic tests the requirement of a heavy truck as reaction load has been removed and the time required per test has been drastically reduced to a few minutes or even less.

Like the in-situ CBR-test, the Clegg Impact Test is of an empirical nature. Although the load applied in the test on impact of the drop weight may be as high as 20 kN (and thereby realistic for truck loading through asphalt on a granular base), the loaded area obviously is not realistic. Furthermore, the test result is expressed in units not

suited for use in pavement design. As noted, the parameter measured is the maximum deceleration of the drop weight upon impact. The electronics of the tester displays this deceleration in CIV-units, 1 CIV being ten times the unit of gravitational acceleration (1 CIV = 10 g). Like the in-situ CBR-test, the Clegg Impact Test too should therefore not be used in attempts to obtain fundamental parameters like E-moduli. The test is an empirical one, and should at all times be used as such. In that light the test was performed on the granular bases of the test pavement discussed earlier and for that reason no attempts will be made here to correlate the obtained CIV-values to the parameters obtained from the fundamentally sound tests.

8.7.2 Test procedure

Figure 8.16: Clegg Impact Test in progress.

Figure 8.16 shows the Clegg Impact Test being carried out on the granular base of the test pavement. The 4.5 kg drop weight is raised to the indicated height of 450 mm above the granular base and then released. The electronics of the tester then display the maximum deceleration on impact in CIV (1 CIV = 10 g).

The Clegg Impact Test was performed on Days -8 (directly after compaction of the granular base) and on Days 20, 73 and 237. The tests were carried out at the center of the measuring points used for the other three tests described earlier. Per measurement, four consecutive blows of the Clegg hammer were applied recording the CIV-value resulting from the fourth blow. No tests were performed on the sand subgrade (section A), since on sands the impact load causes major shear deformation of the material tested and hence no measure of elastic stiffness is obtained.

8.7.3 Test results

Figure 8.17 shows the results of the Clegg Impact Tests. From the results depicted, the following conclusions can be drawn:

1. The Clegg Impact Test shows to work remarkably well. Taking into account the small diameter of the drop weight (approximately 50 mm) relative to the particle size of the base course materials (up to 45 mm), far more scatter was expected then that showing up in the test results. It should be noted here that per measuring point all measurements were performed at exactly the same position on the granular base, with exception of the measurements on Day -8 which were carried out prior to duly marking of the measuring points.

2. For the first series of measurements (Day -8), the difference in quality between the various base course materials is not reflected in the test results. All other three tests discussed earlier showed crushed masonry (section M) to have the poorest quality, crushed concrete (section B1-3 and B4-6) the highest and the two crushed rubble sections (sections E and F) to be of intermediate quality. This order in quality is not reflected in the Clegg Impact Values obtained on Day -8: sections B4-6 for instance yields CIV-values similar to those of section M.

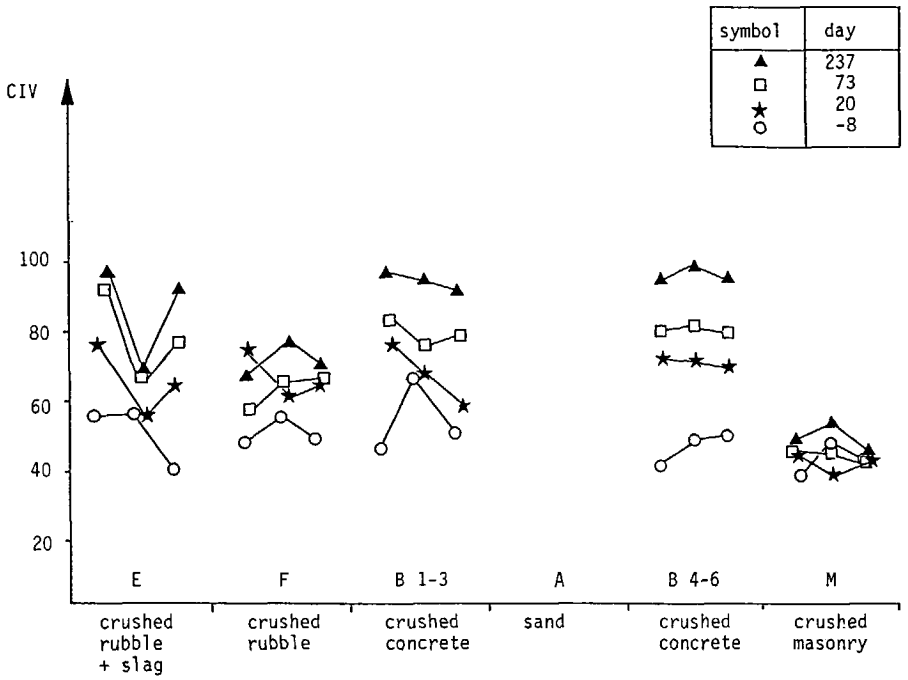

Figure 8.17: Results of Clegg Impact Tests

3. The stiffening of the granular bases with time is indicated by the test results. After this stiffening, the difference in quality of the various materials is reflected. The two crushed concrete sections and the section with crushed rubble with slag show the highest CIV-values, followed by the crushed rubble section. The crushed masonry section shows the lowest CIV-values.

8.8 CONCLUSION

The tests described in this chapter were performed on the granular bases of a specially built test pavement. The pavement was constructed with full scale construction plant, yielding granular bases with realistic densities. The following conclusions can be drawn with respect to the applicability of the tests in proof testing of granular layers:

1. Of the four tests performed, the static Plate Bearing Test, the Dynamic Plate Bearing Test and the Falling Weight Deflectometer Test are fundamentally sound. These tests apply realistic stresses to the granular base and measure the resulting deformation. The Dynamic Plate Bearing Test appears to be the most applicable one for proof testing of granular layers. The test is very fast to perform and no complicated analysis of the measured data is required to arrive at the parameter of interest, being the support provided for the asphalt by the pavement foundation as a whole. The static Plate Bearing Test is too time-consuming to be of practical use in statistically sound proof testing of granular layers. The Falling Weight Deflectometer Test is fast to perform, but the measured data need to be interpreted using a back-analysis program and the back-analysis is somewhat sensitive to variations in layer thickness.

2. The Dynamic Plate Bearing Test should be used in a "forward analysis" approach. At the design stage, the required outcome of the test should be calculated using a suitable analytical tool with laboratory-determined stiffness parameters of the various unbound materials as input. The design-assumptions on the stiffness of the successive unbound layers can then be checked in-situ by performing the Dynamic Plate Bearing Test on each successive layer. This approach is the same as that used in Germany for proof testing and design of granular layers, advocated in Chapter 2 as being a very thorough one indeed. The main advance is that the Dynamic Plate Bearing Test is very fast to perform and can, hence, be applied in a statistically sound way. The second main advance with respect to the German approach is that the basis of the proof testing of the pavement foundation can become an analytical one rather than an empirical one, thereby opening up the proof testing to new materials and new pavement structures.

3. The Clegg Impact Test was shown here to work remarkably well, given the small dimensions of the impact hammer relative to the particle size of the materials tested. The test is an empirical one and should be used as such only. Thanks to its simplicity and speed of operation, its small size and its low price the Clegg Impact Tester, however, does hold a great promise as a contractor's tool for assessing the uniformity of laid-and-compacted granular bases.

9 STRUCTURAL SIGNIFICANCE OF GRANULAR BASES - A CASE STUDY

9.1 INTRODUCTION

As discussed in Chapter 2, today's mechanistic pavement design procedures are based on the principle of calculating stresses and strains in pavement structures and comparing the calculated values to allowable values. Computer programs like BISAR and CHEVRON form the analytical back-bone of such mechanistic design procedures. The main drawback here is that the mechanistic design procedures implemented today use linear elastic theory for the calculation of stresses and strains. The use of linear elastic theory is, by definition, incompatible with a detailed analysis of the structural contribution of stress-dependent granular materials. As long as the main structural element of the pavement is formed by the asphalt layers, the use of linear elastic theory for pavement design is valid. When, however, the granular base plays a structurally important role, then a more detailed form of analysis incorporating stress-dependent material behaviour should be used.

Focusing on resilient stiffness, the determination of that parameter for a granular material in the laboratory yields, in the simplest form, the resilient modulus M_r as a function of the sum of principal stresses θ. When trying to use that resilient stiffness as input to a linear-elastic program like BISAR, the designer is faced with the problem that he cannot obtain a proper value for θ and, hence, for M_r. In case of granular bases having an resilient stiffness substantially higher than that of the lower layers, even negative values of θ indicating the sum of principal stresses being tensile are obtained, which is clearly unrealistic.

The solution to the problem of linear elastic analysis not being able to deal properly with structurally important granular bases lies with the finite element approach. Rather than dividing the pavement for analysis into a number of horizontal layers only, the finite element approach involves dividing the pavement both vertically and horizontally into a large number of so-called elements. Each element can then

be attributed an resilient stiffness consistent with the stress in that particular element.

As stated, the development of a finite element approach to pavement design lies beyond the scope of this dissertation. Yet, to establish by analytical means the structural contribution of granular materials to flexible pavements, such a finite element approach is required. Being unable at the present time to make that analytical assessment of the structural importance of granular materials, this chapter therefore deals with that problem through an experimental approach. A case study of the structural importance of granular bases was performed by actually building a test pavement with different granular bases and a bituminous base and measuring under realistic loads the main design parameter for flexible pavements, being the tensile strain at the bottom of the asphalt layer.

The test pavement with the 10 m wide granular bases discussed in Chapter 8 was for this purpose paved with 6 m wide asphalt, leaving 4 m "unpaved" for the research described in Chapter 8. Strain gauges were incorporated at the bottom of the asphalt layer to measure the asphalt tensile strain caused by loading of the pavement by means of a hydraulic actuator. The structural contribution of the various granular bases and the bituminous base could thus be compared on the basis of the measured asphalt tensile strain. Furthermore, the asphalt strain data obtained were meant for later use in the validation process of the finite element program being developed at the time of writing of this dissertation.

This chapter will focus on the structural contribution of the 25 cm thick granular bases in the test pavement and on comparison of that contribution to that of a 6 cm bituminous base. No attempts will be made to analytically couple the measured asphalt tensile strains to the resilient properties of the granular base course materials as determined in cyclic load triaxial tests. As stated above, such a coupling requires an analytical tool based on a finite element approach, the development of which falls beyond the scope of this dissertation.

Also, no correlations will be sought between the asphalt tensile strains measured in the test pavement and the results of the tests performed directly on the granular base, as discussed in Chapter 8. As

stated there, the tests were performed on the granular bases to assess their applicability in a forward-analysis type of approach, involving determination of material parameters in the laboratory and subsequent control in-situ whether or not the design assumptions on stiffness based on the laboratory values are indeed met in the laid-and-compacted granular base. The purpose of the tests on the granular bases was not determination of material parameters for design and, hence, no correlation will be sought here between the outcome of the tests on the granular base and those on the asphalt.

9.2 THE TEST PAVEMENT AND ITS INSTRUMENTATION

9.2.1 Introduction

The research into the structural contribution of the various granular materials was performed on the asphalt paved part of the test pavement described in Paragraph 8.2. As stated there, the test pavement was built outdoor on the imported subgrade of Eastern Scheldt sand of the Pavement Test Facility. Certainly for tests performed on the asphalt paved part working outdoor has the disadvantage of being open to climatic influences, of which air temperature and direct sunshine are the most important. As will be discussed later, the asphalt temperatures during testing were therefore not constant and a temperature normalizing factor had to be introduced to allow for comparison of the asphalt tensile strains measured in the various sections of the test pavement.

Yet, working outdoor was preferred since testing of indeed a "full-scale" pavement was judged essential. Certainly where the asphalt was concerned, it was judged essential to have a contractor build the pavement with full scale equipment such as an asphalt spreading machine and rolling equipment in order to get a realistic pavement. Furthermore, to allow access of the large equipment needed for the tests on the granular base described in the previous chapter, working outdoor was the only possibility.

9.2.2 Lay-out of the test pavement

Figure 9.1 repeats the lay-out of the test pavement, given earlier in Chapter 8. Note that this time the main measuring points are indicated on the asphalt-paved part of the test pavement. As indicated in the figure, three measuring points were installed in each section of the test pavement, incorporating a strain gauge for measurement of asphalt tensile strain at each measuring point.

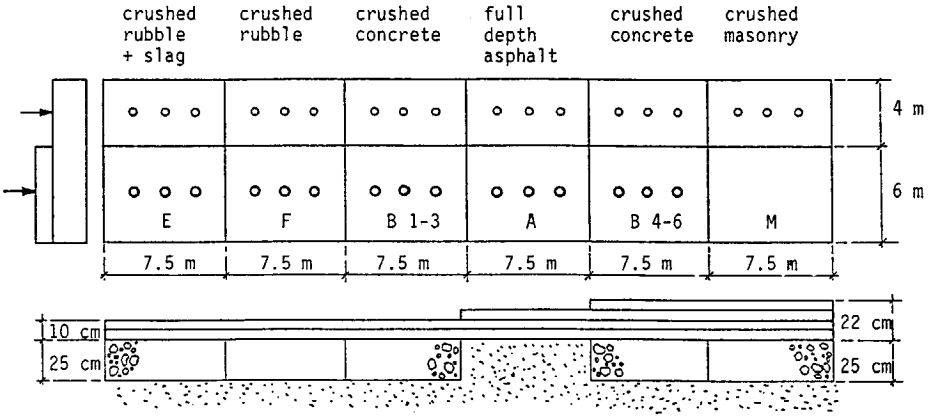

Figure 9.1: Lay-out and cross-section of the test pavement.

Figure 9.1 also shows the longitudinal cross-section of the test pavement. Sections E (crushed rubble with slag), F (crushed rubble) and B1-3 (crushed concrete) had an asphalt thickness of 10 cm. In section A (full depth asphalt) the 25 cm thick granular base was "replaced" by a 6 cm bituminous base. This was achieved by constructing an extra layer of 6 cm asphalt at section A. It should be noted here that the same asphalt was used for all layers of the pavement, namely base course asphalt complying with the Dutch specifications (grindasfaltbeton 4/32-57, Eisen 1978 [7]). For full details on the asphalt used, reference is made to the relevant research report [17]. Section B4-6 had a total of 22 cm thickness of the same asphalt. The main purpose of this section was to gather asphalt strain data for the validation on finite element calculations. The section with the crushed masonry base was not equiped with asphalt strain gauges since this material has an elastic stiffness comparable to that of sand and, hence, does not merit a detailed investigation of its structural contribution to flexible pavements. This section was mainly built for the

in-situ testing described in Chapter 8 and to check the influence of a low quality granular base on the quality of the first layer of asphalt built on that base. Details on the latter subject will not be dealt with in this dissertation.

9.2.3 Instrumentation of the test pavement

In each of the sections, three measuring points were equiped with one asphalt strain gauge per point at the bottom of the lower asphalt layer. The gauges used are so-called "embedment strain gauges" (TML, type KM 100 HAS). Figure 9.2 shows a cross-section of such a gauge. The asphalt strain gauges measure directly the horizontal tensile strain at the bottom of the lower asphalt layer, which is the main design criterion for asphalt pavements in the Netherlands. The strains measured therefore permit a direct comparison of the structural contribution of the granular bases applied and that of the bituminous base of section A. The gauges consist of a low stiffness (E = 1 GPa) brass tube, equiped with flanges at both ends and having a gauge length of 100 mm. The flanges are equiped with small anchor bars to ensure a proper fixation in the asphalt layer. Inside the brass tube a full bridge set of strain gauges is mounted on a beam connecting the two flanges. Connected to a strain gauge amplifier, the gauges measure asphalt tensile strain directly.

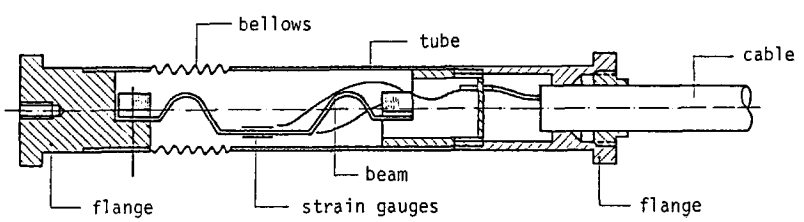

Figure 9.2: Cross-section of asphalt strain gauge.

The gauges were installed on the completed granular base prior to asphalt paving. To fix them at the required place, some bitumen was poured onto the granular base, on which a thin layer (approximately 1 cm) of asphalt was placed. The gauge was then pressed into this asphalt and further fixed with bitumen. This procedure has been found necessary and adequate to prevent the gauge from wandering from its

required position. At the full-depth asphalt section a somewhat different procedure is required since fixation of the gauge to the sand surface would be of little use. Here, a 1 m wide stretch of filter cloth was placed on top of the sand layer, covering the whole length of the particular section at the place of the measuring points. The gauges were then fixed to the filter cloth using the procedure described above. Figure 9.3 shows an asphalt strain gauge on the granular base.

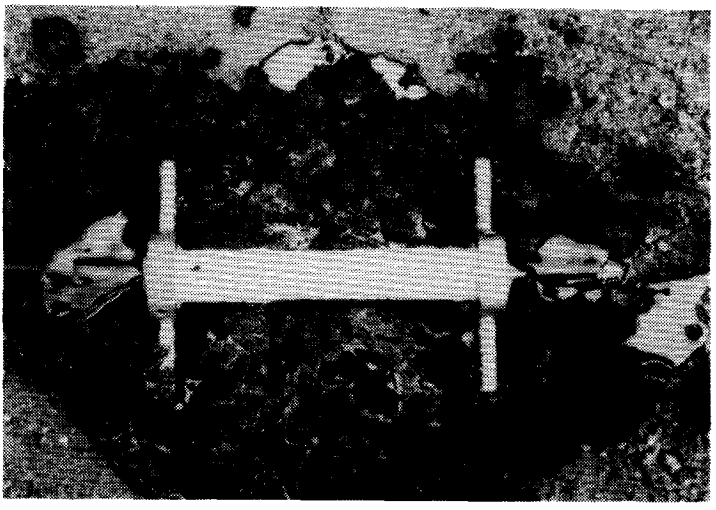

Figure 9.3: Asphalt strain gauge on granular base.

Since the test pavement was built outdoor, the temperature of it could not be controlled. Therefore, detailed measurement of the temperature of the asphalt was required. To allow for this, thermocouples were incorporated at each measuring point at the bottom and on top of the asphalt and in between all asphalt layers.

9.3 TESTING

9.3.1 Introduction

The aim of the research described in this chapter was to establish through experimental means the structural contribution of the various granular materials to a flexible pavement and to compare that contribution to that of a bituminous base. An additional aim was to gather data on asphalt tensile strain needed for validation of finite element calculations.

To achieve these aims, traffic loading was simulated at each of the measuring points of the test pavement using a hydraulic actuator. Since the granular materials applied in the pavement were known to show (self-)cementing effects, the loading of the pavement at the various measuring points was repeated several times. The first series of measurements was performed on Day 10 (counting again from Day 0 being the last day of asphalt paving) and repeated later on Day 38 and Day 77.

9.3.2 Loading and measurements

Each of the three series of measurements (Days 10, 38 and 77) consisted of application of a limited number of cyclic plate loads at each of the measuring points in the test pavements. The cyclic plate loads were 50 kN in magnitude (equal to half of the maximum axle load in the Netherlands) and 0.20 s in duration (half-sine loading signal). The loading was executed with the servo-hydraulic actuator of the Pavement Test Facility, which is supported in a large 22 m long beam spanning the width of the facility. The mass of the beam (11 ton) served as reaction load for the hydraulic actuator. The beam is supported on bogies that travel on rails at either side of the facility, thereby allowing for easy moving of the actuator/beam assembly from one measuring point to another. Performance of a whole series of loadings took several days; as was done with the measurements on the granular base, the day-numbering indicates the first day of the measurements.

Figure 9.4 shows the schematics of the hydraulic actuator used to apply the cyclic load. The 50 kN load is applied to the pavement through a rigid 300 mm diameter steel plate, connected to the actuator by a ball and socket joint. A circular rubber sheet of 10 mm thickness was placed between the steel loading plate and the asphalt. All loads were performed on exactly the same spot. Barksdale [131] reported a similar investigation into the performance of crushed-stone base courses, using an indoor cyclic plate load facility. To prevent "localized punching failure", the position of the actuator applying the plate loading was shifted after given numbers of load applications in a circular pattern around the actual measuring point. Such a shifting of the loading was not done here. Yet, no punching failure occurred even after 10^6 applications of the 50 kN load. It is believed that the good quality of the asphalt achieved by using full-scale construction plant prevented such failure from occurring.

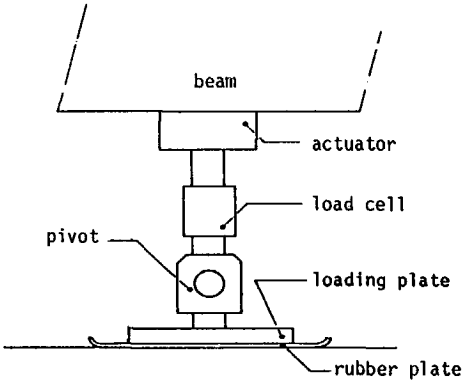

Figure 9.4: Schematics of hydraulic actuator for cyclic plate loading.

During the execution of the measurements, the signals from the full-bridge strain gauge of the asphalt strain transducer were amplified and displayed on a transient recorder, together with the applied load. For later analysis, the signals were stored using an X-Y plotter. The temperatures measured by the thermocouples at the particular measuring point were recorded by hand at frequent intervals.

9.4 INTERPRETATION OF MEASURED STRAINS

9.4.1 Introduction

The structural performance of the granular bases and the bituminous base of the test pavement will be compared in this chapter on the basis of the measured tensile strain at the bottom of the asphalt layer. A direct comparison of as-measured strains, however, is not possible, since the measurements of the strains were performed at different temperatures. As noted, three series of measurements were carried out at intervals of roughly one month, causing the temperature of the asphalt to be different for each series. Moreover, even within one series of measurements substantial differences in asphalt temperature occurred, not only since a series of measurements took several days to be carried out but also because sunshine caused substantial differences in asphalt temperature even within a single day.

To allow for a comparison of asphalt strains, all as-measured strains were multiplied by a normalizing factor dependent on the asphalt temperature during the particular measurement. As will be described in the next paragraph this normalizing factor was obtained from a series of BISAR calculations for the different structures applied in the test pavement.

9.4.2 Determination of temperature normalizing factors

The pavement structures applied in the test pavement can be divided into three groups:

a: 10 cm of asphalt on 25 cm of granular base

b: 16 cm full depth asphalt

c: 22 cm of asphalt on 25 cm of granular base.

For each of these three types of structures the horizontal strain at the bottom of the asphalt layer caused by a 50 kN load of 0.2 s duration on a 300 mm loading plate was calculated with the BISAR-program. The calculations were performed for asphalt temperatures of 10, 15, 20, 25 and 30°C. This range of temperatures covered all as-measured

temperatures. The stiffness parameters for each of the layers of the pavement structures were obtained as follows:

- For the asphalt the stiffness of the bitumen S_{bit} was derived from the well-known Van der Poel-nomogram, assuming a penetration pen (25°C, 100 g, 5 s) = 40, PI = -0.65 and ring-and-ball temperature T_{r+b} = 54.5°C. Rather than using the classic graphical approach of Van der Poel, the formulae describing the Van der Poel nomogram published by Dauzats and Rampal (132) were used to calculate S_{bit} from the parameters given above.

  Having thus obtained the stiffness of the bitumen S_{bit}, the stiffness of the asphalt mix S_{mix} was then calculated using the formulae presented by Bonnaure et al. (133). The following parameters were used as input to the calculation of S_{mix}: volume of aggregate 83%, volume of bitumen 10%, volume of voids 7%. Table 9.1 shows the S_{bit} and S_{mix} values thus obtained. After completion of the test program, the mix parameters mentioned above were confirmed by analysis of cores from the pavement and of the recovered bitumen.

Table 9.1: Stiffness of bitumen S_{bit} and of mix S_{mix} for various temperatures

T |°C|	S_{bit} |MPa|	S_{mix} |MPa|
10	54	5930
15	23	3520
20	10	2030
25	3.8	1130
30	1.4	600

- For the granular base courses an E-modulus of 600 MPa was used. This parameter was obtained through a back-analysis of the measured asphalt tensile strains at measuring points believed to be representative of the average situation of the base courses with respect to elastic stiffness.

- For the sand subgrade of the Pavement Test Facility an E-modulus of 150 MPa was used, which value is consistent with the results of cyclic load triaxial tests on Eastern Scheldt sand (see Paragraph 5.3.3.5).

Poisson's ratio ν was chosen at $\nu = 0.35$ for all materials. The reference temperature to which all asphalt strains were to be normalized was chosen at T = 15°C, which is the asphalt temperature at the weighted Mean Annual Air Temperature in the Netherlands of wMAAT = 12°C. The normalizing factor was defined as:

$$C^{15} = \frac{\text{calculated asphalt strain at } 15^{\circ}C}{\text{calculated asphalt strain at } T^{\circ}C} \qquad (9.1)$$

Table 9.2: Temperature normalizing factor C^{15}

structure	T [°C]	asphalt strain [10^{-6}]	C^{15} [-]
	10	158	1.15
10 cm asphalt	15	181	1.00
25 cm gran. base	20	194	0.93
sand	25	187	0.97
	30	157	1.15
	10	172	1.42
16 cm asphalt	15	245	1.00
sand	20	345	0.71
	25	473	0.52
	30	617	0.40
	10	59	1.32
22 cm asphalt	15	78	1.00
25 cm gran. base	20	100	0.78
sand	25	125	0.62
	30	150	0.52

Table 9.2 shows the normalizing factor C^{15} obtained for the three types of structures of the test pavement, for the various temperatures

for which the BISAR calculations were carried out. For the intermediate temperatures, normalizing factors were obtained through graphical interpretation.

9.5 TEST RESULTS

9.5.1 Asphalt tensile strains

The tensile strain at the bottom of the asphalt layer caused by the 50 kN cyclic plate load was measured at each of the measuring points on Days 10, 38 and 77. The measured strains were multiplied by the temperature normalizing factor C^{15} to obtain equivalent strains at an asphalt temperature of T = 15°C. The resulting normalized strains are shown in Figure 9.5.

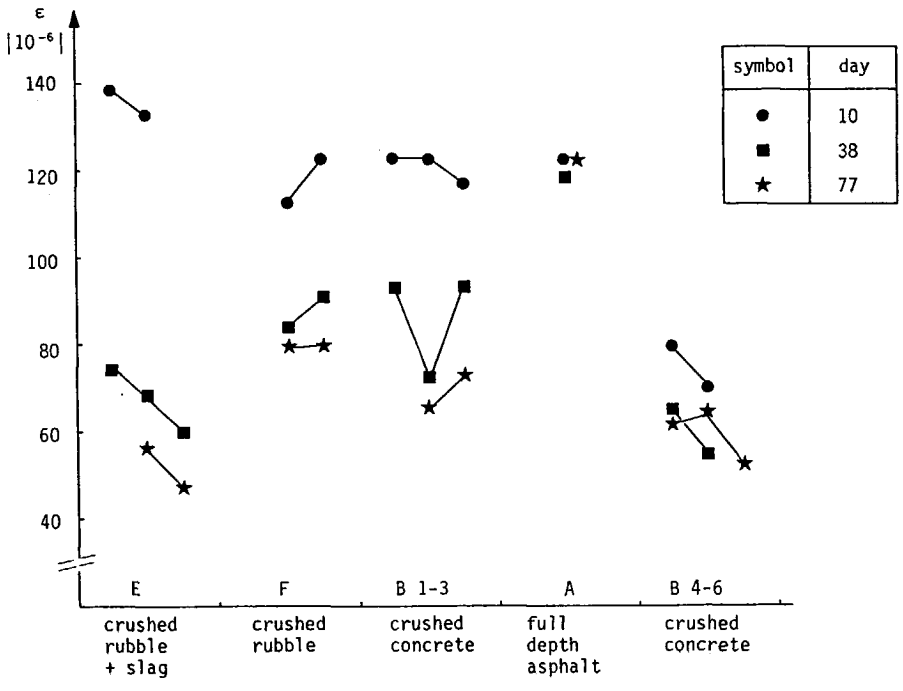

Figure 9.5: Normalized asphalt tensile strains.

As can be seen from Figure 9.5, part of the gauges incorporated in the test pavement did not survive construction of the asphalt layers. It should be noted here that the contractor was given the full go-ahead to obtain an asphalt pavement similar to those in practice. Deliberately, no attempt was made to reduce the compaction effort of the asphalt spreading machine and the dynamic roller equipment. Obtaining a realistic asphalt pavement was deemed more important than the survival of all gauges. The instrumentation of three identical measuring points per section of the test pavement made the loss of one or two gauges per section acceptable. At the measurements on Day 10, the gauges at points E3, F1, A1, A3 and B5 proved not to function properly. Of these gauges, those at points E3 and B6 could later be revitalized by electronic intervention.

Looking at the results depicted in Figure 9.5, the following conclusions can be drawn:

1. The scatter in the asphalt strains per section is limited, indicating a proper functioning of the gauges. It should be noted here that the scatter obtained may originate from actual measuring errors and from the temperature normalization, but also from actual differences in asphalt tensile strain caused by local differences in the pavement structure.

   In section A, only one gauge survived construction and, hence, no remark can be made with respect to the scatter in that section. The results found here for the one surviving gauge are, however, substantiated by those of an earlier test pavement having the same full depth asphalt structure (134).

2. On Day 10, the strains in the three sections with 10 cm asphalt on 25 cm granular base (sections E, F and B1-3) are of the same magnitude as those in the section with the 16 cm full-depth asphalt construction (section A), beit that section E shows somewhat larger strains than sections F, B1-3 and A. In general terms, this indicates that 10 days after paving the structural contribution of the 25 cm granular bases equals that of 6 cm bituminous base.

The asphalt strains in the section with 22 cm of asphalt on 25 cm crushed concrete base (section B3-6) are much smaller than those in the other sections.

3. On Day 38, the comparison of the three 25 cm granular bases in sections E, F and B1-3 with the 6 cm bituminous base in section A clearly yields a favorable result for the granular bases. In all three sections, the increased stiffness of the granular base due to (self-)cementing effects leads to a drastic reduction in asphalt tensile strain. The reduction is of equal magnitude for the crushed rubble (section F) and the crushed concrete (section B1-3) bases, whereas the crushed rubble with addition of the slag (section E) shows a very drastic reduction in strain. The full-depth asphalt construction (section A) shows a negligible change in asphalt strain.

   The asphalt strains in the section with 22 cm of asphalt on 25 cm crushed concrete base also reduce thanks to stiffening of the base, but the effect is far less pronounced because of the large thickness of the asphalt layer.

4. On Day 77, a further reduction in asphalt strain is observed for sections E, F and B1-3, whereas the full depth asphalt section again shows a negligible change in asphalt strain. Hence, the structural contribution of the 25 cm granular bases has further increased relative to the situation on Day 38.

   No further reduction in asphalt strain is observed in section B4-6. Although some further stiffening of the granular base will have taken place here, the effect of this stiffening is completely masked by the thick asphalt layer.

9.5.2 Equivalent E-moduli

Most of the mechanistic pavement design procedures used today rely on linear elastic theory for the calculation of stresses and strains in pavement structures. To each of the pavement layers, a single E-modulus is attributed to characterize its elastic stiffness. Results from cyclic load triaxial tests as described in Chapter 5 cannot be

used directly as input to such a linear elastic analysis, since no realistic stress distribution is obtained for the granular base. Brown and Pappin (70) circumvented this problem by calculating the stresses in the granular base with the finite element program SENOL. Subsequently, they used the obtained stresses as input to the K-θ model describing the stiffness of the granular material as a function of stress. In doing so, an "equivalent stiffness" for the granular base was obtained, which when used as input to linear elastic BISTRO calculations yielded the same values for critical design parameters as did parallel stress-dependent SENOL calculations. Typical values obtained from this analysis for the equivalent stiffness of granular bases were E_2 = 100 MPa for a good quality limestone and E_2 = 50 MPa for a lower quality limestone.

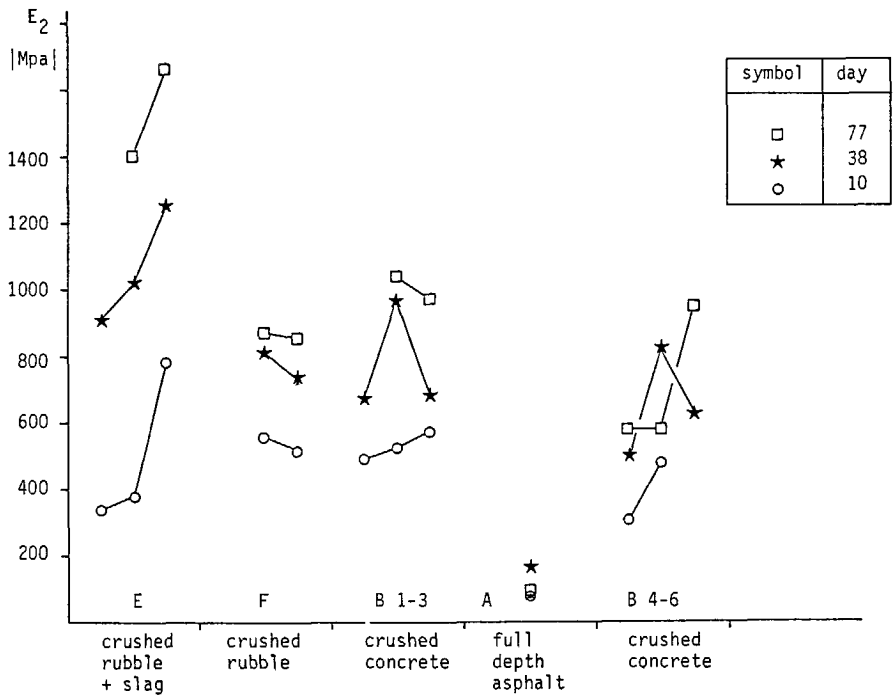

Figure 9.6: Equivalent stiffness E_2 of the granular base.

Figure 9.6 shows values for the "equivalent stiffness" of the granular bases applied in the test pavement as back-analysed directly from the measured asphalt tensile strains. Using fixed values for the stiffness of the asphalt and the sand subgrade, iterative BISAR calculations were run to obtain a single stiffness E_2 for the granular base, which

when used as input to BISAR yielded the measured value of the asphalt tensile strain. For the temperature-dependent stiffness of the asphalt, the values given earlier in Table 9.1 were used in the calculations. For the stiffness of the subgrade, values derived from FWD-measurements on the asphalt paved part of the test pavement were used (E_3 = 150 MPa for sections E, F and B1-3 and E_3 = 200 MPa for section B4-6).

From the results depicted in Figure 9.6, the following conclusions can be drawn:

1. The stiffening of the granular bases with time is clearly reflected in the results of the analysis. The increase in stiffness is largest for the crushed rubble with 10% electro-furnace slag (section E).

2. Comparing the equivalent stiffness obtained for the two crushed concrete sections, the section with 10 cm asphalt thickness (section B1-3) shows a higher stiffness for the granular base than does the section with 22 cm of asphalt (section B4-6). This difference is caused by the stress-dependent behaviour of the crushed concrete. For the same test loading of 50 kN applied on the asphalt, the stresses in the granular base will be higher in the section with 10 cm of asphalt cover and, hence, the equivalent stiffness of the granular base will be higher. It should be noted here that the same granular material was applied at the same thickness in the two crushed concrete sections.

3. For the full-depth asphalt section (section A), the stiffness obtained from the iterative BISAR-calculations is the equivalent stiffness of the sand subgrade. Obviously, this stiffness is lower than that of the granular bases in the other sections of the test pavement.

4. The overall values found for the equivalent stiffness of the granular bases are quite high, certainly when compared to the equivalent stiffness of E_2 = 100 MPa found by Brown and Pappin for a good quality limestone (70). The (self-)cementing potential of the granular materials applied certainly contributed to the high stiffness values found here. It should be noted that the first

measurements of asphalt strain (Day 10) were performed some 20 days after compaction of the bases. Hence, even at the time of the first measerements a certain stiffening of the bases may have taken place. On the other hand, the equivalent stiffness for the non-cementing Eastern Scheldt sand in section A is some 150 kPa, which value is already substantially higher than that found a crushed stone material from the finite element calculations by Brown and Pappin.

9.5.3 Discussion

The test pavement described in this chapter was built and tested to assess through experimental means the structural significance of various granular bases. The research described is a case study, pertaining only to the granular bases applied under the particular conditions of subgrade support and asphalt cover thickness. The results obtained cannot without further preface be extrapolated to other pavements with a different subgrade, different layer thicknesses or other granular materials.

The structural significance of the granular bases applied in the test pavement was first assessed on the basis of the main design criterion for flexible pavements, being the tensile strain at the bottom of the asphalt layer. The results shown in Figure 9.5 indicate that the structural contribution of the 25 cm thick granular bases is larger than that of an extra bituminous layer of 6 cm thickness.

To obtain a reference with present day pavement design practice involving linear elastic analysis, the "equivalent stiffness E_2" was back-analysed from the measured asphalt tensile strains. The values given in Figure 9.6 are no more or less than the stiffnesses that should be used as input to BISAR calculations to obtain the measured asphalt tensile strain, for the given set of subgrade support, materials applied and layer thicknesses. The E_2 values given are, therefore, "structure parameters", pertaining only to the given set of conditions.

A straightforward correlation of the structure parameters E_2 given in Figure 9.6 to the material parameters obtained in cyclic load triaxial

testing of similar materials is not feasible because of the (self-) cementing potential of the materials applied. Focusing on crushed rubble and crushed concrete with 10 cm asphalt cover, the equivalent stiffness found on Day 10 is some 500 MPa for both materials (see Figure 9.6). On Day 77, the crushed rubble has an equivalent stiffness of about 850 MPa, whereas the crushed concrete reaches about 1000 MPa. All these values are higher than the resilient modulus values found in the cyclic load triaxial testing of crushed rubble and crushed concrete described in Chapter 5 (see Table 5.4, Paragraph 5.3.2.5). A direct comparison is only feasible for the Eastern Scheldt sand. Here, the material included in the triaxial test program is the same as that in the test pavement and the material shows no cementing effects. The equivalent stiffness found for the sand subgrade of the test pavement was some 150 MPa (see Figure 9.6), while the triaxial tests yielded a range of stiffness of M_r = 81 MPa to M_r = 281 MPA for stress conditions representative of those in-situ (see Table 5.7, Paragraph 5.3.3.5).

The numerical values found for the equivalent stiffness of the various granular bases in the test pavement (Figure 9.6) indicate a significant structural contribution to the particular pavement construction, as did the measured asphalt strains depicted in Figure 9.5. In fact, the information given in both figures is the same; Figure 9.6 is no more than a translation of the basic information given in Figure 9.5 to linear elastic pavement engineering terminology. In all, the case study presented in this chapter clearly indicates the structural significance of the granular bases applied. Furthermore, the results presented for the various materials indicate a significant difference in the structural capacity of these materials. This finding illustrates that granular materials merit individual laboratory testing to assess their elastic stiffness for use in an appropriate analytical tool for pavement design.

9.6 CONCLUSION

This chapter has dealt with a case study into the structural significance of granular bases as established through experimental means. A test pavement was constructed containing various granular bases and a section with a bituminous base. The structural contribution of the various bases applied was compared on the basis of measured tensile strains at the bottom of the asphalt layer. From the results obtained, the following conclusions can be drawn:

1. The granular bases applied are structurally significant. Directly after construction, the structural contribution of the granular bases is similar to that of the bituminous base applied. Due to cementing effects, the structural contribution of the granular bases is further increased with time.

2. The "equivalent stiffness" E_2 back-analysed from the measured asphalt tensile strain is a structure parameter, pertaining only to the given set of materials, layer thicknesses and subgrade support. The numerical values of E_2 found here are, therefore, of limited interest only. They do, however, indicate the structural significance of the granular bases applied.

10 SUMMARY, CONCLUSIONS AND RECOMMENDATIONS

10.1 SUMMARY

Over the past two decades, flexible pavement design has been gradually evolving from a purely empirical trade towards the analytical/mechanistic approach being used today. This evolution is, however, far from completed. Major pavement design procedures published recently are still empirically based. The AASHTO Guide for the Design of Pavement Structures, for instance, is a purely empirical method based on the performance data gathered during the AASHO Road Test of the late nineteen-fifties. The UK pavement design method published by the Transport and Road Research Laboratory in 1984 too is based on empirical knowledge, although structural theory has been used in the analysis of the performance of the test sections that form the basis of the design method.

The first analytical pavement design procedure to be accepted widely in practice is contained in the Shell Pavement Design Manual, published in 1978. The designs presented therein are based on the calculation of stresses and strains in pavement structures and on limitation of these calculated values to allowable values of stress and strain. The South-African pavement design procedure has evolved farthest towards actual mechanistic design. It couples an analytical approach similar to that of the Shell-method to a vast validation using performance data of existing pavements under normal and accelerated loading.

Pavement design procedures developed for use in tropical areas are still all empirically based. Serviceability criteria that form the basis of the temperate zone mechanistic design procedures hardly play a role in the design of rural roads in the tropics. There, the main function of the road is establishing an all-weather connection between two places. A lower riding quality than in the developed countries has to be accepted here because of budget restrictions. The application of locally occurring natural materials often calls for the use of engineering judgement and experience rather than a sophisticated analytical approach to pavement design.

The empirical design procedures used in temperate zone and tropical areas evidently deal with granular materials in an empirical way. The specifications set out for these materials are based on availability and experience rather than on the required performance in the pavement structure. The specifications are recipe-based rather than end-product based. They prescribe what the material should be like rather than what it should do. Index tests and empirically based strength tests such as the California Bearing Ratio test are used the characterize the materials and assess their structural contribution to flexible pavements. Being based on vast experience and sound engineering judgement, this empirical approach can be quite satisfactory, provided it is used within the limits of the experience on which it is based. Extrapolation towards new materials or heavier axle loads can, however, be quite hazardous.

Contradictory as it may seem, the analytical/mechanistic pavement design procedures of today also use the empirical approach to specifying and characterizing granular materials for use in pavements. Sophisticated mechanistic pavement design procedures are often used in conjunction with empirical, recipe-based specifications and purely empirical tests, such as the California Bearing Ratio, are used to assess fundamental material characteristics such as Young's modulus E. Clearly, if granular materials are to be used in pavement structures to their full structural capacity, this empirical approach to their specification and characterization is not adequate. End-product specifications should be developed on the basis of the required structural capacity and long-term performance of the granular materials. Fundamentally sound laboratory testing techniques should be used to determine the structural characteristics of soils and granular materials for input to the design calculations that form the basis of mechanistic pavement design. In-situ testing techniques should be developed that allow for a proper assessment of the structural capacity of the laid-and-compacted granular bases in a statistically sound way.

This study deals with the testing of granular road base materials to determine their mechanical properties. An extensive experimental program involving laboratory and in-situ tests forms the basis of the data presented. Granular materials ranging from crushed stone through non-bituminous recycled materials and sands to tropical laterites were

investigated. These materials were examined in cyclic load triaxial tests and in a wide range of empirically based standard tests. Correlations between the results of the two groups of tests were checked using the laboratory data. Having established that fundamental material parameters needed as input to design calculations cannot be assessed from the results of the empirical standard tests, an investigation was carried out into possible simplifications of the complex cyclic load triaxial test.

The influence of the degree of saturation on the elastic stiffness of granular materials was investigated in cyclic load triaxial tests. Crushed stone materials, sands and laterites were tested for their elastic stiffness at different levels of the degree of saturation and the observed changes in stiffness were shown to be related to material composition and grading. Next, a study was performed on the modeling of elastic and permanent deformation of granular materials. This modeling was done both in terms of principal stresses and strains and in terms of volumetric and shear components of stress and strain.

The in-situ investigations involved testing of various sections in a specially constructed test pavement. A dynamic version of the well-known static Plate Bearing Test was developed, allowing for rapid and fundamental determination of the in-situ stiffness of granular bases. The structural significance of granular bases was assessed by experimental means. The tensile strain at the bottom of the asphalt layer of the various sections in the test pavement was measured under application of a cyclic plate load of realistic magnitude.

10.2 CONCLUSIONS

The experimental results obtained in this study and the analyses which were performed lead to a number of main conclusions. From the results of the laboratory testing, these conclusions are:

1. For the wide range of materials tested, the resilient modulus M_r shows no correlation with the California Bearing Ratio CBR. Apparently, the widely used rule E [MPa] = 10 CBR is not valid for granular materials and sands. Additional data from literature shows E-CBR relationships to be not valid for soils either.

2. The resilient modulus of granular materials was shown to be affected by grading. For materials with the same maximum particle size, those with a coarse grading were shown to be more stress-dependent than those with a fine grading. The resistance to permanent deformation too was shown to be affected by grading. For materials with the same maximum particle size, those with a coarse grading showed a lower resistance to permanent deformation than those with a fine grading.

3. The resistance to permanent deformation of granular materials in general was shown to be much larger than that of sands. The difference in resilient stiffness between granular materials and sands is less pronounced.

4. In the search for simplified test procedures for determination of resilient properties, the repeated static load triaxial test was shown to yield the same results as the far more complicated cyclic load triaxial test. The time-consuming "static triaxial creep test" procedure suggested in the literature can be replaced by the repeated static load test procedure presented here without loss of accuracy.

5. Methods from the literature that predict permanent strain from the stress ratio at failure or from resilient properties were shown to be inapplicable for the wide range of materials tested here in cyclic load triaxial tests with large numbers of load applications. Apparently, the latter type of testing is required to establish permanent strain properties of granular materials.

6. Determination of the resilient properties of granular materials in cyclic load triaxial tests on 150 mm diameter specimens showed inconsistent results. Results from the literature showed scaling down of the grading itself to cause a decrease in resilient stiffness. Therefore, coarse graded granular materials should be tested for resilient properties in cyclic load triaxial equipment with large specimen diameters.

The study of the influence of water content on the elastic stiffness of a wide range of materials yielded the following conclusions:

7. The suction-dependent behaviour of a granular material is dominated by its grading and the nature of its fine fraction. The stiffness of the sands having a grading much coarser than the Fuller-curve and little or no clay in the fine fraction, showed only a limited dependency on moisture content. On the other hand, the laterites having gradings significantly finer than the Fuller-curve and containing a significant amount of clay in their fine fraction were shown to be extremely suction-dependent. The laterites with gradings closer to the Fuller-curve showed less suction-dependency. Granular materials with gradings on the Fuller-curve nevertheless showed a distinct suction-dependent stiffness, explained by the presence of clay in the fine fraction.

With respect to modelling of the resilient behaviour of granular materials for pavement design, the following conclusions are drawn:

8. The cyclic load triaxial tests described in this dissertation were Constant Confining Pressure tests. Uniaxial Hooke's law can be used to interpret the results of such tests, since increments of strain are measured in the tests as caused by increments of stress. It should however be noted that the stiffness values obtained relate to the boundary condition of the level of confining stress used in the particular test only.

9. The K - θ model gives a good prediction of axial resilient strain. Coupled with a constant value for Poisson's ratio ν a poor prediction of volumetric strain results. The K - θ model used in conjunction with a stress-dependent ν gives a satisfactory prediction of both volumetric and shear strain.

10. A better insight into material behaviour under application of stress can be obtained by separating principal stresses and strains into volumetric and shear components. Rather than using Young's modulus E and Poisson's ratio ν, the stress-strain relationship is then expressed using the bulk modulus K and the shear modulus G. For granular materials, K and G are functions of stress.

11. Elasticity theory sets strict requirements on the relationship between K and G and stress. Boyce's three parameter model meets these requirements, but gives a poor fit of volumetric strains. Releasing the requirements of elasticity by fitting volumetric and shear strain independently to stress leads to a far better agreement between measured and model-predicted values of elastic strain.

With respect to the modelling of permanent deformation, the following conclusions are drawn:

12. For modelling of principal permanent strains as a function of the number of load applications, the log-natural approach $\varepsilon_p = a + b \log N$ used widely in the literature is not accurate when dealing with large numbers of load applications. Using the log-log approach $\log \varepsilon_p = a + b \log N$, a satisfactory fit between model-predicted and measured values of strain can be obtained.

13. As was the case with modelling of resilient strains, more insight into material behaviour under stress can be obtained by separating stresses and strains into volumetric and shear components.

14. Triaxial specimens compacted to typical field densities showed significant permanent dilation under a large number of load applications. In practical engineering terms, this indicates that well-compacted granular bases show an increase in volume under prolonged traffic loading, rather than "post-compaction".

In-situ assessment of granular layers to check design assumptions with respect to stiffness resulted in the following conclusions:

15. The newly developed Dynamic Plate Bearing Test appears most applicable for fundamentally and statistically sound proof testing of granular layers. It combines speed of execution with simplicity of interpretation. The support for the asphalt layers is expressed in a single, easy to interpret parameter. The required outcome of the test can be calculated at the design stage and later checked in the field.

16. The Clegg Impact Tester appears to be very applicable as an empirical contractor's tool for assessing the uniformity of the granular base.

The experimental case study into the structural significance of granular bases in flexible pavements leads to the following conclusions:

17. Directly after construction, the structural contribution of the three granular bases applied in the test pavement was similar to that of a 6 cm bituminous base. This contribution was further increased due to cementing of the particular materials.

18. The "equivalent stiffness" E_2 of the granular bases back-analysed from the measured asphalt tensile strain also indicated the structural significance of the granular bases.

10.3 RECOMMENDATIONS

On the basis of the experimental research and the analyses described in this dissertation, coupled with the extensive literature study, a number of recommendations can be made. With respect to specifications the following recommendations are made:

1. The recipe-specifications presently being used should be replaced by end-product specifications, expressing the required structural parameters of the materials in sound engineering units. Some form of recipe-specifications will, however, still be required to ensure a proper long-term performance of the materials applied.

2. The end-product specifications should only specify the relevant engineering characteristics of the materials. The contractor should be required to meet these specifications, but restrictions beyond that should be omitted.

3. End-product specifications should allow for international exchangeability of the specifications themselves and of the materials concerned.

The laboratory testing performed leads to the following recommendations:

4. Stress-strain properties of granular materials needed as input to pavement design should be determined in fundamentally sound tests. Such material properties should be determined in the laboratory, on specimens of the material isolated from the rest of the materials in the pavement construction.

5. The repeated static load triaxial test should be implemented in the practice of pavement engineering as a fundamentally sound, but relatively simple means of assessing stress-strain characteristics of granular materials.

Research into the dependency of the stiffness of granular materials on the degree of saturation leads to the following recommendations:

6. Granular materials that are likely to become wet during the life-cycle of the pavement should be tested for resilient properties at the worst possible in-situ moisture content. The optimum moisture content from the Proctor test appears to be a reasonable measure for that in-situ moisture content, provided free drainage is allowed in the pavement construction.

7. To minimize the suction-dependency of the stiffness of granular materials, limits should be set in their specifications for the plasticity of the fine fraction.

Study of the modelling of granular materials for pavement design leads to the following recommendations:

8. When performing cyclic load triaxial tests, good account should be taken of which deformations are actually measured and which are

not. A good distinction should be made between incremental and total stresses and strains. In doing so, both Constant Confining Pressure tests and Variable Confining Pressure tests can be used to assess fundamental stress-strain characteristics of granular materials.

9. The approach of interpreting stresses and strains in terms of volumetric and shear components should also be applied to other pavement materials such as asphaltic concrete.

10. Permanent strain tests on granular materials should be run to at least 10^6 load applications. Although time-consuming, such testing is necessary since the permanent deformation behaviour cannot be reliably predicted from tests with limited numbers of load applications, let alone from monotonic loading failure tests.

The research into development of quick means of proof testing of granular layers leads to the following recommendations:

11. The present approach to proof testing of granular layers by measuring in-situ density should be replaced by an in-situ assessment of the parameter which is of direct interest to pavement design, being the elastic stiffness and the resistance to permanent deformation.

12. The applicability of the Dynamic Plate Bearing Test should be further investigated by performing the test on granular bases showing variations in subgrade support and density and thickness of the granular layer itself. Research should be performed into the possibility of using the test as a means of assessing the resistance to permanent deformation. One possibility might be to relate the resistance to permanent deformation to the change in elastic stiffness under repeated application of the dynamic plate load.

13. The Clegg Impact Tester should be used only as an empirical tool for assessing the uniformity of compacted granular layers. Extrapolation of the results of the test towards fundamental stress-strain characteristics is not worth persuing.

With respect to the design of pavements including granular layers, the following recommendations are made:

14. Granular materials should be dealt with as a structural component of the pavement. To assess their structural contribution to pavements analytically, a finite element approach to calculating stresses and strains in pavements is required. Such a new approach requires extensive validation using stress-strain data obtained on specially constructed test pavements such as the one described in this dissertation.

15. The calculation of stresses and strains in pavement constructions only yield the pavement response to a single loading. Such calculations are necessary but not sufficient for proper mechanistic pavement design. They should be supplemented with performance data of actual pavements under normal and accelerated loading.

16. Once thoroughly validated, finite element calculations of stresses and strains in pavements should be applied in the development of mechanistic pavement design procedures that pay proper attention to the structural role of the granular layers. Fundamentally sound testing techniques like the ones described in this dissertation can then be used to assess the structural characteristics of granular materials for pavement design.

11 REFERENCES

1. Kerncijfers verkeer en weg.
   Stichting Weg, The Hague, 1989.

2. The AASHO Road Test.
   Special Reports 61A - 61E, Highway Research Board, Washington, D.C., 1961.

3. Powell, W.D., J.F. Potter, H.C. Mayhew and M.E. Nunn.
   The structural design of bituminous roads.
   Laboratory Report 1132, Transport and Road Research Laboratory, Crowthorne, 1984.

4. AASHTO guide for the design of pavement structures 1986.
   American Association of State Highway and Transportation Officials, Washington, D.C.,1986.

5. Shell Pavemnent Design Manual.
   Shell International Petroleum Company Limited, London, 1978.

6. Jong, D.L. de, M.G.F. Peutz and A. Korswagen.
   Computerprogram BISAR. Layered systems under normal and tangential surface loads.
   External report AMSR.0006.731, Koninklijke/Shell-Laboratorium, Amsterdam, 1973.

7. Eisen 1978 voor bouwstoffen in de wegenbouw.
   Staatsuitgeverij, 's Gravenhage, 1978.

8. Standard specifications for transportation materials and methods for sampling and testing. Part 1. Specifications.
   American Association of State Highway and Transportation Officials, Washington, D.C., 1978.

9. AASHTO interim guide for the design of pavement structures.
   American Association of State Highway and Transportation Officals, Washington, D.C., 1974.

10. Road Note 31. A guide to the structural design of bitumen surfaced roads in tropical and subtropical countries.
    HMSO, London, 1977.

11. Niet-gebonden steenfunderingen.
    Mededeling 27, Study Centre for Road Construction, Arnhem, 1971.

12. Pappin, J.W.
    Characteristics of a granular material for pavement analysis.
    Ph.D.-thesis, Department of Civil Engineering, University of Nottingham, 1979.

13. Thom, N.
    Design of road foundations.
    Ph.D.-thesis, Department of Civil Engineering, University of Nottingham, 1988.

14. Centre R.O.W.
Resten zijn geen afval meer. Puingranulaten.
Publication 12, Centre R.O.W., Ede, The Netherlands, 1988.

15. Centre R.O.W.
Steenfunderingen beter gefundeerd.
Publication 18, Centre R.O.W., Ede, The Netherlands, 1988.

16. Puingranulaat als funderingsmateriaal. Wegbouwkundig onderzoek proefvak Schipluiden.
Public Works Department, Province of Zuid-Holland, The Hague, 1986.

17. Sweere, G.T.H., C.H. Vogelzang and P.J. Galjaard.
De constructieve bijdrage van puingranulaat-funderingen aan flexibele verhardingen. Een vergelijkend meetvakonderzoek.
Report 7-88-209-7, Road and Railroad Research Laboratory, Faculty of Civil Engineering, Delft University of Technology, 1988.

18. Sweere, G.T.H.
Structural contribution of self-cementing granular bases to asphalt pavements.
Proceedings, International symposium on Unbound Aggregates in Roads UNBAR3, Butterworth, 1989, pp. 343 - 353.

19. Specifications for highway works. Parts 1 - 7.
HMSO, London, 1986.

20. Sherwood, P.T., L.W. Tubey and P.G. Roe.
The use of waste and low-grade materials in road construction. Volume 7. Miscellaneous wastes.
Laboratory report 819, Transport and Road Research Laboratory, Crowthorne, UK, 1977.

21. Buchanan, F.
A journey from Madras through the countries of Myson, Canara and Malabar, 2.
East India Company, London, 1807.

22. Sweere, G.T.H.
Genesis of laterites and its engeneering implications.
Proceedings, FURORIS- conference, University of Suriname, Paramaribo, 1982, pp. 61-88.

23. Gidigasu, M.D.
Laterite soil engineering.
Developments in Geotechnical Engineering 9, Elsevier, Amsterdam, 1976.

24. Pannekoek, A.J. and L.M.J.U. van Straaten.
Algemene geologie.
Wolters Noordhoff, Groningen,, The Netherlands, 1982.

25. Sweere, G.T.H. and P.J. Galjaard.
Compaction and strength characteristics of laterites as related to soil composition.
Proceedings, International Conference on Roads and Development, Paris, 1984, pp. 835-841.

26. Standard specifications for transportation materials and methods for sampling and testing. Part 2. Methods for sampling and testing. American Association of State Highway and Transportation Officials, Washington, D.C., 1978.

27. Valerga, B.A., J.A. Shuster, A.L. Love and C.J. van Til. Engineering study of laterite and lateritic soils in connection with construction of roads, highways and airfields. Phase 1 - Southeast Asia (Thailand). Soil and Pavement Consultants of Southeast Asia, Oakland, California, 1969.

28. Morin, W.J. and P.C. Todor. Laterite and lateritic soils and other problem soils of Africa. Lyon Associates and Building and Road Research Institute, Baltimore / Kumasi, 1971.

29. Morin, W.J. and P.C. Todor. Laterite and lateritic soils and other problem soils of the tropics. Lyon Associates and Road Research Institute, Brasilian Highway Department, Baltimore / Brasilia, 1975.

30. Medina, J. and L.M.G. Motta. Design of asphalt pavements using lateritic soils in Brasil. Proceedings, Sixth International Conference Structural Design of Asphalt Pavements, Volume 1, Ann Arbor, USA, pp. 898 - 903.

31. Medina, J, E.S. Preussler, S. Pinto and L. Motta A study of resliency for pavement design in Brasil. Proceedings, Fifth International Conference Structural Design of Asphalt Pavements, Delft, 1982, pp. 726 - 737.

32. Medina, J. and E.S. Preussler. Resilient characteristics of Brazilian soils. Journal of the Geotechnical Engineering Division, ASCE, Vol. 108, No. GT5, May 1982, pp. 697 - 712.

33. British Standard recommendation fot testing of aggregates. Part 1. Compactibility tests for graded aggregates. British Standards Institution, London, 1975.

34. Croney, D. The design and performance of road pavements. HMSO, London, 1977.

35. Soils manual for the design of asphalt pavement structures. Manual series No. 10, March 1978 edition. The Asphalt Institute, Maryland, USA, 1978.

36. Run, L.P.A.J. van, H. de Vroome and G.T.H. Sweere. A user's manual for soil testing with the Hveem stabilometer. Report 7-84-206-1, Road and Railroad Research Laboratory, Department of Civil Engineering, Delft University of Technology, 1984.

37. British Standard methods for sampling and testing of mineral aggregates, sands and fillers. Part 3. Mechanical properties. British Standartds Institution, London, 1975

38. Seed, H.B., C.K. Chan and C.L. Monismith.
Effects of repeated loading on the strength and deformation of a compacted clay.
Proceedings Highway Research Board, No. 34, 1955, pp. 541 - 558.

39. Bishop, A.W. and P.J. Henkel.
The measurement of soil properties in the triaxial cell.
Edward Arnold Publishers Ltd., London, 1957.

40. Seed, H.B., C.K Chan and C.E. Lee.
Resilience characteristics of subgrade soils and their relation to fatigue failures in asphalt pavements.
Proceedings, International Conference Stuctural Design of Asphalt Pavements, Volume 1, Ann Arbor, USA, 1962, pp. 611 - 636.

41. Allen, J.J. and M.R Thompson.
Resilient response of granular materials subjected to time-dependent lateral stresses.
Transportation Research Record 510, 1974, pp. 1 - 13.

42. Barksdale, R.D.
Compressive stress pulse times in flexible pavements for use in dynamic testing.
Transportation Research Record 537, 1975, pp. 32 - 44.

43. Test procedures for characterizing dynamic stress-strain properties of pavement materials.
Special Report 162, Transportation Research Board, Washington, 1975.

44. Donbovand, J.
The results obtained from repeated load triaxial tests.
Internal Report, Pavement Research Group, University of Nottingham, 1987.

45. Brown, S.F. and A.F.L. Hyde.
Significance of cyclic confining stress in repeated-load triaxial testing of granular material.
Transportation Research Record 537, 1975, pp. 49 - 58.

46. Kalcheff, I.V. and R.G. Hicks.
A test procedure for determining the resilient characteristics of granular materials.
Journal of Testing and Evaluation, JTEVA, Vol. 1, No. 6, 1973, pp. 472 - 479.

47. Lentz, R.W. and G.Y. Baladi
Simplified procedure to characterize permanent strain in sand subjected to cyclic loading.
Proceedings, International Symposium on Soils under Cyclic and Transient Loading, Swansea, 1980, pp. 89 - 95.

48. Lentz, R.W. and G.Y. Baladi.
Constitutive equation for permanent strain of sand subjected to cyclic loading.
Transportation Research Record 810, 1981, pp. 50 - 54.

49. Veverka, V.
Raming van de spoordiepte bij wegen met een bitumineuze verharding.
De Wegentechniek, Vol. XXIV, No. 3, 1979, pp. 25 - 45.

50. Descornet, G.
Essais de compression répété sur materiaux granulaires: modulus et déformation permanente.
Ninth International Conference on Soil Mechanics and Foundation Engineering, Tokyo, 1977, pp. 203 - 211.

51. Yong, R.N. and B.P. Warkentin.
Soil properties and behaviour.
Developments in Geotechnical Engineering 5, Elsevier Scientific Publishing Company, Amsterdam, 1975.

52. Bishop, A.W. and G.E. Blight.
Some aspects of effective stress in saturated and partly saturated soils.
Geotechnique, Vol. 13, 1963, pp. 177 - 197.

53. Fredlund, D.G., R.N. Morgenstern and A. Widger.
Shear strength of unsaturated soils.
Canadian Geotechnical Journal, Vol. 15, No. 3, 1978, pp. 313 - 321.

54. Fredlund. D.G.
Appropriate concepts for unsaturated soils.
Canadian Geotechnical Journal, Vol. 16, No. 1, 1979, pp. 121 - 139.

55. Ho, D.Y.F. and D.G. Fredlund.
Increase in strength due to suction for two Hong Kong soils.
Proceedings, ASCE Specialty Conference "Engineering and Construction in Tropical and Residual Soils, Honolulu, Hawaii, 1982, pp. 263 - 295.

56. Thompson, M.R. and Q.L Robnet.
Resilient properties of subgrade soils.
Transportation Engineering Journal, Proceedings of the American Society of Civil Engineers, Vol. 105, No. TE1, 1979, pp. 71 - 89.

57. Fredlund, D.G., A.T. Bergan and E.K. Sauer.
Deformation characteristics of subgrade soils for highways and runways in northern environments.
Canadian Geotechnical Journal, Vol. 12, No. 2, 1975, pp. 213 - 223.

58. Fredlund, D.G., A.T. Bergan and P.K. Wong.
Relation between resilient modulus and stress conditions for cohesive subgrade soils.
Transportation Research Record 642, D.C., 1977, pp. 73 - 81.

59. Motan, E.S. and T.C. Edil.
Repetitive-load behavior of unsaturated soils.
Transportation Research Record 872, 1982, pp. 41 - 48.

60. Jouve, P., J. Martinez, J.L. Paute and E. Ragneau.
Rational model for the flexible pavement deformations.
Proceedings, Sixth International Conference Structural Design of Asphalt Pavements, Volume 1, Ann Arbor, USA, 1987. pp. 50 - 64.

61. Paute, J.L.
Influence de l'état hydrique sur les propriétés méchaniques des sols-support.
Proceedings, Journées de Physique, Laboratoire Central des Ponts et Chaussées, Paris, 1987.

62. Thom, N.H. and S.F. Brown.
The effect of moisture on the structural performance of a crushed limestone road base.
Paper presented to the Annual Meeting of the Transportation Research Board, Washington, D.C., 1987.

63. Boussinesq, V.J.
Applications des potentiels a l'étude de l'équilibre, et du mouvement des solides élastiques avec des notes entendues sur divers points de physique, mathématique et d'analyse.
Gauthier-Villais, Paris, 1885.

64. Burmister, D.M.
The theory of stresses and displacements in layered systems and applications to the design of airport runways.
Proceedings, Highway Research Board, Vol. 23, 1943, pp. 127 - 148.

65. Odemark, N.
Undersoekning av elasticitetsegenskaperne hos olika jordarter samt teori for beraekning av belaegninger enligt elasticitetsteorien.
Meddelande 77, Statens Vaeginstityut, Stockholm, 1949.

66. Duncan, J.M., C.L. Monismith and E.L. Wilson.
Finite element analysis of pavements.
Highway Research Record 228, 1968, pp. 18 - 31.

67. Heukelom, W. and C.R. Foster.
Dynamic testing of pavements.
Journal of Structural Division, ASCE, SM1, February 1960, pp 1 - 29.

68. Brown, S.F., S.C. Loach and M.P. O'Reilly.
Repeated loading of fine grained soils.
Pavement Research Group, Department of Civil Engineering, University of Nottingham, 1987.

69. Heukelom, W. and A.J.G. Klomp.
Dynamic testing as a means of controlling pavements during and after construction.
Proceedings, International Conference Structural Design of Asphalt Pavements, Volume 1, Ann Arbor, USA, 1962, pp. 667 - 679.

70. Brown, S.F. and J.W. Pappin.
Modelling of granular materials in pavements.
Transportation Research Record 1022, 1985, pp. 45 - 51.

71. Hveem, F.N.
Pavement deflections and fatigue failures.
Highway Research Board Bulletin, No. 114, 1955.

72. Hveem, F.N., E. Zube, R. Bridges and R. Forsyth.
The effect of resiliency-deflection relationship on the structural design of asphalt pavements.
Proceedings, International Conference Structural Design of Asphalt Pavements, Ann Arbor, USA, 1962, pp. 649 - 666.

73. Monismith. C.L. H.B. Seed, F.G. Mitry and C.K. Chan.
Prediction of pavement deflections from laboratory tests.
Proceedings, Second International Conference Structural Design of Asphalt Pavements, Ann Arbor, USA, 1967, pp. 109 - 140.

74. Brown, S.F. and P.S. Pell.
An experimental investigation of the stresses, stains and deflections in a layered pavement structure subjected to dynamic loads.
Proceedings, Second International Conference Structural Design of Asphalt Pavements, Ann Arbor, USA, 1967, pp. 487 - 504.

75. Boyce, H.R.
A non-linear model for the elastic behaviour of granular materials under repeated loading.
Proceedings, International Symposium on Soils under Cyclic and Transient Loading, Swansea, UK,, 1980, pp. 285 - 294.

76. Pappin, J.W. and S.F. Brown.
Resilient stress-strain behaviour of a crushed rock.
Proceedings, International Symposium on Soils under Cyclic and Transient Loading, Swansea, UK, 1980, pp. 169 -177.

77. Mayhew, H.C.
Resilient properties of unbound road base under repeated triaxial loading.
Laboratory Report 1088, Transport and Road Research Laboratory, Crowthorne, UK, 1983.

78. Uzan, J.
Characterization of granular material.
Transportation Research Record 1022, Washington, D.C., 1985, pp. 52 - 59.

79. Sweere, G.T.H., A. Penning and E. Vos.
Development of a structural design procedure for asphalt pavements with crushed rubble base courses.
Proceedings, Sixth International Conference Structural Design of Asphalt Pavements, Volume 1, Ann Arbor, USA, 1987, pp. 35 - 49.

80. Barksdale, R.D.
Laboratory evaluation of rutting in base course materials.
Proceedings, Third International Conference Structural Design of Asphalt Pavements, Volume 1, London, 1972, pp. 161 - 174.

81. Annual book of ASTM standards, Sec. 4, Vol. 04.08, Soil and Rock; Building Stones.
American Society for Testing and Materials, Philadelphia, 1985.

82. Gerlach, A., J. Hothan and H. Lücke
Zur Bestimmung der Nachverdichtbarkeit von Tragschichten ohne Bindemittel.
Strasse und Autobahn, No. 4, 1987, pp. 148 - 152.

83. Day, J.B.A.
Proof testing of unbound layers.
Proceedings, Symposium on Unbounb Aggregates in Roads UNBAR 1, University of Nottingham, 1981, pp. 15 - 20.

84. Westergaard, H.M.
Stresses in concrete pavements computed by theoretical analysis.
Public Roads, Vol. 7, No. 2, 1926, pp. 25-35.

85. Burmister, D.M.
Prototype load-bearing tests for foundations of structures and pavements.
ASTM STP No. 23, American Society for Testing and Materials, Philadelphia, 1963, pp. 98 - 118.

86. Richtlinien für die Standardisierung des Oberbaues von Verkehrsflächen RSTO 86.
Forschungsgesellschaft für Strassen- und Verkehrswesen, 1986.

87. Garrick, N.W. and C.F. Scholer.
Rapid determination of base course strength using the Clegg Impact Tester.
Transportation Research Record 1022, 1985, pp. 115 - 119.

88. Brown, S.F., W.S. Tam and J.M. Brunton.
Development of a structural method for the evaluation of pavements.
Proceedings, Second International Conference Bearing Capacity of Roads and Airfields, Plymouth, 1986, pp. 267 - 276.

89. Tam, W.S. and S.F. Brown.
Use of the Falling Weight Deflectometer for in-situ evaluation of granular materials in pavements.
Proceedings of the Australian Road Research Board, Vol. 14, Part 5, 1988, pp. 155 - 163.

90. Brown, S.F., W.S. Tam and J.M. Brunton.
Structural evaluation and overlay design: analysis and interpretation.
Proceedings, Sixth International Conference Structural Design of Asphalt Pavements, Volume 1, Ann Arbor, USA, 1987, pp. 1013 - 1028.

91. Structural design of inter-urban and rural road pavements.
Technical Recommendations for Highways TRH4.
National Institute for Transport and Road Research, Pretoria, 1985.

92. Freeme, C.R., J.H. Maree and A.W. Viljoen.
Mechanistic design of asphalt pavements and verification using the heavy vehicle simulator.
Proceedings, Fifth International Conference Structural Design of Asphalt Pavements, Volume 1, Delft, 1982, pp. 156 - 173.

93. Freeme, C.R., M. de Beer and A.W. Viljoen.
The behaviour and mechanistic design of asphalt pavements.
Proceedings, Sixth International Conference Stuctural Design of Asaphalt Pavements, Volume 1, Ann Arbor, USA, 1987, pp. 333 - 343.

94. Road Note 29. A guide for the structural design of pavements for new roads.
HMSO, London, 1977.

95. Behr, H. and H. Buseck.
Entwicklung eines Schnellverfahrens zur Bestimmung des Verformungsmoduls von Böden.
Stasse und Autobahn 4, 1986, pp. 167 - 168.

96. Addendum to the Shell Pavement Design Manual.
Shell International Petroleum Company Limited, London, 1985.

97. Brown, S.F. and R.D. Barksdale.
Keynote Lecture "Pavement design and materials".
Proceedings, Sixth International Conference Stuctural Design of Asphalt Pavements, Volume 2, Ann Arbor, USA, 1987, pp. 117 - 148.

98. Gerritsen, A.H. and R.C. Koole.
Seven years' experience with the structural aspects of the Shell Pavement Design Manual.
Proceedings, Sixth International Conference Structural Design of Asphalt Pavements, Volume 1, Ann Arbor, USA, 1987, pp. 94 -107.

99. Sweere, G.T.H. and C.H. Vogelzang.
Linear Tracking Apparatus LINTRACK.
ASFALT, Vol. 16. No. 2, June 1989.

100. Grace, H., D.W. Hight and D.G. Toll.
Some recent work on the use of locally occuring materials as bases for bituminous surfaced low-volume roads.
Proceedings, First International Conference on Geomechanics in Tropical Lateritic and Saprolitic Soils TropicaLS'85, Volume 2, Brasilia, 1985, pp. 295 - 309.

101. Guidelines for road construction materials. Technical recomdations for highways TRH 14.
National Institute for Transport and Road Research, Pretoria, South Africa, 1985.

102. Various properties of natural sands for Nethertlands highway engineering.
SCW Record 4, Study Centre for Road Construction, Arnhem, 1978.

103. Sweere, G.T.H., P.J. Galjaard and H.F.J. Tjong Tjin Joe.
Engineering behaviour of laterites in road constructions.
Proceedings, Second International Conference on Soil Mechanics in Tropical Soils, Volume 1, Singapore, 1988, pp. 421 - 427.

104. NEN 2560.
Controlezeven. Draarzeven en plaatzeven met ronde en vierkante gaten.
Nederlands Normalisatie Instituut.

105. Rijkswaterstaat.
Verband tussen vochtgehalte en dichtheid van funderingsmateriaal (Proctorproef). Eénpuntsbepaling.
Notitie MAA-N-83021, Road and Hydraulic Engineering Division, Rijkswaterstaat, 1983.

106. Rijkswaterstaat.
Trilhamerproef. Verdichtingsproef voor ongebonden funderingsmateriaal.
Notitie MAO-N-85092, Road and Hydraulic Engineering Division, Rijkswaterstaat, Delft, 1985.

107. Eerden, M.A.C. van der and G.T.H. Sweere.
Vergelijkend onderzoek naar het gedrag onder herhaalde belasting van gebroken puin, lava en grind.
Report 7-83-201-3, Road and Railroad Research Laboratory, Faculty of Civil Engineering, Delft University of Technology, 1983.

108. Sweere, G.T.H. and C.H. Vogelzang.
Bepaling van de elastische en plastische materiaalkarakteristieken van een aantal alternatieve funderingsmaterialen.
Report 7-85-201-5, Road and Railroad Research Laboratory, Faculty of Civil Engineering, Delft University of Technology, 1985.

109. Sweere, G.T.H. and R.J. Henny.
Bepaling van de vervormingseigenschappen van een drietal puingranulaten.
Report 7-87-201-14, Road and Railroad Research Laboratory, Faculty of Civil Engineering, Delft University of Technology, 1987,.

110. Henny, R.J.H. and G.T.H. Sweere.
Vergelijkend onderzoek steenfunderingsmaterialen. Rapportage Rankingonderzoek.
Report 7-85-201-15, road and Railroad Research Laboratory, Faculty of Civil Engineering, Delft University of Technology, 1988.

111 Thom, N.H. and S.F. Brown.
The mechanical properties of unbound aggregates from various sources.
Proceedings, International Symposium on Unbound Aggregates in Roads UNBAR3, Butterworth, 1988, pp. 130 - 143.

112. Ladd, R.S.
Preparing test specimens using undercompaction.
Geotechnical Testing Journal, Vol. 1, No. 1, pp. 16 - 23.

113. Sweere, G.T.H. and P.J. Galjaard.
Herhaalbaarheid en onderlinge vergelijking van dynamische triaxiaalproeven.
Report 7-86-201-8, Road and Railroad Research Laboratory, Faculty of Civil Engineering, Delft University of Technology, 1986.

114. Henny. R.J. and G.T.H. Sweere.
Vergelijking resilient moduli bepaald met statische en dynamische triaxiaalproeven.
Report 7-89-201-23, Road and Rairoad Research Laboratory, Faculty of Civil Engineering, Delft University of Technology, 1989.

115. Sweere, G.T.H. and P.J. Galjaard.
Determination of the resilient modulus of sands by means of static loading triaxial tests.
Report 7-86-201-10, Road and Railroad Research Laboratory, Faculty of Civil Engineering, Delft University of Technology, 1986.

116. Sweere, G.T.H. and P.J. Galjaard.
Repeated static loading triaxial tests for determination of resilient properties of sands.
Transportation Research Record 1192, 1988, pp. 8 - 15.

117. Bie, B de and G.T.H. Sweere.
Bepaling van de dynamische materiaalkarakteristieken van funderingsmaterialen met behulp van statische triaxiaalproeven.
Report 7-85-201-4, Road and Railroad Research Laboratory, Faculty of Civil Engineering, Delft University of Technology, 1985.

118. Yong, R.N., G.T.H. Sweere, M.L. Sadana, Z.C. Moh and Y.C. Chiang.
Composition effect on suction of a residual soil.
Proceedings, ASCE Specialty Conference on Engineering and Construction in Tropical and Residual Soils, Honolulu, Hawaii, 1982, pp. 296-313.

119. Sweere, G.T.H. and Galjaard, P.J.
The methylene blue test as a rapid means of estimating the cation exchange capacity of soils.
Proceedings, Symposium on Geotechnical Aspects of Mass and Material Transportation, Bangkok, 1984. pp. 533-542.

120. Janssen, P.P.M.K. and P.J. Galjaard.
Onderzoek naar de invloed van fysische en chemische factoren op het zwelgedrag van gronden uit Soedan.
Report 7-85-206-3, Road and Railroad Research Laboratory, Faculty of Civil Engineering, Delft University of Technology, 1985.

121. Fuller, W.B. and F.W. Thompson.
The laws of proporting concrete.
A.S.C.E.-transcipts, Volume 59, Paper No. 1053, 1907

122. Rada, G. and M.W. Witczak.
Material layer coefficients of unbound granular materials from resilient modulus.
Transportation Research Record 852, 1982, pp. 15 - 21.

123. Rada, G. and M.W. Witczak.
Comprehensive evaluation of laboratory resilient moduli results for granular material.
Transportation Research Record 810, 1981, pp. 23 - 33.

124. Brown, S.F. and D.Y. Bush.
Dynamic response of model pavement structure.
Journal of the Transportation Division, Proceedings of the American Society of Civil Engineers, Vol. 98, TE 4, Nov. 1972, pp. 1005 - 1022.

125. Sweere, G.T.H. and P.J. Galjaard.
In-situ determination of granular base course stiffness.
Proceedings, International Symposium on Unbound Aggregates in Roads UNBAR3, Butterworth, 1989, pp. 354 - 366.

126. Sande, H. van de.
Plaatbelastingsproeven op proefvakken TU Delft.
Report WXM-R-88-04, Road and Hydraulic Engineering Division, Rijkswaterstaat, Delft, 1988.

127. Sweere, G.T.H. and R.J. Henny.
Toename van de elastische stijfheid van betongranulaat met de tijd.
Report 7-87-201-16, Road and Railroad Research Laboratory, Faculty of Civil Engineering, Delft University of Technology, 1987.

128. Henny, R.J. and G.T.H. Sweere.
Ontwikkeling van licht-gebonden menggranulaat met de tijd.
Report 7-88-201-19, Raod and Railroad Research laboratory, Faculty of Civil Engineering, Delft University of Technology, 1988.

129. Kroezen, M.F.J.M.
Enige kritische beschouwingen betreffende de plaatbelastingsproef.
Report 7-70-104-1, Road and Railroad Research Laboratory, Faculty of Civil Engineering, Delft University of Technology, 1970.

130. Gurp, CH.A.P.M. van and F. Houtman.
Moduli Information System MISS. Terugrekenen van moduli van wegverhardingen.
Report 7-88-203-5, Road and Railroad Research Laboratory, Faculty of Civil Engineering, Delft University of Technology, 1988.

131. Barksdale, R.D.
Performance of crushed stone base courses.
Transportation Research Record 954, 1985, pp. 78 - 87.

132. Dauzats, M. and A. Rampal.
Mechanism of surface cracking in wearing courses.
Proceedings, Sixth International Conference Structural Design of Asphalt Pavements, Ann Arbor, USA, 1987, pp. 232 - 247.

133. Bonnaure, F., G. Gest, A. Gravois and P. Ugé.
A new method for predicting the stiffness of asphalt paving mixtures.
Proceedings, Association of Asphalt paving Technologists, Volume 46, 1977.

134. Bosch, H.G. van den and G.T.H. Sweere.
Interpretatia meetgegevens Meetvak 1. Deel 1: Meetrapport.
Rapport 7-88-209-5, Road and Railroad Research Laboratory, Faculty of Civil Engineering, Delft University of Technology, 1988.

APPENDIX 1

MATERIALS USED IN TEST PROGRAM

material number	material name (English)	material name (Dutch)	grading	code
C01	lava	lava	fine	LAB
C02			coarse	LAO
C03	porphyry	porfier	fine	POB
C04			coarse	POO
C05	crushed gravel	gebroken grind	fine	GGB
C06			coarse	GGO
C07	limestone	kalksteen	fine	KAB
C08			coarse	KAO
C09	stol	stol	natural	STN
C10	silicon manganese slag	silico-mangaanslak	commercial	SMC
R01	crushed masonry 1	metselwerkgranulaat 1	fine	MGB
R02			coarse	MGO
R03	crushed masonry 2	metselwerkgranulaat 2	fine	M2B
R04			coarse	M2O
R05	crushed concrete 1	betongranulaat 1	fine	BGB
R06			coarse	BGO
R07	crushed clinskers	klinkergranulaat	fine	KGB
R08			coarse	KGO
R09	crushed masonry/concrete	menggranulaat	fine	FFB
R10			coarse	FFO
R11	crushed concrete 2	betongranulaat 2	commercial	B2C
R12	crushed rubble 1	korrelmix 1	commercial	K1C
R13	crushed rubble 2	korrelmix 2	commercial	K2C
R14	crushed rubble 3	korrelmix 3	commercial	K3C
R15	waste incineration slag	AVI-slakken	commercial	AVC

material	material name (English)	material name (Dutch)	grading	code
S01	Echteld sand	Echteld zand	natural	ELN
S02	Echten sand	Echten zand	natural	ENN
S03	Eems sand	Eems zand	natural	EEN
S04	Eastern Scheldt sand	Oosterschelde zand	natural	OSN
S05	Winterwijk sand	Winterswijk zand	natural	WIN
S06	Zeyen sand	Zeyen zand	natural	ZEN
L01	laterite	lateriet	natural	HA2
L02	laterite	lateriet	natural	AB1
L03	laterite	lateriet	natural	BB1
L04	laterite	lateriet	natural	IB1
L05	laterite	lateriet	natural	BB2
L06	laterite	lateriet	natural	AC

APPENDIX 2

MATERIAL INFORMATION SHEETS

MATERIAL INFORMATION SHEET GROUPS C AND R

MATERIAL NUMBER	CODE	MATERIAL NAME
C01	LAB	lava

GRADING

sieve [mm]	percentage passing
.020	...
.063	4.4
.125	8.2
.250	15.7
.500	26.1
1.0	37.3
2.0	50
4.0	60
8.0	76
16.0	90
22.4	95
31.5	98
45.0	100

DENSITY	[kg/m³]	at MC [%]	CBR 0/22.4 at PEN [%]	[in]
MMPD	1889	10.5	...	.1
SPPD	1637	11.4	...	.2
MVHD	1849	11.0		

DEGRADATION

fraction [mm]	value
4.0 - 5.6	VF= 0.66
5.6 - 8.0	0.70
8.0 - 11.2	0.71
11.2 - 16.0	0.71
16.0 - 22.4	0.70
22.4 - 31.5	0.70
31.5 - 45.0	0.69

SPECIFIC GRAVITY

fraction [mm]	Gs [kg/m³]
4-8	1996
8-16	1914
16-31.5	1871
4-31.5	1941

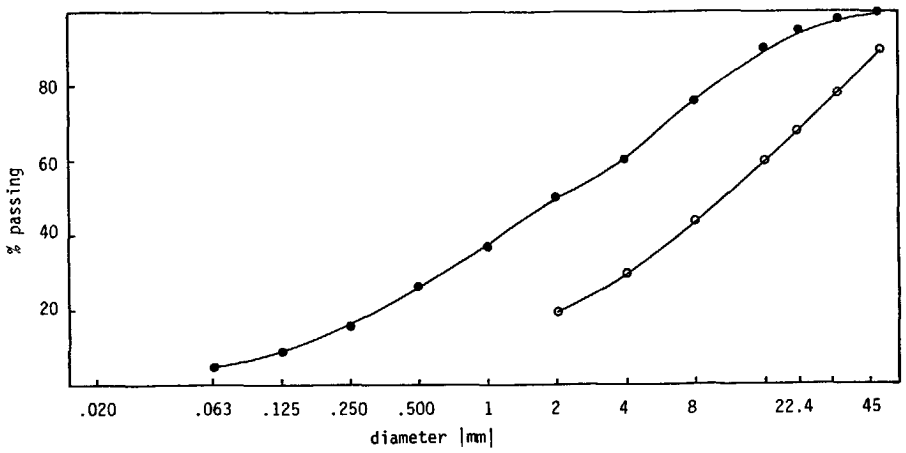

MMPD = Maximum Modified Proctor Density
SPPD = Single Point Proctor Density
MVHD = Maximum Vibrating Hammer Density

VF = Verbrijzelingsfactor

MATERIAL INFORMATION SHEET GROUPS C AND R

MATERIAL NUMBER	CODE	MATERIAL NAME
CO2	LAO	lava

GRADING

sieve [mm]	percentage passing
.020	...
.063	1.8
.125	3.3
.250	6.3
.500	10.5
1.0	14.9
2.0	20
4.0	30
8.0	44
16.0	60
22.4	69
31.5	78
45.0	90

DENSITY	[kg/m³]	at MC [%]	CBR 0/22.4 at PEN [%]	[in]
MMPD	1682	9.3	...	.1
SPPD	1576	12.1	...	.2
MVHD	1678	8.6		

DEGRADATION

fraction [mm]	value
4.0 - 5.6	VF= 0.66
5.6 - 8.0	0.70
8.0 - 11.2	0.71
11.2 - 16.0	0.71
16.0 - 22.4	0.70
22.4 - 31.5	0.70
31.5 - 45.0	0.69

SPECIFIC GRAVITY

fraction [mm]	Gs [kg/m³]
4-8	1996
8-16	1914
16-31.5	1871
4-31.5	1941

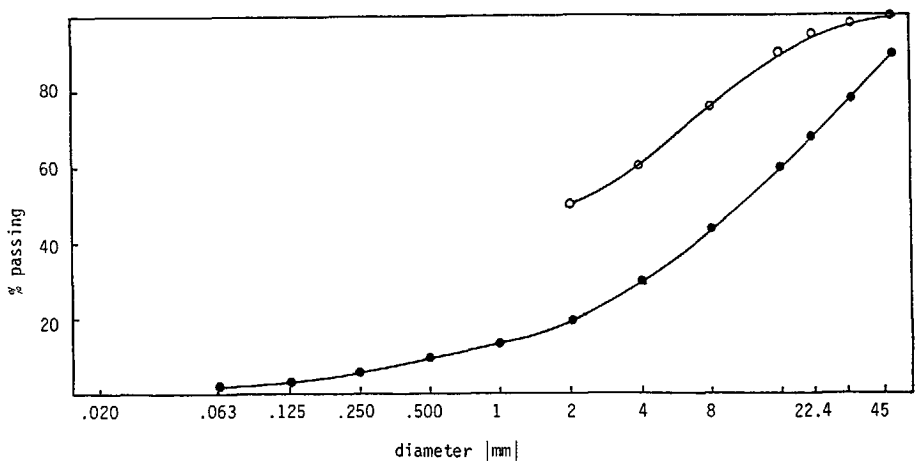

MMPD = Maximum Modified Proctor Density
SPPD = Single Point Proctor Density
MVHD = Maximum Vibrating Hammer Density
VF = Verbrijzelingsfactor

MATERIAL INFORMATION SHEET GROUPS C AND R

MATERIAL NUMBER	CODE	MATERIAL NAME
C03	POB	porphyry

GRADING

sieve [mm]	percentage passing
.020	...
.063	9.6
.125	12.3
.250	16.3
.500	23.4
1.0	33.8
2.0	50
4.0	60
8.0	76
16.0	90
22.4	95
31.5	98
45.0	100

DENSITY	at MC	CBR 0/22.4 at PEN	
[kg/m³]	[%]	[%]	[in]
MMPD 2260	4.5	175	.1
SPPD 2160	5.2	235	.2
MVHD 2340	4.5		

DEGRADATION

fraction [mm]	value
4.0 - 5.6	VF= 0.86
5.6 - 8.0	0.85
8.0 - 11.2	0.88
11.2 - 16.0	0.86
16.0 - 22.4	0.87
22.4 - 31.5	0.85
31.5 - 45.0	...

SPECIFIC GRAVITY

fraction [mm]	Gs [kg/m³]
4-8	2585
8-16	2671
16-31.5	2710
4-31.5	2665

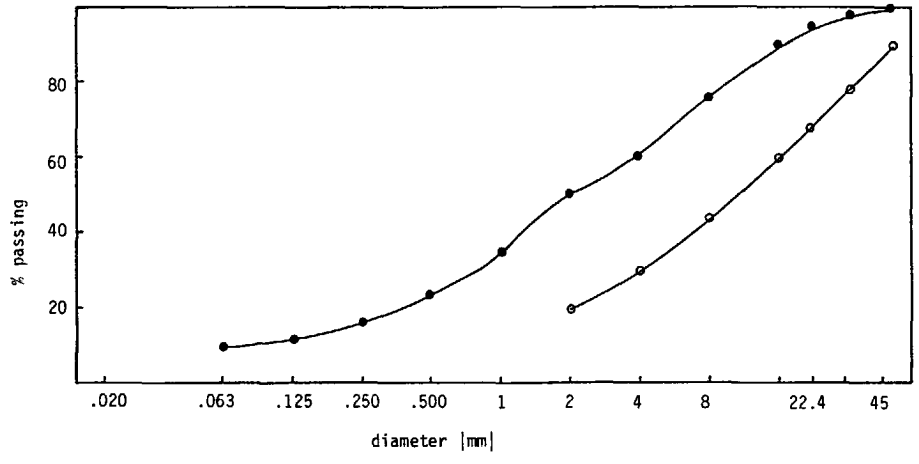

MMPD = Maximum Modified Proctor Density
SPPD = Single Point Proctor Density
MVHD = Maximum Vibrating Hammer Density

VF = Verbrijzelingsfactor

MATERIAL INFORMATION SHEET GROUPS C AND R

MATERIAL NUMBER	CODE	MATERIAL NAME
C04	P00	porphyry

GRADING

sieve [mm]	percentage passing
.020	...
.063	3.9
.125	4.9
.250	6.5
.500	9.4
1.0	13.5
2.0	20
4.0	30
8.0	44
16.0	60
22.4	68
31.5	78
45.0	90

	DENSITY [kg/m³]	at MC [%]	CBR 0/22.4 at PEN [%]	[in]
MMPD	2038	2.6	96	.1
SPPD	2196	3.7	123	.2
MVHD	2166	3.3		

DEGRADATION

fraction [mm]	value
4.0 - 5.6	VF= 0.86
5.6 - 8.0	0.85
8.0 - 11.2	0.88
11.2 - 16.0	0.86
16.0 - 22.4	0.87
22.4 - 31.5	0.85
31.5 - 45.0	...

SPECIFIC GRAVITY

fraction [mm]	Gs [kg/m³]
4-8	2585
8-16	2671
16-31.5	2710
4-31.5	2665

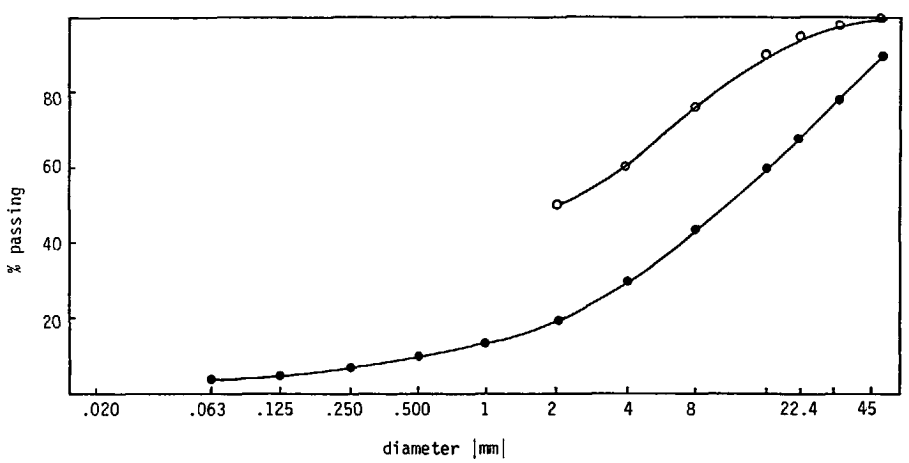

MMPD = Maximum Modified Proctor Density
SPPD = Single Point Proctor Density
MVHD = Maximum Vibrating Hammer Density
VF = Verbrijzelingsfactor

MATERIAL INFORMATION SHEET GROUPS C AND R

MATERIAL NUMBER	CODE	MATERIAL NAME
C05	GGB	crushed gravel

GRADING

sieve [mm]	percentage passing
.020	...
.063	1.1
.125	4.6
.250	13.4
.500	25.9
1.0	39.5
2.0	50
4.0	60
8.0	76
16.0	90
22.4	95
31.5	98
45.0	100

DENSITY at MC	[kg/m³]	[%]	CBR 0/22.4 at PEN [%]	[in]
MMPD	2002	6.6	140	.1
SPPD	1892	6.6	...	.2
MVHD	1917	3.7		

DEGRADATION

fraction [mm]	value
4.0 - 5.6	VF= 0.84
5.6 - 8.0	0.83
8.0 - 11.2	0.87
11.2 - 16.0	0.83
16.0 - 22.4	0.85
22.4 - 31.5	0.84
31.5 - 45.0	...

SPECIFIC GRAVITY

fraction [mm]	Gs [kg/m³]
4-8	2555
8-16	2563
16-31.5	2590
4-31.5	2563

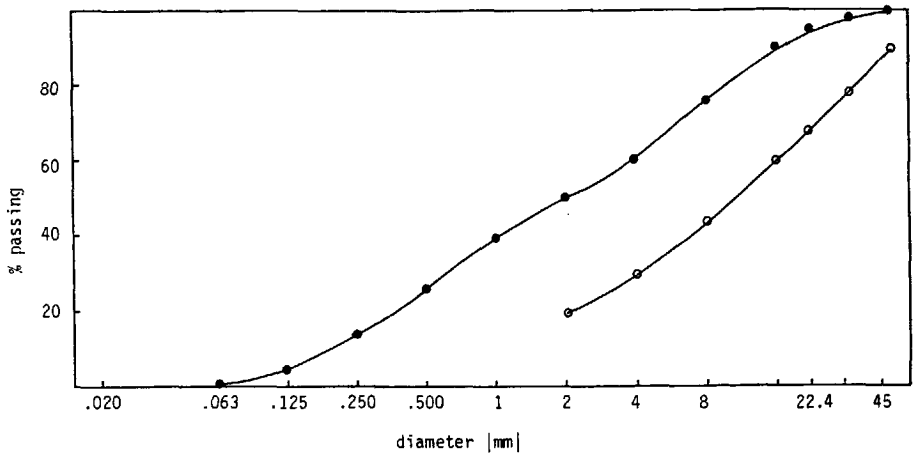

MMPD = Maximum Modified Proctor Density
SPPD = Single Point Proctor Density
MVHD = Maximum Vibrating Hammer Density
VF = Verbrijzelingsfactor

MATERIAL INFORMATION SHEET GROUPS C AND R

MATERIAL NUMBER	CODE	MATERIAL NAME
C06	GGO	crushed gravel

GRADING

sieve [mm]	percentage passing
.020	...
.063	0.4
.125	1.8
.250	5.4
.500	10.4
1.0	15.8
2.0	20
4.0	30
8.0	44
16.0	60
22.4	69
31.5	78
45.0	90

DENSITY	[kg/m³]	at MC [%]	CBR 0/22.4 at PEN [%]	[in]
MMPD	2029	4.8	143	.1
SPPD	2103	4.8	...	.2
MVHD	2084	1.8		

DEGRADATION

fraction [mm]	value
4.0 - 5.6	VF= 0.84
5.6 - 8.0	0.83
8.0 - 11.2	0.87
11.2 - 16.0	0.83
16.0 - 22.4	0.85
22.4 - 31.5	0.84
31.5 - 45.0	...

SPECIFIC GRAVITY

fraction [mm]	Gs [kg/m³]
4-8	2555
8-16	2563
16-31.5	2590
4-31.5	2563

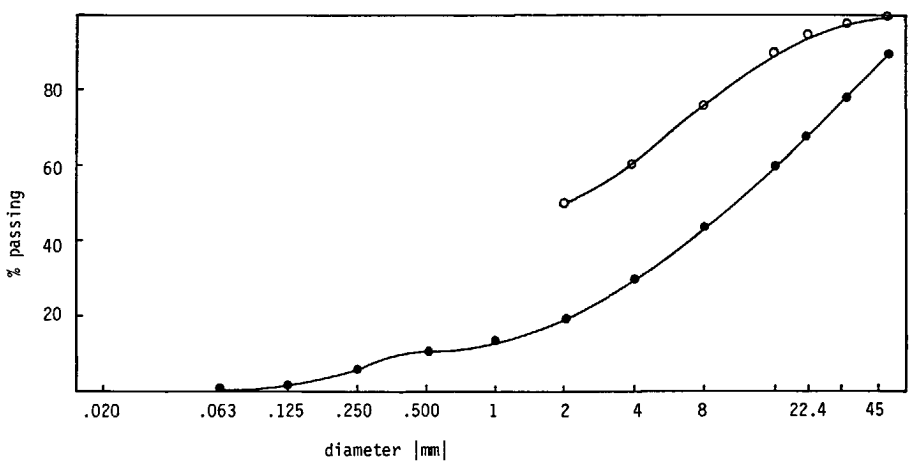

MMPD = Maximum Modified Proctor Density
SPPD = Single Point Proctor Density
MVHD = Maximum Vibrating Hammer Density

VF = Verbrijzelingsfactor

MATERIAL INFORMATION SHEET GROUPS C AND R

MATERIAL NUMBER	CODE	MATERIAL NAME
C07	KAB	limestone

GRADING

sieve [mm]	percentage passing
.020	12.4
.063	17.9
.125	20.8
.250	25.1
.500	32.5
1.0	40.2
2.0	50
4.0	60
8.0	76
16.0	90
22.4	95
31.5	98
45.0	100

	DENSITY [kg/m³]	at MC [%]	CBR 0/22.4 at PEN [%]	[in]
MMPD	2291	4.7	85	.1
SPPD	2182	8.0	112	.2
MVHD	2352	5.0		

DEGRADATION

fraction [mm]	value
4.0 - 5.6	VF= 0.82
5.6 - 8.0	0.80
8.0 - 11.2	0.81
11.2 - 16.0	0.79
16.0 - 22.4	0.79
22.4 - 31.5	0.79
31.5 - 45.0	...

SPECIFIC GRAVITY

fraction [mm]	Gs [kg/m³]
4-8	2637
8-16	2671
16-31.5	2687
4-31.5	2669

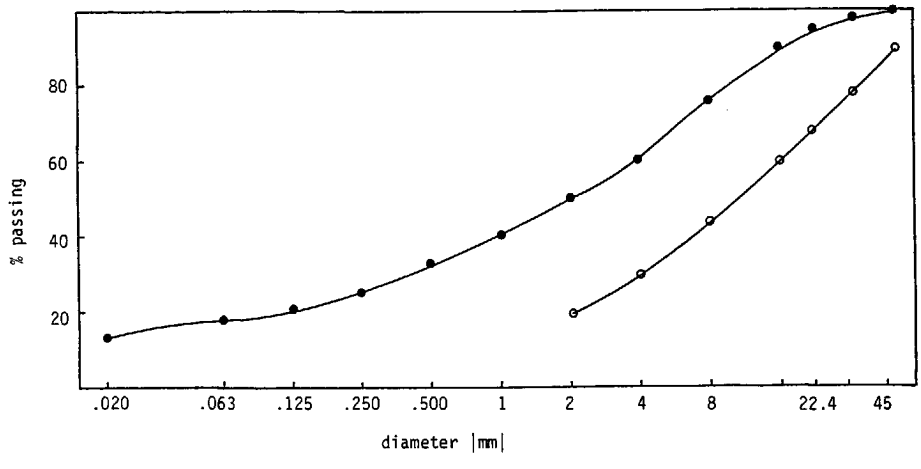

MMPD = Maximum Modified Proctor Density
SPPD = Single Point Proctor Density
MVHD = Maximum Vibrating Hammer Density

VF = Verbrijzelingsfactor

MATERIAL INFORMATION SHEET GROUPS C AND R

MATERIAL NUMBER	CODE	MATERIAL NAME
C08	KAO	limestone

GRADING

sieve [mm]	percentage passing
.020	5.0
.063	7.2
.125	8.4
.250	10.1
.500	13.0
1.0	16.1
2.0	20
4.0	30
8.0	44
16.0	60
22.4	69
31.5	78
45.0	90

DENSITY at MC

	[kg/m³]	[%]
MMPD	2288	6.1
SPPD	2278	5.5
MVHD	2235	3.7

CBR 0/22.4 at PEN

[%]	[in]
66	.1
86	.2

DEGRADATION

fraction [mm]	value
4.0 - 5.6	VF= 0.82
5.6 - 8.0	0.80
8.0 - 11.2	0.81
11.2 - 16.0	0.79
16.0 - 22.4	0.79
22.4 - 31.5	0.79
31.5 - 45.0	...

SPECIFIC GRAVITY

fraction [mm]	Gs [kg/m³]
4-8	2637
8-16	2671
16-31.5	2687
4-31.5	2669

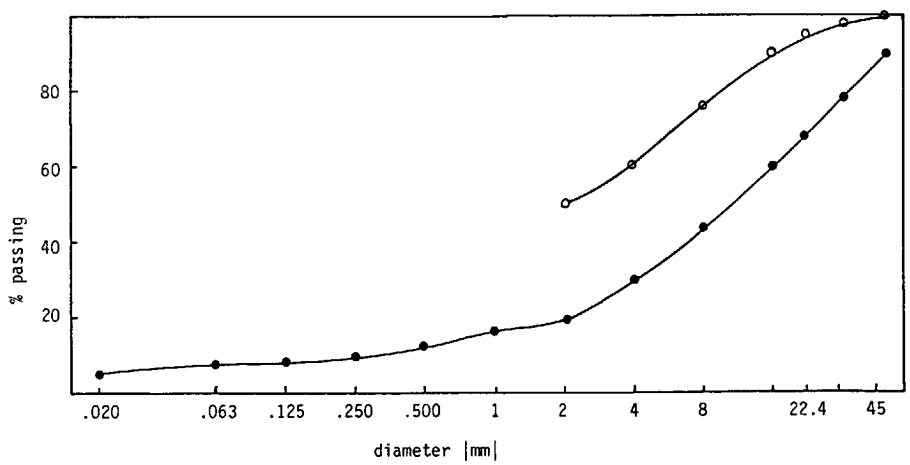

MMPD = Maximum Modified Proctor Density
SPPD = Single Point Proctor Density
MVHD = Maximum Vibrating Hammer Density

VF = Verbrijzelingsfactor

MATERIAL INFORMATION SHEET **GROUPS C AND R**

MATERIAL NUMBER	CODE	MATERIAL NAME
C09	STN	stol

GRADING

sieve [mm]	percentage passing
.020	...
.063	6.0
.125	7.8
.250	11.2
.500	18.0
1.0	22.5
2.0	25
4.0	30
8.0	40
16.0	60
22.4	71
31.5	86
45.0	96

	DENSITY [kg/m³]	at MC [%]	CBR 0/22.4 at PEN [%]	[in]
MMPD	2174	4.4	139	.1
SPPD	2225	4.7	179	.2
MVHD	2265	4.3		

DEGRADATION

fraction [mm]	value
4.0 - 5.6	VF= 0.91
5.6 - 8.0	0.87
8.0 - 11.2	0.90
11.2 - 16.0	0.85
16.0 - 22.4	0.85
22.4 - 31.5	0.82
31.5 - 45.0	...

SPECIFIC GRAVITY

fraction [mm]	Gs [kg/m³]
4-8	2460
8-16	2509
16-31.5	2529
4-31.5	2513

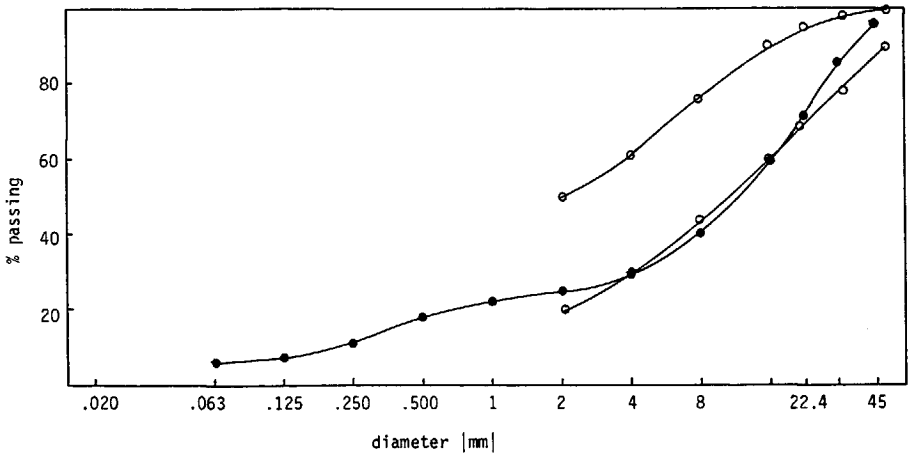

MMPD = Maximum Modified Proctor Density
SPPD = Single Point Proctor Density
MVHD = Maximum Vibrating Hammer Density

VF = Verbrijzelingsfactor

MATERIAL INFORMATION SHEET GROUPS C AND R

MATERIAL NUMBER	CODE	MATERIAL NAME
C10	SMC	silicon manganese slag

GRADING

sieve [mm]	percentage passing
.020	...
.063	3.4
.125	5.2
.250	8.6
.500	12.2
1.0	15.8
2.0	21
4.0	29
8.0	44
16.0	68
22.4	84
31.5	99
45.0	100

DENSITY at MC

	[kg/m³]	[%]
MMPD	1857	4.5
SPPD	1676	5.4
MVHD	1772	5.4

CBR 0/22.4 at PEN

[%]	[in]
95	.1
110	.2

DEGRADATION

fraction [mm]	value
4.0 - 5.6	VF= 0.69
5.6 - 8.0	0.69
8.0 - 11.2	0.71
11.2 - 16.0	0.72
16.0 - 22.4	0.73
22.4 - 31.5	0.75
31.5 - 45.0	...

SPECIFIC GRAVITY

fraction [mm]	Gs [kg/m³]
4-8	2039
8-16	2247
16-31.5	2396
4-31.5	2146

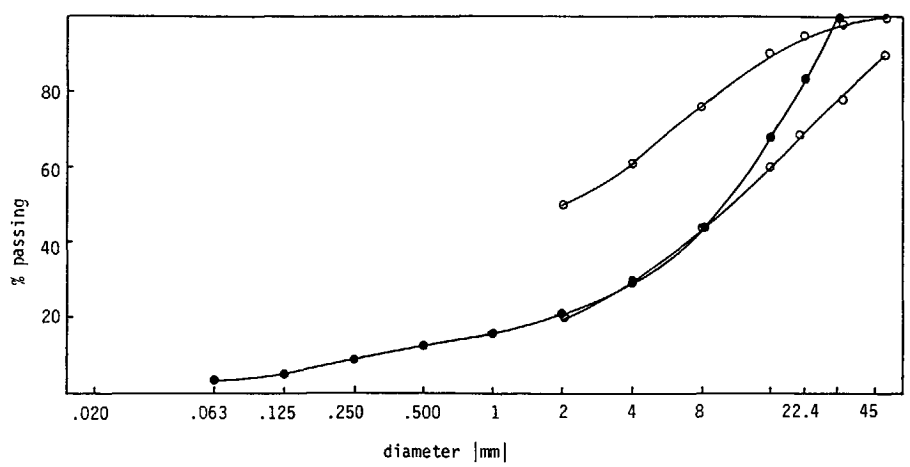

MMPD = Maximum Modified Proctor Density
SPPD = Single Point Proctor Density
MVHD = Maximum Vibrating Hammer Density
VF = Verbrijzelingsfactor

MATERIAL INFORMATION SHEET GROUPS C AND R

MATERIAL NUMBER	CODE	MATERIAL NAME
R01	MGB	crushed masonry 1

GRADING

sieve [mm]	percentage passing
.020	...
.063	5.6
.125	9.4
.250	17.3
.500	28.5
1.0	37.9
2.0	50
4.0	60
8.0	76
16.0	90
22.4	95
31.5	98
45.0	100

	DENSITY [kg/m³]	at MC [%]	CBR 0/22.4 at PEN [%]	[in]
MMPD	1536	18.4	97	.1
SPPD	1430	21.5	110	.2
MVHD	1447	21.2		

DEGRADATION

fraction [mm]	value
4.0 - 5.6	VF= 0.65
5.6 - 8.0	0.63
8.0 - 11.2	0.65
11.2 - 16.0	0.65
16.0 - 22.4	0.67
22.4 - 31.5	0.67
31.5 - 45.0	...

SPECIFIC GRAVITY

fraction [mm]	Gs [kg/m³]
4-8	1535
8-16	1622
16-31.5	1730
4-31.5	1699

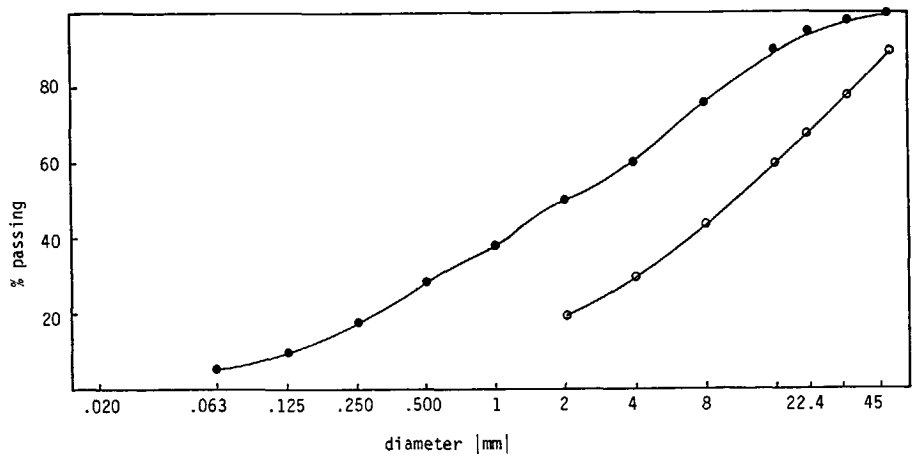

MMPD = Maximum Modified Proctor Density
SPPD = Single Point Proctor Density
MVHD = Maximum Vibrating Hammer Density

VF = Verbrijzelingsfactor

MATERIAL INFORMATION SHEET GROUPS C AND R

MATERIAL NUMBER	CODE	MATERIAL NAME
R02	MGO	crushed masonry 1

GRADING

sieve [mm]	percentage passing
.020	...
.063	2.3
.125	3.8
.250	6.9
.500	11.4
1.0	15.2
2.0	20
4.0	30
8.0	44
16.0	60
22.4	69
31.5	78
45.0	90

	DENSITY [kg/m³]	at MC [%]	CBR 0/22.4 at PEN [%]	[in]
MMPD	1534	18.7	86	.1
SPPD	1437	16.6	106	.2
MVHD	1446	17.0		

DEGRADATION

fraction [mm]	value
4.0 - 5.6	VF= 0.65
5.6 - 8.0	0.63
8.0 - 11.2	0.65
11.2 - 16.0	0.65
16.0 - 22.4	0.67
22.4 - 31.5	0.67
31.5 - 45.0	...

SPECIFIC GRAVITY

fraction [mm]	Gs [kg/m³]
4-8	1535
8-16	1622
16-31.5	1730
4-31.5	1699

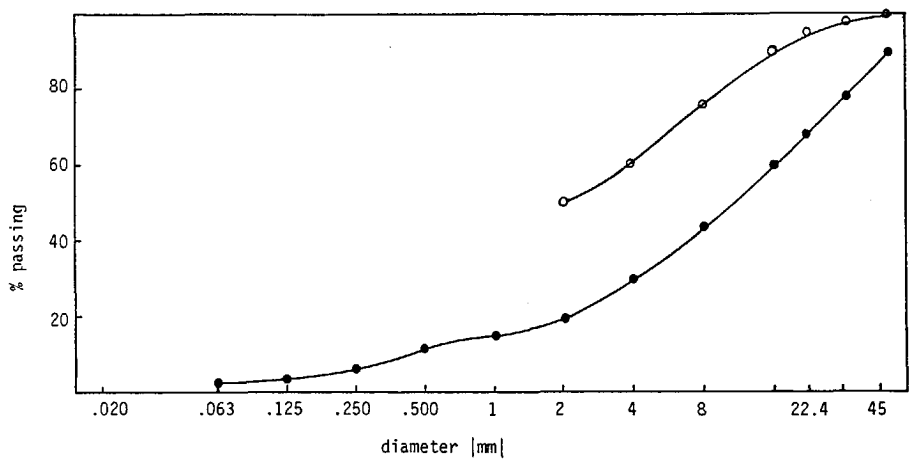

MMPD = Maximum Modified Proctor Density
SPPD = Single Point Proctor Density
MVHD = Maximum Vibrating Hammer Density

VF = Verbrijzelingsfactor

MATERIAL INFORMATION SHEET **GROUPS C AND R**

MATERIAL NUMBER	CODE	MATERIAL NAME
R03	M2B	crushed masonry 2

GRADING

sieve [mm]	percentage passing
.020	...
.063	8.9
.125	14.5
.250	27.9
.500	40.9
1.0	46.2
2.0	50
4.0	60
8.0	76
16.0	90
22.4	95
31.5	98
45.0	100

	DENSITY [kg/m³]	at MC [%]	CBR 0/22.4 at PEN [%]	[in]
MMPD	1629	15.6	103	.1
SPPD	1518	16.5	121	.2
MVHD	1609	17.1		

DEGRADATION

fraction [mm]	value
4.0 - 5.6	VF= 0.67
5.6 - 8.0	0.67
8.0 - 11.2	0.67
11.2 - 16.0	0.65
16.0 - 22.4	0.70
22.4 - 31.5	0.69
31.5 - 45.0	...

SPECIFIC GRAVITY

fraction [mm]	Gs [kg/m³]
4-8	1628
8-16	1726
16-31.5	1769
4-31.5	1697

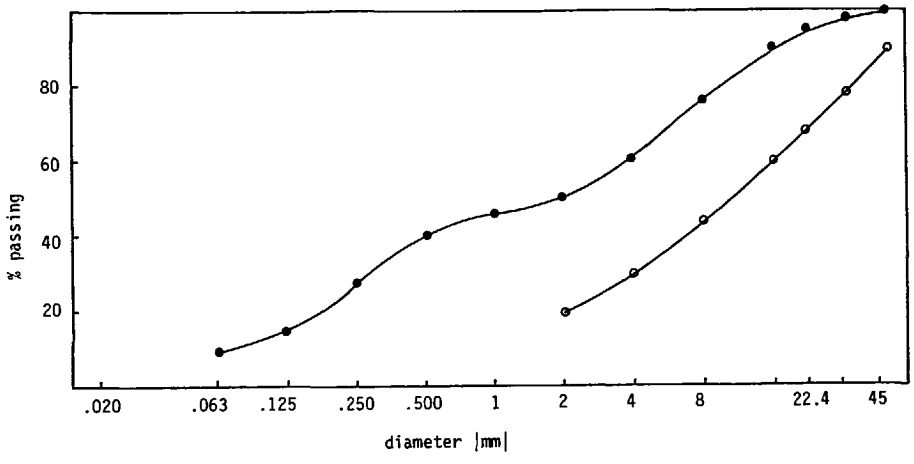

MMPD = Maximum Modified Proctor Density
SPPD = Single Point Proctor Density
MVHD = Maximum Vibrating Hammer Density

VF = Verbrijzelingsfactor

MATERIAL INFORMATION SHEET GROUPS C AND R

MATERIAL NUMBER	CODE	MATERIAL NAME
R04	M20	crushed masonry 2

GRADING

sieve [mm]	percentage passing
.020	...
.063	3.6
.125	5.8
.250	11.2
.500	16.4
1.0	18.5
2.0	20
4.0	30
8.0	44
16.0	60
22.4	69
31.5	78
45.0	90

	DENSITY [kg/m³]	at MC [%]	CBR 0/22.4 at PEN [%]	[in]
MMPD	1570	15.8	97	.1
SPPD	1563	14.0	113	.2
MVHD	1555	15.0		

DEGRADATION

fraction [mm]	value
4.0 - 5.6	VF= 0.67
5.6 - 8.0	0.67
8.0 - 11.2	0.67
11.2 - 16.0	0.65
16.0 - 22.4	0.70
22.4 - 31.5	0.69
31.5 - 45.0	...

SPECIFIC GRAVITY

fraction [mm]	Gs [kg/m³]
4-8	1628
8-16	1726
16-31.5	1769
4-31.5	1697

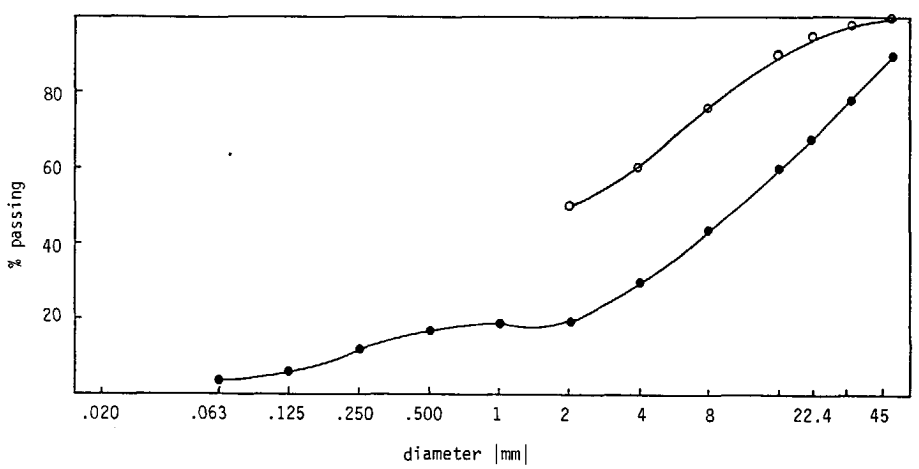

MMPD = Maximum Modified Proctor Density
SPPD = Single Point Proctor Density
MVHD = Maximum Vibrating Hammer Density
VF = Verbrijzelingsfactor

MATERIAL INFORMATION SHEET **GROUPS C AND R**

MATERIAL NUMBER	CODE	MATERIAL NAME
R05	BGB	crushed concrete 1

GRADING

sieve [mm]	percentage passing
.020	...
.063	3.0
.125	6.6
.250	14.0
.500	25.8
1.0	37.7
2.0	50
4.0	60
8.0	76
16.0	90
22.4	95
31.5	98
45.0	100

	DENSITY [kg/m³]	at MC [%]	CBR 0/22.4 at PEN [%]	[in]
MMPD	1864	9.0	76	.1
SPPD	1778	12.1	95	.2
MVHD	1919	12.2		

DEGRADATION

fraction [mm]	value
4.0 - 5.6	VF= 0.79
5.6 - 8.0	0.78
8.0 - 11.2	0.78
11.2 - 16.0	0.79
16.0 - 22.4	0.84
22.4 - 31.5	0.75
31.5 - 45.0	...

SPECIFIC GRAVITY

fraction [mm]	Gs [kg/m³]
4-8	2178
8-16	2291
16-31.5	2307
4-31.5	2207

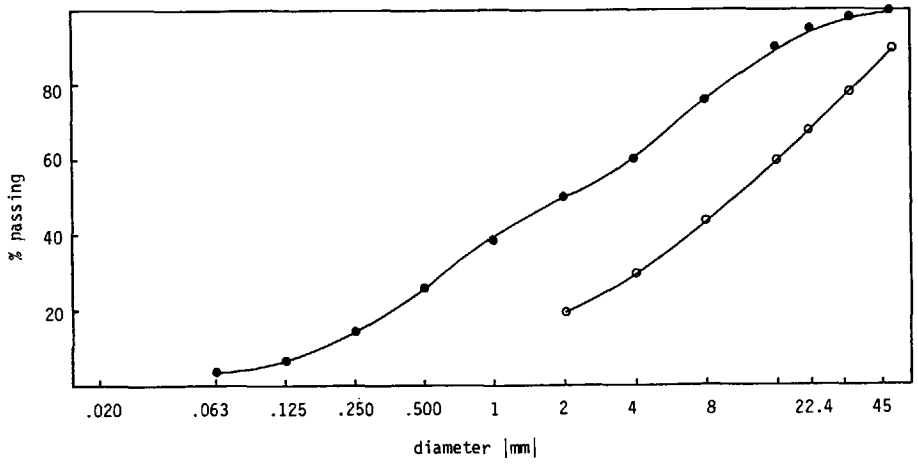

MMPD = Maximum Modified Proctor Density
SPPD = Single Point Proctor Density
MVHD = Maximum Vibrating Hammer Density

VF = Verbrijzelingsfactor

MATERIAL INFORMATION SHEET GROUPS C AND R

MATERIAL NUMBER	CODE	MATERIAL NAME
R06	BGO	crushed concrete 1

GRADING

sieve [mm]	percentage passing
.020	...
.063	1.2
.125	2.6
.250	5.6
.500	10.3
1.0	15.1
2.0	20
4.0	30
8.0	44
16.0	60
22.4	69
31.5	78
45.0	90

	DENSITY [kg/m³]	at MC [%]	CBR 0/22.4 at PEN [%]	[in]
MMPD	1884	8.5	87	.1
SPPD	1806	8.0	112	.2
MVHD	2006	8.8		

DEGRADATION

fraction [mm]	value
4.0 - 5.6	VF= 0.79
5.6 - 8.0	0.78
8.0 - 11.2	0.78
11.2 - 16.0	0.79
16.0 - 22.4	0.84
22.4 - 31.5	0.75
31.5 - 45.0	...

SPECIFIC GRAVITY

fraction [mm]	Gs [kg/m³]
4-8	2178
8-16	2291
16-31.5	2307
4-31.5	2207

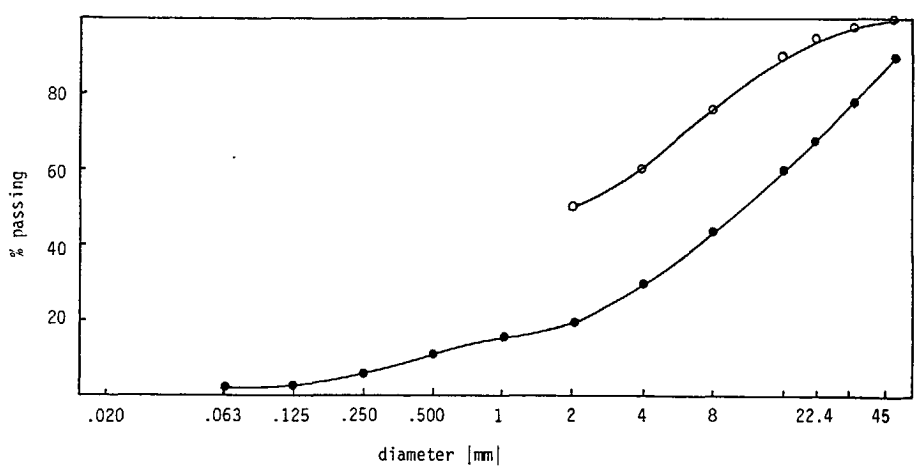

MMPD = Maximum Modified Proctor Density
SPPD = Single Point Proctor Density
MVHD = Maximum Vibrating Hammer Density

VF = Verbrijzelingsfactor

MATERIAL INFORMATION SHEET GROUPS C AND R

MATERIAL NUMBER	CODE	MATERIAL NAME
R07	KGB	crushed clincker

GRADING

sieve [mm]	percentage passing
.020	...
.063	8.7
.125	14.8
.250	23.4
.500	33.9
1.0	42.5
2.0	50
4.0	60
8.0	76
16.0	90
22.4	95
31.5	98
45.0	100

DENSITY	at MC	CBR 0/22.4 at PEN	
[kg/m³]	[%]	[%]	[in]
MMPD 1828	7.5	210	.1
SPPD 1775	9.7	>247	.2
MVHD 1844	8.3		

DEGRADATION

fraction [mm]	value
4.0 - 5.6	VF= 0.76
5.6 - 8.0	0.76
8.0 - 11.2	0.79
11.2 - 16.0	0.77
16.0 - 22.4	0.79
22.4 - 31.5	0.74
31.5 - 45.0	...

SPECIFIC GRAVITY

fraction [mm]	Gs [kg/m³]
4-8	2052
8-16	2085
16-31.5	2094
4-31.5	2086

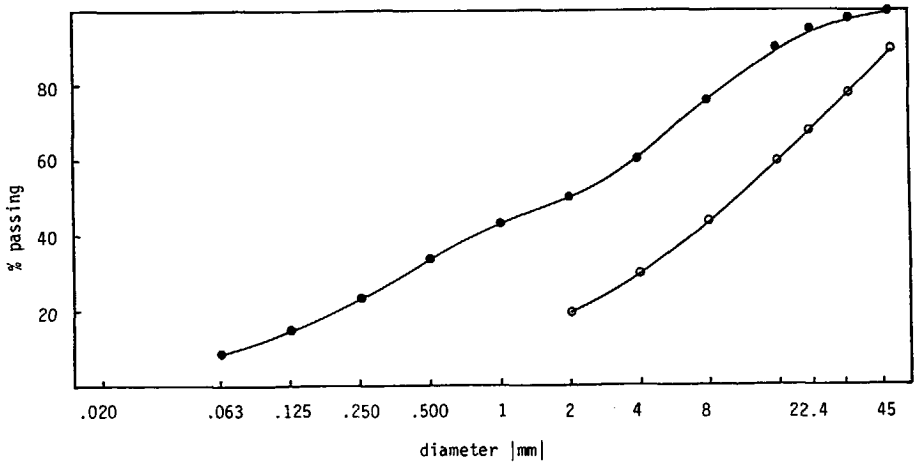

MMPD = Maximum Modified Proctor Density
SPPD = Single Point Proctor Density
MVHD = Maximum Vibrating Hammer Density

VF = Verbrijzelingsfactor

MATERIAL INFORMATION SHEET GROUPS C AND R

MATERIAL NUMBER	CODE	MATERIAL NAME
R08	KGO	crushed clincker

GRADING

sieve [mm]	percentage passing
.020	...
.063	3.5
.125	5.9
.250	9.4
.500	13.6
1.0	17.0
2.0	20
4.0	30
8.0	44
16.0	60
22.4	69
31.5	78
45.0	90

	DENSITY [kg/m³]	at MC [%]	CBR 0/22.4 at PEN [%]	[in]
MMPD	1699	5.5	108	.1
SPPD	1761	6.7	125	.2
MVHD	1717	5.5		

DEGRADATION

fraction [mm]	value
4.0 - 5.6	VF= 0.76
5.6 - 8.0	0.76
8.0 - 11.2	0.79
11.2 - 16.0	0.77
16.0 - 22.4	0.79
22.4 - 31.5	0.74
31.5 - 45.0	...

SPECIFIC GRAVITY

fraction [mm]	Gs [kg/m³]
4-8	2052
8-16	2085
16-31.5	2094
4-31.5	2086

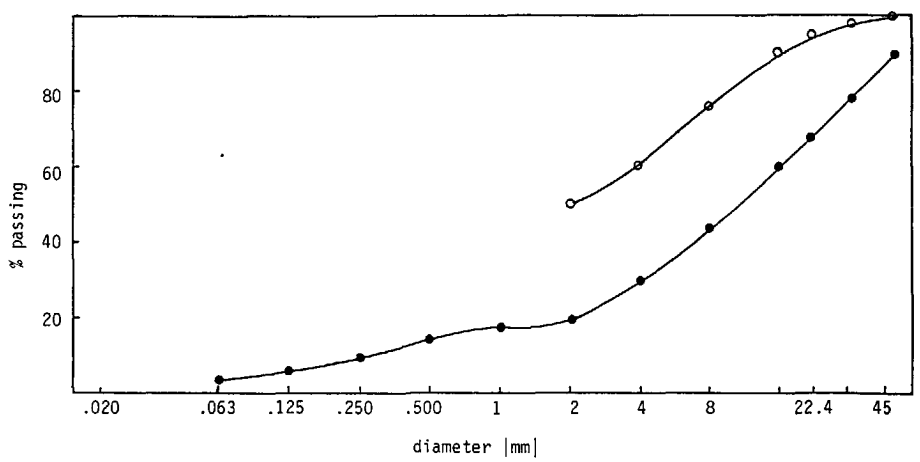

MMPD = Maximum Modified Proctor Density
SPPD = Single Point Proctor Density
MVHD = Maximum Vibrating Hammer Density
VF = Verbrijzelingsfactor

MATERIAL INFORMATION SHEET **GROUPS C AND R**

MATERIAL NUMBER	CODE	MATERIAL NAME
R09	FFB	crushed masonry/concrete

GRADING

sieve [mm]	percentage passing
.020	...
.063	5.9
.125	10.5
.250	20.9
.500	33.1
1.0	41.9
2.0	50
4.0	60
8.0	76
16.0	90
22.4	95
31.5	98
45.0	100

DENSITY at MC **CBR 0/22.4 at PEN**

	[kg/m³]	[%]	[%]	[in]
MMPD	1758	12.5	84	.1
SPPD	1632	13.9	104	.2
MVHD	1747	13.3		

DEGRADATION

fraction [mm]	value
4.0 - 5.6	VF= 0.74
5.6 - 8.0	0.72
8.0 - 11.2	0.75
11.2 - 16.0	0.74
16.0 - 22.4	0.74
22.4 - 31.5	0.73
31.5 - 45.0	0.72

SPECIFIC GRAVITY

fraction [mm]	Gs [kg/m³]
4-8	1989
8-16	2044
16-31.5	2039
4-31.5	2024

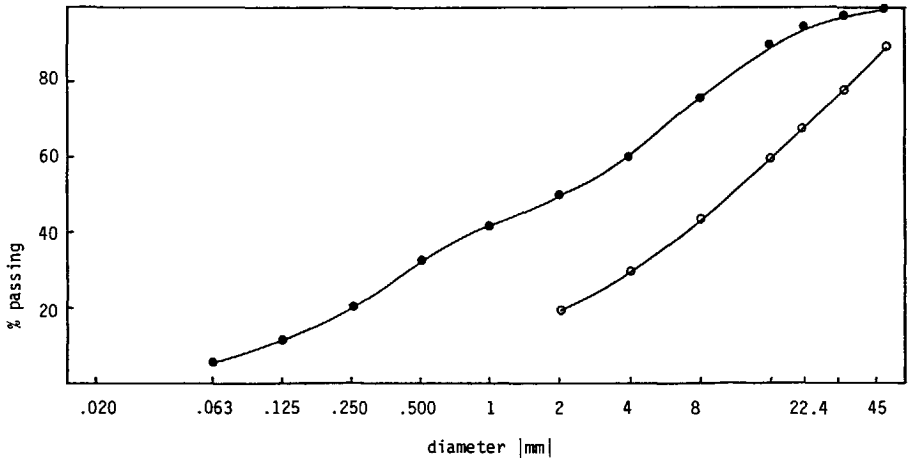

MMPD = Maximum Modified Proctor Density
SPPD = Single Point Proctor Density
MVHD = Maximum Vibrating Hammer Density
VF = Verbrijzelingsfactor

MATERIAL INFORMATION SHEET GROUPS C AND R

MATERIAL NUMBER	CODE	MATERIAL NAME
R10	FFO	crushed masonry/concrete

GRADING

sieve [mm]	percentage passing
.020	...
.063	2.4
.125	4.2
.250	8.4
.500	13.3
1.0	16.8
2.0	20
4.0	30
8.0	44
16.0	60
22.4	69
31.5	78
45.0	90

	DENSITY [kg/m³]	at MC [%]	CBR 0/22.4 at PEN [%]	[in]
MMPD	1713	11.5	88	.1
SPPD	1714	11.9	109	.2
MVHD	1765	10.2		

DEGRADATION

fraction [mm]	value
4.0 - 5.6	VF= 0.74
5.6 - 8.0	0.72
8.0 - 11.2	0.75
11.2 - 16.0	0.74
16.0 - 22.4	0.74
22.4 - 31.5	0.73
31.5 - 45.0	0.72

SPECIFIC GRAVITY

fraction [mm]	Gs [kg/m³]
4-8	1989
8-16	2044
16-31.5	2039
4-31.5	2024

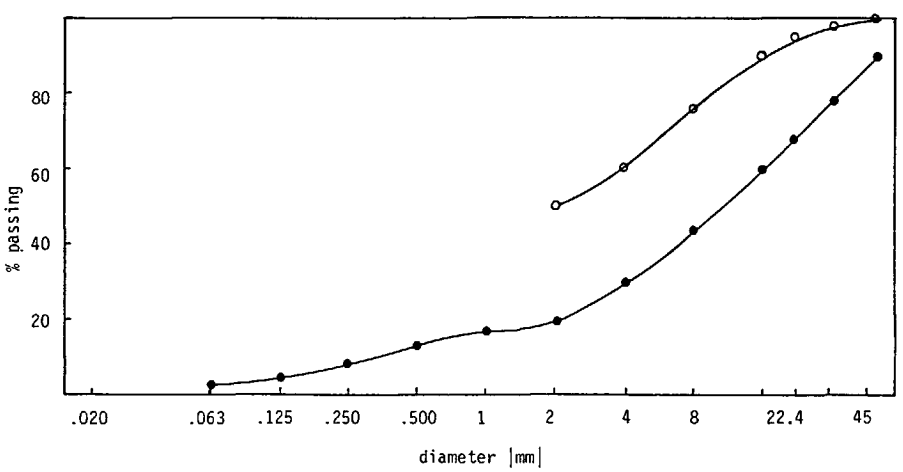

MMPD = Maximum Modified Proctor Density
SPPD = Single Point Proctor Density
MVHD = Maximum Vibrating Hammer Density
VF = Verbrijzelingsfactor

MATERIAL INFORMATION SHEET GROUPS C AND R

MATERIAL NUMBER	CODE	MATERIAL NAME
R11	B2C	crushed concrete 2

GRADING

sieve [mm]	percentage passing
.020	...
.063	1.9
.125	3.1
.250	7.7
.500	12.8
1.0	18.3
2.0	23
4.0	30
8.0	44
16.0	68
22.4	81
31.5	94
45.0	100

DENSITY	at MC	CBR 0/22.4 at PEN	
[kg/m³]	[%]	[%]	[in]
MMPD 1922	9.6	142	.1
SPPD 1800	8.0	...	.2
MVHD 1937	9.6		

DEGRADATION

fraction [mm]	value
4.0 - 5.6	VF= 0.81
5.6 - 8.0	0.79
8.0 - 11.2	0.83
11.2 - 16.0	0.79
16.0 - 22.4	0.78
22.4 - 31.5	0.76
31.5 - 45.0	...

SPECIFIC GRAVITY

fraction [mm]	Gs [kg/m³]
4-8	2278
8-16	2345
16-31.5	2263
4-31.5	2303

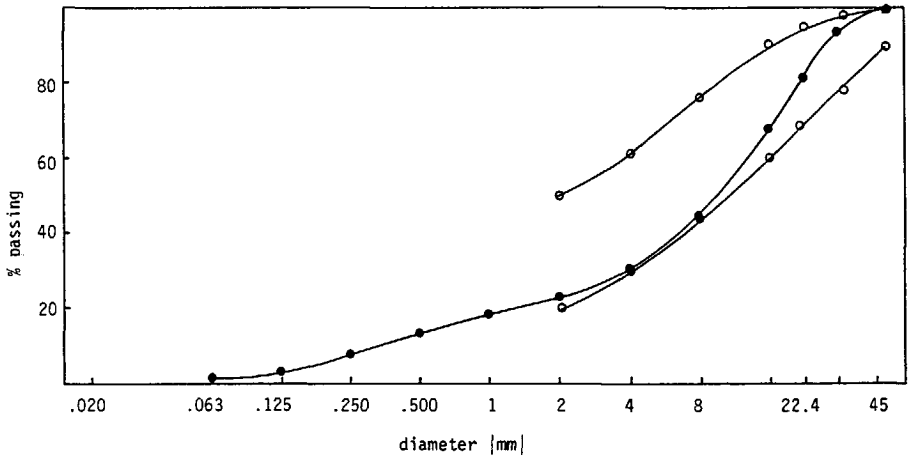

MMPD = Maximum Modified Proctor Density
SPPD = Single Point Proctor Density
MVHD = Maximum Vibrating Hammer Density
VF = Verbrijzelingsfactor

MATERIAL INFORMATION SHEET GROUPS C AND R

MATERIAL NUMBER	CODE	MATERIAL NAME
R12	K1C	crushed rubble 1

GRADING

sieve [mm]	percentage passing
.020	...
.063	2.7
.125	4.5
.250	7.7
.500	13.5
1.0	17.6
2.0	22
4.0	29
8.0	42
16.0	65
22.4	...
31.5	89
45.0	...

DENSITY	at MC	CBR 0/22.4 at PEN	
[kg/m³]	[%]	[%]	[in]
MMPD 1783	11.4	127	.1
SPPD 1687	7.5	156	.2
MVHD 1749	11.7		

DEGRADATION

fraction [mm]	value
4.0 - 5.6	VF= 0.72
5.6 - 8.0	0.70
8.0 - 11.2	0.75
11.2 - 16.0	0.73
16.0 - 22.4	0.73
22.4 - 31.5	0.70
31.5 - 45.0	...

SPECIFIC GRAVITY

fraction [mm]	Gs [kg/m³]
4-8	2061
8-16	2084
16-31.5	2088
4-31.5	2040

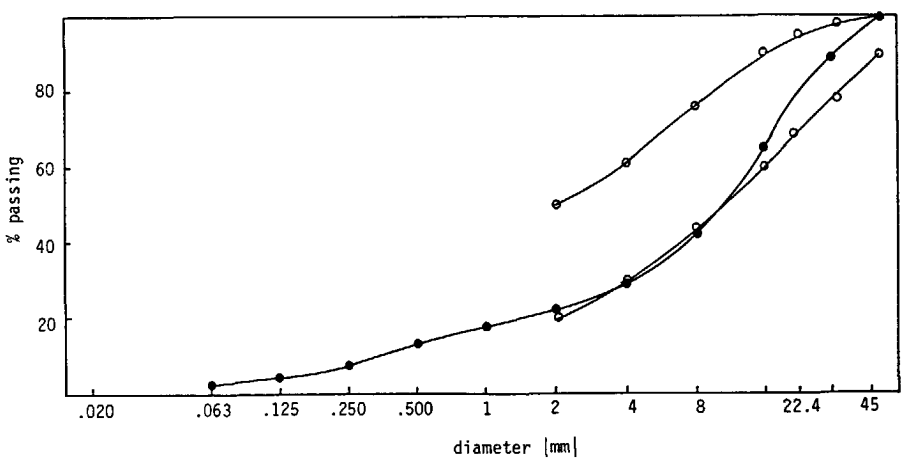

MMPD = Maximum Modified Proctor Density
SPPD = Single Point Proctor Density
MVHD = Maximum Vibrating Hammer Density
VF = Verbrijzelingsfactor

MATERIAL INFORMATION SHEET **GROUPS C AND R**

MATERIAL NUMBER	CODE	MATERIAL NAME
R13	K2C	crushed rubble 2

GRADING

sieve [mm]	percentage passing
.020	...
.063	3.0
.125	5.4
.250	12.9
.500	20.0
1.0	26.5
2.0	32
4.0	40
8.0	53
16.0	75
22.4	...
31.5	95
45.0	...

	DENSITY [kg/m³]	at MC [%]	CBR 0/22.4 at PEN [%]	[in]
MMPD	1806	9.9	128	.1
SPPD	1677	10.1	160	.2
MVHD	1779	12.5		

DEGRADATION

fraction [mm]	value
4.0 - 5.6	VF= 0.75
5.6 - 8.0	0.75
8.0 - 11.2	0.78
11.2 - 16.0	0.74
16.0 - 22.4	0.75
22.4 - 31.5	0.72
31.5 - 45.0	...

SPECIFIC GRAVITY

fraction [mm]	Gs [kg/m³]
4-8	2049
8-16	2088
16-31.5	2025
4-31.5	2030

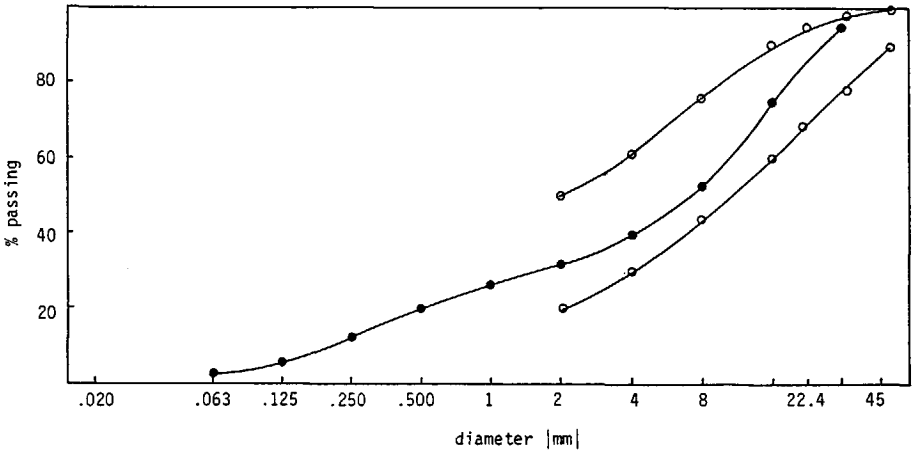

MMPD = Maximum Modified Proctor Density
SPPD = Single Point Proctor Density
MVHD = Maximum Vibrating Hammer Density

VF = Verbrijzelingsfactor

MATERIAL INFORMATION SHEET GROUPS C AND R

MATERIAL NUMBER	CODE	MATERIAL NAME
R14	K3C	crushed rubble 3

GRADING

sieve [mm]	percentage passing
.020	...
.063	3.4
.125	8.0
.250	11.1
.500	15.5
1.0	18.1
2.0	21
4.0	25
8.0	37
16.0	57
22.4	...
31.5	89
45.0	...

DENSITY at MC	[kg/m³]	[%]	CBR O/22.4 at PEN [%]	[in]
MMPD	1742	10.6	120	.1
SPPD	1705	8.7	152	.2
MVHD	1769	9.9		

DEGRADATION

fraction [mm]	value
4.0 - 5.6	VF= 0.73
5.6 - 8.0	0.72
8.0 - 11.2	0.77
11.2 - 16.0	0.71
16.0 - 22.4	0.77
22.4 - 31.5	0.71
31.5 - 45.0	...

SPECIFIC GRAVITY

fraction [mm]	Gs [kg/m³]
4-8	2058
8-16	2123
16-31.5	2163
4-31.5	2095

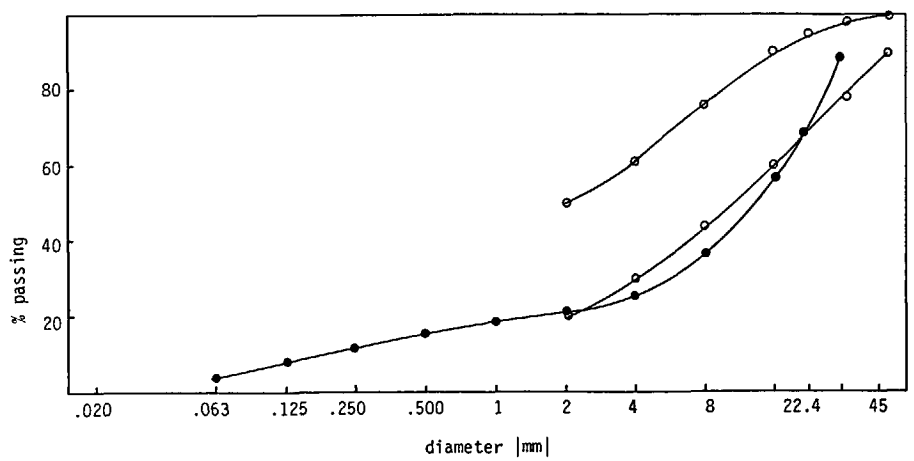

MMPD = Maximum Modified Proctor Density
SPPD = Single Point Proctor Density
MVHD = Maximum Vibrating Hammer Density

VF = Verbrijzelingsfactor

MATERIAL INFORMATION SHEET **GROUPS C AND R**

MATERIAL NUMBER	CODE	MATERIAL NAME
R15	AVC	waste incineration slag

GRADING

sieve [mm]	percentage passing
.020	...
.063	7,0
.125	9,5
.250	18,0
.500	31,3
1.0	40,6
2.0	49
4.0	60
8.0	74
16.0	94
22.4	100
31.5	...
45.0	...

	DENSITY [kg/m³]	at MC [%]	CBR 0/22.4 at PEN [%]	[in]
MMPD	1763	12.7	64	.1
SPPD	1564	11.2	84	.2
MVHD	1621	14.0		

DEGRADATION

fraction [mm]	value
4.0 - 5.6	VF= 0.72
5.6 - 8.0	0.70
8.0 - 11.2	0.72
11.2 - 16.0	0.69
16.0 - 22.4	...
22.4 - 31.5	...
31.5 - 45.0	...

SPECIFIC GRAVITY

fraction [mm]	Gs [kg/m³]
4-8	1796
8-16	2150
16-31.5	....
4-31.5	2051

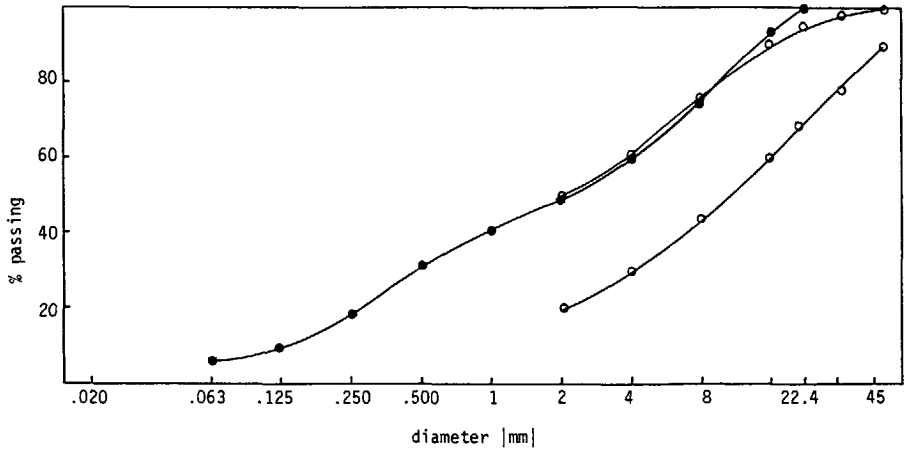

MMPD = Maximum Modified Proctor Density
SPPD = Single Point Proctor Density
MVHD = Maximum Vibrating Hammer Density

VF = Verbrijzelingsfactor

MATERIAL INFORMATION SHEET GROUP S

MATERIAL NUMBER	CODE	MATERIAL NAME
S01	EL	Echteld sand

GRADING		DENSITY	at MC	CBR 0/22.4 at PEN	
sieve [mm]	percentage passing	[kg/m³]	[%]	[%]	[in]
.002	0.6	MMPD 1745	12.7	19	.1
.006	1.7				
.020	5.2			17	.2
.075	8.7				
.175	21.4				
.300	47.2				
.420	68.0	CLASSIFICATION (extended USCS)			
.600	79.7				
1.4	92.4	type: poorly graded sand			
2.0	94.9				
2.8	97.1	code: SP/SF			

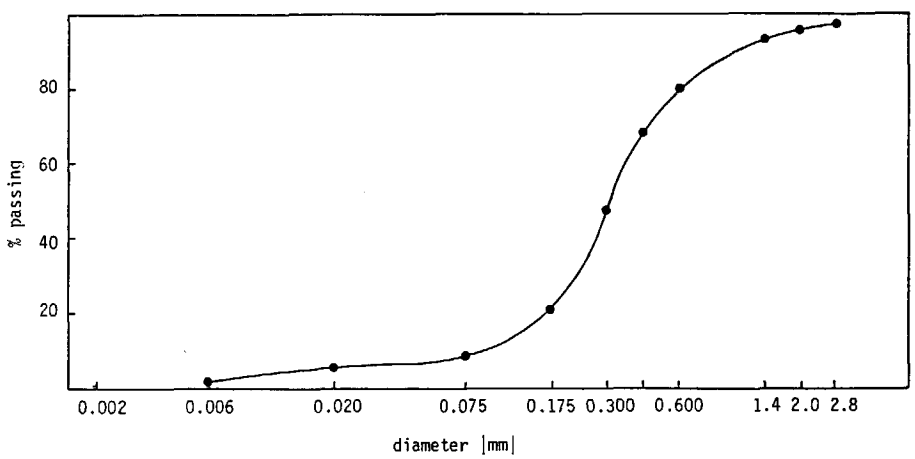

MMPD = Modified Maximum Proctor Density

MATERIAL INFORMATION SHEET GROUP S

MATERIAL NUMBER	CODE	MATERIAL NAME
S02	EN	Echten sand

GRADING		DENSITY	at MC	CBR 0/22.4 at PEN	
sieve [mm]	percentage passing	[kg/m³]	[%]	[%]	[in]
.002	1.7	MMPD 1712	13.7	16	.1
.006	3.0				
.020	5.0			14	.2
.075	8.4				
.175	23.0				
.300	49.2				
.420	72.6	CLASSIFICATION (extended USCS)			
.600	86.6				
1.4	98.4	type: poorly graded sand			
2.0	99.4				
2.8	99.8	code: SP/SF			

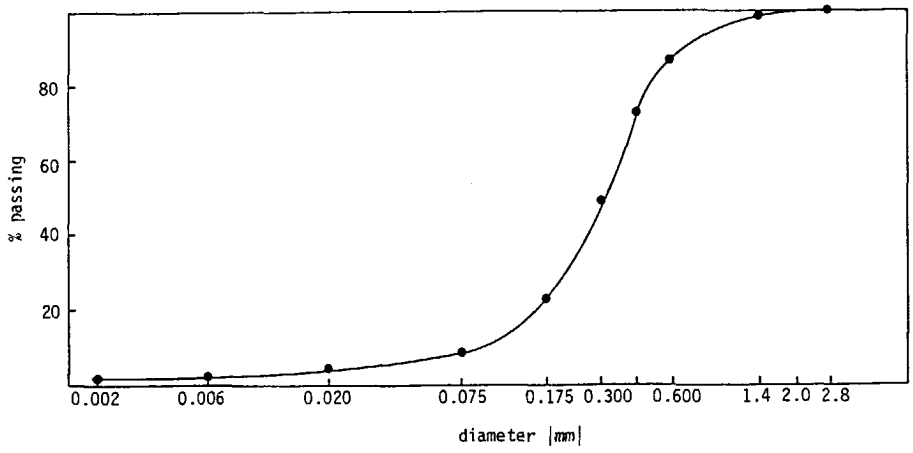

MMPD = Modified Maximum Proctor Density

MATERIAL INFORMATION SHEET GROUP S

MATERIAL NUMBER	CODE	MATERIAL NAME
S03	EE	Eems sand

GRADING		DENSITY	at MC	CBR 0/22.4 at PEN	
sieve [mm]	percentage passing	[kg/m³]	[%]	[%]	[in]
.002	...	MMPD 1665	13.0	21	.1
.006	...				
.020	...			16	.2
.075	5.7				
.175	73.2				
.300	89.7				
.420	95.6	CLASSIFICATION (extended USCS)			
.600	97.8				
1.4	99.6	type: poorly graded sand			
2.0	99.9				
2.8	99.9	code: SP/SF			

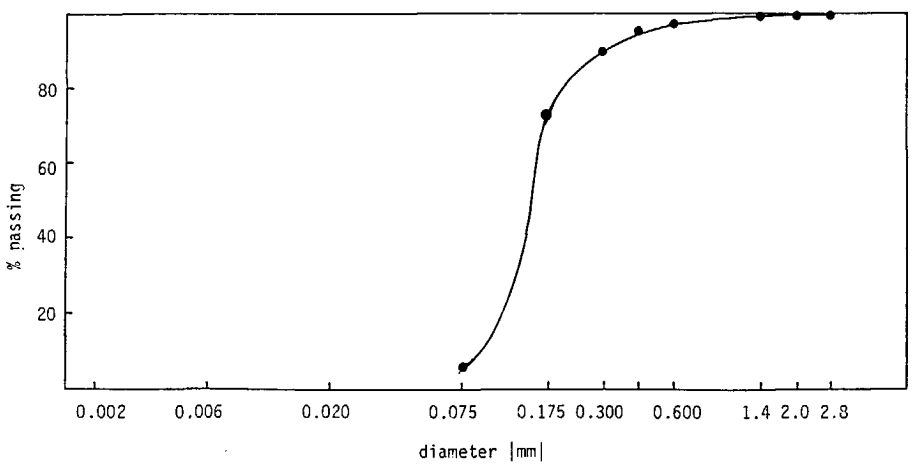

MMPD = Modified Maximum Proctor Density

MATERIAL INFORMATION SHEET GROUP S

MATERIAL NUMBER	CODE	MATERIAL NAME
S04	OS	Eastern Scheldt sand

GRADING		DENSITY	at MC	CBR 0/22.4 at PEN	
sieve [mm]	percentage passing	[kg/m³]	[%]	[%]	[in]
.002	2.9	MMPD 1668	15.7	19	.1
.006	3.9				
.020	5.5			23	.2
.075	11.5				
.175	72.9				
.300	89.2				
.420	96.5	CLASSIFICATION (extended USCS)			
.600	98.7				
1.4	99.6	type: poorly graded sand			
2.0	99.8				
2.8	99.9	code: SP/SF			

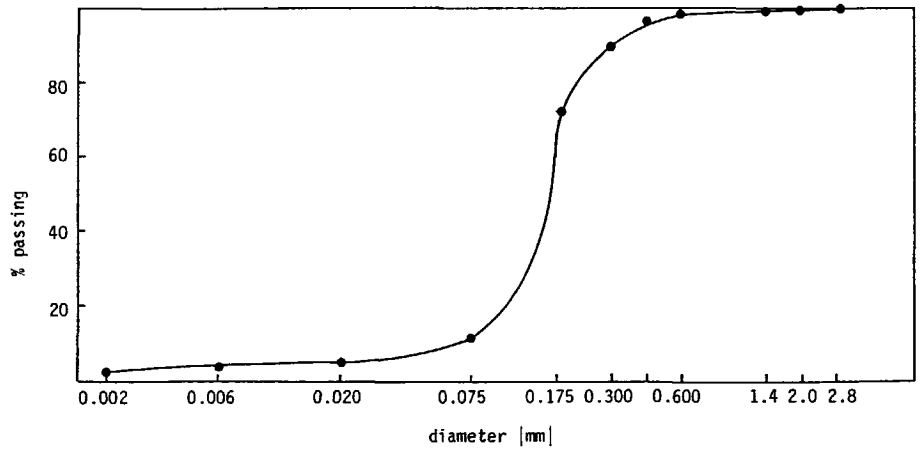

MMPD = Modified Maximum Proctor Density

MATERIAL INFORMATION SHEET GROUP S

MATERIAL NUMBER	CODE	MATERIAL NAME
S05	WI	Winterswijk sand

GRADING		DENSITY	at MC	CBR 0/22.4 at PEN	
sieve [mm]	percentage passing	[kg/m³]	[%]	[%]	[in]
.002	2.1	MMPD 1697	10.5	25	.1
.006	2.4				
.020	3.3			12	.2
.075	11.6				
.175	67.0				
.300	94.2				
.420	98.0	CLASSIFICATION (extended USCS)			
.600	99.1				
1.4	99.8	type: poorly graded sand			
2.0	99.9				
2.8	100.0	code: SP/SF			

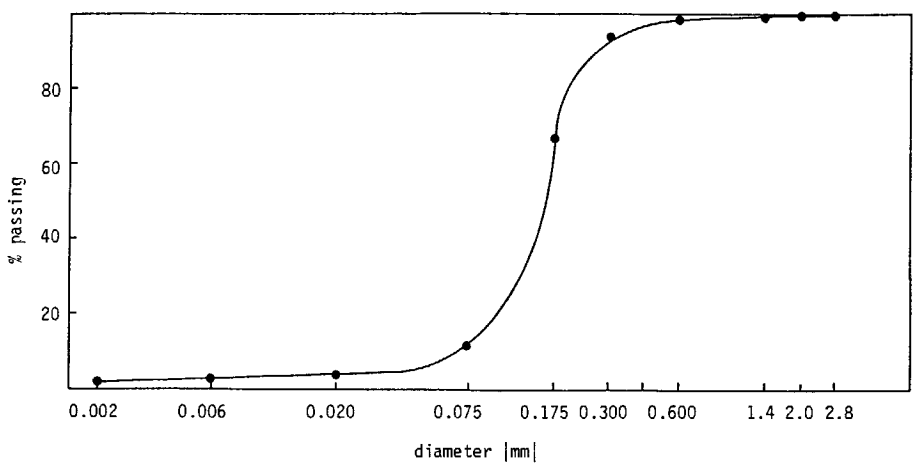

MMPD = Modified Maximum Proctor Density

MATERIAL INFORMATION SHEET GROUP S

MATERIAL NUMBER	CODE	MATERIAL NAME
S06	ZE	Zijen sand

GRADING		DENSITY	at MC	CBR 0/22.4 at PEN	
sieve [mm]	percentage passing	[kg/m³]	[%]	[%]	[in]
.002	2.7	MMPD 1593	15.0	30	.1
.006	3.3				
.020	4.3			26	.2
.075	33.8				
.175	95.1				
.300	98.4				
.420	99.5	CLASSIFICATION (extended USCS)			
.600	99.7				
1.4	99.7	type: silty sand			
2.0	99.8				
2.8	99.9	code: SMF			

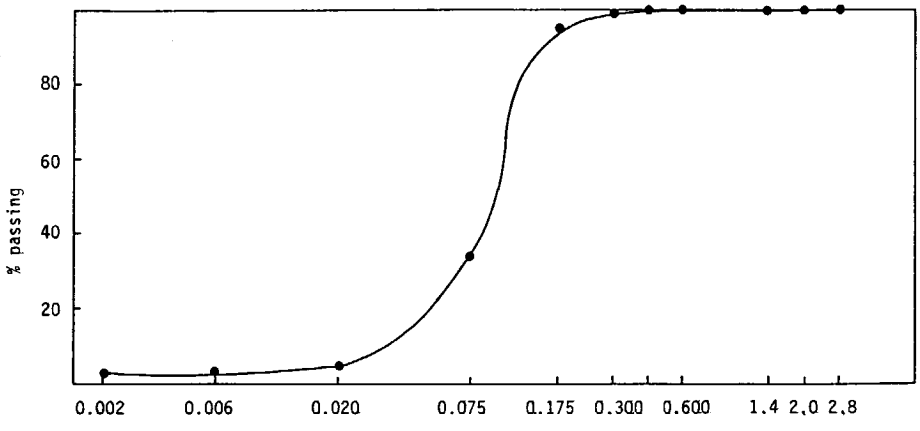

MMPD = Modified Maximum Proctor Density

MATERIAL INFORMATION SHEET GROUP L

MATERIAL NUMBER	CODE	MATERIAL NAME
L01	HA2	laterite

GRADING

sieve [mm]	percentage passing
.075	40.8
.150	44.9
.300	53.2
.600	68.4
2.36	96.8
4.75	100.0
9.52	...
19.05	...
25.40	...

SPECIFIC GRAVITY

fraction [mm]	Gs [kg/m³]
0-19	2.82

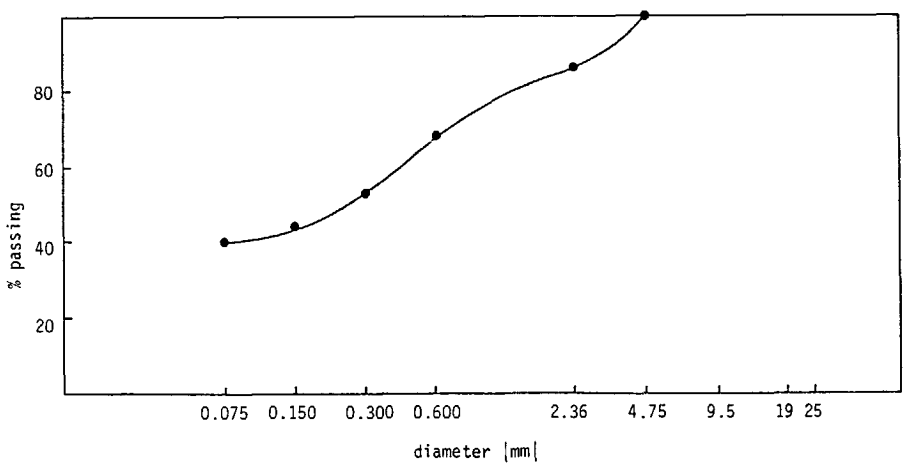

MATERIAL INFORMATION SHEET GROUP L

MATERIAL NUMBER	CODE	MATERIAL NAME
LO2	AB1	laterite

GRADING

sieve [mm]	percentage passing
.075	24.1
.150	25.2
.300	29.0
.600	34.9
2.36	49.5
4.75	54.8
9.52	65.0
19.05	87.3
25.40	92.3

SPECIFIC GRAVITY

fraction [mm]	Gs [kg/m³]
0-19	2.85

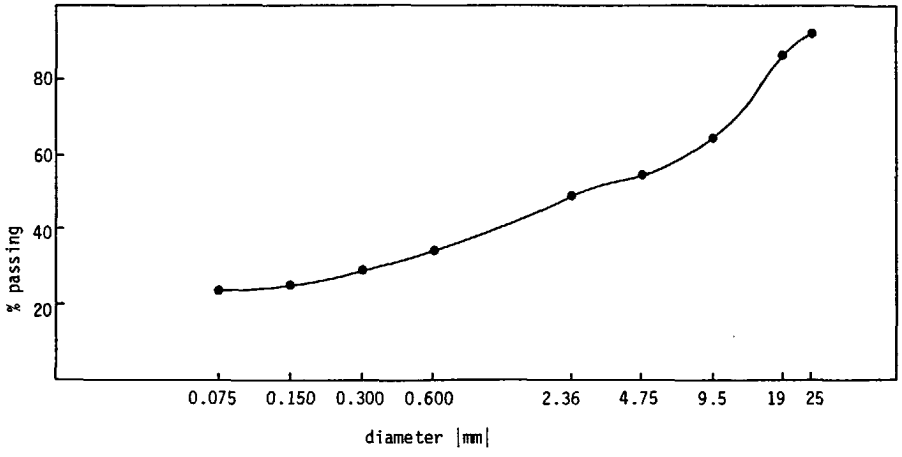

MATERIAL INFORMATION SHEET GROUP L

MATERIAL NUMBER	CODE	MATERIAL NAME
L03	BB1	laterite

GRADING

sieve [mm]	percentage passing
.075	29.4
.150	30.0
.300	32.2
.600	34.4
2.36	55.4
4.75	57.1
9.52	63.0
19.05	85.1
25.40	91.1

SPECIFIC GRAVITY

fraction [mm]	Gs [kg/m³]
0-19	3.08

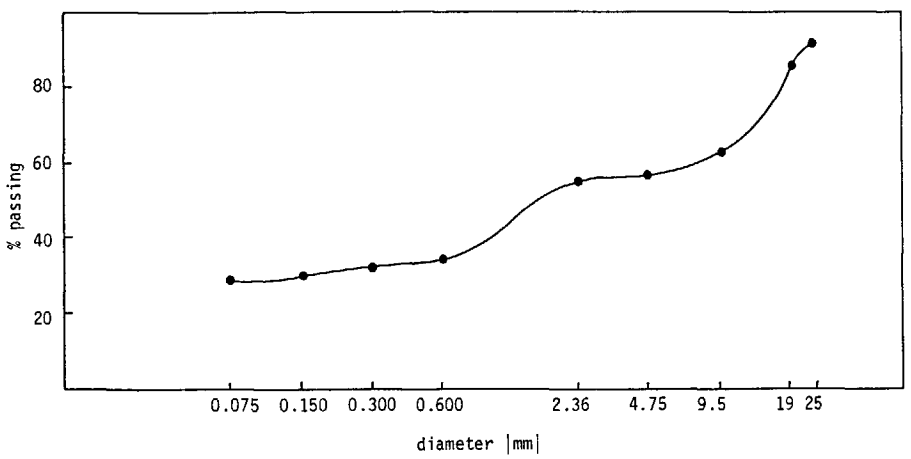

MATERIAL INFORMATION SHEET GROUP L

MATERIAL NUMBER	CODE	MATERIAL NAME
L04	IB1	laterite

GRADING

sieve [mm]	percentage passing
.075	30.7
.150	33.5
.300	41.1
.600	49.0
2.36	76.0
4.75	83.8
9.52	89.1
19.05	97.6
25.40	100.0

SPECIFIC GRAVITY

fraction [mm]	Gs [kg/m³]
0-19	2.90

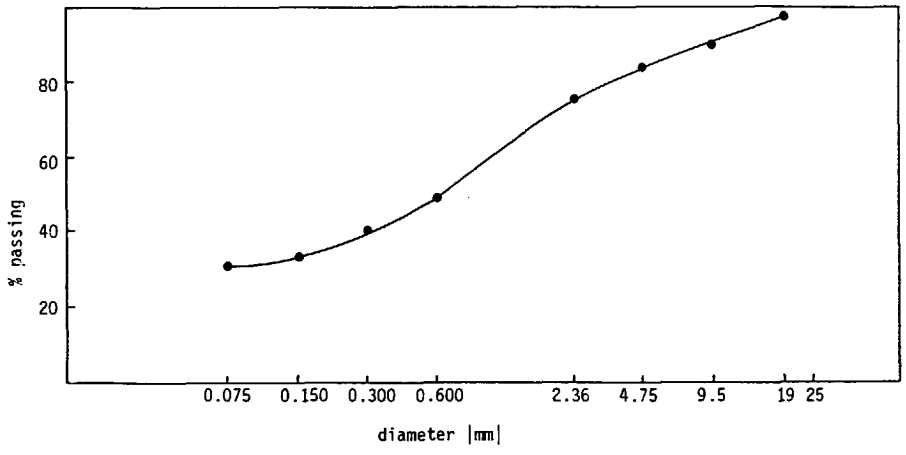

MATERIAL INFORMATION SHEET GROUP L

MATERIAL NUMBER	CODE	MATERIAL NAME
L05	BB2	laterite

GRADING

sieve [mm]	percentage passing
.075	49.8
.150	50.5
.300	53.4
.600	58.4
2.36	92.7
4.75	95.1
9.52	96.0
19.05	100.0
25.40	...

SPECIFIC GRAVITY

fraction [mm]	Gs [kg/m³]
0-19	2.84

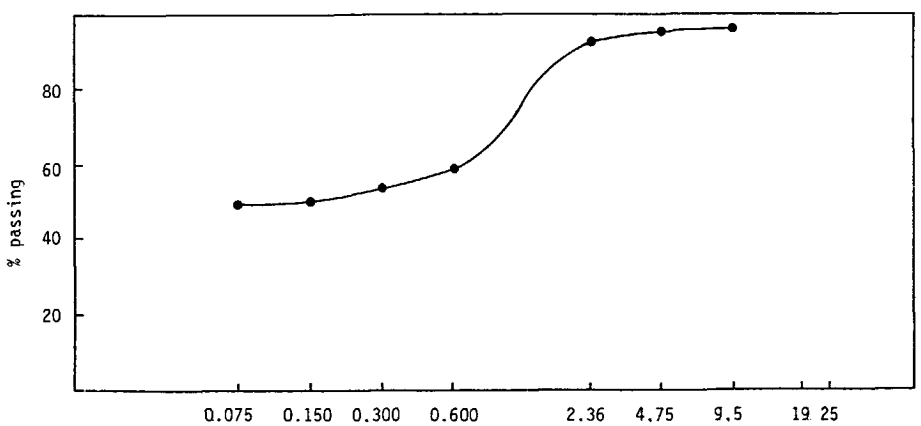

MATERIAL INFORMATION SHEET **GROUP L**

MATERIAL NUMBER	CODE	MATERIAL NAME
L06	AC	laterite

GRADING

sieve [mm]	percentage passing
.075	53.8
.150	57.4
.300	65.4
.600	75.1
2.36	87.3
4.75	91.6
9.52	97.1
19.05	100.0
25.40	...

SPECIFIC GRAVITY

fraction [mm]	Gs [kg/m³]
0-19	2.80

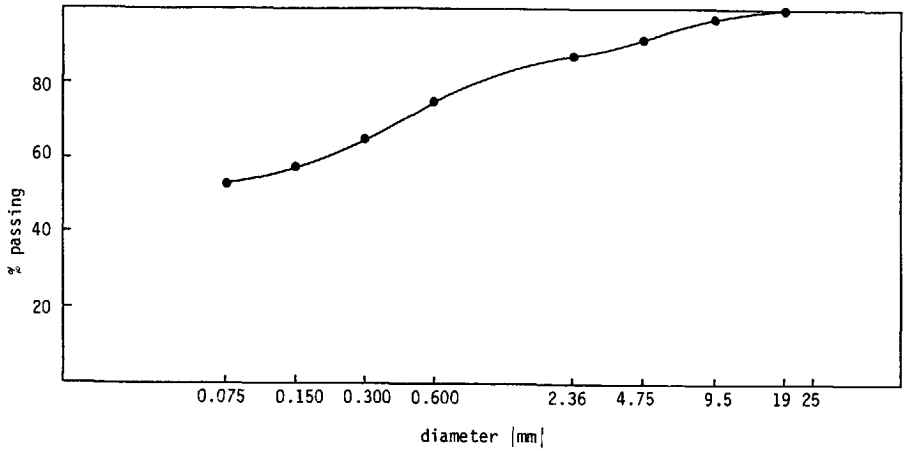

APPENDIX 3

TRIAXIAL SPECIMEN DATA

	TRIAXIAL				PROCTOR		VIBRATING HAMMER	
test code	w	ρ_d	% MMPD	% MVHD	w_{opt}	MMPD	w_{opt}	MVHD
	[%]	[kg/m³]	[%]	[%]	[%]	[kg/m³]	[%]	[kg/m³]
MGBD 06	21.4	1578	103	109	18.4	1536	21.2	1447
07	24.5	1530	100	106				
09	24.5	1530	100	106				
10	20.0	1460	95	101				
MGBS 03	22.0	1485	97	103				
MGOD 10	17.2	1523	99	105	18.7	1534	17.0	1446
11	20.8	1475	96	102				
13	19.1	1481	96	102				
14	19.4	1499	98	104				
M2BD 01	16.0	1585	97	99	15.6	1629	17.1	1609
M2OD 02	13.7	1516	97	97	15.8	1570	15.0	1555
BGBD 01	13.5	1863	100	97	9.0	1864	12.2	1919
03	10.6	1830	98	95				
04	8.9	1815	97	95				
05	11.5	1797	96	94				
BGBS 04	10.7	1815	97	95				
BGOD 01	7.8	1878	100	94	8.5	1884	8.8	2006
03	7.6	1856	99	93				
04	7.9	1879	100	94				
05	8.6	1811	96	90				
BGOS 04	8.0	1882	100	94				
KGBD 01	7.6	1803	99	98	7.5	1828	8.3	1844
03	6.2	1790	98	97				
04	6.8	1768	97	96				
05	7.5	1743	95	95				
KGOD 01	5.3	1695	100	99	5.5	1699	5.5	1717
03	5.4	1695	100	99				
04	3.9	1704	100	99				
06	4.7	1722	101	100				
FFBD 01	14.6	1660	94	95	12.5	1758	13.3	1747
02	11.8	1644	94	94				
03	12.5	1633	93	93				
04	11.8	1613	92	92				
FFOD 01	12.1	1676	98	95	11.5	1713	10.2	1765
02	11.2	1698	99	96				
03	11.9	1669	97	95				
04	11.3	1688	98	96				

test code	TRIAXIAL w [%]	ρ_d [kg/m³]	% MMPD [%]	% MVHD [%]	PROCTOR w_{opt} [%]	MMPD [kg/m³]	VIBRATING HAMMER w_{opt} [%]	MVHD [kg/m³]
LABD 05	9.7	1778	94	96	10.5	1889	11.0	1849
06	7.5	1745	92	94				
07	10.2	1762	93	95				
08	8.2	1802	95	97				
LAOD 03	9.4	1665	99	99	9.3	1682	8.6	1678
04	6.9	1689	100	101				
05	6.1	1739	103	104				
07	8.8	1640	98	98				
LAOS 05	6.9	1681	100	100				
POBD 03	4.2	2113	93	90	4.5	2260	4.5	2340
04	4.5	2072	92	89				
05	1.4	2072	92	89				
POOD 01	2.0	2075	102	96	2.6	2038	3.3	2166
02	1.8	2117	104	98				
03	0.7	2117	104	98				
GGBD 01	5.1	1968	98	103	6.6	2002	3.7	1917
GGOD 01	4.0	2042	101	98	4.8	2029	1.8	2084
KABD 02	5.5	2129	93	91	4.7	2291	5.0	2352
KAOD 01	5.9	2287	100	102	6.1	2288	3.7	2235
STND 01	4.9	2121	98	94	4.4	2174	4.3	2265
02	1.6	2121	98	94				
SMCD 01	4.9	1809	97	102	4.5	1857	5.4	1772
B2CD 01	10.6	1858	97	96	9.6	1922	9.6	1937
02	7.4	1821	95	94				
K1CD 01	9.0	1704	96	97	11.4	1783	11.7	1749
K2CD 01	11.3	1712	95	96	9.9	1806	12.5	1779
K3CD 01	9.6	1710	98	97	10.6	1742	9.9	1769
AVCD 01	16.1	1562	89	96	12.7	1763	14.0	1621

	TRIAXIAL			PROCTOR	
test code	w	ρ_d	% MMPD	w_{opt}	MMPD
	[%]	[kg/m³]	[%]	[%]	[kg/m³]
ELND 01	12.7	1745	100	12.7	1745
ENND 01	13.8	1710	100	13.7	1712
02	13.7	1712	100		
03	13.6	1713	100		
04	13.8	1710	100		
05	13.6	1713	100		
06	6.2	1713	100		
ENNS 01	13.6	1713	100		
EEND 01	12.9	1666	100	13.0	1665
OSND 01	15.8	1667	100	15.7	1668
02	15.8	1668	100		
03	15.6	1669	100		
04	15.4	1672	100		
05	15.7	1668	100		
06	15.6	1669	100		
07	6.9	1669	100		
OSNS 01	16.0	1664	100		
WIND 01	10.5	1698	100	10.5	1697
ZEND 01	15.1	1592	100	15.0	1593
02	14.9	1694	100		
03	14.7	1597	100		
04	15.4	1587	100		
05	14.9	1594	100		
06	7.5	1594	100		
ZENS 01	15.0	1593	100		

TRIAXIAL

test	code	w [%]	ρ_d [kg/m³]
HA2D	01	16.5	1694
	02	21.6	1694
AB1D	01	12.5	1890
	02	15.5	1890
BB1D	01	15.1	1851
	02	18.8	1851
IB1D	01	19.6	1599
IB1D	02	25.1	1599
BB2D	01	13.2	1860
BB2D	02	17.3	1860
ACD	01	19.8	1560
ACD	02	25.1	1560